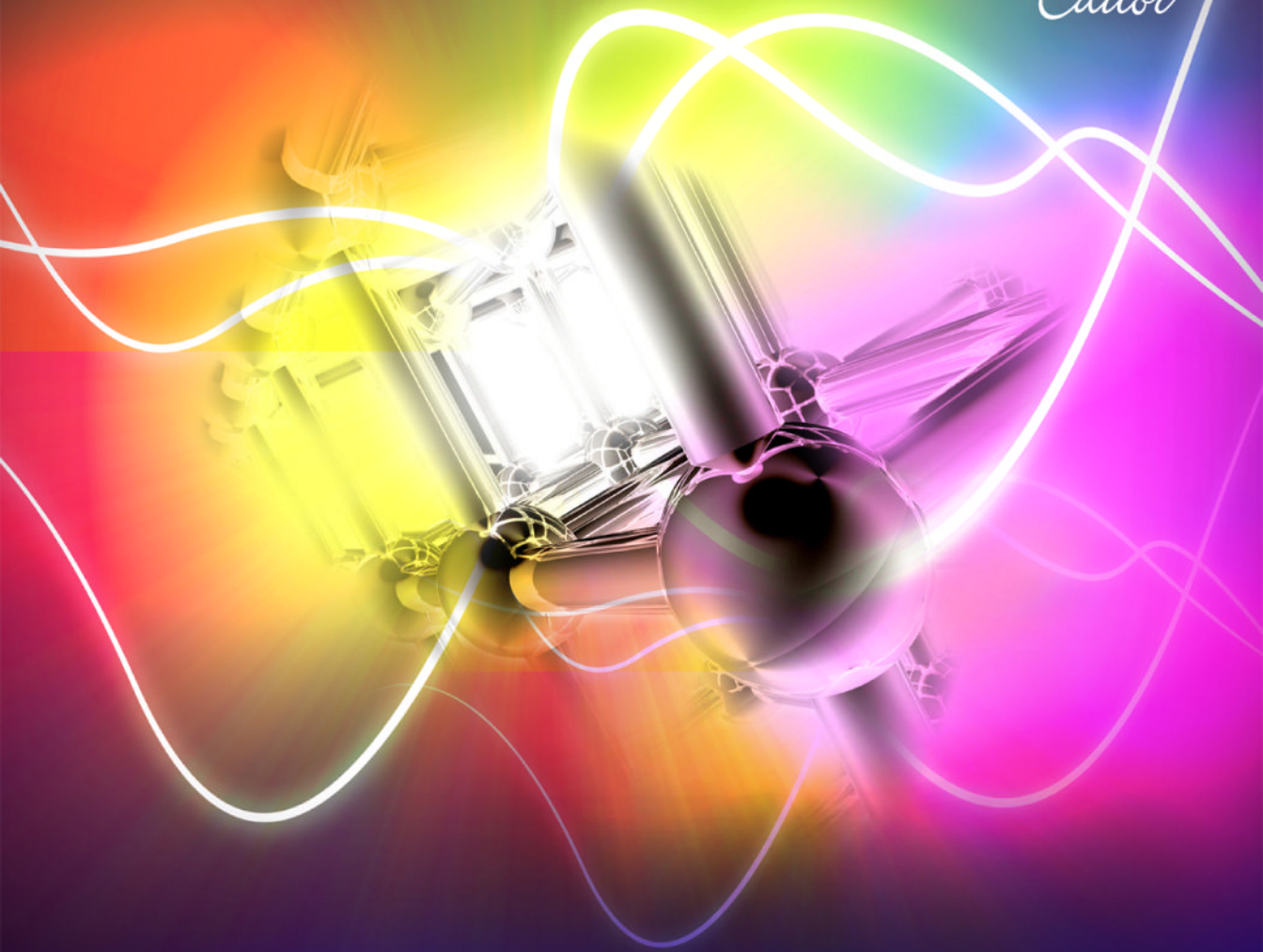




*Nanotechnology Science and Technology Series*

*Armando Barrañón*

*Editor*



# New Nanotechnology Developments

NOVA



**Nanotechnology Science and Technology Series**

# **NEW NANOTECHNOLOGY DEVELOPMENTS**

No part of this digital document may be reproduced, stored in a retrieval system or transmitted in any form or by any means. The publisher has taken reasonable care in the preparation of this digital document, but makes no expressed or implied warranty of any kind and assumes no responsibility for any errors or omissions. No liability is assumed for incidental or consequential damages in connection with or arising out of information contained herein. This digital document is sold with the clear understanding that the publisher is not engaged in rendering legal, medical or any other professional services.

# **NANOTECHNOLOGY SCIENCE AND TECHNOLOGY SERIES**

## **National Nanotechnology Initiative: Assessment and Recommendations**

*Jerrod W. Kleike (Editor)*  
2009. ISBN 978-1-60692-727-4

## **Nanotechnology Research Collection - 2009/2010. DVD edition**

*James N. Ling (Editor)*  
2009. ISBN 978-1-60741-293-9

## **Nanotechnology Research Collection - 2009/2010. PDF edition**

*James N. Ling (Editor)*  
2009. ISBN 978-1-60741-292-2

**Safe Nanotechnology**  
*Arthur J. Cornwelle (Editor)*  
2009. ISBN 978-1-60692-662-8

**Safe Nanotechnology in the Workplace**  
*Nathan I. Bialor (Editor)*  
2009. ISBN 978-1-60692-679-6

## **Strategic Plan for NIOSH Nanotechnology Research and Guidance**

*Martin W. Lang (Author)*  
2009. ISBN: 978-1-60692-678-9

**Nanotechnology in the USA: Developments, Policies and Issues**  
*Carl H. Jennings (Editor)*  
2009. ISBN: 978-1-60692-800-4

**New Nanotechnology Developments**  
*Armando Barrañón (Editor)*  
2009. ISBN: 978-1-60741-028-7

**Nanotechnology Science and Technology Series**

# **NEW NANOTECHNOLOGY DEVELOPMENTS**

**ARMANDO BARRANON  
EDITOR**

**Nova Science Publishers, Inc.**  
*New York*

Copyright © 2009 by Nova Science Publishers, Inc.

**All rights reserved.** No part of this book may be reproduced, stored in a retrieval system or transmitted in any form or by any means: electronic, electrostatic, magnetic, tape, mechanical photocopying, recording or otherwise without the written permission of the Publisher.

For permission to use material from this book please contact us:

Telephone 631-231-7269; Fax 631-231-8175

Web Site: <http://www.novapublishers.com>

#### **NOTICE TO THE READER**

The Publisher has taken reasonable care in the preparation of this book, but makes no expressed or implied warranty of any kind and assumes no responsibility for any errors or omissions. No liability is assumed for incidental or consequential damages in connection with or arising out of information contained in this book. The Publisher shall not be liable for any special, consequential, or exemplary damages resulting, in whole or in part, from the readers' use of, or reliance upon, this material. Any parts of this book based on government reports are so indicated and copyright is claimed for those parts to the extent applicable to compilations of such works.

Independent verification should be sought for any data, advice or recommendations contained in this book. In addition, no responsibility is assumed by the publisher for any injury and/or damage to persons or property arising from any methods, products, instructions, ideas or otherwise contained in this publication.

This publication is designed to provide accurate and authoritative information with regard to the subject matter covered herein. It is sold with the clear understanding that the Publisher is not engaged in rendering legal or any other professional services. If legal or any other expert assistance is required, the services of a competent person should be sought. FROM A DECLARATION OF PARTICIPANTS JOINTLY ADOPTED BY A COMMITTEE OF THE AMERICAN BAR ASSOCIATION AND A COMMITTEE OF PUBLISHERS.

#### **LIBRARY OF CONGRESS CATALOGING-IN-PUBLICATION DATA**

Barrañón, Armando.

New nanotechnology developments / Armando Barrañón.

p. cm.

Includes index.

ISBN 978-1-61761-827-7 (Ebook)

1. Nanotechnology. 2. Nanostructured materials. I. Title.

T174.7.B37 2009

620'.5--dc22

2008055351

*Published by Nova Science Publishers, Inc., + New York*

# CONTENTS

<b>Foreword</b>	vii	
<b>Chapter 1</b>	Bidimensional Ionic Solutions: A Molecular Dynamics Study <i>Gloria Arlette Méndez-Maldonado, Minerva González-Melchor and Honorina Ruiz-Estrada</i>	1
<b>Chapter 2</b>	Children and Teenagers: Seeds for a Next Generation of Nanoscientists Los Niños Y Los Jóvenes: Semillas De La Próxima Generación De Nanocientíficos <i>Melina Tapia, Aristeo Segura and Nikola Batina</i>	9
<b>Chapter 3</b>	Presentation of Some Concepts for the Understanding of the Nanoworld <i>S.J. Castillo, J.C. Lopez-Cervantes, M.E. Alvarez-Ramos, A. Apolinar-Iribar, R.P. Duarte-Zamorano, L.E. Regalado and A. Duarte-Moller</i>	17
<b>Chapter 4</b>	Centers of Educational Excellence in Nanotechnology: The Proposed World Bank Scientific Millennium Initiatives and Nanotechnology in Latin America <i>Guillermo Foladori, Mark Rushton and Edgar Zayago Lau</i>	31
<b>Chapter 5</b>	Elemental Identification by X-Ray Fluorescence Using a Portable Pyro-Electric Generator and a CdTe Detector for an Advanced Laboratory Course <i>M. Castro-Colin, J. A. López and S. K. Valaparla</i>	41
<b>Chapter 6</b>	Properties of the Near Field Produced by a Circular Nanoaperture Using the Bethe Formulation <i>J. M. Merlo, E. Martí-Panameño and F. Aguilar</i>	49
<b>Chapter 7</b>	Teaching Nanostructures Using the Simple Infinite Potential Well Model <i>R. Rodriguez-Mijangos and G. Vazquez-Polo</i>	57

<b>Chapter 8</b>	Synthesis and Characterization of Pt and Pt-Au Nanoparticles for Catalysis and Pem Fuel Cells Applications <i>M. Gutiérrez Arzaluz, B. Ruiz Camacho, V. Múgica Álvarez, O. Solorza Feria and M. Torres Rodríguez</i>	<b>61</b>
<b>Chapter 9</b>	Enhanced Adsorption of Heavy Metals by Nanostructured Composites Based upon Dendrimer-Functionalized MCM-41 <i>M. A. Escalante, E. Delgado, L. F. García and G. Toriz</i>	<b>69</b>
<b>Chapter 10</b>	Cognitive Level of Secondary School Students and Its Relation to Some Conceptual Aspects of Bernoulli Principle <i>María Eugenia Bustamante Estudillo and Honorina Ruiz Estrada</i>	<b>79</b>
<b>Chapter 11</b>	Pharmaceutical Bionanotechnology: Fundamental Principles <i>Emilio Segovia</i>	<b>93</b>
<b>Chapter 12</b>	The Order Parameter of a Binary Alloy Thin Film of Cu <sub>3</sub> Au <i>G. Ramírez-Dámaso, F.L. Castillo-Alvarado, I. Zasada and L. Wojtczak</i>	<b>103</b>
<b>Chapter 13</b>	Green's Function Tight-Binding Formalism for Line-Shape Description of Virtual Electronic States <i>S. J. Vlaev</i>	<b>109</b>
<b>Chapter 14</b>	Gender and Social Interaction in Mexican Nanotechnology and Nanosciences Research Groups <i>Armando Barrañón</i>	<b>117</b>
<b>Chapter 15</b>	On the Manipulation of Microscopic Particles by Optical Tweezers: Flatness Based Approach <i>Carlos Aguilar-Ibañez, Armando Barrañón Cedillo, Hebertt Sirar-Ramirez and Luis Ignacio Rosas Soriano</i>	<b>125</b>
<b>Chapter 16</b>	Structural Features and Catalytic Activity of Ce <sub>1-X</sub> (La <sub>x</sub> , Ru <sub>x</sub> )O <sub>2</sub> /Bi <sub>2</sub> Mo <sub>0.9</sub> W <sub>0.1</sub> O <sub>6</sub> Nanostructured Solid Solutions <i>R. Rangel, F. Huerta, P. Bartolo-Pérez, F. Morales, D. H. Galván and F. Castillón-Barraza</i>	<b>137</b>
<b>Chapter 17</b>	Silver Nanoplates: Synthesis, Growth and Functional Properties <i>Xuchuan Jiang, Qinghua Zeng and Aibing Yu</i>	<b>145</b>
<b>Chapter 18</b>	Study of the Properties of Iron Oxide Nanostructures <i>Arturo I. Martinez, M.A. Garcia-Lobato and Dale L. Perry</i>	<b>183</b>
<b>Index</b>		<b>195</b>

## **FOREWORD**

Nanotechnology is considered an unlimited discipline inasmuch as it is considered as a mother technology by means of a reductionist approach. Nanotechnology is regarded as a fundamental technology that could ground all the technologies in a similar fashion to the unified theory of physics. Nevertheless, nanotechnology definition, in terms of the system size, which should be less than 1000 nanometers, is not related to the properties of objects or application areas. This confers Nanotechnology with a semantic vagueness that has been profited by several research groups to obtain financial funds inasmuch as nanocosmos has turned out to be a new frontier for scientific research. It is not about building a new world “atom by atom” but of miniaturizing the mesocosmic world to a nanometric scale. Having this in mind, it is necessary to integrate physics, chemistry and molecular biology, notwithstanding are open fields which avoids attaining the goal of a unified theory. Hence, Nanotechnology is heavily grounded in frontier sciences and uses instruments developed for natural sciences investigations. Nanotechnology has continuously evolved sharing with past technologies the same approaches to science policy, therefore, it is problematic to consider nanotechnology as a radical change in the development of technology.

Nanotechnology reductionism that considers nanotechnology as a mother technology can inspire economic forces capable of radically changing our world.

Nanotechnology tries to unify all the engineering, extending the heuristic concept of unity of physics to the unity of all technologies. Nanotechnology considers itself as a converging technology following a metaphysical perspective that subsumes diverse technological areas such as spintronics, Ion Beams Fabrication, nanometric lithography, etc.

This metaphysical perspective goes back to Greek philosophy and relies on nature unity, which nowadays is incorporated in the term NBIC (nanotechnology-biology-informatics-cognitive sciences), to denote the conjunction of sciences and technologies that should lead to an explosive development and a radical transformation of our existence. Reductionism is related to Descartes since Descartes considers a self-sufficient Reason that can be used to derive knowledge and that allows for a scientific knowledge based on mathematics. In his third rule, Descartes advises the reader to start considering the simplest objects, gradually advancing to the most complex ones. This is the bottom-up approach publicized by the technological reductionism of nanotechnology.

Nanotechnology research can lead to the development of patents in the emerging economies. It is expected that by 2015, nanotechnology industry will comprise one trillion dollars in USA and that two million workers will be needed in the nanotechnology labor

market. USA National Nanotechnology Initiative seeks for incorporating half of American universities and Center of Research to Nanotechnology. Also NNI strives for education a quarter of the students of American Research Universities. As long as the number of articles published on ethical and societal aspects of nanotechnology has grown exponentially, it is understandable that several Mexican research groups are devoted to these aspects.

Several experiences of Nanoeducation in Mexico follow the trend of incorporating nanotechnology from Kindergarten to Graduate Studies. This was the motivation to implement a Nanoeducation Seminar at UAM-Azcapotzalco in order to educate instructors in philosophical and environmental aspects of nanotechnology. Several posters were exhibited on Science and Technology Education by the participants of Nanoeducation Seminar. And several articles were contributed to this volume by Mexican researchers, in a number close to half the total of research groups registered in the Mexican Department of Education. These articles were contributed by authors belonging to the following universities and research centers: ESFM-IPN, University of Lodz, Tecnológico de Estudios Superiores de Ecatepec; Centro Universitario de Los Lagos de la U. de Guadalajara, Benemérita Universidad Autónoma de Puebla, Universidad de Guadalajara, Universidad Autónoma Metropolitana-Azcapotzalco, Universidad Autónoma Metropolitana-Iztapalapa, Universidad de Sonora, Instituto de Física de la UNAM, Instituto Nacional de Astrofísica, Óptica y Electrónica, University of Texas at El Paso, Universidad Autónoma de Zacatecas, CINVESTAV-IPN, Centro de Investigación en Computación-IPN, Centro de Investigación en Química Aplicada. I acknowledge support from CONACYT-58939 Fund and División de Ciencias Básicas e Ingeniería of UAM-Azcapotzalco, as well as support from CONACYT-75722 Grant.

Dr Armando Barrañón  
El Paso, Texas, USA. October, 2008.

***Chapter 1***

# **BIDIMENSIONAL IONIC SOLUTIONS: A MOLECULAR DYNAMICS STUDY**

***Gloria Arlette Méndez-Maldonado<sup>\*1</sup>,  
Minerva González-Melchor<sup>\*2</sup>  
and Honorina Ruiz-Estrada<sup>1</sup>***

<sup>1</sup> Facultad de Ciencias Físico-Matemáticas, Benemérita Universidad Autónoma de Puebla, Río Verde y Av. San Claudio, San Manuel. CP 72570, Puebla, Mexico

<sup>2</sup> Instituto de Física “Luis Rivera Terrazas”, Benemérita Universidad Autónoma de Puebla, Apartado Postal J-48, 72570 Puebla, Mexico

## **ABSTRACT**

A numerical study of a binary mixture of charged discs immersed in a solvent at fixed temperature is presented. Bidimensional molecular dynamics simulations of a modified version of the restricted primitive model of ionic liquids were performed. The bidimensional Ewald summation method to calculate the long-range electrostatic interactions was implemented in the program. We obtained the radial distribution function and the internal energy of the system.

**Keywords:** Bidimensional ionic liquids, molecular dynamics, radial distribution function, Ewald method.

## **INTRODUCTION**

The study of complex fluids is nowadays a very active field of research in the area of materials science or materials engineering. We call complex fluids those whose relevant properties (thermal, rheological and transport, for instance) are described in a regime

---

<sup>\*</sup> arlette.mm@gmail.com

<sup>\*</sup> minerva@sirio.ifuap.buap.mx

intermediate between molecular and macroscopic scales. Among these systems we have micelles, liquid crystals, polymeric solutions and colloidal suspensions. A colloidal suspension is an electrically neutral system consisting of two phases: the solvent and the colloidal particles immersed in it [Evans and Wennerström, (1999)]. Being the latter several orders of magnitude larger than solvent molecules, colloidal particles are about  $10^{-8} - 10^{-5}$  m in size, and have typical masses of  $10^{-15}$  gr. Quantitative comparisons between theoretical calculations, computer simulations and experimental data have been possible due to the synthesis and characterization of spherical colloidal particles, which can help to understand more complex systems. Contrary to the case of three dimensional colloidal suspensions and ionic solutions, the study of their bidimensional counterparts has been less undertaken [Gao, et al. (1997); Weis and Levesque (1998), Méndez Maldonado G. A. (2006)]. In the last few decades, bidimensional or quasi-bidimensional systems have also grown in importance due to the possibility of technological manipulation and their use in applications involving surface phenomena.

In this work we present a numerical study of a bidimensional 1:1 ionic solution by using computer simulations. We developed a molecular dynamics program [Allen and Tildesley (1987); Frenkel and Smit (1996)] where the bidimensional Ewald summation method to calculate long-range electrostatic interactions was included [Gao, Zeng, Wang (1997)]. The radial distribution function and the internal energy at a fixed temperature were then calculated.

## THE SYSTEM

We consider a 1:1 bidimensional ionic solution at fixed temperature  $T$ , contained in a surface of area  $A$ . The two dimensions the restricted primitive model (RPM) is an electrically neutral mixture consisting of  $N$  charged hard discs of equal diameter  $\sigma$ , half of which carry a point charge  $+Ze$  and the other half  $-Ze$ . Particles of species  $i$  have a number density  $\rho_i = N_i / A$  and a charge  $q_i = Z_i e$ . Overall charge neutrality is assumed so that

$$\sum_i \rho_i Z_i = 0$$

A typical configuration is shown in figure 1.

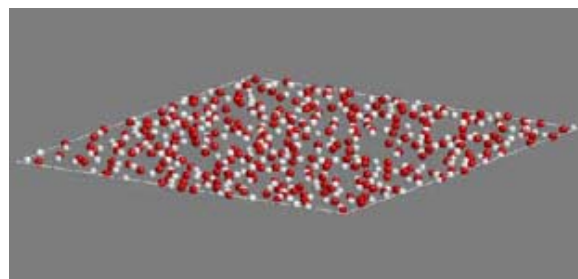


Figure 1. A typical configuration of the 1:1 bidimensional ionic solution.

In this work we consider a modified version of the RPM, so the interaction potential between two particles is given by

$$u(r) = \begin{cases} A_s \left( \frac{\sigma_{ij}}{r} \right)^n, & r \leq \sigma_{ij}, \\ \frac{1}{4\pi\epsilon_0\epsilon_s} \frac{q_i q_j}{r}, & r > \sigma_{ij} \end{cases} \quad (1)$$

where  $r$  is the distance between discs  $i$  and  $j$ ,  $\sigma_{ij} = (\sigma_i + \sigma_j)/2 = \sigma$  for particles of the same diameter.  $A_s$  is a positive parameter with units of energy and  $n$  is an integer. The solvent is assumed as a continuum structureless background of dielectric constant  $\epsilon_s$ , and  $\epsilon_0$  is the dielectric permittivity of vacuum. This interaction, named soft primitive model (SPM), has been used in the study of three dimensional ionic fluids [González-Melchor, et al. (2005)] and provides practically the same results as the RPM. A comparison between the reduced RPM potential and the SPM is shown in figure 2 for charged particles of the same and opposite sign.

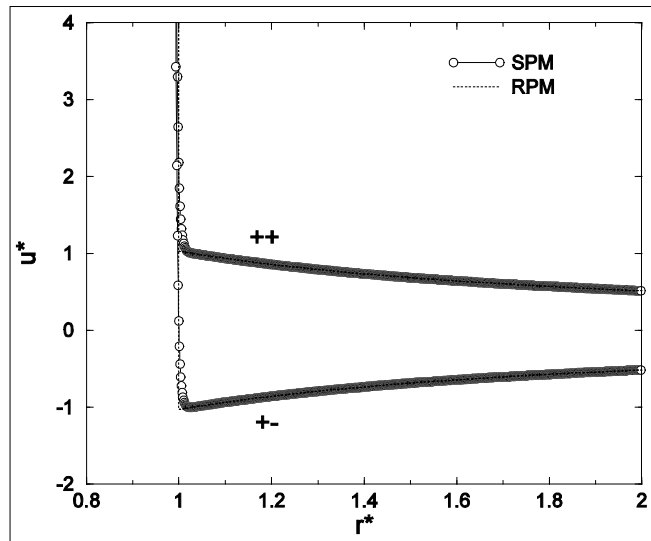


Figure 2. Comparison between the RPM and the SPM interaction potentials, as stated on the figure. The integer  $n$  was taken to be  $n=225$ . RPM: open circles, SPM: dotted lines.

## MOLECULAR DYNAMICS METHOD

We developed a molecular dynamics (MD) simulation program, where classical Newton's equations of motion are solved in time [Allen and Tildesley (1987); Frenkel and Smit (1996)],

$$\mathbf{F}_i = m_i \mathbf{a}_i \quad (2)$$

where  $\mathbf{F}_i$  is the force exerted on the particle  $i$ ,  $m_i$  is its mass and  $\mathbf{a}_i$  is its acceleration. From the knowledge of the force, it is possible to determine the acceleration of each atom in the system. Starting from an initial configuration, the integration of the equations of motion then yields a trajectory that describes the positions, velocities and accelerations of the particles as they vary with time. From this trajectory, the average values of properties can be determined. Given the total interaction potential  $U$ , the force acting on each particle is obtained through

$$\mathbf{F}_i = -\nabla_{\mathbf{r}_i} U \quad (3)$$

The method is deterministic; i.e., once the positions and velocities of each particle are known, the state of the system can be predicted at any time. To integrate the equations of motion several good algorithms have been developed, we used the velocity Verlet algorithm [Allen and Tildesley (1987)], described by the relations

$$\begin{aligned} \mathbf{r}_i(t+dt) &= \mathbf{r}_i(t) + \mathbf{v}_i(t)dt + \frac{1}{2} \frac{\mathbf{F}_i}{m_i} dt^2, \\ \mathbf{v}_i(t+dt) &= \mathbf{v}_i(t) + \frac{1}{2m_i} [\mathbf{F}_i(t+dt) + \mathbf{F}_i(t)]dt. \end{aligned} \quad (4)$$

As is usually done, periodic boundary conditions and the minimum image convention [Allen and Tildesley (1987)] were used in the simulations. By rescaling the velocities of particles at each time step, we kept the temperature constant along the simulations [Allen and Tildesley (1987)]. In order to capture the full Coulombic interactions in two dimensions, the Ewald expression for the total electrostatic energy in a bidimensional systems was used as described in Refs. [Gao, et al. (1997)]. So, the electrostatic contribution to the potential energy is given by

$$\begin{aligned} U^{Coul} = & \frac{1}{4\pi\epsilon_0\epsilon_s} \left[ \sum_{i=1}^{N-1} \sum_{j=1}^N \frac{q_i q_j}{r_{ij}} \text{erfc}(\kappa r_{ij}) + \right. \\ & \frac{\pi}{A} \sum_{i=1}^N \sum_{j=1}^N \sum_{G \neq 0} \frac{q_i q_j}{G} \text{erfc}\left(\frac{G}{2\kappa}\right) \exp(-\hat{i}\mathbf{G} \cdot \mathbf{r}_{ij}) \\ & \left. - \sum_{i=1}^N \frac{\kappa q_i^2}{\sqrt{\pi}} \right], \end{aligned} \quad (5)$$

where  $\text{erfc}(\kappa r_{ij})$  is the complementary error function,  $\kappa$  is the parameter governing the convergence of the Ewald sums.  $\mathbf{G} = (2\pi/L)(n_x \hat{i} + n_y \hat{j})$  is the reciprocal vector,  $A = L^2$

and  $L$  is the length of the simulation cell. Equation (5) is an excellent approximation to the total electrostatic energy of a periodic system of  $N$  point charges. The first and second terms in Eq. (5) are known as the real and the reciprocal part, respectively [Gao, et al. (1997)]. The last one is a constant known as the self energy term.

The short repulsive contribution to the total potential energy, coming from the first part of Eq. (1) can be written as

$$U^s = \sum_{i < j} u_{ij}^s(r) \quad (6)$$

where, we have defined

$$u_{ij}^s(r) = A_s \left( \frac{\sigma_{ij}}{r} \right)^n. \quad (7)$$

Therefore, the total potential energy of the systems is given by

$$U = U^{Coul} + U^s. \quad (8)$$

The forces needed to evolve the positions and velocities from time  $t$  to time  $t + dt$  in Eq. (4), are obtained from Eqs. (3) and (8).

## SIMULATION DETAILS

We chose as unit of energy the quantity  $E_{ref} = A_{ref} f(n)$ , where  $A_{ref} = e^2 / (4\pi\epsilon_0\epsilon_s\sigma)$ ,  $f(n) = (n^{\eta_{1-n}} - n^{\eta_{1-n}})$ ,  $e$  is the electron charge and  $n$  is the integer appearing in the short range repulsive interaction. It was taken to be  $n = 225$  as in Ref. [González-Melchor, et al. (2005)]. The unit of length was chosen as the diameter  $\sigma$  and the time was measured in terms of  $t_0 = (m\sigma^2/\epsilon)^{1/2}$ . In this form, reduced distance, energy, force, temperature and time are written as

$$r^* = \frac{r}{\sigma}, \quad u^* = \frac{u}{E_{ref}}, \quad f^* = \frac{f\sigma}{E_{ref}}, \quad T^* = \frac{k_B T}{E_{ref}}, \quad dt^* = \frac{dt}{t_0}.$$

The values for the Ewald parameters were  $\kappa L = 5$  and the maximum number of reciprocal vectors used to calculate the reciprocal contribution were  $n_x^{\max} = 5, n_y^{\max} = 5$ . For comparison purposes we used a cut-off distance  $r_c^* = 8$  for the real part as in [Weis and

Levesque (1998)]. To integrate the equations of motion we used a time step  $dt^* = 0.005$ . This time step was found to obey the criterion of energy conservation in a microcanonical simulation (at number of particles, energy and area fixed). The total simulation time was given by  $T_{sim}^* = N_c dt^*$ , where  $N_c$  is the number of time steps used to calculate average properties. After some equilibration period, we used  $N_c = 2 \times 10^5$  steps for production time.

## RESULTS

We performed molecular dynamics simulations at constant number of particles, temperature and area for the 1:1 ionic solution. In figures 3 y 4 we show the radial distribution function  $g_{++}(r)$  y  $g_{+-}(r)$  at temperature  $T^* = 0.166$ . In figure 3, the total number density is  $\rho = 3.3 \times 10^{18} \text{ part./m}^2$  and in figure 4,  $\rho = 6.6 \times 10^{18} \text{ part./m}^2$ . When we increased the density, the structure is enhanced as is observed from the figures.

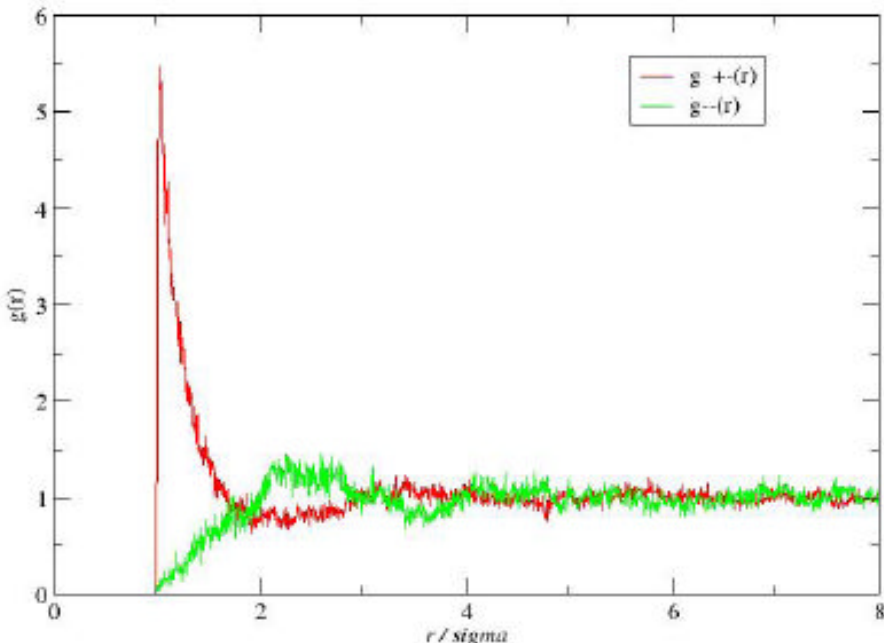


Figure 3. Radial distribution function  $g(r)$  for  $\rho^* = 0.3$  and  $T^*=0.166$ .

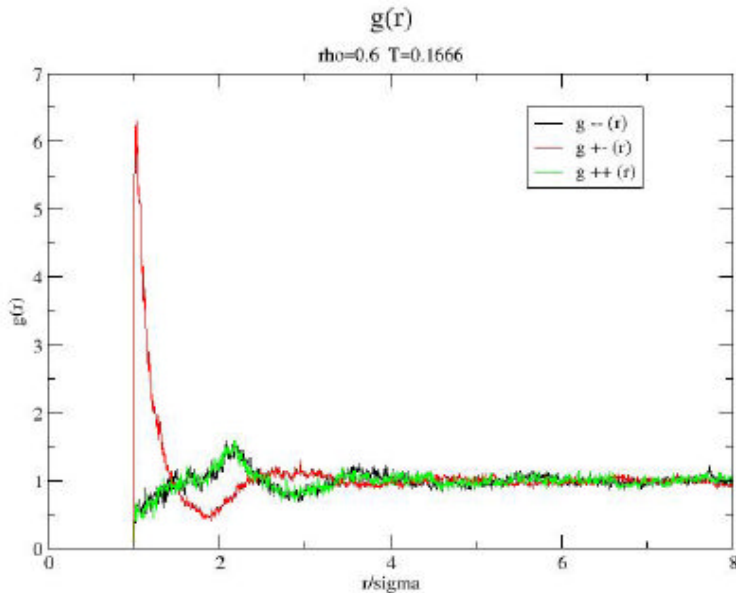


Figure 4. Radial distribution function  $g(r)$  for  $\rho^* = 0.6$  and  $T^*=0.166$ .

When we compared our MD results of electrostatic potential energy with data obtained via the Monte Carlo method [Weis and Levesque (1998)], we found the same values within statistical error, as shown in table 1 for the two thermodynamic states at the reduced densities  $\rho^* = \rho\sigma^2$ .

**Table 1. Electrostatic potential energy for the solution at  $T^*=0.166$**

$\rho^*$	$T^*$	$U^*$	$U^* [\text{Weis (1998)}]$
0.3	0.16	$-2.9375 \pm 0.0029$	-2.93
0.6	0.16	$-3.5052 \pm 0.0041$	-3.47

## CONCLUSIONS

We developed a molecular dynamics simulation program to study a 1:1 ionic solution at fixed temperature. The radial distribution functions and the internal energy of the system were obtained. When we compared our MD energy data with those published in Ref. [Weis and Levesque (1998)] obtained by using Monte Carlo simulations good agreement was found. We emphasize that computer MD method allows us the calculation of dynamic properties which is not possible with the Monte Carlo technique. Some work in this direction is in progress.

## ACKNOWLEDGMENTS

Financial support from VIEP and PROMEP is gratefully acknowledged.

Gloria Arlette Méndez Maldonado is a MSc student at Facultad de Ciencias Físico-Matemáticas, Dr Minerva González Melchor is a researcher in computer simulation of fluids at Instituto de Física “Luis Rivera Terrazas”. Dr Honorina Ruiz Estrada is a Faculty Member at Facultad de Ciencias Físico-Matemáticas, all them from Benemérita Universidad Autónoma de Puebla.

## REFERENCES

- Allen, M.P., and Tildesley, D.J. (1987). *Computer simulation of liquids*, Clarendon Press, Oxford.
- Frenkel, D., and Smit, B. (1996). *Understanding Molecular Simulation: from algorithms to applications*, Academic Press, Amsterdam.
- Evans D.F., Wennerström, H. (1999). *The colloidal domain: where physics, chemistry, biology, and technology meet*, Advances in Interfacial Engineering, Wiley-VCH, Minneapolis.
- Gao, G.T., Zeng, X. C., and Wang, W. (1997), “Vapor-liquid coexistence of quasi-two-dimensional Stockmayer fluids.”, *J. Chem. Phys.* 106, 3311.
- González-Melchor M., Bresme, F., and Alejandre J. (2005), “Molecular dynamics simulations of the surface tension of ionic liquids”. *J.Chem. Phys.* 122, 104710.
- Méndez-Maldonado G.A. (2006). *Un estudio de soluciones iónicas bidimensionales*. Thesis, Facultad de Ciencias Físico-Matemáticas, BUAP.
- Weis, J.J., and Levesque, D. (1998), “Restricted primitive model of an ionic solution confined to a plane.”, *J. Chem. Phys.* 109, 7486.

*Chapter 2*

## **CHILDREN AND TEENAGERS: SEEDS FOR A NEXT GENERATION OF NANOSCIENTISTS**

## **LOS NIÑOS Y LOS JÓVENES: SEMILLAS DE LA PRÓXIMA GENERACIÓN DE NANOCIENTÍFICOS**

***Melina Tapia<sup>1</sup>, Aristeo Segura<sup>2</sup> and Nikola Batina<sup>3</sup>***

<sup>1</sup> Laboratorio de Nanotecnología e Ingeniería Molecular,  
Departamento. de Química, CBI, UAM-Iztapalapa.

<sup>2</sup> Facultad de Ciencias Químicas, Universidad Autónoma  
Benito Juárez, Oaxaca, Oaxaca, México.

<sup>3</sup> Laboratorio de Nanotecnología e Ingeniería Molecular,  
Departamento. de Química, CBI, UAM-Iztapalapa

A primary factor in nanoscience strengthening is to train scientific researchers capable to understand nanometric phenomena, which requires joint efforts from society and scientific community in order to attract younger students during their early academic education. The present work proposes the incorporation of seminars and workshops about nanotechnology as a part of elementary school teaching programs, this strategy will allow kids to be acquainted with areas related to nanotechnology such as mathematics, physics, biology, medicine among others. All this with the final end to increase their curiosity in nanotechnology.

### **1. INTRODUCTION**

Nowadays nanotechnology, nanoengineering and nanoscience, are areas of research with increasing relevance at the international level, this is because they are strongly linked with areas of study such as biology, chemistry, physics and mathematics, which embrace all the scientific knowledge gained so far by the Humankind (Deal, 2002).

To develop these nanoareas, research has made impressive efforts in improving and developing technologies that allow us to study and analyze the phenomena to study at

nanometric scales. Some of these improvements ranging from enhanced resolution and modes of operation in the electron microscopy, until the creation of new visualization tools as those of sonda microscopy, atomic force microscopy and tunnel effect, among others. These new microscopes allow for visualization and analysis of physical properties of materials at the nano and atomic level and they have been instrumental in generating new materials. All these developments have been used in the manufacture of what is currently called "smart materials" (Deal ,2002) .

However, this technological development, is not enough, because to exploit the potential use of nanoscience is not only necessary to invest in equipment and laboratories, but investing also in primary education and generating a genuine enthusiasm for nanoresearch in younger generations.

Based on studies in the field of learning, we know that children and young people between 7 and 16 years old, are in a stage characterized by the search for explanations of the world around them. Particularly, for ages going from 4 to 12 years, there is a critical and crucial stage for the development of their intellect and their socialization (Rico, 2004), since in this age children have the highest rate of curiosity and interpretative ability about the causes of phenomena surrounding them.

Since antiquity it is well known the lust for knowledge in children, however, nowadays children and young people are much more aware of the advantages offered by new technologies because they live immersed in them. This awareness and curiosity about the world around them, as well as children desire to transform what they already know, are useful to promote a rapprochement between children and nanoscience. The main objective of this paper is to propose some initiatives or strategies, which favor closer ties, teaching and dissemination of various areas of nanotechnology among children and young people who are in Secondary and High school.

## **1.2. The Problematics of Nanoeducation**

The obstacles for a rapprochement between nanoscience and children, lie in two main points. First, there is a poor dissemination to the general public of knowledge and developments in the field of nanoscience, without conveying relevant applications and benefits of nanotechnology to society. And also there is a lack of recognition of children and youth as a group of high impact on scientific and technological development.

Nanotechnology is not explained in K12 instruction, since it is not included in curricula. We believe that there are three factors that govern this issue: the economic factor, the social perception about science and researchers and finally, the role of educators and nanoscientists.

### **1.2.1. Economic Aspect**

On the economic side we know that scarce funding is directed to education and national technological development, which results in low wages to teachers, lack of resources in schools to comply with the contents of curricula, poor infrastructure for the development of scientific research, lack of support for children with fewer resources to access education. This turns into low satisfaction for faculty, students and society at large (Vazquez-Queen, 2007).

During the presentation of the report “The State of World Children 2007“, Oliver Degreef, representative of UNICEF in Mexico, said that the reduction in education spending

is a danger to our country. This comment stems from the premise that "the development of a nation is directly dependent on its level of education", nevertheless the Education Federal Budget has been recently reduced (Degreef, 2006); (Amir, 2006).

Another consequence of the low educational budget is the difficulty of updating curricula, limiting access of teachers and students to new research being conducted not only in our country but also globally. This way that infants have a limited picture and therefore will be apathetic to research and science. However, given the importance of scientific and technological activities in its three components: i) Research and Experimental Development (IDE), ii) education and scientific and technical education (postgraduate education) and iii) science and technology and in spite of current economic perspectives, efforts are under way to invest in science and technology among which are the areas of nanotechnology, nanoengineering and nanoscience (CONACYT, 2006).

### **1.2.2. Social Perceptions About Science and Researchers**

Some Mexicans consider that education is not a key factor for having success either as individuals or as a country. This creates a greater distance between the society and scientific activities, which explains ignorance on the part of society about the existence of nanoscience and the impact on quality of life that can be derived from studying nanosciences. An important segment of population, namely the labor sector and students' parents, do not see education as a source of support to improve their living conditions. According to recent surveys about the personal opinions of Mexicans with ages between 18 and 50 years (*Cómo se siente el Mexicano?* ), 9.1% of this sector is interested in education. Education is almost the last in a list of six priorities for Mexicans, being Employment (84.1%) and Economics (56.9%) their top priorities (Fields and Penna, 2006). This perception is strongly influenced by the fact that many students graduate with the feeling that they lost time while studying, because they do not find work areas to apply their knowledge and end up working in another field unrelated to their major. This results in social frustration on the part of the student, and is perceived as a waste of economic resources in the family (SEP, 2006).

Another point which feeds the estrangement between science and society is that "scientists" or "researchers" belong to a selected group, in terms of wealth and intellectual capacities, demoralizing youngsters who feel attracted to science. Besides, researchers contribute to this mythification by using an obscure language when addressing audiences which restricts social understanding of science.

### **1.2.3. The Role of Educators and Nanoscientists**

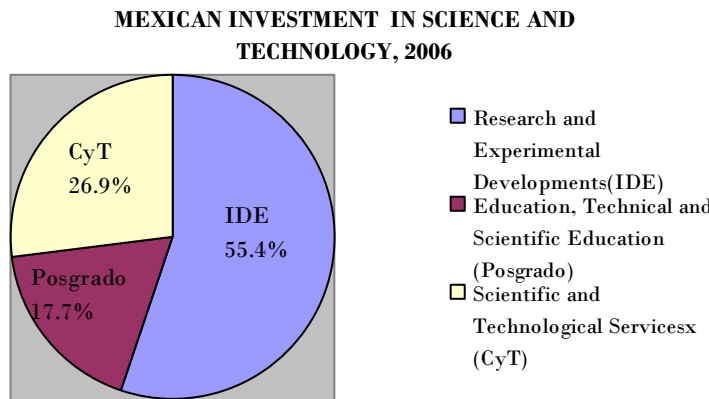
Regardless of the education given by parents to children, in most cases the first rapprochement of children and youth with science is through their teachers who usually explain them why happen the phenomena that surround them. The role of teachers in K12 education is of great importance, not only at the level of assimilation of knowledge by students, because it is supposed to develop a positive perception on study and learning.

The problem here is that in Mexico, teachers do not receive an adequate level of job satisfaction. This feeling is mainly attributable to factors such as lack of involvement in given targets, lack of autonomy in the development of activities, not being able to be regularly updated, lack of advice and expert help, lack of recognition of their work by parents and pupils, also lack of promotion based on performance, and of course and unpleasant economic situation (Vazquez-Queen, 2007). This dissatisfaction and the fact students do not always

want to learn, discourages teachers whose frustrations and stress affect negatively students and the quality of education (Garcia-Garrido, 2004).

Scientific community shares the same factors of disappointment mainly due to the lack of recognition of their research and in most cases because of the impossibility to apply such knowledge to practice. In the specific case of nanoscientists, the challenge of overcoming the uncertainties associated with a cutting-edge science developed at an atomic scale. But nanotechnology, nanoengineering and nanoscience deal with research activities with applications to technology, industry, biology, physics, chemistry, medicine, computer science, among many others (SEP-IPN, 2007).

Unlike educators, researchers, including nanoscientists, will have no direct impact on children's perception of science although researchers are responsible for social perception of science and can be promoters of youngsters' involvement with science which might lead to the development of human resources capable to understand and create better beneficial technologies to our country.



## 2. PROPOSAL

Our goal is to propose some strategies which favor teaching and dissemination of various areas of nanotechnology among children and young people attending K12 instruction. Considering dissemination of nanoscience to K12 students, we propose:

### I. I Direct collaboration between nanoscientists and educators.

This is the cornerstone of any initiative on "nanoeducation" because it is necessary to unite the skills and experience of both researchers and specialists of nanoscience with educators and K12 teachers.

Seminars aimed at K12 teachers about global research efforts on Nanoscience and Nanotechnology.

Seminars on teaching methods and groups management by K9 teachers addressed to nanoscience researchers.

Detection of K9 students' areas of interests in order to show how these areas are benefited everyday by nanotechnology. To attain this end, toys and video games can be useful as well as examples based on body performance during sickness and sport activities.

## II. Links between scientists and young people

These links will enable youngsters to interact with researchers, opening the possibility for students to become acquainted with nanoresearch, sharing research experiences that will help students to develop their own research in the future. Coexistence among students and researchers can occur in schools under topics such as science week, also allowing parents to be present in these talks, so that the community begins to participate in scientific efforts.

These collaborations can lead to the development of forums aimed particularly at children and young people, where researchers are supported by teachers to convey their work to public audiences in a didactic fashion.

## III. Group visits to research centers and Labs.

It is convenient for a child or young person to become acquainted with the places where nanosearch is conducted, the equipment employed, so that students have a better idea about this type of research activities, the social use of nanotechnology as well as the future impact of nanoresearch.

Development of educational materials.

Collaboration and ideas exchange between educators and researchers will help to design teaching materials useful for students, scientific and technological update of educators and enhancement of teaching strategies.

Creation of a multidisciplinary committee on "Dissemination of Nanoscience and Nanotechnology". This will be a committee composed of K12 instructors, nanoeducators and nanoresearchers from various fields of nanoscience, promoting collaboration between educators and researchers that would allow a better organization of teaching programs, designing programs, update for educators and researchers, development of educational materials and a better attitude of students and teachers with respect to nanoscience.

## 3. CONCLUSIONS

Nowadays, due to social and cultural factors, children are not considered as a high impact group in regards to scientific and technological development. However, men where children develop their character and interests at this stage. It is necessary to introduce youngsters and infants to the basics of Nanotechnology, Nanoengineering and Nanosciences, so that children may understand the importance of this research, and the role they can play in future efforts to develop such beneficial areas as environmental protection, medicine, development drugs, development of smart materials and technological developments. It is also important to note that nanoscience should be incorporated to national education programs (SEP, 2001). Another important point to stress is that the engine for bringing youth with nanoscience is the close

cooperation between educators and nanoresearchers as an optimal strategy of giving publicity to nanoscience.

## ACKNOWLEDGEMENT

We are grateful to Physics Education Group of UAM-Azcapotzalco, Nanotechnology and Molecular Engineering Lab at UAM-Iztapalapa, financial support from CONACyT/104746 Fund and help from Eng. Andrés de Luna Bugallo and Eng. Israel Morales Reyes.

This work is supported by Nanotechnology and Molecular Engineering Laboratory, UAM-Iztapalapa, Mexico.

## REFERENCES

- Campos R. y Penna C. (2006). “Cambio de año 2006-2007 ¿Cómo se siente el Mexicano?”, *Consulta Mitofsky*. [www.consulta/interna/sentirmexicano/.com.mx](http://www.consulta/interna/sentirmexicano/.com.mx)
- Consejo Nacional de Ciencia y Tecnología. (2006). “Gasto en Actividades Científicas y tecnológicas”, *Reporte anual de Recursos Humanos y Ciencia y Tecnología*, [www.Ciencia TecCONACYT\\_mitofsky.pdf](http://www.Ciencia TecCONACYT_mitofsky.pdf)
- Deal F.W. III (2002). “Under the Microscope: Nanotechnology”, *The Technology Teacher*, 62:9, 21-23.
- Degreff O. (2006). “Estado Mundial de la Infancia”, *Reporte del fondo de las naciones Unidas para la Infancia Unicef*, Reporte presentado en el informe del Estado Mundial de la Infancia, N.Y. [www.consulta.com.mx/interiores/14\\_entorno\\_int/ei\\_infancia2007.html](http://www.consulta.com.mx/interiores/14_entorno_int/ei_infancia2007.html)
- Emir Olivares A. (2006). “Reducir el gasto educativo es un peligro para Mexico, señala la Unicef”, *La Jornada*, 12-Diciembre-Política, México.
- García Garrido J.L. (2004). “La Clave para Mejorar la Educación la tiene la Sociedad”, *Consumer Erosky-Entrevista*. Abril, 10-12. España.
- Rico L. (2004). “Programación Infantil”, *Consumer Erosky*. Mayo 43, 15-31, España.
- Secretaría de educación Pública (2001). “Programa Nacional de Educación 2001-2006”, *SEP*, México. <http://basica.sep.gob.mx/pagina/index.html>
- Secretaría de Educación Pública (2006). “OCDE-Nota informativa de México”, *Panorama de la Educación OCDE*, [www.consulta.com.mx/interiores/14\\_entorno\\_int/ ei\\_panorama\\_educacion07.html](http://www.consulta.com.mx/interiores/14_entorno_int/ ei_panorama_educacion07.html)
- Secretaría de Educación Pública-Instituto Politecnico Nacional (2007). “Nanotecnología y Medio Ambiente”, *Innovación Educativa* 7, núm. 36, Mexico.
- Vazquez-Reina M. (2007). “Satisfacción laboral del profesorado”, *Consumer Erosky*. Diciembre, España. <http://revista.consumer.es/web/es/20070401/68481.php>

## **Biographical Note of Authors**

### **M. Sc. Melina Tapia T.**

M.Sc. in Biomedicine and molecular biotechnology in I.P.N.

- Expert in cancerogen cell lines culture.
- Immunefluorescence, preparation and visualization of samples by Fluorescence Optical Microscopy in INP (National Institute of Pediatrics)
- Preparation and visualization of different biological samples with Scanning Electron Microscopy (SEM) and Transmission Electron Microscopy.
- Expert in organical and inorganical materials analysis (morphology and force measurements studies) with Atomic Force Microscopy (AFM) and Scanning Tunneling Microscopy (STM)

***M. Sc. Aristeo Segura S.***

Benito Juárez University

Positions and Employment

- Bio-Nanotechnology (expert in biological macro-molecule adsorption phenomena by Scanning Probe Microscopy (AFM and STM))
- Past-director's Assistant at U.A.B.J.O.
- Past-director of Facultad de Ciencias Química de la U.A.B.J.O.
- Professor of Chemistry at Facultad de Ciencias Química de la U.A.B.J.O

***Ph.D.Nikola Batina***

Ph.D. in Chemistry,1986,The Rudjer Boskovic Institute, University of Zagreb,Croatia.

Member of “Sistema Nacional de Investigación”, SNI-CONACyT, LEVEL III

Manager of Nanotechnology and Molecular Engineering Laboratory. Universidad Autonoma Metropolitana-Iztapalapa (UAM-I). Mexico City.

Research Interest:

- Molecular adsorption phenomena at the metal surface: identification of molecules, ions, active sites for nucleation and catalysis, metal underpotential and bulk deposition, influence of adsorbed layer on the energy and mass transfer at the modified interfaces.
- Fisico-chemical characterization of nanoparticulate material and development of new methodologies in the field of nanotechnology with especial emphasis for industrial applications.



### **Chapter 3**

## **PRESENTATION OF SOME CONCEPTS FOR THE UNDERSTANDING OF THE NANOWORLD**

**S.J. Castillo<sup>1</sup>, J.C. Lopez-Cervantes<sup>2</sup>, M.E. Alvarez-Ramos<sup>2</sup>,  
A. Apolinar-Iribé<sup>2</sup>, R.P. Duarte-Zamorano<sup>2</sup>,  
L.E. Regalado<sup>1</sup> and A. Duarte-Moller<sup>3</sup>**

<sup>1</sup> Departamento de Investigación en Física de la Universidad de Sonora. Blvd. Rosales y Transversal s/n, Hermosillo, Son. 83000. México

<sup>2</sup> Departamento de Física de la Universidad de Sonora. Blvd. Rosales y Transversal s/n, Hermosillo, Son. 83000. México

<sup>3</sup> Centro de Investigación en Materiales Avanzados. Miguel de Cervantes 120, Complejo Industrial Chihuahua, Chih.31109, México

### **ABSTRACT**

This work, starting from a hard historical review, try to generate a kind of update of the actual stage of the concepts related with nanometers scales, also try to deduce something about the further develop in this science, at the same time that comment a little of our experiences in the area. We hope it will be capable to push to the readers to involve in this new age of the sciences.

**Keywords:** Nanoscience, nanotechnology, nanoworld, semiconductors, photonics.

For write about the nanoworld firstly it is necessary to establish a minimal set of concepts over which it would be possible to built our compose concept of the “nanoworld”. Let us start, for the moment, with a basic understanding for such a concept like “*regions of the real world whose longitudinal sizes are between one to a few hundreds of a millionth of millimeter*”. For real world we mean portions of the space filled of material substances under certain energy conditions.

Due to the enough and rapid growing of the knowledge, it is necessary that any scientist have as global as precise points of view about a philosophy of the world, about the society and the politics, and about the science. Many times due to the deficiency of such points of

view, the scientific develop looks truncated. Examples of relatively big jumps in the human knowledge were the developments of Albert Einstein, see Einstein (1949), Karl Marx and Friedrich Engels, see Woods (1995), among others. Now, let us to consider the turn to recall the famous lecture: "*There's plenty of room at the bottom*", given for Richard Feynman in 1959, in a meeting of the American Physical Society at the Caltech where he insisted about describing nanotechnology as an important field for future.

Let us go to make a small review in the formal history of the nanoworld. There exist the evidence that in 1952 *Radushkevich* and *Lukyanovich* published clear images of 50 nanometer diameter tubes made of carbon, see *Radushkevich* (1952); Abrahamson J. , in 1971 worked and wrote in his PhD thesis "*The reactions of coal in a high intensity electric arc.*" At the University of Canterbury, Christchurch, NZ.; Also Abrahamson, J. published in 1973 "*The surface energies of graphite*" , see Abrahamson (1973); from 1974 to 1979 were published the works "*Graphite sublimation temperatures, carbon arcs and crystallite erosion*", "*Filamentous growth of carbon through benzene decomposition*", "*Carbon fiber layers on arc electrodes - I their properties and cool-down behavior*", "*Structure of carbon fibers found on carbon arc anodes*"; and a PhD thesis "*The production of acetylene by a carbon arc*" containing additional observations of fine fibers on carbon cathodes, see Abrahamson (1974), Oberlin (1976), Wiles (1978), Abrahamson (1979), Wiles (1979).

For that moment carbon fibers have been prepared by pyrolysing a mixture of benzene and hydrogen at about 1100°C. These fibers have been studied by high resolution electron microscopy showing various external shapes and contain a hollow tube with a diameter ranging from 20 to more than 500 Å along the fiber axis, see Oberlin (1976) . It was until 1981 when Binnig and Rohrer created the STM to image individual Atoms, and in the same year, K. Eric Drexler published his first article on the subject of the nanotechnology in the prestigious scientific journal, Proceedings of the National Academy of Sciences, titled "Molecular engineering: An approach to the development of general capabilities for molecular manipulation". After that another isolated advance was done by Abrahamson John and Maclagan Robert G.A.R. (1984), it was about theoretical studies of interstitials in graphite , see Abrahamson (1984).In 1985 Curl, Kroto and Smalley discovered C60; in 1986 the Invention of AFM image was done by Mike Tiner; in 1986 K. Eric Drexler published his book "*Engines of Creation*"; 1989-First atomic manipulation at IBM by Don Eigler; 1992 K. Eric Drexler published his book "*Nanosystems: Molecular Machinery, Manufacturing, and Computation*"; in 1993 Iijima, Bethune, et al. discovered single wall carbon nanotubes; in 1998 Cees Dekker's group created a TUBEFET; and in the same year the Nobel Laureate Horst Stormer said: "*Nanotechnology has given us the tools... to play with the ultimate toy box of nature – atoms and molecules. Everything is made from it... The possibilities to create new things appear limitless.*"

Already for the present century in 2000 Nano-tube AFM tips were prepared, see Wong (2007); in 2001 was obtained or prepared or synthesized or designed, or we do not know which a term to choose, a Nanowire ZnO laser; in 2002 were done Super lattice Nano-wires; in 2007 was published in *Science Express* on January 18th, the work "*A Molecule Carrier*", see Yonghui Deng (2008); and finally a work Received for publication on September 17th 2007, and Accepted for publication on November 23rd 2007 and First published on the web on December 14th 2007 about "*A novel approach to the construction of 3-D ordered macrostructures with polyhedral particles*", here we can see how the domain of nanotechniques can to get results in other areas like in this case in the photonic. As we can

see there is a lot of work involving ideas, techniques and devices about the nanoworld, so we can find works like: Atom Manipulation, Molecular electronics, matter emitting devices, Self-Assembled monolayer, Nanowires, Semiconductor Nanowires, Nano-Lasers, Nanotube AFM and STM tips, Hydrogen Storage in Carbon Nanotubes, Nanobiology, Nano-optics, and an unsuitable or incredible mix of terms with the prefix NANO.

Now, before to go to the further develops those like Feynman pointed up at the end of the 50's, i. e., before to be predictive, let us to present some about our work related with the nanoworld, see Castillo (2000), Castillo (2001), Sotelo-Lerma (2001). We have worked structural, optical and surface morphology changes of the In/CdS/glass system subjected to thermal annealing in air. In figure 1. We show AFM surface images of the In/CdS/glass, system without annealing and annealed at temperatures of 300 and 400°C. A gradual change is observed in the surface morphology from the sample without annealing, which displays the surface morphology of the In, to the sample annealed at 400°C. At this annealing temperature, the surface is completely oxidized and then the image corresponds to the surface morphology of  $\text{In}_2\text{O}_3$ .

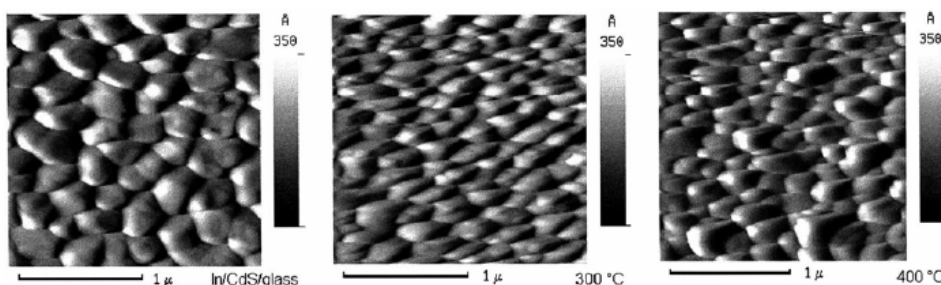


Figure 1. AFM surface images of the In/CdS/glass, system without annealing and annealed at temperatures of 300 and 400°C.

Also we have worked with ZnO/CdS bilayers prepared by concurrent deposition from a chemical bath (CBD). Here we have in figure 2, a SEM photograph that display the surface film morphology in a portion of  $8 \times 6 \mu\text{m}$  of the surface, the orientation and elongated shape of the ZnO grains is evident. From this image, it can be observed that the cross-section of the grains has an average size of about  $0.3 \mu\text{m}$  and it is possible to see several grains with a length of about  $1 \mu\text{m}$ , but more accurate lengths can be confirmed by another technique shown in the figure 3. The information about the thickness, homogeneity and the formation of two different layers of ZnO and CdS on the glass substrate was given by the cross sectional studies by Electron Microprobe Analysis. In figure 3(a) we observe an image with a bright cross-section of the film. To the left of the film, in gray color, is the substrate and to the right of the film, in black color, is an epoxy resin used to prepare the film for this measurement. There are also dotted sections in backscattered electron (BSE) image, these dots represent sections of higher mean atomic number of Cd or Zn. The width of X-ray distribution peaks is partly a function of the minimum interaction volume diameter achievable by electron beam excitation of X-rays, which is approximately 1-2 microns. The elemental distributions in figure 3(b) indicate that Cd and S are present together, and occur as a very thin film of about 300 nm at the boundary between the glass and the film, indicated by an arrow in this graph. The diameter of the X-ray generation volume is sufficient to explain the apparent greater

width observed. On the other hand, Zn and O also are present together and occur as a mass of mixed crystals, having a thickness of approximately  $2 \mu$  in the external part of the film.

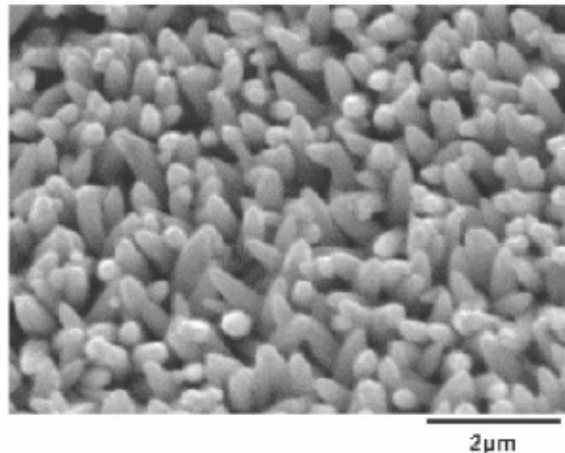


Figure 2. SEM image in a surface portion of 8 X 6 microns of the ZnO/CdS bilayer film.

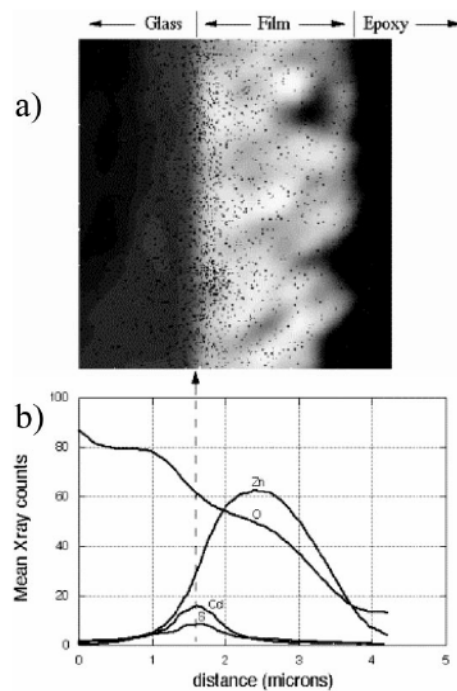


Figure 3. (a) Backscattered electron image of the cross section of the ZnO/CdS bilayer film. (b) Spatial distribution of the elements in the substrate and in the ZnO/CdS bilayer film.

Also we are interested in study absorptions-transmitions, photosensitivity and others optical, electrical, structural or non linear properties, because there are interest in such as applications like photo sensors, solar cells, photo emissions and radioactive dosimeters,

among others. In figure 4, in order to obtain some information about the photosensitivity of thin films (continuing with the ZnO/CdS system), we use to exposed them to dark-light-dark intervals for light periods of at least 300 s. We measured the change in the electrical current applying a bias voltage of 10 V between two electrodes on the film. Figure 4 shows the photosensitivity curves of the ZnO/CdS film and it is compared with that of a pure ZnO film deposited by DBQ technique. The curve corresponding to the ZnO/CdS film displays an increase of five orders of magnitude in the electrical current under illumination. This is an indication of a very good photosensitivity of the bilayer film. On the other hand, the curve corresponding to the pure ZnO film shows an increase of about four orders of magnitude in the electrical current under illumination. The photosensitivity of this ZnO film is not as good as that of the ZnO in the bilayer film. The decay of the electrical current after illumination is slow in both kinds of ZnO films. From these electrical measurements, we also obtained the dark electrical resistivity of both films, they were  $1.4 \times 10^8$  and  $4.6 \times 10^4$  V  $\Omega$ cm for the pure ZnO and ZnO/CdS films, respectively.

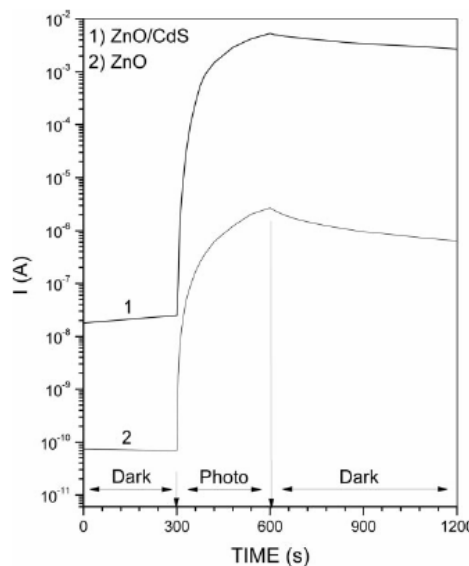


Figure 4. Photocurrent responses  $I(A)$  vs. time of the ZnO/CdS bilayer film and of a pure ZnO film.

We have experience in to prepare CdTe coatings on glass, by the reaction between films of cadmium hydroxide previously deposited on the glass, and a solution prepared by the dissolution of tellurium in hydroxymethane sulfenic acid. The films of CdTe having thicknesses in the range of 1  $\mu\text{m}$  have been deposited by immersing the cadmium hydroxide coatings in an alkaline solution containing tellurium ions. This interest is due that the Cadmium telluride is a II-VI semiconductor compound which is considered of great importance for applications in optoelectronic devices. In particular, it is a very promising material for use in photovoltaic devices because of its optimum bandgap (ca. 1.5 eV) for energy solar conversion and its high optical absorption coefficient ( $>10^4 \text{ cm}^{-1}$ ). Several reports in the last few years have described solar cell efficiencies as high as 15.8% based on CdTe/CdS heterojunctions, with CdTe as the absorber layer and CdS as the window layer. This application of CdTe films has increased the importance of research concerning the

properties of this material and the chemical deposition technique, which lead to the formation of CdTe films. CdTe thin films have been prepared by several techniques, including MBE, CSVT, r.f. sputtering, thermal evaporation and electrodeposition. A search of the literature reveals that among these techniques the aqueous chemical bath deposition method has not lent itself to the preparation of CdTe thin films. This is one of the simplest and most economical techniques for the preparation of semiconductor thin films. It consists in the deposition of a semiconductor film on a substrate immersed in an aqueous solution which contains a source of the chalcogenide and dissolved metal ions. This technique of thin film preparation has been utilized for the preparation of semiconducting binary chalcogenides. Among these are PbS, PbSe, CdS, CdSe, CuS, ZnS and others. In the figures from figure 5 to figure 11 it is shown a more or less complete characterization for these CdTe thin films. The figure 5. Show the optical absorption spectrum of CdTe film, basic for to calculate the absorption edge of the material semiconductor and its bandgap energy. The figure 6. Show the numerical derivative of the absorption spectrum of the figure 5, like a better or more sensible mathematical method. In the figure 7. It has plotted the square of the multiplication of the energy times optical density, vs. the energy, it gave us graphically its bandgap energy. The figure 8. shows XRD spectrum of CdTe film and the wide behave is due to the glass substrate. The SEM photograph of CdTe film in the figure 9, shown that the crystalline aggregates are fairly uniform in size and theirs mean size is about 500 nm. The individual crystal size, as calculated from the Debye-Scherer equation, is approximately 21 nm. Figure 10, show a cross-sectional photograph by Back Scattered Electron Microscopy (BSEM) of the CdTe films, also graphs of ion distributions are shown. From this, it is possible to conclude that the conversion to CdTe is not 100%. The results of XPS measurements, figure 11, demonstrate the presence of Te and Cd with binding energies of 579.2 and 412 eV, respectively. In the same figure, we can see a 3.2 eV shift from Te° (44 and 576 eV) powder peaks, measured with the same equipment.

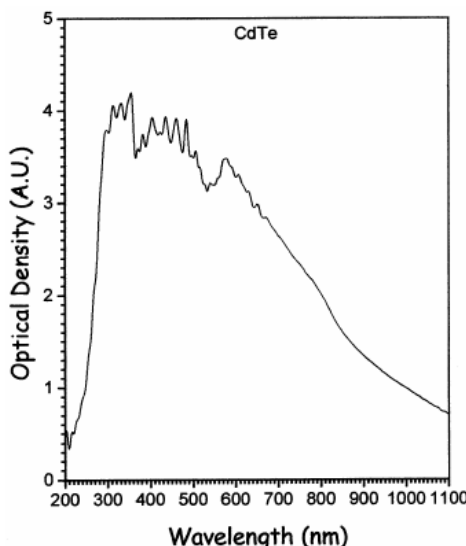


Figure 5. Optical absorption spectrum of CdTe film.

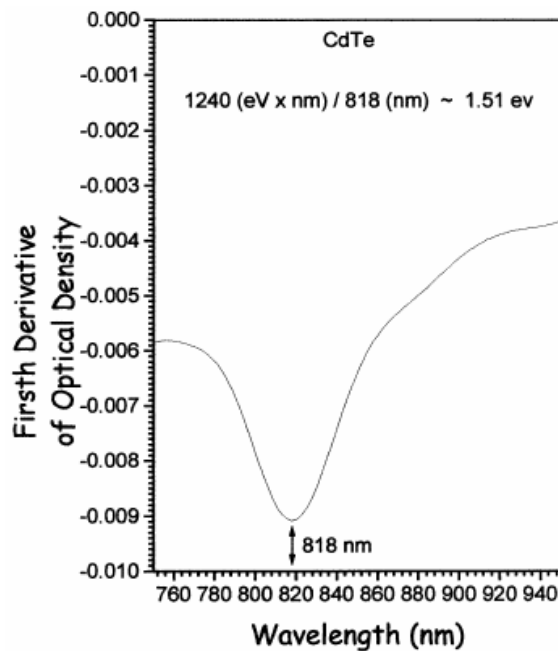


Figure 6. Numerical derivative of the absorption spectrum in figure 5.

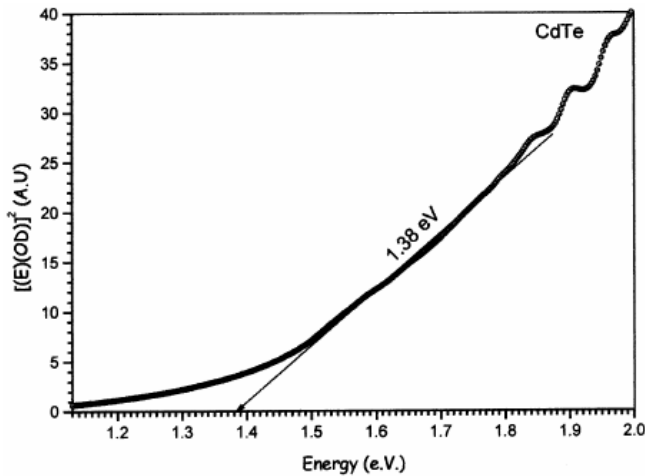


Figure 7. Plot of the square of energy times optical density vs. energy.

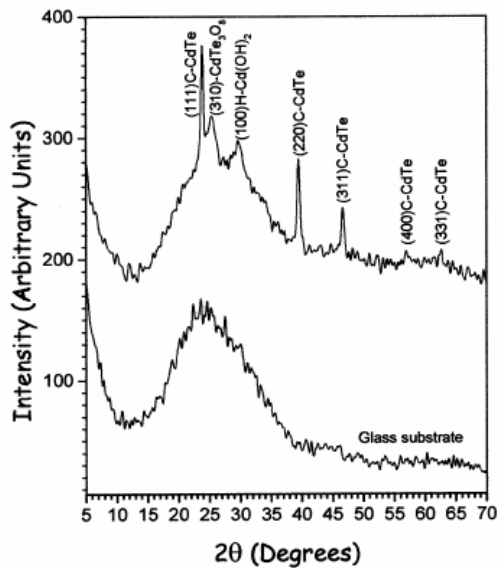


Figure 8. XRD spectrum of CdTe film and glass substrate.

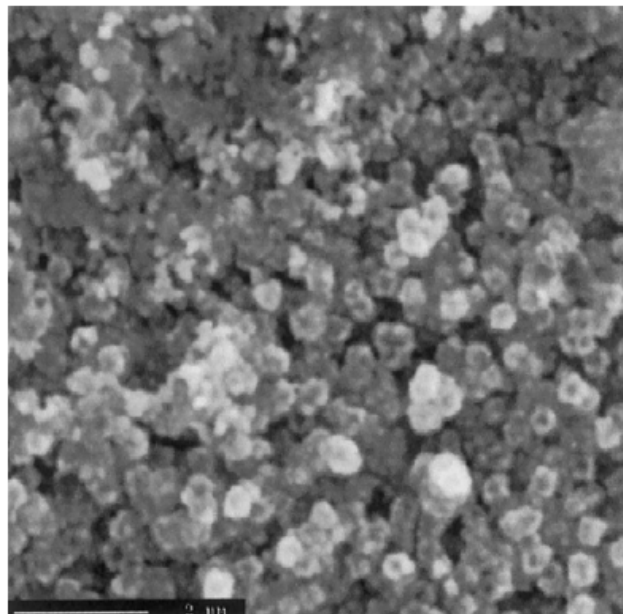


Figure 9. SEM photograph of CdTe film.

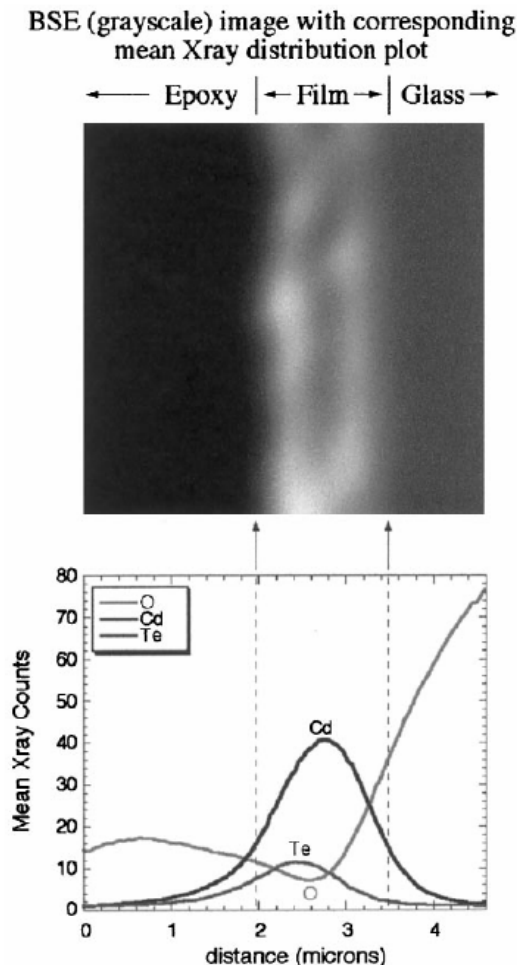


Figure 10. Cross-section photograph by BSEM of the CdTe film, including graphs of ion distributions.

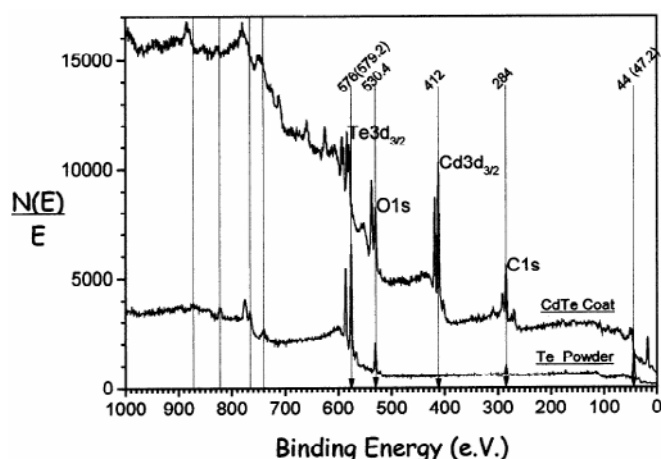


Figure 11. XPS-measured spectra of CdTe film and Te° powder.

Another field of interest for us is of the composites of semi organic crystals or organic-inorganic crystals containing amino acids. The why are we interested interested in to study these semi organic systems?, is because with them it is possible to make frequency duplicator devices, the which could be considered like new electromagnetic radiation sources, i.e., that is due what those systems presents non- linear optical properties. So we have acquired the experience to synthesize Glycine Sodium Nitrate (GSN) crystals, simply by evaporation of aqueous solutions at room temperature, the crystals are characterized by IR, UV-Vis, XRD, thermal analysis and SEM. For certain conditions<sup>(17)</sup>, the UV-Vis shows that the crystals are transparent in the range of 500-1000 nm indicating the materials are desirables for second harmonic generation. The XRD results confirm that the materials have a monoclinic structure and a spatial group Cc with lattice parameters of  $a = 14.329 \text{ \AA}$ ,  $b = 5.2662 \text{ \AA}$ ,  $c = 9.1129 \text{ \AA}$  and  $\beta = 119.10^\circ$ . While the thermal analysis show that the crystals are stables under  $190^\circ\text{C}$ , which is very important for future applications.

We will continue experimenting by changing the conditions and the reagents, for instance using other amino acids. In the figure 12, we can see in the part (a) a  $3 \text{ mm} \times 0.5 \text{ mm} \times 0.5 \text{ mm}$  GSN crystal image, and in the part (b) the early recrystallization of a nano-monocrystal of the same compound. This nano-monocrystal was created from the atomization over a substrate of the adequate solution for the growing, and let it to evaporate.

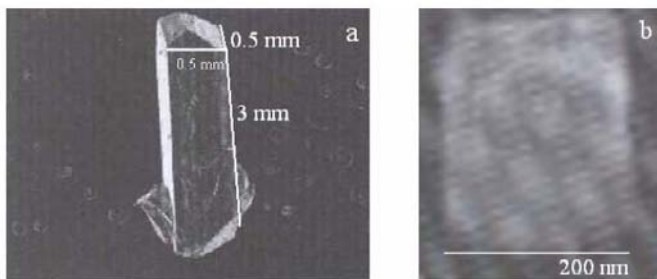


Figure 12. Part (a) crystal of GSN, with sizes of  $3 \text{ mm} \times 0.5 \text{ mm} \times 0.5 \text{ mm}$ , part (b) nano-monocrystal of GSN, with frontal size of the order of  $200 \text{ nm}$ .

In the near future we will participate preparing vitreous dyes lasers, light diffusion on vibrating nanotubes media, organic semiconductors, and others more, but here we should stop the explanations about our research interests, in order to comment that we believe must be the next future steps of the science. Nevertheless that the electronics already is handling 45 nm technologies and smaller, we want to point at that is very difficult to control such a technology. So, we think that there will have a relaxation time where the nanotechnology gets a strong stability and good efficiency. We think that the next obligated step for the nanoscience must be related with the transmutation of the matter and the un-radioactivation of the substances. In other words: "There's a finite flux of life in the limits of the universe". For transmute the matter or disappear its radioactive properties it should be necessary to review the concepts of time, life and intelligence. For example, time ago Roger Penrose commented to his student Richard Feynman "Would it be possible, that in the complete atom there is only an electron, but in different energy states?"

For these and other reasons, it is necessary to summon to all scientific community for convince to the common society to built a structure for the control of the hard sciences, in

order to avoid a society collapse and the bad richness distribution. For instance, in such a scientific structure the scientific journals would be supported in order have the human right to accede to the science development. The financial supporting would become independent from the politicians, and the decisions involving armament would not be taken so slightly.

Then, now must be the historical moment for a conscious growing and emancipation of the science, throughout of the handling of the matter to nanoscales and a wide ignorance in the domain of the elementary particles, see Einstein (1934), Einstein (1935), Einstein (1938), Penrose (1989).

## REFERENCES

- Abrahamson, J. (1973). "The surface energies of graphite", *Carbon* vol. 11, 337-362.
- Abrahamson, J. (1974). "Graphite sublimation temperatures, carbon arcs and crystallite erosion", *Carbon*, vol. 12, 111-141.
- Abrahamson, J. and Maclagan, R. G.A.R. (1984). "Theoretical studies of interstitials in graphite". *Carbon*, vol. 22 , 291-295. Y. Nakayama *et al*, Nanotube AFM tip, *J. Vac. Sci. Tech.*, B18 (2000) 661.
- Abrahamson, J., Wiles, P.G., and Rhoades, B.L. (1979). "Structure of carbon fibers found on carbon arc anodes", 14<sup>th</sup> Biennial Conference on Carbon, insert for p254-255, June 25- 29, Penn. State Univ., University Park, Penn., USA.
- Castillo, S.J., Mendoza-Galván, A., Ramírez-Bon, R., Espinoza-Beltrán ,F.J., Sotelo-Lerma, M., González-Hernández, J., Martínez, G., "Structural, optical and electrical characterization of In/CdS/glass thermally annealed system", *Thin Solid Films*, 373,10-14, (2000).
- Castillo, S.J., Sotelo-Lerma, M., Zingaro, R.A., Ramírez-Bon, R., Espinoza-Beltran, F.J., Guillemette, R., Domínguez, M.A., " ZnO/CdS bilayers prepared by concurrent deposition from a chemical bath", *Journal of Physics and Chemistry of Solids*, 62, 1069-1073, (2001).
- Einstein, A. (1949), "Monthly Review", New York.
- Einstein, A. and Infeld, L., "The Evolution of Physics". New York: Simon & Schuster, 1938, p. 294.
- Einstein, A., "The World as I See It", New York: Philosophical Library, 1934.
- Einstein, A., Podolsky, B. and Rosen, N., "Can QuantumMechanical Description of Physical Reality Be Considered Complete?", *Physical Review*. 47, 777, 1935, p. 780.
- Hernández-Paredes, J., Castillo, S.J., Esparza-Ponce, H.E., Téllez-Flores, E., Durante-Moller, J.A., "Síntesis y caracterización de nano-monocristales de Glicina-Nitrato de Sodio, GSN, con propiedades ópticas no-lineales", Tecnura, año 9, No.18, pág. 4-9, primer semestre del 2006.
- Oberlin, A. and Endo-T-Koyama, M. (1976). "Filamentous growth of carbon through benzene decomposition", *Journal of Crystal Growth*, Volume 32, Issue 3, Pages 335-349.
- Penrose, R., "The Emperors New Mind", Oxford University Press,(1989).
- Radushkevich and Lukyanovich (1952). *Soviet Journal of Physical Chemistry*, Pages 88-95.
- Sotelo-Lerma, M., Zingaro , R.A., Castillo, S.J. , "Preparation of CdTe coatings using the chemical deposition method", *Journal of Organometallic Chemistry*, 623, 81–86, (2001).

- Wiles, P.G. (1979) "The production of acetylene by a carbon arc", PhD thesis, University of Canterbury, Christchurch, NZ.
- Wiles, P.G. and Abrahamson, J. (1978). "Carbon fiber layers on arc electrodes – I. Their properties and cool-down behavior". *Carbon*, vol. 16, 341-349.
- Wong, K. L., Pawin, G., Kwon, K.-Y., Lin, X., Jiao, T., Solanki, U., Fawcett, R. H. J. , Bartels, L., Stolbov, S., Rahman , T. S., "A Molecule Carrier", *Science* 9, Vol. 315, No. 5817, pp. 1391 – 1393, March 2007.
- Woods, A. and Grant, T. (1995). "Reason in Revolt. Marxism and Modern Science", Wellred Publications, Londres.
- Yonghui Deng, Chong Liu, Jia Liu, Fan Zhang, Ting Yu, Fuqiang Zhang, Dong Gu and Dongyuan Zhao, "A novel approach to the construction of 3-D ordered macrostructures with polyhedral particles", *J. Mater. Chem.*, 18, 408-415, DOI: 10.1039/b714288a., 2008,

## RESUMES OF THE AUTHORS

### Castillo, S.J.



Mexican scientist born in Empalme Sonora Mexico in 1961, my interest fields are general relativity, synthesis of semiconductors and molecular electronic. I got my PhD in the Sonora University in Mexico, where now I am a full time Researcher. I had a post-doc position in the University of the North of Texas (2001), USA. I have a son, and now I am so happy with a new wife. I think that Albert Einstein yet is irreplaceable.

### Lopez-Cervantes, J.C.

Professor, Department of Physics, University of Sonora Mexico. Taught courses of theoretical physics at all levels of the curriculum, including modern physics, relativity and mechanics. Actually I am studying the PhD in Physics in the Astronomy area.

**Alvarez-Ramos, M.E.**

President of the Optical Properties Academic Group (CA), Full Professor in Physics Department of the University of Sonora in Mexico. My interest areas are the synthesis and Optical characterization of Luminescent Materials as well as the optical-nanodevices. I have facilities in optics laboratory. I teach advanced courses of optics and research laboratory.

**Duarte-Moller, A.**

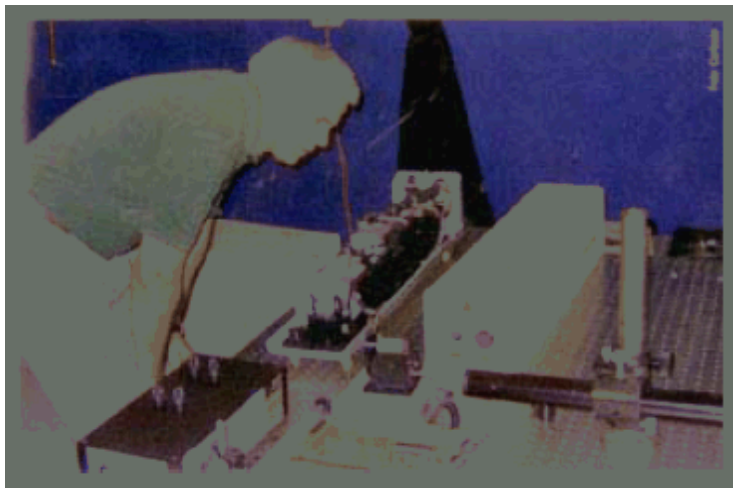
Full Professor in the Physics of Materials Department in the Advanced Materials Research Center, Chihuahua, México. Visitant Researcher in the Physics Department University of Sonora. My interest area is nanotechnology and materials characterization by using TEM, XPS/Auger, EELS and EXAFS techniques.

**Apolinar-Iribar, A.**

I am developing a optics laboratory. I am Full Professor in Physics Department of the University of Sonora Mexico. I have been employers review commissioner of the human resources in my University. I use to teach basic and optional courses on physics for engineer and physics students. My principal topic is the study of the non linear properties of the matter. I was Chair Faculty of my Department.

**Duarte-Zamorano, R.P.**

Full Professor in Physics Department of the University of Sonora Mexico. I have taught several basic courses on physics. My topics are atomic and computational physics. In my opinion the nanotechnology is changing the complete scope of the world.

**Regalado, L.E.**

Professor of Optics. At present, I am investigator of the Departments of Investigation in Physics of the University of Sonora (DIFUS), I lead the works destined to develop a system called LIDAR (initials of Light Detection and Ranking), consisting of a radar laser to detect molecules pollutants in the air. Actually I am director of TxTec, an institutional program of transference of technology. I was general Chair of Centro de Investigaciones en Optica, A. C.

***Chapter 4***

## **CENTERS OF EDUCATIONAL EXCELLENCE IN NANOTECHNOLOGY: THE PROPOSED WORLD BANK SCIENTIFIC MILLENNIUM INITIATIVES AND NANOTECHNOLOGY IN LATIN AMERICA**

***Guillermo Foladori<sup>\*1</sup>, Mark Rushton<sup>\*2</sup>  
and Edgar Zayago Lau<sup>\*3</sup>***

<sup>1</sup> Professor, Doctoral Program in Development Studies, Universidad Autónoma de Zacatecas, México. Member of the Latin American Nanotechnology and Society Network (ReLANS)

<sup>2</sup> Doctoral Program in Development Studies,  
Universidad Autónoma de Zacatecas, México.

<sup>3</sup> Doctoral Program in Development Studies,  
Universidad Autónoma de Zacatecas, México. Member of the Latin American Nanotechnology and Society Network (ReLANS)

### **ABSTRACT**

This article analyses the World Bank Millennium proposals to support research in nanotechnology in Latin America. The proposals are based on the theory of the “knowledge economy.” It concludes by raising some concerns regarding the sustainability of the proposals as foundations for development.

**Keywords:** Nanotecnology, Latin America, Knowledge Economy, Scientific Millennium Initiatives, Development.

---

\* fola@estudiosdeldesarrollo.net  
\* mrushton@mac.com  
\* edzlau@yahoo.com

## 1. NANOTECHNOLOGY AND THE QUESTION OF DEVELOPMENT

Nanotechnology is rapidly becoming the technological platform of the next industrial revolution. Although the world market in products that contain nanocomponents is currently quite small, analysts anticipate an exponential growth in the coming years. The table below provides an idea of the current situation and projections:

**Current and Projected Sales of Products Containing Nanoparticles (World)**

Year	Billion US\$	Reference
2005	32	Lux Research, 2006
2008	100	Lawrence, 2005
2010	500	Baker and Aston, 2005.
2014	2,900	Lux Research, 2007, 2.9 trillion by 2014 Científica 2007, 2.95 trillion by 2015.

Note: By way of comparison, consider that the total exports of Latin America and the Caribbean in 2004 were approximately 500 billion dollars.

What will be the role of nanotechnology in development and, in particular, of those countries in the process of development?

To describe this new industry, proponents usually cite the potential that nanotechnology possesses for developing countries to resolve their innumerable problems, from those relating to the purification of water, the generation of energy and the creation of medicines. Another advantage of nanotechnology lies with the creation of new economic opportunities. This technology is seen as a way to “catch up” to the industrialized countries. The Centre for Bio-Ethics at the University of Toronto, Canada (UTJCB) and the *Task Force on Science, Technology and Innovation* of the Millennium Project of the United Nations, refer to the potential benefits of this technology for development, although there is little detail provided on exactly how this is to be done (Salamanca-Buentello, et al., 2005; Juma and Yee-Cheong, 2005).

So, how can developing countries develop their capacities in Science and Technology (S and T) in order that they attain a technological leap? The answers to this question have come in various international forums since the early 1990s. However, dealing specifically with nanotechnology, the discussion begins at the end of the decade and has been mostly developed in very recent years. In February, 2005, for example, the International Centre for Science and the United Nations Industrial Development Organization organized the conference, *North-South Dialogue on Nanotechnology: Challenges and Opportunities*, focused specifically upon the participation of developing countries in nanotechnology (Brahic, 2005a, 2005b; Brahic and Dickson, 2005). Of particular interest was the message from the president of the Third World Academy of Sciences, Mohamed Hassan (2005). He proposed the establishment of Centres of Excellence in Africa, noting that S and T development is a necessity for the success of developing countries. The same view was discussed by leaders of the industrialized nations (Group of Eight) from 2000 onward, with explicit support for the idea of the formation of Centres of Excellence in Africa, to instigate

the transfer and sharing of S and T between developed and developing countries, during their annual meeting in Scotland in 2005 (Dickson, 2005).

The World Bank ranks countries according to the percentage of high technology that is contained in their products for export. High-technology products are considered to be those that incorporate an intensive Research and Development (R and D) component, which includes computers, pharmaceuticals, industrial instrumentation and equipment, and aerospace products, among others. In 2004, for example, 34% of Ireland's exports were high technology products; in South Korea, 33%; in the United States, 32%; but in Latin America, Chile exported only 5%; Brazil 12%; and Mexico 21% (World Bank, 2006).<sup>1</sup> The World Bank's analysis suggests that R and D has an essential role in development, and a strong investment in R and D that results in productive innovation and an improvement in international competitiveness would be the path that these developing countries should follow.

In Latin America, the proposal to create Centres of Excellence to drive S and T has been one of the World Bank's most significant projects since the end of the 1990s, as part of its series of Millennium Projects.

## **2. WORLD BANK MILLENNIUM PROJECTS AND NANOTECHNOLOGY IN LATIN AMERICA**

Since the end of the 1990s, the World Bank and various other institutions have planned for the creation of a global network of *Millennium Scientific Initiatives* (MSI). These have the function of being centres of excellence in underdeveloped countries, with the objective of promoting research in S and T with equal measures of infrastructure and resources as exist in developed countries (Macilwain, 1998).

Chile's project was the prototype. In 1999, the World Bank allocated a loan of 5-million dollars for the first two-and-a-half year period, which was matched by 10-million dollars from the national budget (ICM, n/d a). The objectives of the MSIs were:

...to foster growth in scientific research capacities, employing and stimulating the best talent in the country, as a key factor for sustainable socio-economic development. The Programme anticipates that the creation of Centres of Scientific Excellence will give rise to Scientific Institutes and Scientific Nuclei under a competitive and transparent process. These centres will pursue scientific research on the frontier, the training of scientists and the establishment of links with the productive sector and other institutional agreements (ICM, n/d a).

Additional MSI objectives in Chile included the attraction of foreign skilled workers and stemming the "brain drain." In this case, the World Bank's plan in Chile was implemented as a pilot project, from the top-down. The Centres of Excellence were staffed by the most distinguished scientists, with the hope that this would facilitate alliances and agreements with private industry and oversee domestic productive innovation.

---

<sup>1</sup>In the case of Mexico, the weight of maquilladora production and the strong inter-firm trade between companies suggests that a careful analysis is required (Delgado Wise & Invernizzi, 2002).

The MSI initially called for the creation of three Institutes and five Nuclei. One of the Nuclei was oriented toward research in nanotechnology (Physics of Condensed Material), with its headquarters at the Universidad Técnica Federico Santa María (ICM, n/d a). Its second recommendation was the formation of the five new research Nuclei, none of which was oriented toward nanotechnology. The third recommendation, announced in 2002 and undertaken in 2003, chose a new project in nanotechnology, with the headquarters at the Universidad Andrés Bello (Material and Nanotechnology Sciences, Organic Physio-Chemistry and Theory of Density Functions); and extended for an additional three years the Physics of Condensed Materials (ICM n/d b). The table which follows summarizes the initiatives chronologically, highlighting those related to nanotechnology:

#### **Millennium Scientific Initiatives. Chile 1999 -2006<sup>2</sup>**

<b>Start Date</b>	<b>Number of Institutes and Nuclei founded</b>	<b>Institute or Nuclei Name</b>	<b>Host University</b>
1999	3 Institutes 5 Nuclei	Physics of Condensed Materials (Nuclei)	Universidad Técnica Federico Santa María
2001	5 Nuclei	-----	-----
2002	3 Institutos	Applied Quantum Mechanics and Computational Chemistry (Nuclei)	U. Andrés Bello
2003	3 Institutes 8 Nuclei	Physics of Condensed Materials (Nuclei - revised)	U. Técnica Federico Santa María
2004	3 Institutes 12 Nuclei	-----	-----
2005	3 Institutes 15 Nuclei	-----	-----
2006 (augmented by funds from the “Ley royalty”)	5 Institutes 17 Nuclei	-----	-----

Source: ICM, 2006; ICM n/d a; ICM n/d b).

The MSIs only marginally supported nanotechnology, being oriented more toward biology and biotechnology, areas in which Chile has a long history (although it is possible that under “biotechnology” there exist projects of nanobiotechnology which are not considered in the above table). However, this limited support with two nanotechnology projects over 9 years of financing (including the revision of one of those) constitutes significant support, given the scarcity of nanotechnology development in Chile.

Other countries in Latin America were beneficiaries of the World Bank’s MSIs. The following table shows those Latin American countries with MSIs and the areas of development in which the projects were undertaken: Excellence will give rise to Scientific Institutes and Scientific Nuclei under a competitive and transparent process.

<sup>2</sup> Information about nanotechnological projects is approximate. The criteria employed was the use of keywords in the title or description of the project: nanotechnology, nanoscience or nanoscopic.

These centres will pursue scientific research on the frontier, the training of scientists and the establishment of links with the productive sector and other institutional agreements (ICM, n/d a).

### **Millennium Scientific Initiatives in Latin America 1999 -2005<sup>3</sup>**

Country	Start Date	# of institutes / nuclei / networks created	Nanotechnology Institutes or Nuclei created under the initiatives	Host Institution
Chile	1999	3 Institutes 5 Nuclei	Physics of Condensed Materials Nucleus	U. Técnica Federico Santa María
Chile	2001	5 Nuclei	-----	-----
Chile	2002	3 Institutes	Applied Quantum Chemistry and Computatinal Chemistry	U. Andrés Bello
Chile	2003	3 Institutes 8 Nuclei	Physics of Condensed Materials Nucleus (revised)	U. Técnica Federico Santa María
Chile	2004	3 Institutes 12 Nuclei	-----	-----
Chile	2005	3 Institutes 15 Nuclei	-----	-----
Chile (funds supplemented by the mining royalty law)	2006	5 Institutes 17 Nuclei	-----	-----
México	2001	4 Institutes	Physics, Chemistry and New Material Studies	UASLP
Venezuela	2001 (closed)	3 Institutes 8 Nuclei	-----	-----
Brasil (World Bank)	2001 - 2004	17 Networks	Millennium Institute of Complex Materials Nanosciences Institute of UFMG Research Network in Microchips, Microsystems and Nanoelectronics	UNICAMP UFMG UNICAMP

Source: ICM, 2006; CNPQ, 2005; MSI, 2005; and World Bank, 2005; ICM n/d a; ICM n/d b).

Although the spirit of the MSIs was to create institutes and nuclei of research with resources comparable to the developed countries, in practice, the resources were meagre. In Chile, for example, the World Bank provided a 5-million dollar loan for the first two-and-a-half year stage, supplemented by another 10-million dollars from the national budget (ICM, n/d a). The projects had an average budget of 290-thousand dollar budget over three years,

<sup>3</sup> Information about nanotechnology is approximate. In the search criteria employed, the title or description of the projects were searched for such keywords as: nanotechnology, nanoscience, nanoscopic, nanostructure y nanocapsules.

with the possibility of a single renewal, which hampered their long-term sustainability. In Brazil, during the first stage (the second was completely funded nationally), the financing was approximately 36-million dollars over three years, with an average of 2.1-million for networking. In the Brazilian case, and with regard to the networks, the number of institutions and participating researchers was very large in each network. The Nanosciences Institute, for example, although its headquarters was in the Universidade Federal de Minas Gerais (UFMG), included 13 institutions and more than 60 researchers with PhDs across 17 research projects (MCT-CNPq, 2002).

### **3. SUSTAINABILITY OF THE CENTRES OF EXCELLENCE AS CRUCIBLES FOR DEVELOPMENT**

- Although the spirit of the MSIs was to create research Institutes and Nuclei with comparable resources as had the developed countries, in practice, the financed projects had an average budget, in the case of Chile, of 290-million dollars over three years, with the possibility of only one renewal, which weakened its sustainability over time (Angel, 2003).
- Some additional funds, provided by the “royalty law” approved in 2006 in Chile, constituted a tax on the exploitation of natural resources destined for scientific innovation, will allow for an increase of the research nuclei and projects, but the resources are plainly lacking in relation to the country’s economy, as was noted by the Chilean economist and member of the Millennium Initiative council, Ffrench Davis (2006).
- Although the plan’s concept was to create conditions where scientists would not be inclined to migrate to the developed countries, it is debatable whether this can be achieved by “centres of excellence,” with little support and without any complementary reform in basic, secondary and higher education to nourish and contribute to a plan for technological innovation over the long term. These centres of excellence have to survive in countries where, like Chile, only 0.7% of the Gross Domestic Product (GDP) is allocated to S and T; a very low figure, although higher than that which Mexico diverts (0.3%) and obviously more than that which is allocated by Brazil (0.1%). These are low percentages in comparison with that which is destined for S and T in the developed countries. The United States, for example, which is not one the more significant examples, dedicates 2.7%. Countries like South Korea, which declined in recent decades, still allocates 2.6% (OECD, 2005).
- Nanotechnology is considered as one of the most important areas in the process of contemporary innovation, and a paradigmatic example of the research that must be developed in the transformation process toward a knowledge economy. However, technological innovation in and of itself is not the most important objective, but rather the incorporation of that innovation in the manufacture of products with competitive international advantages. In fact, competitiveness is one of the justifications - and in many cases, the only one - for the use of public resources in new technology research. The National Initiative for Nanotechnology in the United States illustrates this idea, but it is also present in other nanotechnology programmes,

such as that of Argentina and Brazil, and also in the reports published by the governments of Mexico and Costa Rica (Foladori, 2006). Therefore, beyond the spirit behind the discourse of competitiveness as the engine of development, and presumably, benefits to society in general, the historical experience which is the body of evidence supporting that spirit, in fact indicates the opposite. That is to say, a country can improve its competitiveness without necessarily improving the standards of living for its population, with a cost in increasing inequity - the case of Mexico being a prime example.

- Thus, the idea behind the discourse of competitiveness is that the MSIs would result in research nuclei being integrated into national industry, and that public-private agreements would enable continued research funding once the external support was withdrawn. The gamble that private initiative would make up much of the financing of scientific research is simply not practical in Latin America, where most research is undertaken by universities and public research centres. In Brazil, for example, more than 80% of research is done in public institutions. In some cases, public-private partnerships in research have begun to play a greater role, although cautiously, such as in Mexico and Brazil. But still, in the case of those public-private partnerships that have been successful, it is the private partner that determines the research priorities.
- One other problem which remains unresolved is sustainability, from the perspective of training. The Chilean and Mexican cases are illustrative. There, post-graduate programmes of excellence coexist with a primary and secondary education system which are underfinanced and increasingly privatized. In México, in 2000, only 19% of the population of university age were enrolled in studies; the figure for those in secondary education reached 57% (Delgado Wise and Invernizzi, 2002). Post-graduate programmes are subjected to pressure to produce graduates, which calls into question the quality of that education (Guzmán del Prío, 2006).

## REFERENCES

- Angel V., Eliette (2003). Iniciativa Científica Milenio. Química y neurociencia no tienen fondos. *El Mercurio*, September 29, 2003. <http://www.ceo.cl/609/printer-48524.html> [Consulted May 22, 2007]
- Baker, Stephen and Aston, Adam (2005). The Business of Nanotech. *Business Week*. February 14.
- Brahic, Catherine (2005a). Developing world 'needs nanotech network'. *SciDev.Net* February 11, 2005. <http://www.scidev.net/news/index.cfm?fuseaction=printarticle&itemid=1923&language=1> [Consulted July 27, 2006]
- Brahic, Catherine (2005b). Nanotech revolution needs business know-how. *SciDev.Net* February 18, 2005. <http://www.scidev.net/News/index.cfm?fuseaction=readnews&itemid=1938&language=1> [Consulted July 27, 2006]
- Brahic, Catherine and David Dickson (2005). Helping the poor: the real challenge of nanotech. *SciDev.Net* February 21, 2005. <http://www.scidev.net/content/editorials/eng/helping-the-poor-the-real-challenge-of-nanotech.cfm> [Consulted July 27, 2006]

- Científica (2007). Half Way to the Trillion-Dollar Market? A Critical Review of the Diffusion of Nanotechnologies. [http://www.cientifica.eu/index.php?option=com\\_content&task=view&id=68&Itemid=111](http://www.cientifica.eu/index.php?option=com_content&task=view&id=68&Itemid=111) [Consulted April 24, 2007]
- CNPQ (2005). Institutos do Milênio. <http://www.cnpq.br/programasespeciais/milenio/projetos/2005/05.htm> [Consulted May 20, 2007]
- Delgado Wise, Raúl and Invernizzi, Noela (2002). México y Corea del Sur: Claroscuros del crecimiento exportador en el contexto del globalismo neoliberal. *Aportes, Revista Mexicana de Estudios sobre la Cuenca del Pacífico*, II, 2, 4, 63-86.
- Dickson, David (2005). G8 leaders give indirect boost for science in Africa. *SciDevNet*, September 3. <http://www.scidev.net/news/index.cfm?fuseaction=printarticle&itemid=2549&language=1> [Consulted September 1, 2006]
- Ffrench-Davis, Ricardo. (2005). Entrevista a Ricardo Ffrench-Davis. *Boletín de la Academia Chilena de Ciencias*. September. <http://www.academia-ciencias.cl/index.php?module=boletin&boletin=57&task=boletin&page=2> [Consulted May 19, 2007]
- Foladori, Guillermo. (2006). Nanotechnology in Latin America at a Crossroads. *Nanotechnology Law and Business Journal*, 3(2), 205-216.
- Guzmán del Prío, Sergio A. (2006). Los posgrados y la formación de recursos humanos. La Jornada. México D.F. <http://www.jornada.unam.mx/2006/07/26/a03a1cie.php> [Consulted July 26, 2006].
- Hassan, Mohamed (2005). Nanotechnology: Small things and big changes in the developing world. *Science*, 309, 5731, 65-66.
- ICM. (2006). *Iniciativa Científica Milenio. Memoria Trienal 2003-2005*. [www.mideplan.cl/milenio/?q=node/113](http://www.mideplan.cl/milenio/?q=node/113) [Consulted May 12, 2007]
- ICM. (n/d a). *Iniciativa Científica Milenio. Memoria Bianual 1999-2000*. Santiago: MIDEPLAN. <http://www.mideplan.cl/milenio/?q=node/34> [Consulted May 23, 2007]
- ICM. (n/d b). *Iniciativa Científica Milenio. Memoria Bianual 2001-2002*. Santiago: MIDEPLAN. <http://www.mideplan.cl/milenio/?q=node/35> [Consulted May 23, 2007]
- Juma, C. and Yee-Cheong, L. (Eds.). (2005). *Innovation: applying knowledge in development*. UN Millennium Project. Task Force on Science, Technology, and Innovation. London, Sterling, Va.: Earthscan. <http://www.unmillenniumproject.org/documents/Science-complete.pdf> [Consulted May 29, 2007]
- Lawrence, Stancy (2005). Nanotech Grows Up. *Technology Review*, June.
- Lux Research (2006). *The Nanotech Report*, 4th Edition. New York: Lux Research Inc.
- LuxResearch (2007). *Nanomaterial Forecast: Volumes and Applications*.
- Macilwain, Colin (1998). World Bank backs Third World centres of excellence plan. *Nature*, 396, 711, 24-31.
- MCT-CNPq (2002). A Iniciativa Brasileira em Ciência e Tecnologia. *Parcerias Estratégicas*, (2004), 18, 105-135.
- Mideplan (2006). Programa Iniciativa Científica Milenio aprobó propuesta de distribución presupuestaria para 2007 <http://www.mideplan.cl/final/noticia.php?regid=&idnot=1083> 16/11/2006. [Consulted May 20, 2007]
- MSI (Millennium Science Initiative). (2005) Current and Planned Initiatives. <http://www.msisig.org/msi/current.html> [Consulted May 12, 2007]
- OECD (Organisation for Economic Co-operation and Development) (2005), *Main Science and Technology Indicators 2005-2*.

- Salamanca-Buentello, F.; Persad, D. L.; Court, E. B.; Martin, D. K.; Daar, A. S.; Singer, P. (2005). Nanotechnology and the Developing World. *PLoS Medicine*, 2 (5). <http://medicine.plosjournals.org/perlServ/?request=get-document> and doi=10.1371/journal.pmed.0020097 [Consulted May 22, 2007]
- World Bank. (2005). Implementation Completion Report on a Loan in the Amount of USD \$5.0 Millions to the Bolivarian Republic of Venezuela for the Millennium Science Initiative Project (scl-45720) [http://www-wds.worldbank.org/external/default/WDSContentServer/WDSP/IB/2005/06/27/000012009\\_20050627102527/Rendered/PDF/317310rev.pdf](http://www-wds.worldbank.org/external/default/WDSContentServer/WDSP/IB/2005/06/27/000012009_20050627102527/Rendered/PDF/317310rev.pdf) [Consulted May 12, 2007].
- World Bank. (2006). *World Development Indicators 2006*. CD-ROM. Washington, D.C..



*Chapter 5*

# ELEMENTAL IDENTIFICATION BY X-RAY FLUORESCENCE USING A PORTABLE PYRO- ELECTRIC GENERATOR AND A CdTe DETECTOR FOR AN ADVANCED LABORATORY COURSE

***M. Castro-Colin, J. A. López and S. K. Valaparla***

Department of Physics, University of Texas at El Paso,  
El Paso, TX 79968, U.S.A.

## ABSTRACT

We present an analysis of elemental content carried out by means of a pyro-electric generator and a cadmium telluride (CdTe) energy dispersive detector. The setup presented can be easily assembled and is meant to be used in an advanced laboratory physics course where students can observe with ease the effect of X-rays as they interact with matter to yield a characteristic fingerprint, a phenomenon that directly relates to atomic theory as well as to practical aspects. In the present case three pieces of metal are analyzed and their elemental content shown. Additionally the raw spectrum produced by the pyro-electric generator is also presented.

**Keywords:** XRF, fluorescence, non-destructive analysis, teaching.

## RESUMEN

Se presenta el análisis del contenido de elementos químicos, efectuado por medio de un generador pyroeléctrico y un detector de cadmio-telurio (CdTe) capaz de discriminar distintas energías. El arreglo experimental puede ser fácilmente ensamblado y esta diseñado para ser usado en el laboratorio avanzado, donde los estudiantes pueden observar con facilidad, el efecto que los rayos X tienen cuando interactúan con el material para producir espectros característicos. Los experimentos asocian fenómenos de la teoría con aspectos prácticos. En los experimentos presentados tres muestra de metales varios son analizadas y su contenido

elemental es indicado. Adicionalmente, se presenta el espectro que el generador pyroeléctrico produce.

**Descriptores:** FRX, fluorescencia, analysis no destructivo, enseñanza.

## INTRODUCTION

Elemental analysis, particularly when done in a nondestructive manner is a powerful technique that is within easy access to almost any laboratory. Students that are concurrently taking or have taken a Modern Physics course can greatly benefit their instruction from using a non-destructive technique based on a portable X-ray generator, an energy dispersive detector and a multichannel analyzer (MCA) connected to a personal computer. The X-ray generator, here used, takes advantage of polarization achieved by a crystal, LiTaO<sub>3</sub>, encapsulated together with a copper plate. A repeated warm-up and cool-down cycle is responsible for the generation of a potential difference adequate to yield tantalum (Ta) and copper (Cu) characteristic radiation superimposed on a bremsstrahlung profile. Thus the students confront themselves with reviewing the concepts of atomic structure and its relation to characteristic radiation, by contraposition to the concept of continuous radiation. Not only do the students experiment the basic aspects of the mechanisms involved, but they also appreciate more practical matters, as are the qualitative identification of elements present in a piece of material; in the current study, aluminum, lead and nickel, containing trace elements.

Typically, fluorescence analysis experiments have been performed using radioactive sources, Americium<sup>1</sup> (<sup>241</sup>Am) and Cobalt (<sup>57</sup>Co) (Dasgupta 1988 and Bennal 2005, respectively). The source activities were  $\approx 10^5$  Bequerel (Bq) ( $\approx 0.1$  milli-Curie) which required data collection times of about one hour. The alternative of using a pyro-electric crystal, as has been noted (Ida 2004), offers the possibility of a higher-activity-equivalent source,  $\approx 10^7$  Bq, that can be powered as required and is fairly portable, that additionally, has been configured in a compact setup that encloses a solid state detector (described below) inside a box made up of polyoxymethylene (known with the DuPont™ brand name, Delrin®).

## THEORY

To carry out elemental identification the technique of X-ray fluorescence offers a convenient option. X-ray photons (or some other particle) interact with inner-shell electrons of an atom delivering the energy to one of those electrons, creating thus a vacancy. Energy stability conditions in the atom will require that another electron from a higher shell would move to occupy the previously formed vacancy, but while doing so the electron gives off X-ray radiation that corresponds to the energy difference of the two positions. For instance, using the Siegbahn notation (Siegbahn 1930), K $\alpha$  radiation is produced when an electron from an L-shell occupies a position in the K-shell. At this point, it should be pointed out the

---

<sup>1</sup> Actually, the source of X-rays, or gamma-rays, is the decay product, Neptunium-237 (<sup>237</sup>Np).

there is competing phenomenon, known as Auger process (Auger 1927, Robinson 1923), a radiationalless transition, where the energy difference between shells is actually used to eject another electron, resulting in double ionization of the atom (Auger 1927, Robinson 1923, Beiser 2003). Whether an X-ray photon or an Auger electron is produced can be relatively well described by the fluorescence yield (Jenkins 1988):

$$\omega = \frac{Z^4}{A + Z^4} \quad (1)$$

where  $Z$  = atomic number and  $A$  = constant that depends on the atomic shell involved. The Auger yield is given as  $-(1-\omega)$ . A plot of both yields would show that for low  $Z$  elements, the Auger phenomenon will be predominant.

The phenomenon of pyro-electricity was clearly discussed using a crystal of cesium nitrate ( $\text{CsNO}_3$ ), which was basically a cryostat, with some additions, that took advantage of the large potential difference, about  $10^6$  V, developed during the cool-down cycle of  $\text{CsNO}_3$  (Brownridge 1992). Certainly, there are also other crystals, known to possess such advantageous feature, like lithium niobate ( $\text{LiNbO}_3$ ) and lithium tantalate ( $\text{LiTaO}_3$ ), as has been indicated elsewhere (Brownridge, 1999). In all cases, the residual electrons present in the vacuum, strike against the crystal or against a metallic plate, that also forms part of the vacuum chamber, as the potential difference mounts during polarization and depolarization (Brownridge 1999), i.e, the warm-up and cool-down cycles.

## EXPERIMENTAL SETUP

Figure 2 contains a schematic of the experimental setup used. The X-ray source is an Amptek COOL-X pyro-electric generator. The detector, which has a resolution of  $\approx 200$  eV at 22 keV, is of the solid state type, a 7-mm<sup>2</sup> CdTe crystal from Amptek, model XR-100T which is connected to the Amptek PX-2T module that contains the pre-amplifier, amplifier and power supply. Both, detector and pyro-electric generator, are Peltier cooled and thus affixed to 6-mm thick aluminum plates serving as heat sinks. The detector, as well as the source, make an angle of 45° respect to the sample surface. The output from the PX-2T is sent to a multichannel analyzer (MCA), Amptek pocket MCA 8000A, controlled via the serial port of a computer where all information is recorded. Detector sample and source are enclosed in a polyoxymethylene enclosure, of 20-mm thick walls, that serves a radiation shield to prevent from accidental radiation exposure.

The spectrum produced by the pyro-electric generator, figure 2, contains the bremsstrahlung, a broad feature that spans up to  $\approx 25$  keV. The narrower and more prominent features are the characteristic X-ray lines excited during the warm-up and cool-down cycles: (1) Cu KL<sub>3</sub> = 8.048 keV and Ta L<sub>3</sub>M<sub>5</sub> = 8.146 keV, (2) Cu KM<sub>2b</sub> = 8.9053 keV, (3) Ta L<sub>2</sub>M<sub>4</sub> = 9.3429 keV and (4) Ta L<sub>2</sub>N<sub>4</sub> = 10.895 keV; using the IUPAC nomenclature (Jenkins 1991). The Cu KL<sub>3</sub> and Ta L<sub>3</sub>M<sub>5</sub> lines are not resolved and represent the most intense line observed. It should be highlighted that Ta and Cu radiation are not produced simultaneously, Ta radiation occurs during temperature decrease, timed to 70 s duration. Cu radiation is

produced during temperature increase, during a time interval of 30 s. The excitation time intervals, of each element, stabilize after a three minute warm-up period.

The characteristic lines, figure 2, are also used for calibration purposes. The student here makes use of simple linear regression to find out the constants that correlate channel number with energy. In the present case:  $A \propto +B$ ; where  $A = 0.9237 \text{ keV}$  and  $B = 0.007113 \text{ keV}/\text{ch}$ .

No attempt was made to select one single radiation line since this allows for a higher equivalent source activity. The full spectral output is then directed at the sample to be analyzed for a predetermined time interval of 600 s. Samples of Nickel foil (99.95% purity, 0.009 mm thick produced by Goodfellow), aluminum (Al) and lead (Pb) scrap plates were irradiated. The Nickel (Ni) foil was placed in a self-supported holder that did not have the polymethyl methacrylate backing indicated in figure 1. The Pb and Al plates were 15 mm and 10 mm thick, respectively, therefore opaque to the X-rays.

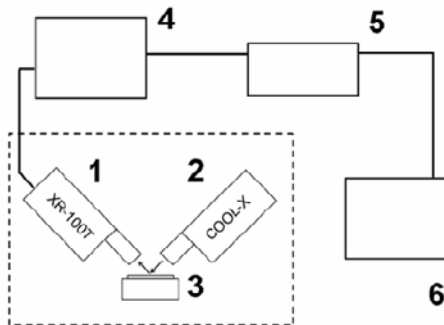


Figure 1. Experimental setup: (1) CdTe detector, (2) pyro-electric X-ray generator, (3) sample and polymethyl methacrylate (plexiglass) sample holder, (4) pre-amplifier and amplifier, (5) multichannel analyzer, and (6) computer. The dashed line represents the polyoxymethylene radiation enclosure that contains the sample, detector and source.

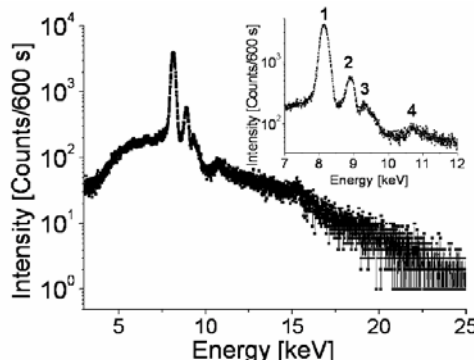


Figure 2. The spectrum produced by the pyro-electric generator consists of several characteristic lines and a bremsstrahlung that extends to about 25 keV. The inset indicates the energies that correspond to the characteristic lines: (1) Cu KL<sub>3</sub> = 8.048 keV and Ta L<sub>3</sub>M<sub>5</sub> = 8.146 keV, (2) Cu KM<sub>2b</sub> = 8.9053 keV, (3) Ta L<sub>2</sub>M<sub>4</sub> = 9.3429 keV and (4) Ta L<sub>2</sub>N<sub>4</sub> = 10.895 keV.

## RESULTS AND DISCUSSION

Irradiation of the Ni foil for 600 s produced the spectrum observed in figure 3. Lines (1) Co KM<sub>2</sub> = 7.649 keV, Co KM<sub>3</sub> = 7.649 keV, Ni KL<sub>2</sub> = 7.461 keV and Ni KL<sub>3</sub> = 7.478 keV, figure 3, are not resolved individually, but given the full-width-at-half-maximum (FWHM) it is relevant to consider the Co lines. Co is a common impurity found in Ni (Ramsden 1966). Line (2), figure 3, includes Cu KL<sub>3</sub> = 8.048 keV, Ta L<sub>3</sub>M<sub>5</sub> = 8.146 keV, Ni KM<sub>2</sub> = 8.265 keV, Ni KM<sub>3</sub> = 8.265 keV. Cu and Ta lines are not unexpected since they are contained in the source. Line (3) Zn KL<sub>3</sub> = 8.639 keV, indicates the presence of another impurity in the Ni foil.

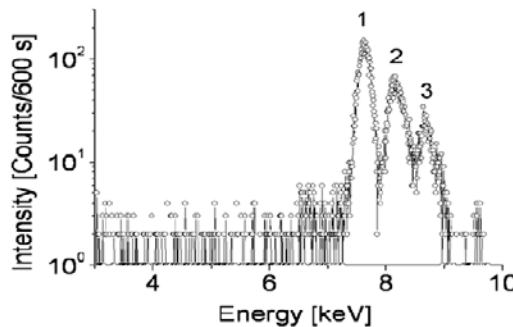


Figure 3. Spectrum from Ni foil after irradiation for 600 s. The characteristic lines identified are: (1) Co KM<sub>2</sub> = 7.649 keV, Co KM<sub>3</sub> = 7.649 keV, Ni KL<sub>2</sub> = 7.461 keV and Ni KL<sub>3</sub> = 7.478 keV, (2) Ta L<sub>3</sub>M<sub>5</sub> = 8.146 keV, Ni KM<sub>2</sub> = 8.265 keV, Ni KM<sub>3</sub> = 8.265 keV, and (3) Zn KL<sub>3</sub> = 8.639 keV.

In figure 4, the spectral content of a Pb plate, irradiated for 600 s, shows four statistically resolvable characteristic lines. Line (1) Cu KL<sub>3</sub> = 8.048 keV, Ta L<sub>3</sub>M<sub>5</sub> = 8.146 keV. Line (2) is formed by the superposition of Zn KL<sub>2</sub> = 8.616 keV, Zn, KL<sub>3</sub> = 8.639 keV, Cu KM<sub>2</sub> = 8.905, Cu KM<sub>3</sub> = 8.905 keV, while lines (3) Pb L<sub>3</sub>M<sub>4</sub> = 10.450 keV, and (4) Pb L<sub>1</sub>M<sub>2</sub> = 12.307 keV are singly defined, as it appears by their  $\approx$  200 eV FWHM. Some peaks appear to be located at  $\approx$  3 keV and 6.7 keV, which are probably escape peaks; statistically it was not possible to assign an elemental line.

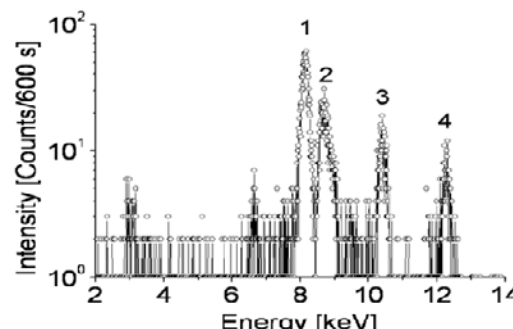


Figure 4. Spectrum from Pb plate irradiated for 600 s. Characteristic lines identified are: (1) Cu KL<sub>3</sub> = 8.048 keV, Ta L<sub>3</sub>M<sub>5</sub> = 8.146 keV, (2) Zn KL<sub>2</sub> = 8.616 keV, Zn, KL<sub>3</sub> = 8.639 keV, Cu KM<sub>2</sub> = 8.905, Cu KM<sub>3</sub> = 8.905 keV, (3) Pb L<sub>3</sub>M<sub>4</sub> = 10.450 keV, and (4) Pb L<sub>1</sub>M<sub>2</sub> = 12.307 keV.

The XRF spectrum from Al plate, figure 5, was recorded at 600 s and 1200 s, open circles and open triangles, respectively. The peak, Al KM<sub>3</sub> = 1.554 keV, is not easily discernible due to its proximity to the (1) Ta M<sub>5</sub>N<sub>7</sub> = 1.710 keV peak, which is a source peak and also contaminates the Al plate spectrum. The signal at, figure 5, (2) corresponds to Fe KL<sub>2</sub> = 6.391 keV, and that at (3) to Gd L<sub>2</sub>M<sub>4</sub> = 6.713 keV. Gadolinium is often added to Al alloys to improve the physical properties of the alloy, like strength or workability (Ohtsubo 2006 and Vakhobov 2003). Other source components, figure 5, are also found at (4) Cu KL<sub>2</sub> = 8.028 keV, Cu KL<sub>3</sub> = 8.028 keV, and Ta L<sub>3</sub>M<sub>5</sub> = 8.146 keV. Finally, figure 5, one more can be identified (5) Zn KL<sub>2</sub> = 8.616 keV, Zn, KL<sub>3</sub> = 8.639 keV, Cu KM<sub>2</sub> = 8.905 keV, and Cu KM<sub>3</sub> = 8.905 keV; source peaks closely overlap with Zn peaks. Statistically, no further peaks were identified at least within the collection times set.

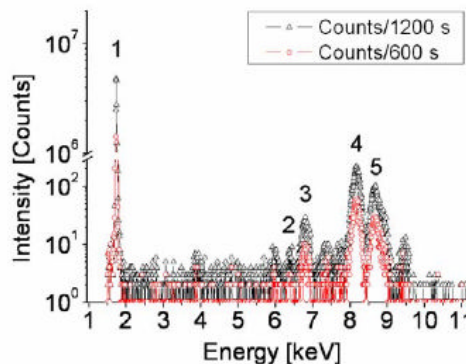


Figure 5. Spectrum from Al plate irradiated during two times intervals, 600 s (open circles) and 1200 s (open triangles). The characteristic lines identified were: (1) Al KM<sub>3</sub> = 1.554 keV (such elemental peak should actually be here but the current setup does not permit to observe it, due to air absorption and window loss; the peak shown is due to electronic noise), (2) Fe KL<sub>2</sub> = 6.391 keV, (3) Gd L<sub>2</sub>M<sub>4</sub> = 6.713 keV, (4) Cu KL<sub>2</sub> = 8.028 keV, Cu KL<sub>3</sub> = 8.028 keV, and Ta L<sub>3</sub>M<sub>5</sub> = 8.146 keV, (5) Zn KL<sub>2</sub> = 8.616 keV, Zn, KL<sub>3</sub> = 8.639 keV, Cu KM<sub>2</sub> = 8.905 keV, and Cu KM<sub>3</sub> = 8.905 keV.

The spectral content in all samples irradiated, has been identified by manually exploring the database in the X-ray data booklet, from the Center of X-ray Optics and Advanced Light Source (Kortright 2001). It would be additionally instructive that the student used Moseley formula (Moseley 1913, Moseley 1914) to express, in an approximate manner, the interrelation between atomic number, and energy difference between participating shells:

$$E = A(Z - b)^2 \quad (2)$$

where E = energy, A and b are constants related to the characteristic X-ray line and Z = atomic number.

The counting times employed in the set of experiments presented, are considerably below, an order of magnitude, than those presented when using radioactive sources (Dasgupta 1988 and Bennal 2005), but about six times larger than commercially available equipment already configured for XRF analysis, like, for instance, the X-MET300 from Oxford Instruments.

## CONCLUSIONS

A simple experimental setup has been suggested to explore, in the advanced laboratory, some aspects of the atomic theory, like the Bohr frequency relation, Moseley's law, and competing mechanisms that appear during X-ray excitation in a practical setting. In these experiments the students, even by solely identifying qualitatively the elemental composition of the samples, are compelled to research whether the energy values found during inspection of the spectrum are real or not. The student gets the opportunity of exploring more closely the origin of some of the impurities found in the samples, like Co, in the Ni-foil and Gd in the Al plate.

The experimental setup shown entails the need, and the instructional benefit, of improvement. Addition of a monochromator crystal, would permit the student to select a particular wavelength and open the possibility for additional analysis of the samples. Shaping energy filters could also be added.

Although commercial instruments are readily available in the market, a setup as the one discussed, is an uncomplicated system that the students in the average advance laboratory can assemble and use for practical purposes and rehearse their knowledge in material learned from the Modern Physics course.

## REFERENCES

- Auger, P., "Etude expérimentale des directions d'émission des photoélectrons", *J. de Phys. et le Radium*, 8 (2) pp. 85 (1927).
- Beiser, A., "Concepts of Modern Physics" (McGraw Hill, New York, NY, USA, 6<sup>th</sup>. Ed., 2003), pp. 258-260.
- Bennal, A.s., Shidling, P. D., Badiger, N. M., Thontadarya, S. R., and Hanumaiah, B., "Measurements of K X-ray fluorescence analysis". *Am. J. Phys.*, 73 (9) pp. 883 (2005).
- Brownridge, J. D. and Raboy, S., "Investigations of pyroelectric generation of x rays", *J. Appl. Phys.*, 86 (1) pp. 640 (1999).
- Brownridge, J. D., "Pyroelectric X-ray generator", *Nature*, 358 (6384) pp. 287 (1992).
- Dasgupta, M., Sharma, B. K., Ahuja, B. L., and Mohammad, F. M., "Some experiments on X-ray fluorescence for the student laboratory", *Am. J. Phys.*, 56 (3) pp. 245 (1988).
- Jenkins, R., Manne, R., Robins, R., and Senemaud, C., "Nomenclature system for X-ray spectroscopy", *Pure and Appl. Chem.*, 63 (5) pp. 735 (1991).
- Kortright , J. B., and Thompson, A. C., "X-ray emission energies" in "X-ray data booklet" (Ed. by A. C. Thompson and D. Vaughan, Lawrence Berkeley National Laboratory, Riverside, CA, USA, 2<sup>nd</sup> Ed., 2001), pp. 1.2-1.27.
- Moseley, H. G., "The high frequency spectra of the elements. Part II", *Philos. Mag.*, 27, pp. 703 (1914).
- Moseley, H. G., "The high frequency spectra of the elements", *Philos. Mag.*, 26, pp. 1024 (1913).
- Ohtsubo, H., Nakagawa, N., Shimizu, K., Shibata, K., Mitani, A., and Waku, Y. "Microstructure and high temperature strength characteristics of unidirectionally

- solidified  $\text{Al}_2\text{O}_3/\text{GdAlO}_3$  eutectic composite”, *Sc. Eng. Ceramics III Key Eng. Mat.*, 317-318, pp. 437 (2006).
- Ramsden, A. R., and Cameron, E. N., “Kamacite and taenite superstructures and a metastable tetragonal phase in iron meteorites”. *Am. Mineral.* 51, pp. 37 (1966).
- Robinson, H., “The secondary corpuscular rays produced by homogenous X-rays”, *Proc. Roy. Soc. London A*, 104 (727) pp. 455 (1923).
- Vakhobov, A. V., Shchevelev, Y. V., “High-temperature strength of high-purity aluminum alloyed with various elements”, *Metal Sc. Heat Treat.*, 45 (5-6) pp. 74 (2003).

***Chapter 6***

## **PROPERTIES OF THE NEAR FIELD PRODUCED BY A CIRCULAR NANOAPERTURE USING THE BETHE FORMULATION**

***J. M. Merlo<sup>1</sup>, E. Martí-Panameño<sup>2</sup> and F. Aguilar<sup>1</sup>***

<sup>1</sup> Coordinación de Óptica del Instituto Nacional de Astrofísica, Óptica y Electrónica, Luis Enrique Erro No.1, Tonantzintla, Puebla, México.

<sup>2</sup> Laboratorio de Fotónica, FCFM, Benemérita Universidad Autónoma de Puebla, Av. San Claudio S/N, C.U. , Puebla, Puebla, México

### **ABSTRACT**

Using Bethe's formulation and the complete Green function, we have found an analytic expression for the description of the nearby field that is produced by a circular nanoaperture. We also present the patterns of the square electric field that were obtained, which were similar to those reported before, and which have an exponential decay of the intensity in the direction that is perpendicular to the plane of the aperture.

### **1. INTRODUCTION**

At the end of the thirties past century, Stratton [1] proposed a solution to the problem of the electromagnetic wave diffraction that is produced by any type of aperture, with an arbitrary size. In order to achieve this, Stratton makes the hypothesis of the existence of charge densities and magnetic currents, with out a physical sense. Nevertheless, this represents a mathematical tool that makes possible the compensation of the inconsistencies of Kirchhoff's theory. A few years later, using this formulation, Bethe [2] obtains an analytic expression for the field that has been diffracted by a circular aperture whose diameter is much less than the wavelength of the incident radiation. The physical conditions of this problem are: a perfect conductor metallic screen that is sufficiently thick to not be transparent, while being thin enough to prevent the generation of modes in the interior of the aperture. Afterwards, we consider a circular aperture, which in the case of the optical range, is called

nanoaperture. Here, it is important to point out that Bethe found an analytic expression for charge densities and magnetic currents (senseless) which allowed him to find a closed expression for the electromagnetic field diffracted by the aperture in the far field approximation.

There are some papers [3,4] that were published some years ago that describe the electromagnetic field in the neighborhood of the small circular aperture. Nevertheless, it is important to state that all of them show computational results, obtained through the numerical solution of Maxwell's equations with their respective boundary conditions.

In this paper, we obtain an analytic equation for the near field, produced by a nanoaperture, which has the same characteristics as those that were considered by Bethe. In our theoretical development we are using the complete Green's function.

The paper is structured in the following way: the next section has a brief description of the theoretical basis. In section 3, we present the results that were obtained, and finally, in section 4, we conclude this article and present a guideline of future research.

## 2. THEORETICAL BASIS

Following Stratton's formulation [1], Bethe [2] obtains the expressions for the electric and magnetic fields that are diffracted by a circular aperture with arbitrary size:

$$\vec{E} = \int_S \vec{K}^* \times \nabla \phi d\sigma, \quad (1)$$

$$\vec{H} = \int_S (ik\vec{K}^* \cdot \nabla \phi - \eta^* \nabla \phi) d\sigma. \quad (2)$$

where  $\vec{K}^*$  y  $\eta^*$  are respectively the magnetic current density and the magnetic charge density. These magnitudes can be described considering the following boundary conditions:

$$\vec{K}^* = \frac{1}{\pi} \left[ ik(a^2 - r'^2)^{\frac{1}{2}} \vec{H}_0 + \frac{1}{2(a^2 - r'^2)^{\frac{1}{2}}} \vec{r}' \times \vec{E}_0 \right], \quad (3)$$

$$\eta^* = \frac{1}{\pi^2 (a^2 - r'^2)^{\frac{1}{2}}}. \quad (4)$$

where  $k$  is the propagation vector,  $a$  is the aperture radius,  $r'$  is the integration coordinate and which lies on the same plane as the aperture, and  $\vec{E}_0, \vec{H}_0$  are the incident electric and magnetic fields, respectively.

In his paper, Bethe made the approximation  $1 \ll kr$ , where  $r$  is the observation point, in order to calculate the expression for a field that is far away from the circular aperture. This results in the Green function:

$$\varphi = \frac{e^{ikr}}{r} \quad (5)$$

This is the point in which our research separates from Bethe's work. We now propose that  $kr \ll 1$ , which obliges us to make a detailed analysis of the term,

$$|\vec{r} - \vec{r}'| \quad (7)$$

of the Green function (7):

$$\varphi = \frac{e^{ik|\vec{r} - \vec{r}'|}}{|\vec{r} - \vec{r}'|}, \quad (8)$$

Basing ourselves on figure 1, we make the analysis of (7), resulting in:

$$|\vec{r} - \vec{r}'| = r \left[ 1 + \left( \frac{r'}{r} \right)^2 - 2 \frac{r'}{r} \cos \theta \right]^{\frac{1}{2}}, \quad (9)$$

where  $\theta$  is the angle that is formed by the vectors  $r$  and  $r'$ . In the particular case which is being analyzed, we suppose that the size of  $r \sim a$ ; therefore,  $r' \sim r$ , thereby implying that:

$$|\vec{r} - \vec{r}'| = r [2 - 2 \cos \theta]^{\frac{1}{2}}, \quad (10)$$

Note that in eq. (10), there is an additional term that is not present in Bethe's approximation, which is  $\cos \theta$ . This term changes the configuration of the field.

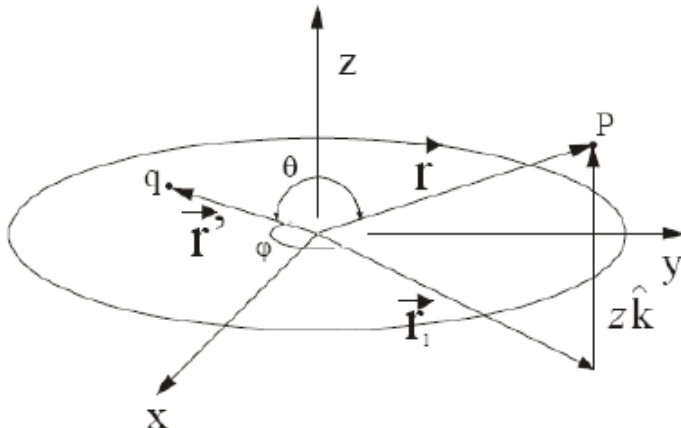


Figure 1. Scheme of the analysis of the circular aperture.

Further, from figure 1 we can see that

$$\cos\theta = \frac{(r^2 - z^2)^{\frac{1}{2}} \cos\varphi}{r}, \quad (11)$$

where  $\varphi$  is the angular coordinate that lies on the aperture plane.

Substituting eq. (11) in eq. (8), we obtain the Green function in the approximation of a nearby field:

$$\varphi = \frac{\exp\left(ikr\left[1 + \left(\frac{r'}{r}\right)^2 - 2r' \frac{(r^2 - z^2)^{\frac{1}{2}} \cos\varphi}{r^2}\right]^{\frac{1}{2}}\right)}{r\left[1 + \left(\frac{r'}{r}\right)^2 - 2r' \frac{(r^2 - z^2)^{\frac{1}{2}} \cos\varphi}{r^2}\right]^{\frac{1}{2}}}, \quad (12)$$

Lastly, the analytical expression of the electric field is given by:

$$\vec{E}(\vec{r}) = -\frac{\hat{r}}{2^{5/2}} \frac{1}{\pi^2} \times (2ik\vec{H}_0 E_H(z) + \vec{E}_0 \times \vec{r}' E_E(z)), \quad (13)$$

where

$$E_H = a - \frac{z^3 \sqrt{1 + \left(\frac{a}{z}\right)^2} \operatorname{Arcsinh}\left(\frac{a}{z}\right)}{a^2 + z^2} + \frac{8a^5 Hgeom2F1\left[2, 3, \frac{7}{2}, -\left(\frac{a}{z}\right)^2\right]}{15z^4} \quad (14)$$

and

$$E_E(z) = \frac{1}{16\sqrt{2} \sqrt{1 + \left(\frac{a}{z}\right)^2} (a^2 + z^2)} \left( a^4 \left( -35 + 12\sqrt{1 + \left(\frac{a}{z}\right)^2} \right) + 12a^2 \left( -7 + 5\sqrt{1 + \left(\frac{a}{z}\right)^2} \right) z^2 \right) + \\ + 48 \left( -1 + \sqrt{1 + \left(\frac{a}{z}\right)^2} \right) z^4 + \frac{a^2}{2}. \quad (15)$$

### 3. RESULTS OBTAINED

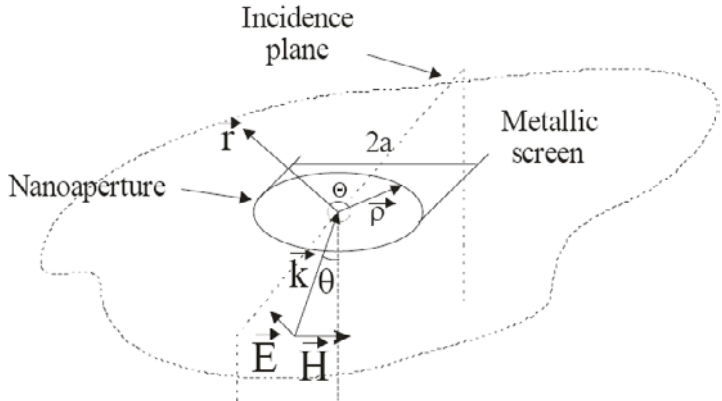


Figure 2. Scheme used for the calculation of the patterns of the squared electric field that are shown in this section.

In figure 2, we show the scheme used in our calculations. In all the disused results one of the main parameters is the elevation over the nanohole where we are calculating the values of the field intensity, here we point out that this elevation corresponds to the center of the nanoaperture.

In this section, we present the intensity patterns of the squared electric field, for the particular case of an aperture with a radius of  $a=\lambda/60$ , that is being illuminated from below of the sheet by a normally incident plane wave. The heights ( $z$ ) that were used for the calculations are specified at the caption of each figure. The arrows that are shown in the upper part of the patterns display the polarization of the incident field.

In figure 3, it is possible to see the presence of the bipolar behavior of the aperture, as predicted by Bethe's model. It is also possible to see that in the center of the aperture has the highest intensity. This implies that the optical entrapment of particles is possible, due to the conditions of our approximation.

In figure 4a), we have two lateral lobules in the direction of the polarization of the incident field, which constitutes a result that has already been reported in Moerland [5]. Nevertheless, in our model, we do not discard the higher order terms in the Green function.

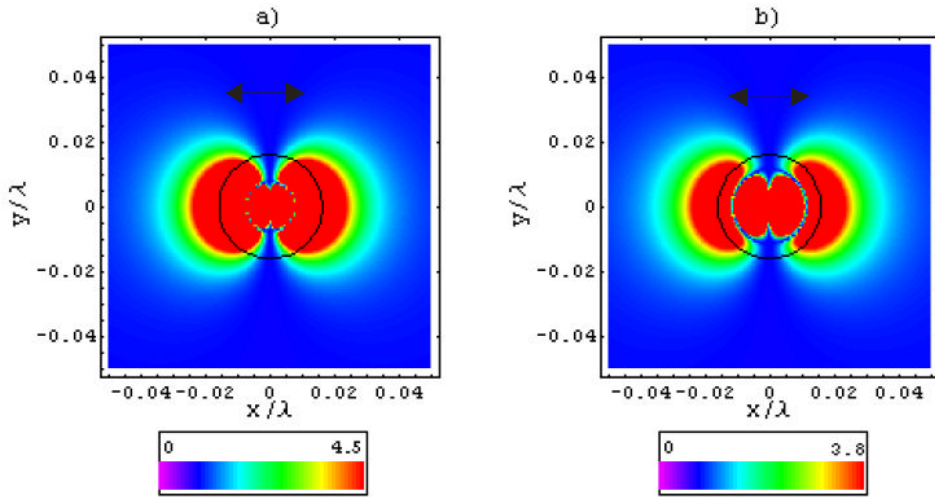


Figure 3. The patterns of the squared electric field produced by a nanoaperture under normal incident radiation. The heights that were used in the calculations are: a)  $z=0.15a$ , b)  $z=0.225a$ . The black circular line shows the position of the aperture.

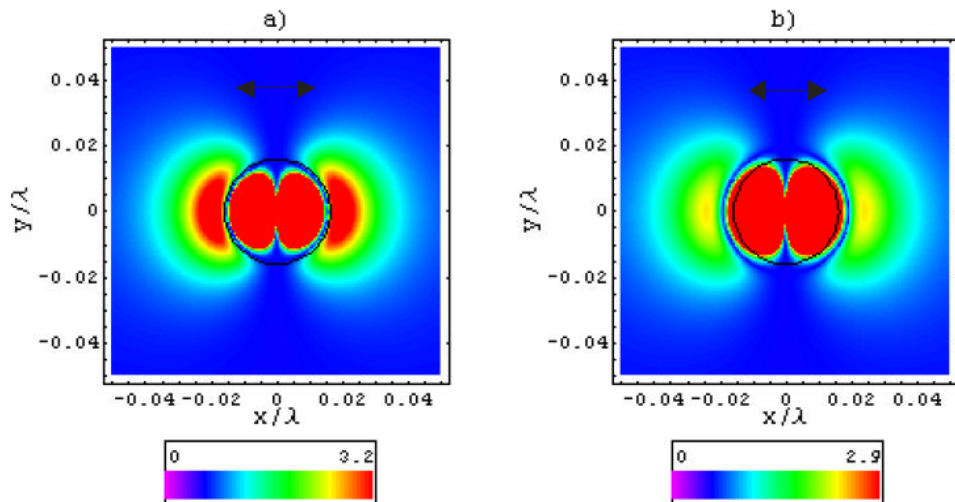


Figure 4. The patterns of squared electric field produced by a nanoaperture at a normal incident direction. The heights that were used for the calculations are: a)  $z=0.3a$ , b)  $z=0.375a$ . The black circular line shows the position of the aperture.

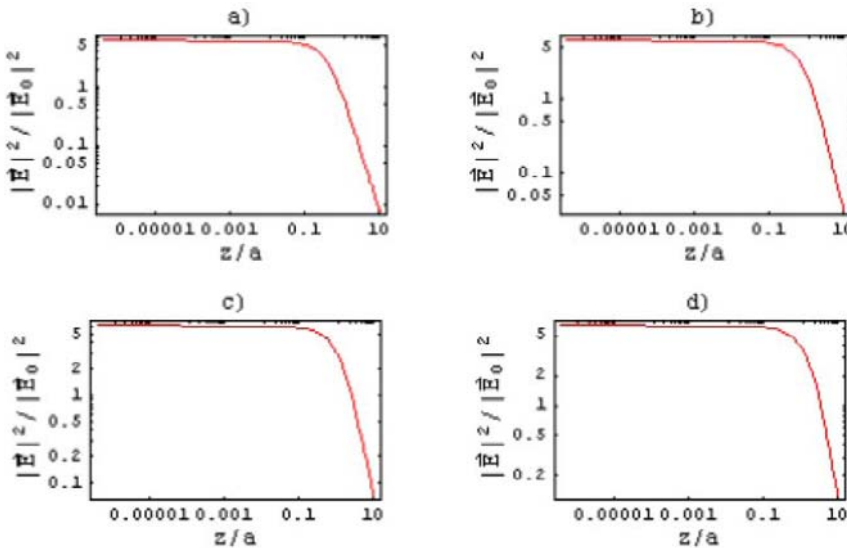


Figure 5. The decay of the normalized squared electric field. The nanoaperture radio are: a)  $a=5\text{ nm}$ , b)  $a=10\text{ nm}$ , c)  $a=20\text{ nm}$ , d)  $a=30\text{ nm}$ . The incident wavelength is 600 nm. The plots have a log-log scale.

In figure 5, the dependence of the squared electric field respect to the distance is presented. Here is possible to observe that this dependence has an exponential like decay that is typical of the evanescent wave. Note that the decay is more pronounced when the size of the aperture increases, due to the effects of diffraction.

Other calculations of the intensity patterns under oblique incident directions, entrapment forces that are produced in the near field of the aperture, and the new configuration for an optical nano tweezers can be found in [6].

#### 4. CONCLUSIONS

In this paper, we show the explicit expression of the nearby field that is produced by circular nanoapertures, using the complete Green function. The field has a behavior that had already been reported. We reproduced the exponential decay of the magnitude of the squared electric field, which implies that the model reproduces the conditions of a real experiment. We also propose the conditions that are necessary for the entrapment of conducting particles that have size that is smaller than the diameter of the aperture, in a selective mode. We also report the use of beams that have different profiles for the illumination of the sheet.

#### Biographic Note of the Authors

Juan Manuel Merlo studied his B. Sc. in the Physical-Mathematical Sciences Faculty of the BUAP from 1998 to 2003, and his M. Sc. in Optoelectronics in the same place from 2004 to 2006. Right now he is into his third year of his Ph. D. thesis in Optical Sciences in the INAOE.

## REFERENCES

- [1] Stratton (1939)., et. al. Phys. Rev. 36, 99.
- [2] Bethe, H.A. (1944) The Physical Review 66, 7.
- [3] Leviatan, Y. J. (1986) App. Phys. 60, 1577-1583..
- [4] Roberts, A. (1993) “*Near field optics*”. Ed. Kluwer Academic Publishers, pp. 221-228
- [5] Moerland, (2005) et. al. Opt. Exp. 13, 5.
- [6] Merlo R, J.M. y Martí P, E. (2006). “Propiedades del campo cercano producido por nanoaberturas y condiciones de atrapamiento óptico de partículas”. Tesis de Maestría, BUAP.

*Chapter 7*

## TEACHING NANOSTRUCTURES USING THE SIMPLE INFINITE POTENTIAL WELL MODEL

***R. Rodriguez-Mijangos and G. Vazquez-Polo<sup>1</sup>***

Centro de Investigación en Física Universidad de Sonora

A.P. 5-88,83190; Hermosillo, Sonora Mexico

<sup>1</sup> Instituto de Física UNAM, A.P.

20-364, 01000, MÉXICO D. F; México

### ABSTRACT

In this work we use the know result for the ground state energy of the infinite potential well. Such energy value is compared to that obtained using the finite potential well result taken from technical literature using formal quantum mechanics. We used this result and current thermal concepts in semiconductors to estimate the size of novel quantum structures such as the so called nanostructures quantum devices, currently under study in electronic solid state physics. This idea could be useful in teaching undergraduate introductory applied physics courses.

**Keywords:** Applied Modern Physics, Infinite Potential Well, Nanostructures devices.

### INTRODUCTION

Before the advent of the formal development of Quantum Mechanics a few simple and fundamental problems were worked out exactly. That was the case of the Bohr atomic model for the Hydrogen atom. This kind of problems are treated in quantum mechanics and modern physics textbooks prior to the introduction of Schrödinger's equation with which more rigorous and general solutions can be obtained than those using the primitive approach. In this work we use the ground state energy of infinite potential well related with a semiconductor system with a nanostructure architecture.

The result presented here using the ground state of an infinite potential well are quite simple and .this could stand as a quantum mechanics example to be included in introductory

textbooks of the subject for students not familiar with this concepts,, serve to introduce the concept of infinite potential well later treated with Schrödinger's equation in more advanced courses.. We know that in most standard text books on Quantum Mechanics usually discuss three problems with exact analytical solution: The infinite potential well, the harmonic oscillator and the Hydrogen atom [Saxon, D. S. (1968)]. Is possible find out other problems with a exact analytical solution in the research literature [Cooper, F. (1995), Plastino, A. R. (1999)]. The infinite potential problem is calculated in a simple form and is possible handled in a simple formulation. The approach presented here, given the quantum mechanics result for a infinite potential well, permit handle the calculation of a nanostructure if is used it as a starting point., this is valuable as a teaching tool to introduce for first time in the class room or a textbook simple quantum mechanics results and its use for application in nanostructures..

## THEORY

The ground state energy of the potential well, with width L is:

$$E = \frac{\hbar^2}{8mL^2} \quad (1)$$

That value of the equation (1) corresponds to the ground state of an infinite potential well [Saxon, D. S. (1968)].

The consideration of infinite well barrier is meaning physically that the trapped particle has energy much smaller than the size of the well barrier.

For application of the result for a quantum well we consider an electron moving in a nanostructure (with quantum size effects) confining this electron in a region L.[Rodriguez-Mijangos, R. (2005)]. In particular in semiconductor materials we observe this quantum confinement by absorption and emission of light; that is, by its optical properties.

What is the dimension of that system for an electron moving to T temperature? The electron is in move only in one direction, using the energy equipartition principle it has energy of the order of  $\frac{1}{2}(kT)$ , where k is the Boltzman constant [Sears, F. W. (1982)] then, using the last equation, L is:

$$L = \frac{1}{2} \frac{\hbar}{\sqrt{mkT}} \quad (2)$$

In a semiconductor, the electron is not free, is linked to periodic potential of the crystal, is possible represent that movement in a simple form, it's inertia to move is simulated with a "different mass" is moving with a equivalent mass  $m^*$  in the semiconductor, such statement is rigorously demonstrate in solid state textbooks [Kittel, C. (1986)], a typical value is  $m^* = 0.1m_0$ . At room temperature  $kT = 1/40$  electron Volts (eV.). With these values we find that we must have L approximately to 10 nanometers, this is the origin of the nanostructure word that is a structure of nanometers size. Thus a "thin semiconductor layer of thickness of 1

micrometer is not thin for confinement effects. It is in fact a crystal which would not exhibit any quantum size effects. To observe quantum size effects we require thinner layers.

The very small crystal dimensions required to observe quantum confinement in semiconductors are recorded in a laboratory by optical spectroscopy, linked with the observation of the absorption light of an electron for up form ground state to an excited state. Is possible the theoretical knowledge of the excited status using Quantum mechanics methods [Singh, J. (1997)].

The ground state of a 10 nm GaAs quantum wells using the energy value for the infinite well has a value of 57 meV [Fox, M. (2001)]; a more realistic value accordingly with the experiment is 32 meV that is obtained using a finite potential well. We have this result only using quantum mechanics methods [Gasiorowicz, S. (1974)].

Although in this problem, the infinite well model overestimates the confinement energies, it is a useful starting point for the discussion of the physics because of its simplicity. For more exactly values you can see [Harrison, P. (2000)].

Semiconductor quantum wells are examples of nanostructures, build by artificial crystals in. layers of different materials grown on top of a thicker crystal. The structures are made by the specialized epitaxial crystal growth techniques. The layer thicknesses of the crystal growth can be controlled with atomic precision. This makes it easy to achieve the thin layer thicknesses required to observe quantum confinement of the electrons in a semiconductor room temperature. An example of nanostructure devices is a series of single GaAs/AlGaAs quantum wells- The single quantum well is formed in the thin GaAs layer sandwiched between AlGaAs layers. This type of structure is either multiple quantum wells. In this system the individual are isolated from each and other, are isolated from each other, and the properties are essentially as those of single quantum wells. They are often used in optical applications to give a usable optical density. It would be very difficult the optical absorption of a single 10 nm thick quantum well, simply because is so little material to absorb the light. By growing many additional properties, the absorption increase of the individual quantum wells. [Fox, M. (2001)].

Also is possible make a nanostructure system with semiconductor doped glasses such as CdS, ZnS, they are place into the glass in the melt process become smaller crystals inside the glass. The dimensions of the small crystals depend of the glass fabrication, with careful preparation is possible to have nanocrystals with good size uniformity

## CONCLUSION

The expression knows of the infinite potential well and the exact value of the ground state of energy are useful the for introduce an idea of modern systems handled in solid state The, use of simple arguments give to undergraduate students, in First courses of Applied Modern Physics in Engineering, Chemistry and Physics Programs given, the opportunity of obtain a primary knowledge of the nanostructures build and a first idea of this novel systems handled actually in applied solid state physics.

## **ABOUT THE AUTHORS**

R..Rodríguez-Mijangos

Realized studies of Physics and Ph D in the Universidad Nacional Autonoma de Mexico  
Researcher in the Universidad de Sonora, Mexico, in the Solid State Academy of Physics

Investigation Department.

Themes of interest: Optical properties of solids, Thermal Physics, Superconductivity, Crystallography, Nanostructures, Mechanics of Fluids.

The last works are associated to mixed dielectric crystals.

Author of many scientific articles in international arbitrated journals.

Teach Statistical Mechanics in graduate level in the Universidad de Sonora.

Direction of several thesis.

Member of American Physical Society, Sociedad Mexicana de Cristalografía and others.  
[mijangos@cajeme.cifus.uson.mx](mailto:mijangos@cajeme.cifus.uson.mx)

G. Vazquez-Polo

Realized studies in Physics and Ph D in the Universidad Nacional Autonoma de Mexico.

Researcher in the Universidad Nacional Autonoma de México, in Solid State Department of Institute of Physics..

Themes of interest: Optical properties of solids, composite materials, Electronic Microscopy, polymeric materials, computational diffraction spectra. Cuasi-crystals, Nanostructures.

Author of many scientific articles in international arbitrated journals.

Teach Materials Science in Engineering Faculty of Universidad Nacional Autonoma de Mexico.

Direction of several thesis.

Member of Academia Mexicana de Ciencias, Sociedad Mexicana de Fisica and others

[vazquez@fisica.unam.mx](mailto:vazquez@fisica.unam.mx)

## **REFERENCES**

Cooper, F., Khare A., and Sukhatme, (1995), *Phys. Rep.*251, 267.

Fox M. (2001), “Optical Properties of Solids” *Master series in Condensed Matter Physics*

Gasiorowicz, S. (1974), “Quantum Physics” *John Wiley and Sons.*

Harrison, P. (2000). “Quantum Wells, Wires and Dots” *John Wiley and Sons.*

Kittel, C.(1986). “Introduction to solid state physics” *john Wiley and Sons.*

Plastino, A. R. , Rigo, A., Casas, F., Garcias, F. and Plastino, A. (1999), *Phys Rev. A*, 60, 318.

Rodriguez-Mijangos, R., Vazquez-Polo, G. and Cervantes, M. (2005), *Rev. Mex. de Fis E* 51, 83.

Saxon, D. S. “Elementary Quantum Mechanics” (1968). *Holden Day San Francisco.*

Sears, F. W., Zemansky, M. W. and Young, H. D. (1982), “University Physics 6<sup>th</sup> Edition”  
*Addison Wesley Publisher.*

*Chapter 8*

## **SYNTHESIS AND CHARACTERIZATION OF PT AND PT-AU NANOPARTICLES FOR CATALYSIS AND PEM FUEL CELLS APPLICATIONS**

***M. Gutiérrez Arzaluz<sup>1</sup>, B. Ruiz Camacho<sup>1</sup>,  
V. Múgica Álvarez<sup>1</sup>, O. Solorza Feria<sup>2</sup>  
and M. Torres Rodríguez<sup>\*1</sup>***

<sup>1</sup> Área. de Química Aplicada, Universidad Autónoma Metropolitana,  
Av. San Pablo 180, CP 02200 Azcapotzalco,  
México D.F., Tel: 53189075, Fax: 53189000 ext 2088

<sup>2</sup> Depto. de Química, Centro de Investigación y de Estudios  
Avanzados del IPN, CP 07360, México D.F.

### **ABSTRACT**

This work reports the synthesis and characterization of platinum, Pt, and platinum-gold, Pt-Au, nanoparticles having 2-5 nm, for their application in catalysis and low temperature fuel cells. The Pt and Pt-Au, with a 2:1 molar ratio, nanoparticles were prepared through a chemical reduction method of the complexes H<sub>2</sub>PtCl<sub>6</sub>·6H<sub>2</sub>O and HAuCl<sub>4</sub>·3H<sub>2</sub>O, used as precursor's salts and polyvinylpyrrolidine as complexing agent. The resulting nanoparticles were supported on Vulcan carbon powder XC-72R using two impregnation methods, in situ and mechanical. The materials obtained Pt/C and Pt-Au/C were characterized by TEM and XRD. The results of the former indicated a homogeneous distribution of nanoparticles having 5 nm as average size over the carbon, aside some nanometric agglomerates. Further, the XRD results allowed identification of crystallographic distances for both metals, though in the bimetallic case with a small shift from the standard position reported, possibly due to the Pt-Au interaction.

---

\* trm@correo.azc.uam.mx

## 1. INTRODUCTION

The nanoparticles' synthesis of different metals has attracted enormous interest due to their potential uses as catalysts, sensors, optoelectronic devices, among others. Their properties are mainly dependent on size, shape and structure. For catalysis applications, control of their properties is of fundamental relevance to achieve significant activity and selectivity.

In the future, refining and petrochemical processing will show lower energy consumption, small or nearly null pollutants generation, lower operations costs, being in general environmentally friendly. The possibility to comply to each of the last four essential demands is based on the use of much more efficient catalysts having proper control of their properties. The synthesis of nanoparticles bearing controlled sizes may indeed assist in the preparation of the catalysts having such features that may be completely different to those displayed by their normal size counterparts.

Modern colloids science is attributed to Michael Faraday (Toshima N. y Yonezawa T.) who developed in 1857 a method to prepare a dispersion of metal Au nanoparticles [1] which are now frequently produced via chemical reduction of the corresponding Au<sup>III</sup> salt to Au<sup>0</sup>, using citrate ions that adsorb on the surface of the Au nanoparticles, becoming stabilized by electrostatic repulsive forces. The citrate ions reduce the Au<sup>III</sup> ions, control the growth of the Au atoms and stabilize the Au nanoparticles obtained [2].

The oxidation of volatile organic compounds, VOCs, can be efficiently achieved using Au nanoparticles that are active at temperatures lower than 100 °C. The possibility to operate commercially with catalysts based on this sort of materials would facilitate significant VOCs reduction or elimination, without having to resort to an additional heating system, which means that process cost reductions can be achieved to the level of the precious metal costs. Other interesting reactions include hydrocarbon selective and unselective oxidation, the hydrogenation of unsaturated hydrocarbon and that of CO [3, 4], and NO<sub>x</sub> reduction with H<sub>2</sub>, C<sub>3</sub>H<sub>6</sub> o CO [5].

On another respect, during the last decades the direct conversion of chemical energy into electric energy via fuel cells, PEMFC, has increasingly become a focal point of electrochemical research and technology development to generate efficiently clean energy for many important applications, like in transport [6], to name a basic one in particular for large air-polluted urban areas. However, one of the key factors that has slowed down massive use of PEMFC is their still elevated cost, which is associated to availability of cost-effective Pt-based electrocatalysts, because of the inherent precious metal costs. A second problem to be solved with the use of Pt is its poisoning tendency since the CO molecules present in the feed fuel strongly adsorb on the metal surface, thus provoking significant efficiency reductions. Considering that the efficiency in a PEMFC is directly related with the electrocatalysts' activity, this is, with its particle size, its geometry and composition, its dispersion and interaction with the support, it is fundamentally important to control such factors during the catalysts synthesis process by adequate selection of the synthesis and impregnation methods.

Nord and Turkevich evolved on Faraday's idea and used a synthetic polymer like polyvinyl alcohol as colloid protector to stabilize the Pd or Pt nanoparticles and its application in catalysis [7]. Further, Turkevich et al., introduced Pd, Pt and Au particles [8] produced through the citrate reduction reaction, and used them as supported catalysts.

The metal nanoparticles can be prepared in two different forms, one by bulk subdivision called the physical method, and the other through particles' growth from the metal atoms, derived from molecular or ionic precursors, termed the chemical method, see figure 1. This preparation method is most convenient to obtain small uniform nanoparticles, because in this case the atomic aggregation is the most important step to control the size and uniformity of the resulting metal particles.

One of the methods proposed in the literature [9-15] to synthesize colloidal nanoparticles, having high catalytic activity, is the chemical reduction method, which is very simple and reproducible, based on the metal salt reduction to its corresponding zerovalent metal atom, by means of a reducing agent, like H<sub>2</sub>, alcohols, hydrazine, diboranes, and others. The said metal atoms tend to group to gather as atomic clusters that can form particles, the growth of which can be controlled through a complexing or stabilizing agent, like a polymer, EDTA, surfactants, P, S and N ligands, phosphines, and some others.

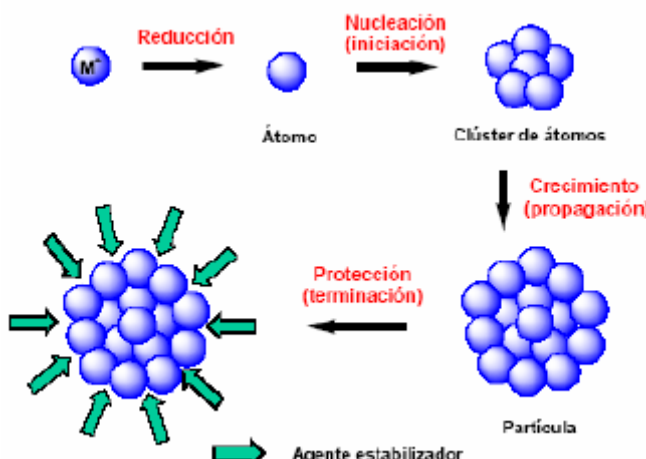


Figure 1. Scheme of formation, growth and stabilization of nanoparticles, chemical method.

This work presents the results obtained during the synthesis of Pt and Pt-Au nanoparticles with particle size smaller than 10 nm and their characterization. The outcomes indicate that the catalysts obtained can be considered candidates to evaluation during hydrogenation reactions in liquid phase and used as cathode in PEM.

## 2. EXPERIMENTAL

### 2. A. Synthesis of Pt Nanoparticles

The synthesis method used, consisted in reducing the Pt precursor salt following equation (1) below; the actual procedure is based on formation of a metal complex of the salt H<sub>2</sub>PtCl<sub>6</sub>·6H<sub>2</sub>O and the stabilizing agent polyvinylpyrrolidone, MM = 55000, at 96 °C as reflux temperature and a molar ratio Pt/PVP = 15. The metal complex was reduced to zerovalent metal by addition of the reducing agent C<sub>2</sub>H<sub>5</sub>OH.



The reaction (1) was carried out in basic media at pH = 12 using NaOH and NH4OH 0.5M to adjust the pH. In the literature [10] it is reported that to control the particle size as a function of the initial pH of the solution because the pH influences the reduction rate of the complex, which in alkaline media this is faster thus giving a smaller particle size. Two different hydroxides were used to examine their effect on the catalytic activity of the final product. NaOH is the hydroxide normally reported in the literature [11-15] for the purpose of pH adjustment. However, when using NaOH the reaction between this base and the precursor salt H<sub>2</sub>PtCl<sub>6</sub>·6H<sub>2</sub>O produces NaCl, which if not fully eliminated for it remains deposited on the surface of the Pt catalyst, thus affecting adversely its activity. This situation is not observed when using NH<sub>4</sub>OH; the Pt powders obtained were dried and calcined for 3 h at 450 °C under air flow at 20 ml/min to eliminate the polymer and to activate the surface of the nanoparticles. Subsequently, a second heat treatment to 350 °C under a H<sub>2</sub> stream with 20 ml/min for 2 h, allowed further reduction.

## 2. B. Synthesis of Bimetal Pt-Au Nanoparticles

Regarding the bimetal Pt-Au catalyst with a 2:1 molar ratio, the synthesis method used was the so-called successive reduction [11], taking into consideration that the Au reduction potential is greater than that of Pt [12] and following the same Pt nanoparticles synthesis method, after initiated the Pt reduction it was then added 1 ml of Au 1.38 x 10<sup>-3</sup> M solution. Once obtained the Pt and Pt-Au nanoparticles, these were supported on Carbon Vulcan XC-72R, using two impregnation methods: 1) in-situ and 2) mechanical, to evaluate the effect of the dispersion and interaction of the nanoparticles with the support on their activity. There were four catalytic materials obtained through these methods that were classified as indicated in table 1.

**Table 1. Pt and Pt-Au electrocatalysts obtained by chemical reduction**

Catalyst	Impregnation method	Sample
Pt	Mechanical	M1
Pt-Au	Mechanical	M2
Pt/C (NaOH)	In-situ	M3
Pt/C (NH <sub>4</sub> OH)	In-situ	M4

Hence, when assessing the four catalysts, it can be inferred from samples M1 and M2 the effect of Au on the catalytic activity, whereas from samples M1 and M4, it would be the catalytic effect exhibited as derived from the impregnation method, either mechanical or in-situ. Lastly, from consideration of samples M3 and M4, the effect of the hydroxide used can be discussed.

## 2. C. Physicochemical Characterization

The catalysts obtained were characterized by means of XRD and TEM. The diffractograms were recorded with the aid of a Bruker D8 Discover diffractometer, from  $20^\circ$  to  $90^\circ$   $2\theta$  at  $1^\circ/\text{min}$  with Cu K $\alpha$  at 40 kV. The TEM preparation included ultrasonic dispersing by dripping the ethanol-suspended samples onto carbon coated copper grid.

## 3. RESULTS AND DISCUSSION

Figure 2 shows the XRD diffractograms for samples M1 and M2 that reveal the Pt peaks for planes (111) and (200) located at  $39.76^\circ$  and  $46.24^\circ$ , respectively, which confirms that all samples contain Pt. For the bimetal sample M2, aside the Pt peaks there were also those for Au (111) and (200) located at  $38.18^\circ$  and  $44.39^\circ$ ; these values are slightly shifted, which is ascribed to the interaction Pt-Au. The diffractogram for sample M3 displayed three peaks located at  $31.75^\circ$ ,  $45.4^\circ$  and  $56.6^\circ$   $2\theta$  degrees, that corresponded to NaCl, thus suggesting that the sample was synthesized using NaOH as an obvious residue from synthesis the reaction, which undesirably deposited onto the catalyst's surfaces. However, the corresponding signal was not detected with sample M4 that was synthesized under the same conditions as sample M3, though using NH<sub>4</sub>OH instead, which leads one to assume that this hydroxide decomposes and is eliminated at the synthesis temperature as NH<sub>3</sub>(g) and HCl(g).

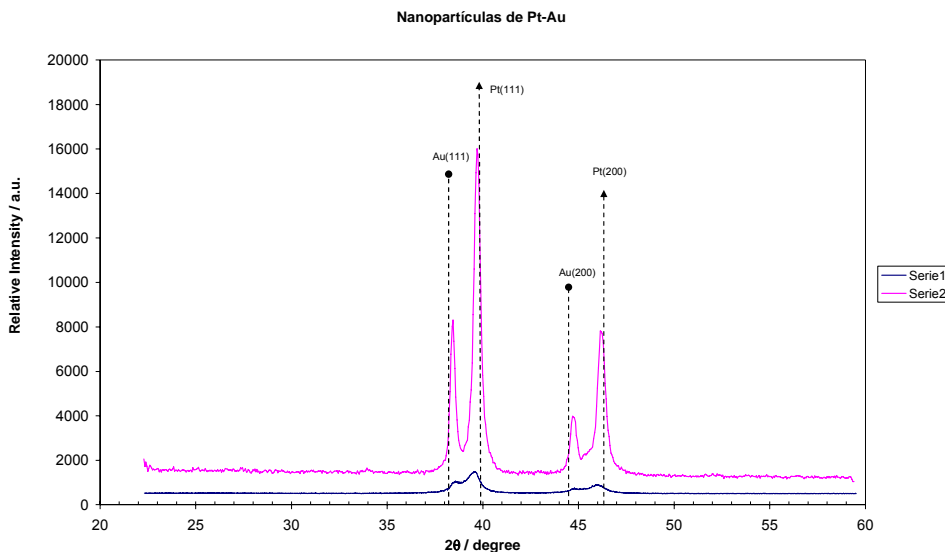


Figure 2. Diffractograms of the Pt and Pt-Au, M1 and M2 electrocatalysts.

Figure 3 shows the transmission electron microscopy micrographs bright field of the Pt-Au catalyst M2. The magnification bars indicate the relative scales of 20 and 5 nm respectively. Also a distribution of the Pt-Au nanoparticles is observed on the support where few of them appear to have agglomerated randomly over the carbon-copper support. Nevertheless, their spherical shape becomes obvious with an average size of  $<10$  nm,

however, the Pt-Au agglomerates have greater sizes. Also, the figure displays the elemental analysis as obtained from the sample M2 through energy dispersive analysis, EDS, on the particles; the diagram gives the relative intensity peaks as cps for Pt and Au indicating that height of the peaks plotted gives an idea of the relative amounts of the element present at the zone where the electron beam interacts with the sample; the carbon and copper signals are expected as they are the supports and another peak that resulted from the interaction between the two metals.

In order to proceed to a more detailed crystallographic description, the Rapid Fourier Transform, RFT, was applied to the high resolution micrographs by means of the Digital Micrograph software, which permitted to emulate the electron diffraction patterns, not shown here; the results corroborated that the analysis performed of the possible crystallographic planes and the corresponding distances matched with presence of Pt and Au, as reported in the literature [13]

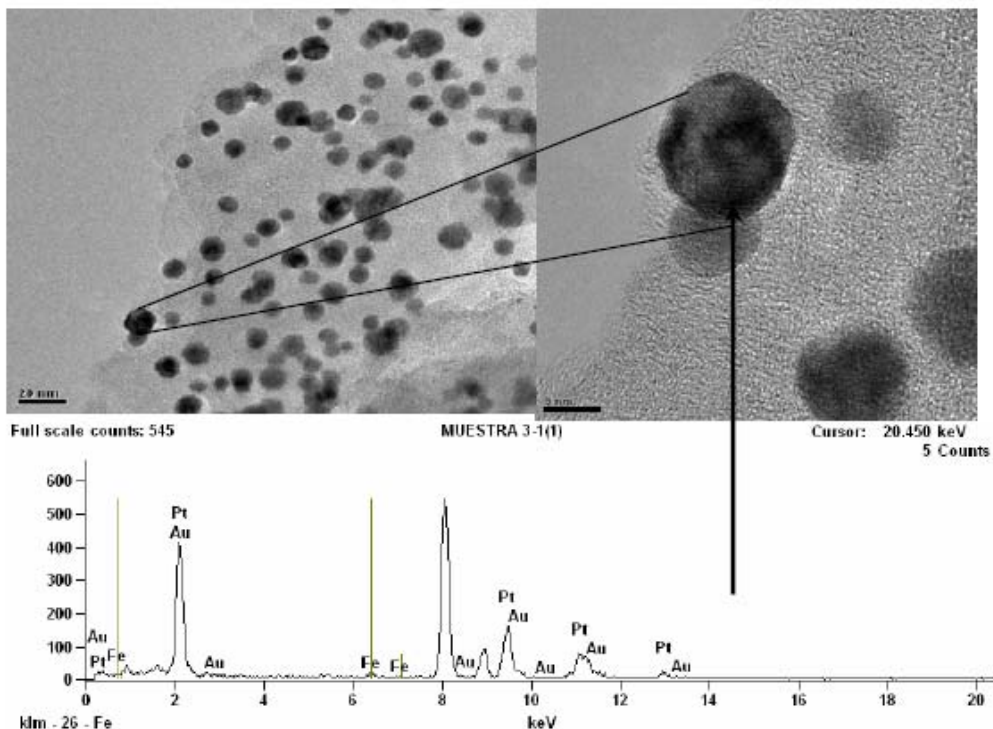


Figure 3. Transmission electron micrograph of the nanoparticles contained in sample M2 supported on C indicating that Pt, Au and Pt-Au are present.

#### 4. CONCLUSIONS

The synthesis method used was simple and reproducible, which allowed the study of three synthesis parameters: a) the synergic effect of both metals in the catalyst over the RRO, b) the impregnation method, namely in-situ and mechanical, and c) the type of hydroxide used, NaOH or NH<sub>4</sub>OH to adjust the solution's pH.

The results of XRD characterization indicated a shift of the peaks corresponding to the pure components Pt and Au, which confirms that the samples were also constituted by an alloy and that there were no other segregated or intermediary unknown phases. This conclusion was supported by the EDS results as applied to different regions of the samples, which indicates that the Pt-Au nanoparticles observed by TEM belong to an alloy system at nanometric scale with a size smaller than 10 nm.

## ACKNOWLEDGEMENTS

The authors are indebted to the Instituto Mexicano del Petróleo, for the use of the analytic facilities to perform the physicochemical characterization, in particular to Dr. Ascensión Montoya of the XRD lab and to Dr. Vicente Paz del Ángel of the TEM lab. Also, VMA, OSF and MTR thank the SNI for the distinction of their memberships and the stipend received. 6

## REFERENCES

- [1] F. Pinna et. al., “Pd-Fe/SiO<sub>2</sub> Catalysts in the Hydrogenation of 2,4-Dinitrotoluene”, *Journal of Catalysis* 150,, (1994), 356-367
- [2] M. Faraday, *Philos. Trans. R. Soc. London*, 1857,147,145
- [3] Masatake Haruta,: Preparation, Working Mechanism and Applications, *Gold Bulletin, Gold as a Novel catalyst in the 21 st Century* 37/1-2 (2004)
- [4] Asbørn Klerke et al, “Pt-Ru colloid nanoparticles for CO oxidation in microfabricated reactors”, *Catalysis Letters*, 109, 1-2 (2006).
- [5] Masatake Haruta, Masakatu Daté, “Advances in the catalysis of Au nanoparticles”, *Applied Catalysis A: General* 222, 427-437.
- [6] González H. R., “Electrocatalysis de una celda de combustible de membrana de intercambio protónico”, Memorias curso Tecnologías del Hidrógeno 2006, Sociedad Mexicana del Hidrógeno- UNAM, (2006).
- [7] J. Turkevich and G. Kim, “Palladium: Preparation and Catalytic Properties of Particles of Uniform Size”, *Science*, 169, (1970),873-879.
- [8] Naoki Toshima and Tetsu Yonezawa, “Bimetallic nanoparticles- novel materials for chemical and physical applications”, *New J. Chem*, (1998), 1179-1201
- [9] Mott D. et al., “Synergistic activity of gold-platinum alloy nanoparticle catalysts”, *Catalysis Today*, 122, (2007), 378-385.
- [10] Teranishi T, Hosoe M., Tanaka T. and Miyake M., “Size Control of Monodispersed Pt Nanoparticles and Their 2D Organization by Electrophoretic Deposition”, *J. Phys. Chem. B*, 103, (1999), 3818-3827.
- [11] Teranishi T and Miyake M., “Size Control of Palladium Nanaoparticles and Their Crystal Structures”, *Chem. Mater.* 20, (1998), 594-600.
- [12] Teranishi T., Weiyong Yu, “Preparation of Polymer-Stabilized Noble Metal Colloids”, *Journal of Colloid and Interface Sci.*, 210, (1999), 218-221
- [13] Hwai P., C., Kong Y. L. and Hanfan L., “Factors affecting the size of polymer stabilized Pd nanoparticles”, *Journal Materials Chemistry*, 12, (2002), 934-937

- 
- [14] Naoki T. and Tetsu Y., "Bimetallic nanoparticles novel materials for chemical and physical applications", *New Journal Chem.*, (1998), 1179-1201.
  - [15] Bonet F Guéry C, et al., "Electrochemical reduction of noble metal compounds in ethylene glycol", *International Journal of Inorganic Materials*, 1, (1999), 47-51.

***Chapter 9***

# **ENHANCED ADSORPTION OF HEAVY METALS BY NANOSTRUCTURED COMPOSITES BASED UPON DENDRIMER-FUNCTIONALIZED MCM-41**

***M. A. Escalante, E. Delgado,  
L. F. García and G. Toriz\****

Departamento de Madera, Celulosa y Papel, CUCEI. Universidad de Guadalajara.  
Km 15.5 Carretera Guadalajara-Nogales, Las Agujas, C.P. 45020. Zapopan, Jalisco

## **ABSTRACT**

The assembly of a multifunctional polymer to a porous substrate was carried out in order to design nanostructured porous composites. Polyamidoamine dendrimers generation 2 (dendrimers) were assembled to silica MCM-41 (MCM-41) and amino functionalized porous composites were obtained. Dendrimer-surface modified MCM-41 was prepared by direct reaction of dendrimers with the silica. Trimethylchlorosilane (TMCS) was reacted with surface hydroxyls of MCM-41 and then the dendrimers were allowed to diffuse and penetrate the pores of the silica. Bare MCM-41 and composites dendrimer-MCM-41 were characterized by Diffuse Reflectance Infrared Fourier Transform Spectroscopy (DRIFTS), X ray powder diffraction (XRD), and surface area (calculated by the method of Brunauer, Emmett and Teller, BET). The BET of untreated MCM-41 was near to  $1300 \text{ m}^2 \cdot \text{g}^{-1}$  while the BET of composites decreased to around  $200-500 \text{ m}^2 \cdot \text{g}^{-1}$  when TMCS was used to cap surface hydroxyls on MCM-41. On the other hand, the surface area of composites was increased to about  $1800 \text{ m}^2 \cdot \text{g}^{-1}$  when dendrimers were allowed to react with the surface hydroxyls on the silica. DRIFT spectra of composites showed an increased signal related to primary amino groups. XRD signals at 2-3 and 5-6  $2\theta$  angles which corresponded to the hexagonal lattices of MCM-41 decreased (at 2-3) or even vanished (at 5-6) in the composites. Adsorption of arsenic (V) and chromium (VI) was evaluated on the materials under study. It was found that MCM-41 was not able to adsorb either of the elements. 17 and 42 mg As and Cr respectively were adsorbed per g of dendrimers. The adsorption on composites was increased up to 22 and 69 mg As and Cr respectively per gram of dendrimers.

---

\* gtoriz@dmcyp.cucei.udg.mx; Tel. (33) 36-82-01-10 Ext. 230. Fax. (33) 36-82-06-43.

**Keywords:** Silica MCM-41, PAMAM dendrimers, nanostructured composites, adsorption, arsenic, chromium.

## INTRODUCTION

Society faces numerous problems such as the improvement of human health, cessation and control of pollution, generation of energy, efficient transformation of raw materials to products, and the imminent depletion of natural resources, just to name a few. Science and technology are continuously coping with the challenges that modern society faces. In order to deal with some of these problems, advances in research and development of new materials have led to the synthesis and design of materials that have dimensions in the nanoscale range (2-50 nm). These materials have superior physical and chemical properties as compared to regular materials. Nanoporous materials have, for instance, an enormous internal surface area available for separation, catalysis and adsorption operations.

Silica MCM-41 is a versatile nanoporous material that has been under study for more than 20 years. The pore size of this inorganic material can be designed in the range from 15 to 100 Å by template polymerization of silica on surfactants (Beck 1992). In addition, hydrothermal restructuration and synthesis at different temperatures have been utilized to control the size of the pores in these materials (Zhao 1996). The nanostructure of silica is thus controlled by combining the procedures aforementioned to achieve large surface areas and a narrow range of porosities.

The usefulness of these materials can be improved by chemical surface modification to control not only physical properties but also its chemistry in order to enhance chemical separation, catalysis and environmental cleansing. These modifications allow controlling the hydrophilic/hydrophobic and the electrostatic character of the surface of the material by incorporation of surface organic functional groups. For example, Moller and Bein (1998) have reported in a review the chemical modification of silica MCM-41 and MCM-48 with regard to their ionic exchange properties, absorption followed by reduction, and also the grafting of several reactive compounds such as metal alcoxydes, metallic complexes, silane coupling agents, as well as polymerization of reactive monomers into the channels of these materials.

The modification of MCM-41 with amino groups has been carried out in order to improve adsorption of several substances such as inks and heavy metals, and also to prepare redox materials. Ho *et al.* (2003) modified silica MCM-41 with both amino and carboxyl functional groups for the selective adsorption of inks. In order to adsorb oxyanions (chromate and arsenate) under acidic conditions, Yoshitake and Yokoi (2002) fixed triaminosilanes onto silica MCM-41 and found improved adsorption of these heavy metals. MCM-41 has been also synthesized from aminoacids containing gels, as reported by Diaz and Pérez-Pariente (2002). In addition, Díaz *et al.* (2003) reported a new kind of redox hybrid materials by the modification of silica MCM-41 with ferrocenyl dendrimers.

The modification of MCM-41 with dendrimers opens up many technological opportunities for the design of nanostructured composites. Dendrimers are branched polymers with very specific, controlled composition. For instance, dendrimers can be designed to obtain geometrical nanostructures such as spherical, cylindrical, or conical with monodisperse

sizes in the range from 2-10 nm. In addition to controlling the nanostructure of dendrimers, the chemical groups at their surfaces can be tailored to meet specific needs. In order to take full advantage of these properties, dendrimers have been immobilized on porous supports, as reported elsewhere (Dvornic 2002, Furuta 2003 y Sivanandan 2002). In this study, we modified Silica MCM-41 with dendrimers to improve the separation of heavy metals from water by introducing primary amino groups on the surface of the material.

## MATERIALS AND METHODS

### Materials

Silica MCM-41 was kindly provided by the Department of Chemical Engineering at the University of New Brunswick (NB, Canada).  $\text{KH}_2\text{AsO}_4$  (99.9%) and polyamidoamine dendrimers generation 2 (PAMAM G-2) were purchased from Sigma-Aldrich (Milwaukee, WI).  $\text{K}_2\text{CrO}_4$  (99.2%) was obtained from J. T. Baker S.A. de C.V. Xalostoc, Mexico. Ultra high purity nitrogen and helium, for adsorption studies, were supplied by INFRA de Mexico, S. A. de C. V. All the other reagents used were analytic grade.

### Methods

#### *Preparation of Arsenate and Chromate Solutions*

$\text{KH}_2\text{AsO}_4$  and  $\text{K}_2\text{CrO}_4$  were weighted and dissolved in distilled water in order to obtain solutions at  $5.4 \text{ mg}\cdot\text{L}^{-1}$  in arsenic and  $11.8 \text{ mg}\cdot\text{L}^{-1}$  in chromium. Adsorption isotherms were taken at a pH 4. The pH was adjusted either with NaOH 0.1N or HCl 0.1N. The concentration of arsenic and chromium were determined by absorption spectrometry in a HACH DR5000 spectrometer at wavelengths of 520 and 540 nm respectively.

#### *MCM-41 Surface Modification*

In order to cap the silica surface hydroxyl groups MCM-41 was treated with mixtures of dry ether/trimethylchlorosilane (TMCS) during 1 h. TMCS was added in sufficient amounts to react only with surface hydroxyl on the silica. Samples in which the surface hydroxyl groups were not capped were treated only with dry ether during 1h. After those treatments, the samples were centrifuged, dried at  $45^\circ\text{C}$  under vacuum and weighted. The dried silica was then added to a mixture of dichloromethane with PAMAM dendrimers generation 2 and left under agitation for 24 h and then centrifuged, dried under vacuum at  $45^\circ\text{C}$  for 24 h and weighted to determine the amount of fixed dendrimers.

#### *Arsenic and Chromium Adsorption Isotherms*

Samples of MCM-41, PAMAM G-2 dendrimers, and dendrimer-modified silica were added to 125 mL arsenic or chromium solution and placed under agitation. Aliquots were taken at the indicated time and the adsorption of arsenic or chromium was quantified. All adsorption tests were carried out at pH 4 and ambient temperature.

### **Scanning Electron Microscopy (SEM)**

Surface imaging of the gold sputtered samples were obtained in a scanning electron microscope JEOL JSM-5400 LV at 15kV working energy.

### **Surface Area and Pore Volume**

MCM-41 and the modified silica were characterized by nitrogen adsorption porosimetry in a Horiba SA-9601-MP apparatus. BET surface area and pore volume were determined at liquid nitrogen temperature.

### **X-Ray Diffraction**

X-ray diffraction patterns of virgin and modified MCM-41 samples were determined by X-Ray powder diffraction in a Siemens diffractometer (Diffraktometer SIEMENS) at 20 angles between 2-40 °.

### **Infrared Spectroscopy**

Samples were subjected to diffuse reflectance infrared fourier transform spectroscopy (DRIFTS) in a Perkin Elmer GX spectrophotometer in the range of 400-4000 cm<sup>-1</sup> in order to detect and monitor functional groups on the samples.

## **RESULTS AND DISCUSSION**

### **Scanning Electron Microscopy**

Figure 1 shows two micrographs of untreated MCM-41 silica at two magnifications. It can clearly be seen clusters of hexagonal particles, agglomerated into groups with dimensions from 10 to 30 micrometers (Figure 1a). Individual particles are flat hexagons of about 2 micrometers in each side (Figure 1b). SEM micrographs of modified silica did not show any differences with the micrographs of untreated MCM-41.

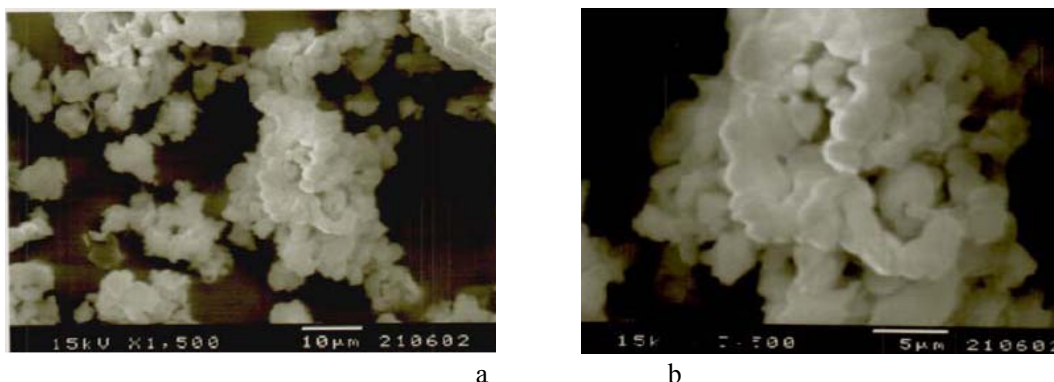


Figure 1. SEM micrographs of silica MCM-41.

## Surface Area and Pore Volume

Table 1 shows the surface area and pore volume, determined by nitrogen adsorption, of virgin MCM-41 and treated MCM-41 (six treatments). Treatments one and two consisted only on the reaction of trimethylchlorosilane with surface hydroxyl groups on the silica. Virgin silica had a surface area close to  $1300 \text{ m}^2 \cdot \text{g}^{-1}$ . The treatment with  $31 \mu\text{L} \cdot \text{g}^{-1}$  TMCS decreased the surface area to  $1260 \text{ m}^2 \cdot \text{g}^{-1}$  and down to  $1160 \text{ m}^2 \cdot \text{g}^{-1}$  when  $37 \mu\text{L} \cdot \text{g}^{-1}$  TMCS were used to cap the surface hydroxyl groups. Quite small amounts of TMCS were used to confine the modification only to the surface and the decrease in surface area was minimal. However, the larger the amount of TMCS added, the higher the decrement on surface area. The pore volume was also decreased on treatments one and two. It is likely that the modification slightly blocks the pores of the silica.

Treatment 3 is the modification of the silica only with dendrimers whereas treatments 4-6 include the modification of the silica with both reagents, i.e. TMCS and dendrimers. Treatments 3-5 have a weight percentage, which represents the amount of dendrimers fixed on the silica. The largest incorporation of dendrimers onto the silica (94% wt:wt) was achieved when the surface hydroxyl groups were available, that is in treatment 3. In this treatment the incorporation of dendrimers resulted in the increment of surface area of the composite near to  $1800 \text{ m}^2 \cdot \text{g}^{-1}$  although the pore volume was slightly diminished. Although it was not possible to determine the surface area of dendrimers because they collapse in the solid state, it can be seen that they contributed to the surface area of the composite. It is possible that the dendrimers attached to the surface of the silica, without blocking its pores and hence contributed to the surface area.

**Table 1. Surface area and pore volume on MCM-41 and modified silica**

Sample	Surface area ( $\text{m}^2 \cdot \text{g}^{-1}$ )	Pore volumen ( $\text{mL} \cdot \text{g}^{-1}$ )
Untreated MCM-41	1294	1.0285
Treatment 1 $31 \mu\text{L} \cdot \text{g}^{-1}$ Trimethylchlorosilane (TMCS)	1257	0.9098
Treatment 2 $37 \mu\text{L} \cdot \text{g}^{-1}$ TMCS	1163	0.8351
Treatment 3 Dendrimer treated (94% wt:wt)	1790	0.8525
Treatment 4 $31 \mu\text{L} \cdot \text{g}^{-1}$ TMCS plus dendrimer (85% wt:wt)	500	0.3602
Treatment 5 $31 \mu\text{L} \cdot \text{g}^{-1}$ TMCS and dendrimer (60% wt:wt)		
Free particles	369	0.4155
Agglomerates	202	0.1760
Treatment 6 $37 \mu\text{L} \cdot \text{g}^{-1}$ TMCS and dendrimer	nq <sup>a</sup>	nq <sup>a</sup>

<sup>a</sup> Non-quantified.

The reaction of TMCS with surface hydroxyl groups on silica plus the addition of dendrimers resulted in a diminished surface area and pore volume of the composites. Since surface hydroxyl groups were not available, it is likely that dendrimers went into the pores of the silica, occupying and blocking them and, therefore, reduced both surface area and pore volume. Treatment 4 yielded a uniform sample, whereas in treatment 5 the composite was recovered in two parts, one with free particles and the other as thin agglomerates. Treatment five was then divided in these two categories. These materials contained different amounts of dendrimers and were difficult to quantify. However, it was worth to notice that is possible to adjust the amount of dendrimers fixed and in that way control the nanostructure of the composite. On the other hand, increasing the content of TMCS to 37  $\mu$ L and adding dendrimers resulted in a gummy-like material which was not amenable for determination of surface area or pore volume. That was due to the complete blockage of the pores of the composite both from TMCS and dendrimers.

## X-Ray Diffraction

Figure 2 shows the X-ray diffraction pattern of untreated MCM-41 and the modified silica. Virgin MCM-41 shows a peak between the angles 2 $\theta$  two and three which indicates the plane 100 of this kind of materials. Planes 110 and 200 reflect at about 5-6 2 $\theta$  angles. These reflections have been attributed to the bidimensional, hexagonal structure of the silica. However due to the strong signal of the plane 100 these signals were weak. Modification of the silica with TMCS did not change the X-ray diffraction pattern. Modification only with dendrimers seemed not to drastically alter the structure of the silica, although the signals were less strong. Since these modifications were confined to the surface of the silica, it seems that the bulk of the material was not severely altered. Modification of silica with TMCS followed by the addition of dendrimers seemed to diminish the signal for the plane 100 and for treatment six that signal almost disappear. Apparently, the blockage of the surface hydroxyl groups forced the dendrimers to penetrate the pores of the silica and then affecting its crystal structure. Otherwise, a large accumulation of dendrimers on the surface of silica could have blocked the crystalline signals from MCM-41.

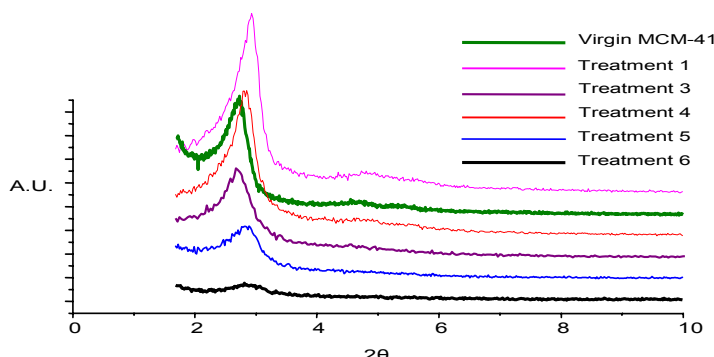


Figure 2. X-ray diffraction patterns of virgin MCM-41 and modified silica with TMCS, dendrimer, and the sequential treatment of TMCS and dendrimer.

## Diffuse Reflectance Infrared Spectroscopy

Diffuse reflectance infrared spectroscopy is a technique suitable to analyze powders. In addition, infrared spectroscopy is useful to provide information about the crystal structure in ordered solids and, therefore, this technique is appropriate to analyze these samples. Figure 3a shows the DRIFT spectra of virgin MCM-41 and 3b shows the DRIFT of silica treated with TMCS, according to treatment one. It can be seen that virgin MCM-41 has a distinctive band at  $3740\text{ cm}^{-1}$  which correspond to Si-O groups. A broad band in the region  $3000\text{-}3700\text{ cm}^{-1}$  corresponds to OH groups. The signal at  $1600\text{-}1700$  indicates amino groups which originate from the surfactant used to prepare the silica. The broad region at  $3000\text{-}3700\text{ cm}^{-1}$  may include also amino groups. Figure 3b shows additional signals at  $2970$  and  $2870\text{ cm}^{-1}$  which can be assigned to asymmetric and symmetric stretching of  $\text{CH}_2$  groups, whereas signals at  $1450$ ,  $1390$  and  $1350\text{ cm}^{-1}$  can be assigned to  $\text{CH}_2$  and  $\text{CH}_3$ , showing the methyl groups from TMCS and that the modification proceeded efficiently.

Figure 4 shows the DRIFT spectra of virgin MCM-41 and treated MCM-41 according to treatments three to six. It can be clearly seen that additional signals appeared due to the presence of dendrimers. MCM-41 treated according to treatments 3-5 retained the signal at  $3740$  which is the signal of  $\text{SiO}_-$  group in the silica, whereas in treatment 6 this signal was not clearly distinguished. Figure 4b shows the spectrum of MCM-41 treated only with dendrimers. The asymmetric-symmetric stretching vibrations of  $\text{CH}_2$  present in the dendrimers can easily be seen. In all the other treatments these signals are not so clear. The shifted signals of amino and carboxyl groups can be seen in treatments three to six, indicating the presence of the dendrimers. These facts suggest that even though dendrimers could have gone inside the pores of the silica, the chemical structure both of dendrimers and silica was up to some extent preserved.

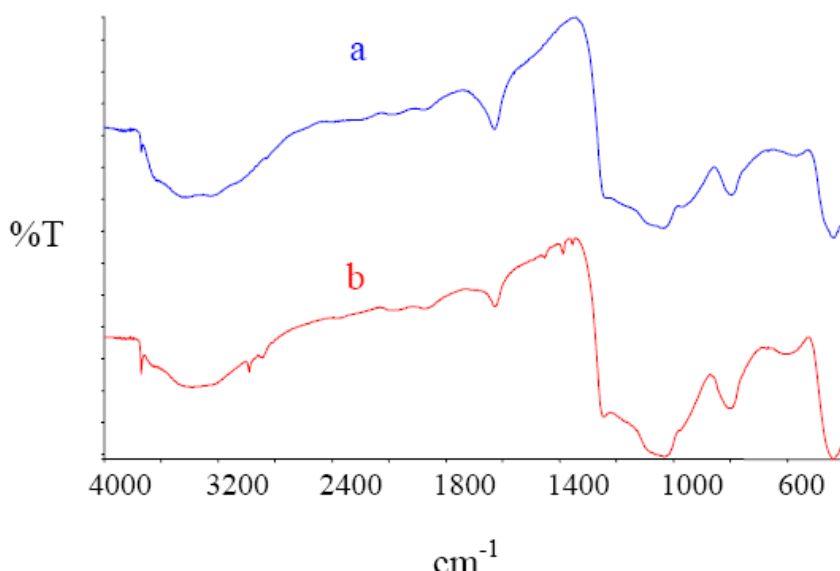


Figure 3. Diffuse reflectance infrared spectra of a) virgin MCM-41, and b) MCM-41 treated with TMCS (Treatment 1).

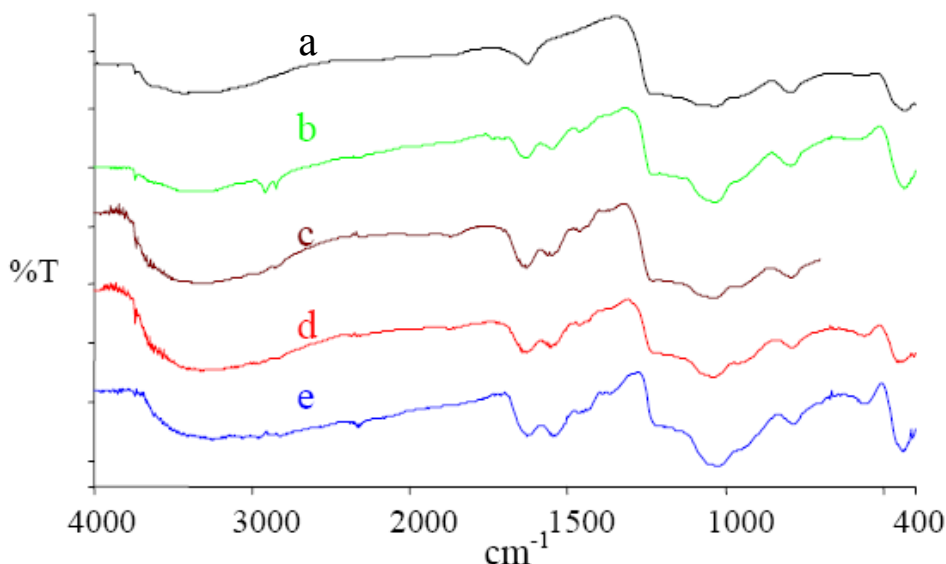


Figure 4. Diffuse reflectance infrared spectra of virgin MCM-41 (a), and modified MCM-41 according to: Treatment 3 (b), Treatment 4 (c), Treatment 5 (d), and Treatment 6 (e).

### Adsorption of Chromium/Arsenic

Table 2 shows the results from adsorption of chromium or arsenic on bare MCM-41, on dendrimers, and on MCM-41-dendrimers composites. These composites correspond to the treatment of MCM-41 with dendrimers alone (treatment 3), and with TMCS followed by dendrimer addition (treatment 4). Neither chromium nor arsenic were adsorbed on bare MCM-41 at the conditions tested on the adsorption experiments, that is at pH 4 and ambient temperature. The lack of adsorption was due to the surface chemistry of the material, since there was enough surface area. Chromate and arsenate ions were most likely repelled by the surface due to electrostatic interactions.

**Table 2. Arsenic/chromium adsorption on MCM-41, dendrimers, and MCM-41 modified with dendrimers**

Sample	Sample weight (g)	Dendrimers weight (g)	Adsorption per g of sample		Adsorption per g of dendrimers	
			As (mg)	Cr (mg)	As (mg)	Cr (mg)
MCM-41	1.0	0.0	0.0	0.0	0.0	0.0
Dendrimers	0.02466	0.02466	17.23	42.00	17.23	42.00
Composite 1 <sup>a</sup>	0.1364	0.0175	1.31	4.11	10.28	32.25
Composite 2 <sup>b</sup>	0.0415	0.0059	3.11	9.91	21.75	69.40

<sup>a</sup> Composite 1: MCM-41 treated with dendrimers (Treatment 3)

<sup>b</sup> Composite 2: MCM-41 treated with TMCS and then with dendrimers (Treatment 4).

On the other hand, dendrimers alone had an adsorption of 42 mg chromium per gram of dendrimers and 17.23 mg arsenic per gram of dendrimers. The numerous free amino groups present at the dendrimers' surface were protonated at pH 4 and able to interact with arsenate and chromate ions. When MCM-41 was treated with dendrimers (treatment 3, composite 1 in Table 2) an improved adsorption of arsenic and chromium was observed with respect to the bare MCM-41, but a decreased adsorption was observed with respect to the dendrimers. 32.3 mg chromium per gram of dendrimers on the composite were adsorbed, whereas 10.3 mg arsenic per gram of dendrimers on the composite were adsorbed. This can be due to the decreased number of amino groups available to participate in the adsorption process, since many of them were utilized to attach to the surface of MCM-41. It is worth to mention that nonetheless this composite had the largest surface area, was not the best for the adsorption of the elements of interest.

MCM-41 treated with TMCS and thereafter with dendrimers, resulted in a composite with an improved adsorption capacity as compared to the dendrimers alone. Chromium was adsorbed in 69.4 mg per gram of dendrimers in the composite as compared to 42 mg per gram of dendrimers alone (65% improvement). The adsorption of arsenic was also enhanced in this composite up to 21.75 mg per g of dendrimers on the composite (26% improvement). It is worth also to point out that even though the surface area of MCM-41 decreased to less than a half, the adsorption of chromium and arsenic was improved because the chemical interactions with the dendrimers dominated the adsorption process. The attachment of dendrimers to MCM-41 provided to dendrimers the support to better accommodate arsenic or chromium during the adsorption process. However, functional groups must be preserved to achieve a better, increased adsorption. Capping the surface hydroxyl groups on MCM-41 allowed dendrimers to attach only with few amino groups leaving most of them free to interact with the elements involved in the adsorption process.

## CONCLUSIONS

In this study we report the modification of MCM-41 with PAMAM dendrimers generation 2 in order to improve the adsorption of arsenic and chromium. Bare and modified MCM-41 were analyzed with respect to the surface area, pore volume, X-ray diffraction pattern, morphology, and chemistry at the surface and these characteristics were related to the ability of these materials to adsorb arsenic and chromium. It could be seen by these analytical techniques that the modification of MCM-41 was efficient and that can be controlled. The modification of MCM-41 with dendrimers resulted in materials with improved adsorption of chromium and arsenic. However, it is important to preserve as many chemical functional groups that will interact with the elements of interest. In this way we were able to design a nanostructured composite with enhanced adsorption capacity as compared to the adsorption with dendrimers alone. In addition, this composite has the advantage that the dendrimers are chemically attached to the MCM-41 support, and can be regenerated and reused many times.

## REFERENCES

- Beck, J. S.; Vartuli, J. C.; Roth, W. J.; Leonowicz, M. E.; Kresge, C. T.; Schmitt, K. D.; Chu, C. T. W.; Olson, D. H.; Sheppard, E. W; McCullen, S.B.; Higgins, J.B.; and Schlenker J. L. (1992). "A new family of mesoporous molecular sieves prepared with liquid crystal templates", *J. Am. Chem. Soc.* 114(27), 10834-10843.
- Diaz, I., García, B., Alonso, B., Casado, C., Morán, M., Losada, J., and Pérez-Pariente, J. (2003). "Ferrocenyl Dendrimers Incorporated into Mesoporous Silica: New Irid Redox-Active Materials", *Chem. Mater* 15, 1073-1079.
- Diaz, I., Pérez-Pariente, J. (2002). "Synthesis of Spongelike Functionalized MCM-41 Materials from Gel Containing Amino Acids", *Chem. Mater* 14, 4641-4646.
- Dvornic R. P., Li J., de Leuze-Jallouli A. M., Reeves S. D., and Owen M. J. (2002). "Nanostructured Dendrimer-based network with hydrophilic poly(amidoamine) and hydrophobic organosilicon domains", *Macromolecules* 35, 9323.
- Furuta P. and Fréchet J. M. J. (2003). "Controlling solubility and modulating peripheral function in dendrimer encapsulated dyes", *J. Am. Chem. Soc.* 125, 13173
- Ho, K. Y., McKay, G., and Yeung, K. L. (2003). "Selective adsorbents from ordered mesoporous silica", *Langmuir* 19, 3019-3024.
- Moller K, Bein T. (1998). "Inclusion chemistry in periodic mesoporous hosts", *Chem. Mater* 10, 2950-2963.
- Sivanandan K., Vutukuri D. and Thayumanavan S. (2002). "Functional group diversity in dendrimers", *Org. Lett.* 4, 3751.
- Yoshitake H., Yokoi T., Tatsumi T. (2002). "Adsorption of Chromate and Arsenate by Amino-Functionalized MCM-41 and SBA-1", *Chem. Mater* 14, 4603-4610.
- Zhao X.S., Lu G.Q., Millar G.J. (1996). "Advances in Mesoporous Molecular Sieve MCM-41", *Ind. Eng. Chem. Res.* 35, 2075-2090.

***Chapter 10***

## **COGNITIVE LEVEL OF SECONDARY SCHOOL STUDENTS AND ITS RELATION TO SOME CONCEPTUAL ASPECTS OF BERNOULLI PRINCIPLE**

***Maria Eugenia Bustamante Estudillo\****  
***and Honorina Ruiz Estrada\****

<sup>a</sup> Facultad de Ciencias Físico Matemática,  
Benemérita Universidad Autónoma de Puebla, Apdo.  
Postal 1152, Puebla, Pue., C.P. 72001

<sup>b</sup> Instituto de Física Luis Rivera Terrazas, Apartado Postal J-48, 72570 ,  
Benemérita Universidad Autónoma de Puebla, Puebla,Pue., México

### **ABSTRACT**

The main goal of this research is to determine the possible correlation between the reasoning level of students attending the third year of Secondary school by means of a scientific reasoning test called Anton E. Lawson, and the capacity of these students to properly use such concepts as “area, volume” as well as the conservation and proportionality schemes. Lawson argues that the boy gradually assimilates scientific reasoning in a natural way and to identify this Lawson is based in studies about rational understanding development processes taking on account Piaget’s epistemology. In a similar fashion Arnold B. Arons used Piaget epistemology to explain scientific initiation and scientific education for K12 students by means of logical activities related to the understanding of concepts such as those previously mentioned, and suggests some activities that will allow the learning of some aspects linked to Bernoulli Principle, according to the scientific level of students. Piaget taxonomy is used in pedagogy, due to its involvement with Lawson and Arons theories. As a strategy to attain this correlation problem solving and collaborative teams will be used.

---

\* marub67@hotmail.com  
\* hruiz@facfm.buap.mx

## **INTRODUCTION**

This educational research has its inspiration and benchmarks in the reports that were generated in the decade of the 70s, following the pioneering work of Piaget. Piaget's theory is a genetic psychology built during the first half of the twentieth century, and since then it has had a huge impact on education, both for developing theories and in daily pedagogical practice. The influence of this theory in education remains very important today as a referent framework and is commonly used to identify the intellectual development of students.

According to Piaget, by the age of 11 years, children reach specific operations which are related to objects and specific physical processes with which children are in direct contact and are operations linked to sensory experience. In terms of children cognitive development such objects and experiments are not important by themselves, what is important is children activity on them (concrete thinker). In opposition, a formal thinker does not require direct physical objects and experiments since a formal thinker can think using abstractions by means of logical propositions. . Piaget levels model states that the transition from the concrete level to the formal level is: (1) universal and (2) occurs between 11 and 15 years old. Studies in the 70's in the United States of America and England show that the first assertion is false and that the second is not fully achieved. According to Arons and Kaplus [1] the distribution of reasoning levels in the preparatory level of American students is uniform at all three Piaget levels and such distribution does not change if a sample is taken from adults. Shay [2 ] found that less than 20% of British schoolchildren become formal thinkers at the age of 16 years due to a change of the structures of thought generally specified from the logical point of view [3].

In order to identify the reasoning stage of Secondary school students we consider the Lawson reasoning test [4], in the recently version used by Colleta et.al. [5]. Lawson studies the rational thought development processes [6], argues that children acquires scientific knowledge in a natural way. Arons [7] considers that university students lack of a scientific education, do not have conceptual grounds and lack of reasoning schemes

Learning planning [8] is a didactic teaching in problem solving; Traditionally teaching-learning was based in conveying information although lately it came out to be experimentation and quantitative application. In the case of the strategy based in problem solving, information is gathered about a given case and finally we come back to the problem.

## **LAWSON TEST**

The first activity has been to use an instrument that detects the reasoning level of the students. We employed the "Scientific Reasoning School Test", designed and used by Anton E. Lawson [7]. The test was applied from August, 31st, up to Sept, 6th, in four modules each one with three questions. Students answered a module each one of these days in fifteen minutes, so that they could have a break without loosing attention. Test has 12 tasks that require different types of scientific reasoning. According to the number of right answers obtained students are classified in two reasoning levels:

- From 0 to 4 right answers, scientific reasoning level is Empiric – Inductive (Concrete in words of Piaget);

- From 9 to 12 right answers, scientific reasoning level is Hypothetical – Deductive (Formal in words of Piaget).

Scores in the intermediate zone (5 to 8 right answers) indicate a transitional reasoning level.

Eleven of the twelve are multiple option, both in the answer and in the explanation..The last problem calls for building the answer and the explanation of the answer. The answer and its explanation must be consistent and assertive in solving the problem. Only this way is considered a correct answer and a point is given to the answer. Essentially, Lawson Test evaluates six aspects of reasoning:

- 1) Physical Magnitudes Conservation,
- 2) Proportionality Reasoning,
- 3) Identification and Control of Variables,
- 4) Probabilistic Reasoning,
- 5) Correlational Reasoning and
- 6) Combinatory Reasoning.

These aspects are evaluated in the twelve questions of the Test. Table I lists the different aspects evaluated.

**Table 1. Skills Evaluated in Lawson Test**

Question	Evaluated Ability
1	Mass Conservation
2	Displaced Volume Conservation
3	Proportionality Reasoning
4	Advanced Proportionality Reasoning
5	Identification and Control of Variables
6	Identification and Control of Variables
7	Identification and Control of Variables, Probabilistic Reasoning
8	Identification and Control of Variables, Probabilistic Reasoning
9	Probabilistic Reasoning and Proportionality Reasoning
10	Probabilistic Reasoning
11	Correlational Reasoning and Probabilistics
12	Combinatory Reasoning

Hereby we use Lawson Test results to determine which aspects of reasoning are used by students. This information is compared with the results obtained that involve some aspects of Bernoulli Principle and it is verified whether students were able to apply the reasoning schemes combined with their knowledge about the motion of incompressible fluids in pipes.

## FLUIDS

The trajectory described by a fluid element in motion is called flow line, the speed of the element changes in magnitude and direction along a flux line. If each element that passes by a given point follows the same flux line as the other elements, we say that the flow is stable. The speed in the pipe cross sections increases when the pipe is narrow and decreases when the cross section widens. When an incompressible fluid moves along an horizontal pipe its speed changes when the cross section fluctuates and the pressure changes at the same time since the required force to produce this acceleration also varies. If the pressure were the same all along the pipe, the net force on every element of the fluid would be zero. Therefore when the cross sections changes, pressure should change all along the pipe even when there is no height contrast. When there is a change in the height there is also an additional pressure. Bernoulli equation is a general expression that relates the pressure difference between two points along a flux pipe with both speed fluctuations and height changes [9, 10, 11]. Bernoulli applies the theorem of Work-Energy to a fluid contained in a flux tube for a given interval of time and in the space contained between two cross sections. In an interval of times  $\Delta t$ , the fluid that initially was in  $a$ , moves up to  $b$  through a distance  $\Delta s_1 = v_1 \Delta t$ , where  $v_1$  is the speed along that section of the tube. In the same interval the fluid that was initially in  $c$ , moves up to  $d$  a distance  $\Delta s_2 = v_2 \Delta t$ . The cross sectional areas are  $A_1$  and  $A_2$

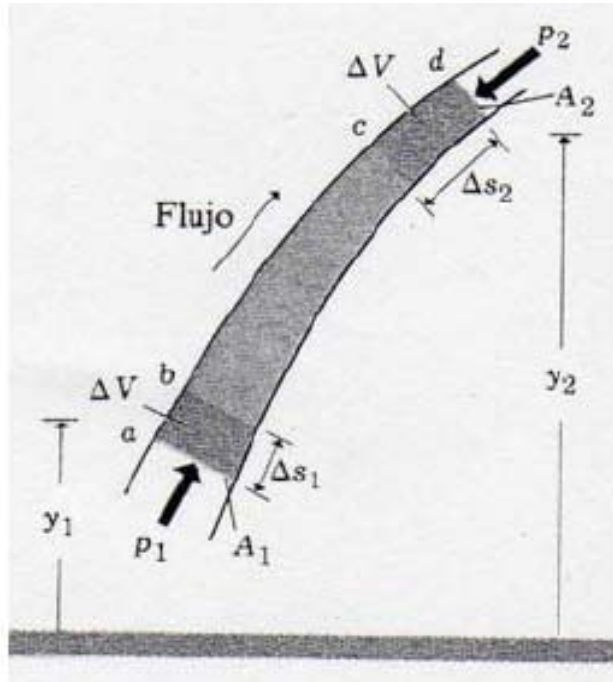


Figure 1. Net Work performed on the fluid tube between  $a$  and  $c$ , is equal to the increase in Kinetic and Potential Energy.

Therefore we have four parameters: Pressure  $P$ , density  $r$ , speed  $v$  and height  $h$ . When these parameters are integrated, we obtain Bernoulli equation that establishes Energy Conservation along a stream line (Tipens Paul 2004) (Streeter, Wylie, Bedford 1999). [11]

Integration constant usually changes from a stream line to other stream line, but remains constant along a given stream line whenever there is no friction and fluid is incompressible. This four conditions are necessary and should always be fulfilled to apply Bernoulli equation. Each term has units of a Newton:

$$\frac{\text{m. N}}{\text{kg}} = \frac{\text{m. kg. m/s}^2}{\text{kg}} = \frac{\text{m}^2}{\text{s}^2}$$

Since fluid has a mass, it is supposed to obey the same conservation laws for solids. In consequence, the work required to move a given volume of fluid all along the pipe should be equal to a total change in potential and kinetic energy. Therefore, net work should be equal to the SUM of the work performed by the applied force  $F_1$  and the negative force applied by the resistant force  $F_2$ . Each one of these terms in Bernoulli equation, the energy of a mass if the liquid in motion is made up by the potential, kinetic and pressure. All these are nothing but the conservation of energy applied to a flow when there are no energy losses (Streeter, Wylie, Bedford 1999). The area times the distances are equal to the volume displaced by the flow since the volume downstream is equal to the volume upstream.

## SCHOOL ACTIVITY (VID. APPENDIX)

The first two activities involve two pipes one meter long: one has three quarters of inch diameter and the other is half an inch. The third and fourth activities consider a pipe made of two sections half meter long. One of these sections diameters is three quarters of an inch wide and the diameter of the other section is half an inch wide. Students are faced with a thought experiment where the pipes are connected for a while to a faucet with water flowing to a recipient. The questions answered by students deal with: the amount of water collected, the distance where the water falls into the collecting recipient, the speed with which water leaves the pipes. Students worked individually and in teams the questionnaires related to previous ideas. The activity ends with a practice of activities 1 and 4, this work was performed in teams. Students contrast their predictions versus experimental evidences collected in the experiments implemented by these students to verify their predictions. Piaget reasoning schemes involved in these experiments are: mass conservation for water as well as identification and control of variables (distance and volume). As a matter of fact, the first of these reasoning determines the way in which the variables involved are related to each other.

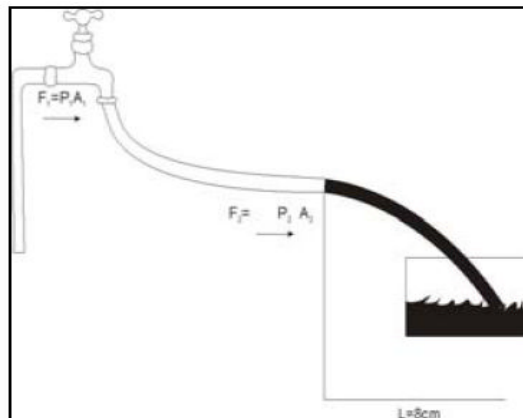


Figura 2. Manguera de  $\frac{3}{4}$  “, la distancia que alcanza el chorro de agua hasta el recipiente es en menor.

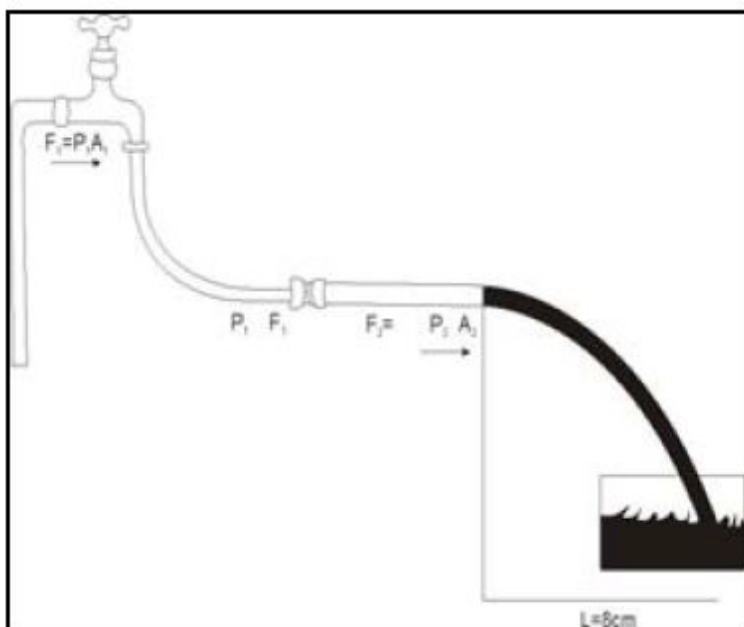


Figure 3. Composite Pipe hose  $\frac{1}{2}$  “ linked by a connector to a pipe hose  $\frac{3}{4}$  “, the distance reached by the water jet until the smaller recipient.

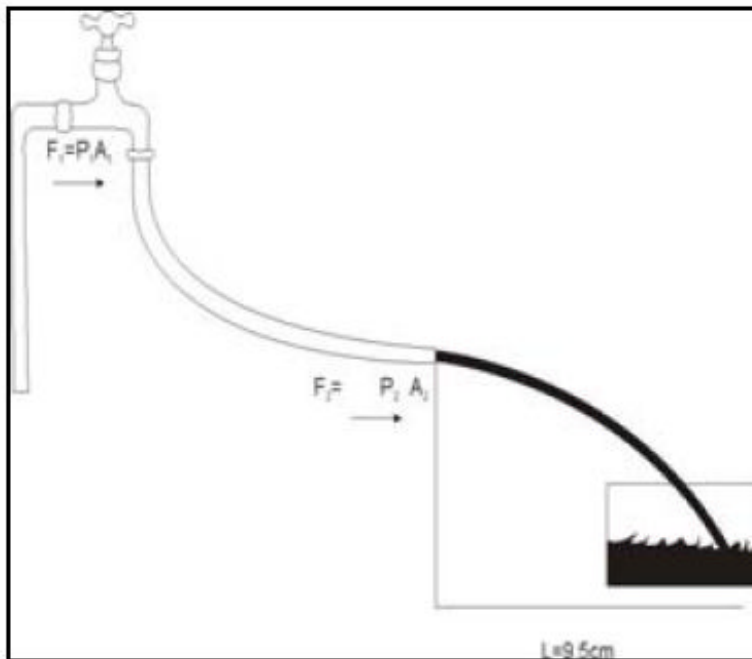


Figure 4. Pipe hose  $\frac{1}{2}$  " ,the distance reached by the water jet until the larger recipient.

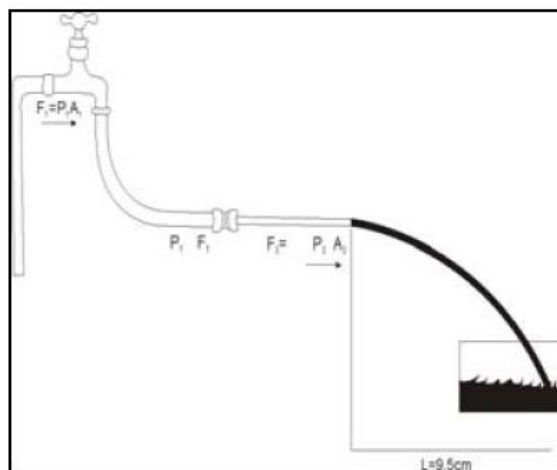


Figure 5. Combined Pipe hose from  $\frac{3}{4}$  " to  $\frac{1}{2}$ ", the distance reached by the water jet until the larger recipient.

## LAWSON TEST GLOBAL RESULTS

We consider a population of 106 youngsters of third year of Secondary School with ages between 13 and 15 years (50.5% are women). Students belong to three school groups, nine students did not participate in the activities. We have found that 60% of the population

understands mass conservation (reactive 1) and 15% understands displaced volume (reactive 2). Questions relative to identification and control of variables (reactives 5 to 8) were answered by a percentage lower than 10%. After reactive 1, the second highest score by students was that ONE belonging to reactive 10 (Advanced Probabilistic Reasoning); this is awkward because reactive 9 involves basic probabilistic reasoning and was assertive only for 3.7%. Scores obtained in each one of these questions of Lawson Test are shown in figure 6.

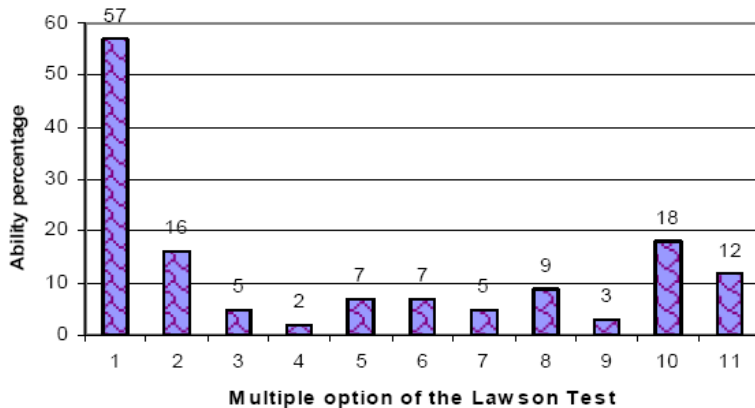


Figure 6. Percentage of right answers of a population of 97 students for each ONE of the 12 questions of Lawson Test.

Students belong to concrete thinkers in a 96.87% and this was reflected in the way that students faced the quizzes. Individual activities were problematic but students had a better performance working in team and when students did the experiments, they realized that their team predictions were not always in agreement with the results of the experiments, which turned out to be shocking for them.

## ACTIVITIES GLOBAL RESULTS

According to Piaget, every form of reasoning or knowledge that requires imagining other possibilities beyond the real or immediate and working with these possibilities as a formalized model will be considered as a concrete thinking. Hence, considering the results obtained in the Lawson cognitive level, 96.87% of the students in the sample turned out to be concrete thinkers. Concrete reasoning is based on mediate reality although Secondary school students are able to perform operations beyond perception by means of conceptualization; their thought is still operatively linked to immediate reality. Students are still unable to formulate and prove hypothesis, therefore students only use six structures to evaluate and create the activity involved, notwithstanding there are twelve structures, which are composed on three stages: 1. Mass and Volume Conservation; 2. Proportional Thinking, direct and inverse; and 3. Identification and control of variables in a low and high level. The rest of the structures belong to formal thinking [12] which is based on symbolic system, by means of object representation and conceptual systems, building up the syntaxes of the explicative nucleus. Without the domain of this symbolic code it is difficult to understand the

interpretation of the proposed activity since students are limited for reasoning as long as students remain in the real objects and do not reach the symbolic level.

Students predicted the result of connecting two pipes one meter long and with different cross sections to the same faucet, each one at a time. All the questions were multiple options, but the explanation of each one was provided by students. Only if the answer and its explanation are right, a point is granted. The students answered four questionnaires, each one with three questions:

- In the first setting: Mass and Volume Conservation,
- In the second: Proportional Thinking, direct and inverse (distance) and
- In the third setting: Identification and control of variables, high and low level (speed).

Maximum grade to be obtained is 12 points. Grades are reported to the range from 1 to 10. For the practical activity, the water container that provided water to the faucets was so full of water that the flow should be steady. Each group was divided in teams. Table 2 shows results obtained by students. In the first row shows the grade obtained in scientific reasoning, described in the first part of this section.

Figure 7 shows the correlation of the grades for concrete thinking (Lawson Test) with the grades for predictive skills (strategy).

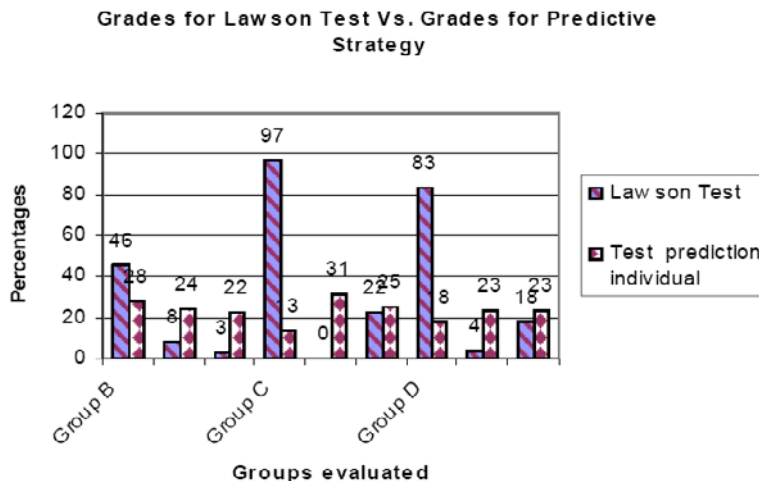


Figure 7. Percentages of students Vs. Obtained evaluation of the four questions grades predictive skills.

Questions 1.1, 2.1, 3.1 and 4.1 are related to conservation of water provided to the faucet was correct for the 20.40%, 17.34%, 22.44% and 26.53% of the samples.

Incorrect answers addressed the reasoning that a larger cross section of the pipe ejects more water. The distance traveled by the jet leaving the pipes and the jet speed is a consequence of water mass conservation. Table 3 shows these results.

**Table 2. Grades for Lawson Test vs. Grades for Predictive Strategy**

Tasks	Group			Group			Group		
	B			C			D		
Skills	Mass Cons	D.I.	I.C.V.	Mass	DI	I.C.V	Mass Cons.	DI	I.C.V
Lawson Test	45.7	7.7	2.7	97	0	22	83	3.8	17.9
TEST PREDICTION INDIVIDUAL	28.37	24.3	21.62	13.1 9	30.5	25	18.18	22.72	22.72

**Table 3. More frequent wrong answers**

Tasks	Group			Group			Group		
	B			C			D		
Skills	M.C	DI	I.C.V	M.C.	DI	I.C.V	M.C.	D. I.	I.C.V
Lawson Test	45.7	7.7	2.7	97	0	22	83	3.8	17.9
Individual Test	28.37	24.32	21.62	13.19	30.55	25	18.18	22.72	22.72
Team Test	56.25	37.5	31.25	35	35	45	56.25	56.25	31.25

**Table 4. Percentage of right answers in predictive activities Vs. Physical variables**

Physical Variables	% Right Answers			
	Single Pipe		Composite Pipe	
	Wide	Narrow	Wide-Narrow	Narrow-Wide
Conservation of mass of water arriving to faucet	25.23	23.36	28.03	31.75
Distance of the stream leaving the pipe	38.31	45.79	33.64	17.75
Jet speed of water leaving the pipe	37.38	49.53	31.77	24.29

As can be seen, about 33.64% of the sample understands mass conservation in a given situation (See the first row in the Table). To answer the question related to the distance of the jet of water and the speed of the jet, students apply empirical ideas. That is why there is a spread in the percentages of the second and third row in the Table. Students are confused when they use composite pipes, in that case they do not have an answer.

## CONCLUSION

Concepts such as are, volume and proportional reasoning involved in Bernoulli equation are not related with the understanding peculiar to students, mainly volume and proportion are not recognized in the activity. Time and mass conservation are more understandable to their level of reasoning. Although students talk about distance, they relate it to several distinct ideas. Considering plots, previous ideas have nothing to do with the level of reasoning, they are independent. In the result of the confrontation between the grope activity and the individual activity, it seems to be that collaborative work turns out to be more efficient for the understanding of concepts and the creation of ideas. School activities must be designed according to the student cognitive levels since standardization leads to a localization of the cognitive development process.

## APPENDIX: ACTIVITY FOR THIRD YEAR SECONDARY SCHOOL STUDENTS

The first two activities involve two pipes one meter long: one has a diameter three quarter inch (wide pipe) and the other pipe is half of an inch wide (narrow pipe). Activities 3 and 4 involve a composite pipe with a section of three quarters of an inch wide and the other section is half an inch wide. Pipes are connected to a faucet and water runs through the pipes coming from a large recipient. In each activity choose the right answer among the three options given in the questionnaire and write it down in the Answer Sheet at the space indicated. Make sure that you are writing an explanation of your selected answer..

## ACTIVITY 1

1.1 The amount of water accumulated in the recipient when the pipe is connected to the faucet of a wider diameter (wide pipe) is:

- a. Larger than the amount collected when the faucet is connected to the pipe with a smaller diameter (narrow pipe)
- b. Smaller than the amount collected when the faucet is connected to the pipe with a smaller diameter (narrow pipe).
- c. Equal to the amount collected when the faucet is connected to the pipe with a smaller diameter (narrow pipe).

1.2 When the pipe is connected to the faucet, the jet will fall:

- a. At a larger distance than when it is connected to the narrow pipe.
- b. The same distance as when it is connected to the narrow pipe hose.
- c. An smaller distance than hen it is connected to the narrow pipe.

1.3 When the wide pip hose is connected to the faucet, the speed with which the jet exits from the pipe is:

- a. Smaller than when it is connected to the narrow pipe hose.
- b. Largent than when it is connected to the narrow pipe hose.
- c. The same as when it s connected to the narrow pipe hose.

ACTIVITY 2: In questions 1.1 to 1.3 the wide pipe hose is changed by the narrow one.

ACTIVITY 3: In questions 1.1 to 1.3 the wide pipe hose is changed by the composite pipe hose and it is connected to the faucets by the wide section.

ACTIVITY 3: In questions 1.1 to 1.3 the wide pipe hose is changed by the wide pipe hose and it is connected to the faucet by the narrow part.

## REFERENCES

- Arons, A. B. y Karplus, R. (1976). Implications of accumulating data on levels of intellectual development, *American Journal of Physics*, 44, 396. [1]
- Guillen, M. (2007) Cinco ecuaciones que cambiaron el mundo, 87. [2]
- Lawson, A. E. (1995). *Science teaching and the development of thinking*. Belmont, CL: Wadsworth Publishing Company. [3]
- McKinnon, J. W. y Renner, J. W. (1971). Are colleges concerned with intellectual Development? *American Journal of Physics*, 39, 1047 – 1052. [4]
- Piaget, J. y Inhelder, B. (1958). *Growth of Logical Thinking*. New York: Basic Books. [5]
- Pozo, J.I. Gómez M.A(2204) Aprender y Enseñar Ciencia. Morata cuarta edición, 77, 78 [12]

- Renner, J. W. (1976). Significant physics content and intellectual development: cognitive development as a result of interacting with phycis content, *American Journal of Physics*, 44, 218 - 222. [6]
- Renner, J. W. y Paske, W.C. (1977). Comparing two forms of instruction in college physics. *American Journal of Physics*, 45, 851 - 859. [7]
- Sears, W F., Zemansky, Mark W; y Young, Hugh, D. (1990)Física Universitaria Sexta Edición Addison Wesley Iberoamericana, 316 [9]
- Tippens, P.Física de Conceptos (2001) Edit. Mc. Graw Hill sexta edición 325,326,328,329, 341,342 [10]
- Streeter, V.L.; Wylie E. B y Bedford K. W (1999) Mecánica de fluidos. Edit. Mc Graw Hill Novena edición 202-205 [11]
- Whitaker, R. J. y Renner, J. W. (1974). Teaching practices in introductory physics vourses, *American Journal of Physics*, 42, 820 - 829. [8]



***Chapter 11***

## **PHARMACEUTICAL BIONANOTECHNOLOGY: FUNDAMENTAL PRINCIPLES\***

***Emilio Segovia***

Laboratorio de Bionanotecnología, Departamento de Ciencias de la Vida y de la Tierra,  
Centro Universitario de Los Lagos, Universidad de Guadalajara

### **RESUMEN**

Cuando un grupo de moléculas farmacológicamente activas encerradas en nanocápsulas biodegradables inciden en los tejidos del organismo, el sistema en su conjunto podría compararse a un ejército de minúsculos caballos de Troya de los cuales se liberan y liberan estas moléculas a manera de guerreros combatiendo y derrotando a enemigos tales como microorganismos patógenos o virus.

La Bionanotecnología Farmacéutica puede ser definida como el estudio de los mecanismos de interacción entre nanocápsulas cargadas de moléculas bioactivas y los diversos tejidos corporales. Se ha encapsulado una variedad de moléculas con actividad terapéutica, así como vacunas y ADN. Aquí se presentan una serie de opciones de medicamentos encapsulados para su administración a través de las mucosas.

### **ABSTRACT**

When a group of pharmacologically active molecules enclosed in biodegradable nanocapsules is delivered into the body, the system as a whole could be compared to an army of tiny Trojan horses from which these molecules are released resembling warriors combating and defeating enemies such as pathogen microorganisms or virus.

Pharmaceutical Bionanotecnology can be defined as the study of interaction mechanisms between bioactive molecules charged capsules and human tissues. A number

---

\* Paper presented at the *Educating the next generation of scientists and engineers: Nanotechnology in the K-16 science curriculum*, Universidad Autónoma Metropolitana, Campus Azcapotzalco, Mexico, D.F., September 24-28, 2007.

of molecules such as vaccines, DNA and some drugs provided with pharmacological activity have been successfully encapsulated. A number of options of nanoencapsulated compounds for mucosal administration are presented in this paper.

**Keywords:** Pharmaceutical Bionanotechnology, nanocapsules, mucosal barrier.

## INTRODUCTION

When a group of pharmacologically active molecules are filled into biodegradable capsules reaches live tissues, the overall system could be compared to minuscule Trojan horses from which these molecules are released as if they were warriors to defeat their enemies such as pathogen microorganisms and viruses.

Biodegradable capsules can be obtained from polymers obtained from the polymerization of several organic acids (table 1). Once the acids are polymerized, the compounds yielded are by themselves biodegradable polymers suitable to generate nanocapsules to be charged with pharmacologically active molecules (table 2).

**Table 1. Examples of substances to obtain biodegradable polymers**

Name	Structure	Molecular weight
Acetic acid		60.05
Glycolic acid		76.05
Lactic acid		90.08

**Table 2.** Some biodegradable polymers to manufacture nanocapsules

Name	Structure
Polylactic acid	
Gelatin	
Lecithin (Phosphatidylcholine) e)	$\text{R''COO}-\overset{\text{CH}_2-\text{OOCR}'}{\underset{\text{O}}{\text{CH}}}-\overset{\text{O}}{\underset{\text{O}^-}{\text{P}}}(\text{O}^-)-\overset{+}{\text{O}-\text{CH}_2\text{CH}_2\text{N}(\text{CH}_3)_3}$

These molecules inside the nanocapsule are eventually released when in contact with tissues (figure 1).

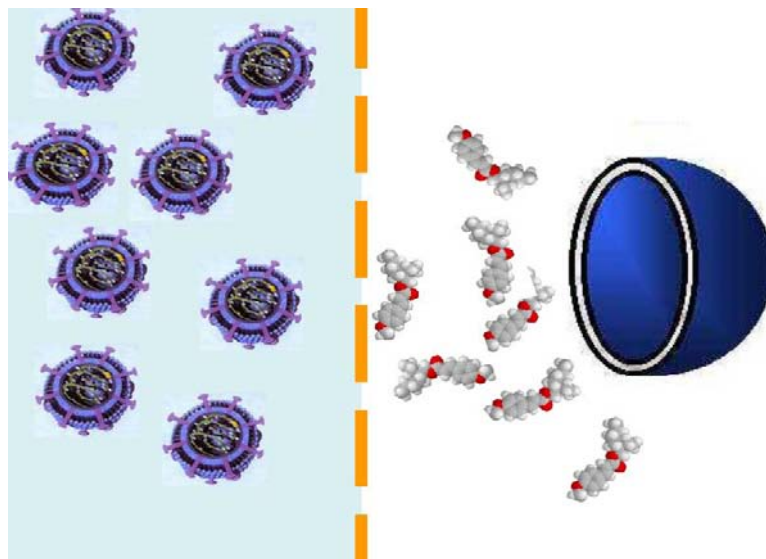


Figure 1. Molecules being released from nanocapsules.

## NANOENCAPSULATED SUBSTANCES

A variety of substances have been nanoencapsulated: *Drugs*: chlorpheniramine maleate, indometacine, Insulin. *Biologicasl*: tetanic toxoide, *Yeseenia pestis*, hepatitis B virus, diphtheria, blood substitutes, DNA, and many more.

Singh *et al.*, using nanoparticles, prepared using a water-in-oil-in-water (w/o/w) double emulsion solvent evaporation method and using Poly-(epsilon-caprolactone) (PCL), a poly(lactide-co-glycolide) (PLGA)-PCL blend and co-polymer nanoparticles encapsulating diphtheria toxoid (DT) were investigated for their potential as a mucosal vaccine delivery system.

Poly (L-lactic acid) (PLA) microparticles encapsulating Hepatitis B surface antigen (HBsAg) with alum and chitosan were investigated by Pandit *et al.* for their potential as a vaccine delivery system. The microparticles, prepared using a water-in-oil-in-water (w/o/w) double emulsion solvent evaporation method with polyvinyl alcohol (PVA) or chitosan as the external phase stabilizing agent showed a significant increase in the encapsulation efficiency of the antigen.

## MANUFACTURING PROCESS

The more efficient nanocapsule manufacturing process is based upon high or medium pressure homogenisation of single and double emulsions of three main ingredients: active biomolecules, a selected polymer and an organic solvent (figure 3). Nanocapsule laboratory manufacturing techniques have been developed some years ago mainly at pharmaceutical research laboratories from some universities of several European countries. Nevertheless these techniques still remain at laboratory scale although some unsuccessful attempts have been done to produce nanocapsules at production scale level.

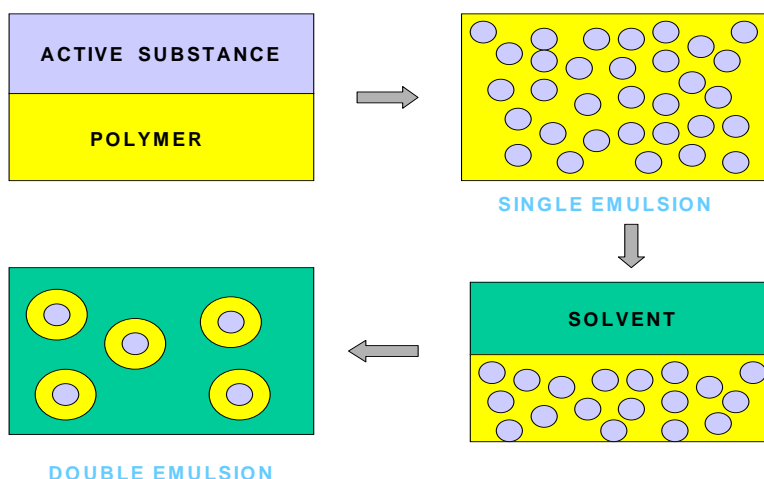


Figure 2. Single and double emulsions.

## EQUIPMENT

The aims for the nanocapsules manufacturing equipment building can be described as follows:

1. The development of existing single emulsion jet homogenisation technology to provide a process for the manufacture of double emulsion micro- and nanoparticles in a way that can be scaled up.
2. Engineer a system that will prove suitable for the production of clinical trial batches of successful vaccine formulations providing 100% protection *in vivo* after nasal administration.
3. To investigate the formulation effects within the process, and the process parameters that control the final particle characteristics.

To deal with the production level scale Segovia has proposed to build up an special equipment that includes the following components:

- Mixing chambers (Homogenizers)
- Exchangeable orifice plates
- 0.22  $\mu$  filtering station
- Heat control jackets
- Pressure regulation valves
- Supply vessels
- Collection vessels

Some of these components are schematically depicted in figure 3.

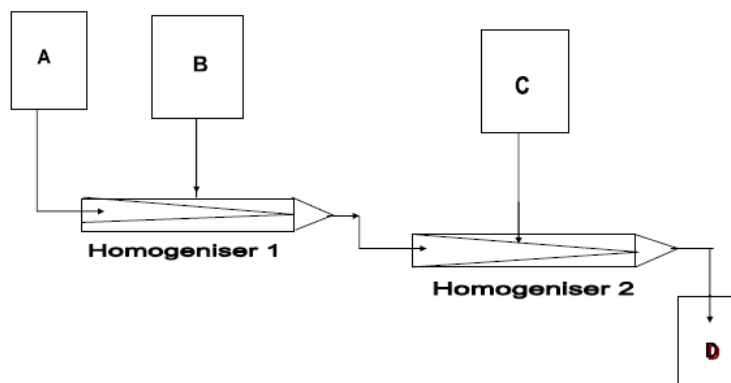


Figure 3. Components of the manufacturing equipment.

The manufacturing equipment described has to comply with certain requirements such as:

- Parts in contact with product made of 316 L stainless steel
- Capable of taking pressures up to 500 Bar (gas or pump)

- Easy to clean and assemble
- Ease to change orifice plates
- Suitable for large volumes (100-500 ml)
- Suitable for continuous process
- Ease to obtain spare parts and
- Not to be expensive

Once the requirements are properly fulfilled, the completion of the equipment from the design up to the final approval to start the initial operation has to follow a number of stages:

- Design
- Find a suitable workshop
- Build up
- Assembling
- Testing
- Modify design
- Reassembling
- Testing
- Final approval
- Initiate experimental work

The full program should be carried out in a number of successive actions, some of them pain-taking and time consuming such as:

1. Development of an homogeniser – machine building
2. Development of a solvent extraction system. (it can be carried out simultaneously to the homogeniser building)
3. Development of a control system
4. Development of a monitoring system (simultaneously to the development of the control system)
5. Integration of control and monitoring systems
6. Evaluation of homogenisation efficiency and function
7. Evaluation of solvent extraction efficiency and function
8. Investigation of process parameters
9. Process development
10. Initiate scale-up to manufacturing level
11. Evaluation of product suitability for clinical trials
12. Evaluation of GMP compliance
13. GMP registration. (If compliance is satisfied)
14. Formulation of clinical trial batches
15. Optimisation of existing formulations
16. Production of a first clinical batch

## SELECTION CRITERIA FOR MOLECULES TO BE NANOENCAPSULATED

In order to test the nanocapsule manufacturing equipment it will become necessary to select initially a placebo for setting equipment conditions, that is, temperature, pressure, plate orifice diameter at the exit of homogenizer and temperature and coolant water in the cooling jackets of the homogenizers. Once the conditions are set up a drug to be nanoencapsulated will be selected. The drug is required to be therapeutically appealing, readily available, fully characterised, water soluble and of low cost. Parameters to be taken into consideration before the encapsulation is started are the nature of the molecule to be encapsulated, pH of the drug in solution, viscosity, mixing time, volume/weight ratio of internal/external phase, orifice diameter and flow rate through orifice.

## EXPERIMENTAL DESIGN

The selected experimental design will be the Evolutionary Operation method (EVOP) defined by Ridgway as the introduction of a repetitive pattern of small perturbations into the input parameters of a manufacturing process and studying the resultant changes in the rate of manufacturing, the quality of the product or its cost. The parameters selected can be size, stability and sphericity of the obtained nanocapsules and drawing of the area where these parameters resulted satisfactory within a range of temperature of 25 to 60 °C and a range of pressure of 350 and 400 Bar (figure 4). Then, superposing the three selected individual areas will yield an area common to the three which will represent the ideal operation conditions (figure 5)

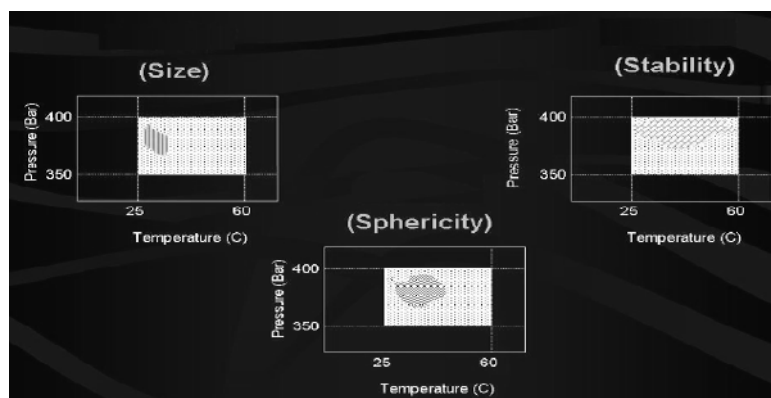


Figure 4. EVOP graphs of three parameters (size, stability and sphericity).

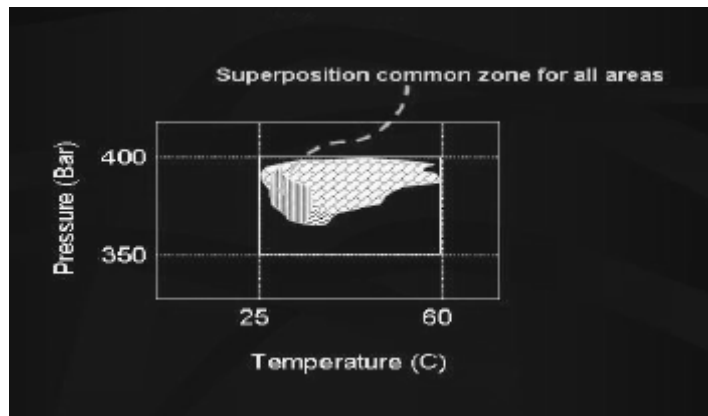


Figure 5. EVOP Superposition of size, sphericity and stability areas.

### EFFECTIVITY OF NANOENCAPSULATED DRUGS VERSUS DISSOLVED ONES

Nanoencapsulated drugs are much more effective than a drug in solution as can be seen in figure 6.

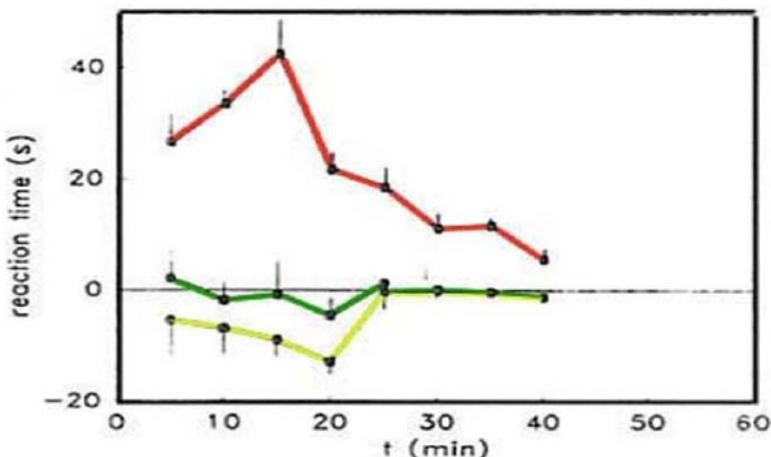


Figure 6. Comparative analgesic action of 2% dispersion of nanoencapsulated Lidocaine (red), 2% solution of Lidocaine (green) and a control solution (Yellow) during topical administration. (Analgesic intensity is measured as a function of the time taken to react to a painful stimulus).

### ADMINISTERING DRUGS THROUGH THE MUCOSAL BARRIER

The more effective way to administer nanoencapsulated drugs is by spraying it from a suspension into a mucosal tissue such as the nasal mucosa. As soon as the nanocápsulas enter into the mucosa barrier they get rid of the polymer capsule liberating the drug. The polymer

(Polylactic acid) decomposes generating lactic acid. The later breaks producing carbon dioxide and water:

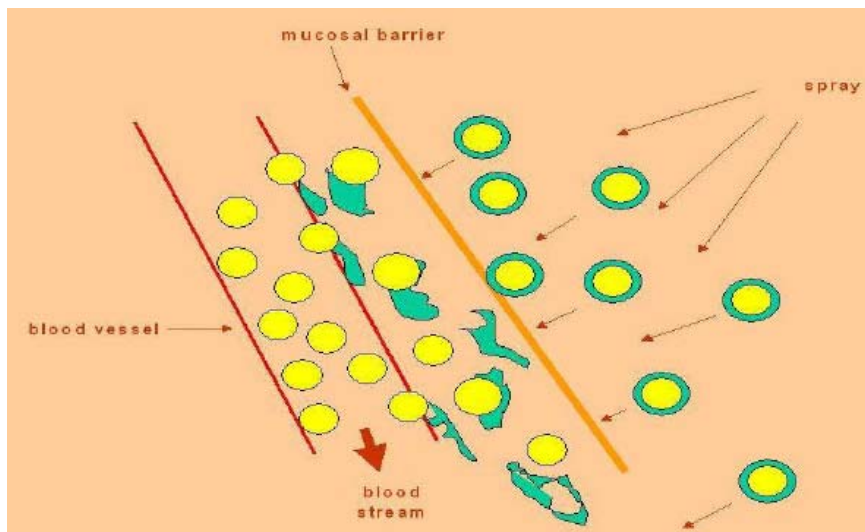


Figure 7. Nanoencapsules trespassing the nasal mucosal barrier while drug reaches blood vessels.

By the time the drug enters the blood stream through the vessels, the therapeutic effect starts taking place.

## CONCLUSION

It can be concluded that the most efficient way to administer drugs into the blood stream is through a spray applied to the mucosal tissues.

## ACKNOWLEDGEMENTS

Dr. Emilio Segovia holds a PhD degree from University of London. He is a full professor and research worker in charge of the Bionanochnolgy Laboratory at Los Lagos University Centre University of Guadalajara in Mexico where he has been working in the subject for the last three years. His areas of interest are Water purification and Pharmaceutical Bionanotechnology. Dr. Segovia has delivered more than 200 conferences talks and short courses in many meetings around the world.

## REFERENCES

- Pandit S, Cevher E, Gulrez Zariwala M, Somavarapu S and Alpar H O (2007). Enhancement of immune response of HBsAg loaded poly (L-lactic acid) microspheres against Hepatitis B through incorporation of alum and chitosan. *J. Microencapsul.* Sep;24 (6):539-52.
- Ridgway, K. (1970). Improving production by using evolutionary operation: aspects of pharmaceutical engineering. *Pharmaceutical Journal.* 205 (Sep 5): 265-267.
- Segovia, E. (2002). High and medium pressure homogenisation for producing particles carrying biomolecules: A Report on Research Progress. Centre for Delivery Drug Research. School of Pharmacy, University of London.
- Singh J , Pandit S, Bramwell V W and Alpar H O. (2006) Diphtheria toxoid loaded poly-(epsilon-caprolactone) nanoparticles as mucosal vaccine delivery systems. *Methods.* Jan 25;164.

**Chapter 12**

## **THE ORDER PARAMETER OF A BINARY ALLOY THIN FILM OF Cu<sub>3</sub>Au**

**G. Ramírez-Dámaso<sup>\*1, 2, 5, 6</sup>, F.L. Castillo-Alvarado<sup>2, 4</sup>,  
I. Zasada<sup>3</sup> and L. Wojtczak<sup>3</sup>**

<sup>1</sup> Becario CONACyT; <sup>2</sup> Escuela Superior de Física y Matemáticas del IPN,  
Edificio 9, Zacatenco, C. P. 07738 México D. F. México

<sup>3</sup> Departament of Solid State Physics, University of Lodz,  
ul. Pomorska 149/153, 90236 Lodz, Poland.

<sup>4</sup> Becario COFAA-IPN, EDD-IPN.

<sup>5</sup> Escuela Superior de Ingeniería y Arquitectura “Unidad Ticomán”  
del I. P. N., Av. Ticomán No. 600, Col. San José Ticomán, C. P. 07330,  
Del. G. A. M., México D. F., México.

<sup>6</sup> Tecnológico de Estudios Superiores de Ecatepec, Av. Tecnológico s/n esq.  
Av Carlos Hank González, Col. Valle de Anáhuac, C. P. 55210,  
Ecatepec Edo. de México, México

### **ABSTRACT**

We describe the degree of the ordering of components in an alloy Cu<sub>x</sub>Au<sub>1-x</sub> thin film using a lattice order parameter t(i), being i the number of layers in the system. The formulations reported by Hill [1] in the context of small particles can be applied to the film structure when we treat a thin film as a system divided into subsystems equivalent to two-dimensional monoatomic layers parallel to the surfaces. The film thickness d is then the characterization of a sample and it can be expressed by the number n of monoatomic layers d = na, so i(1,n) with a standing for the average spacing between the neighbouring layers. Then we can use the thermodynamic relation F(d)=U(d)-T S(d) between the free energy F, the internal energy U, and the entropy S. In order to obtain t(i) in equilibrium vs T, we minimize the free energy respect to the lattice order parameter. We apply this

---

\* Corresponding author: Phone: 52-55-57-29-61-39, Fax: 52-55-55-86-29-57. E-mail address:  
gramirezd@ipn.mx

theory to the case of a fcc Cu<sub>3</sub>Au binary alloy. We obtain t(i) vs T and x(i) vs T, with n = 17 where we observe the correct behaviour.

**Keywords:** Thin films; Alloys; Surface disordering.

## 1. INTRODUCTION

The order-disorder phenomena for binary alloys have been studied as theoretically as experimentally by many authors [2-5]. In our case we study a three-dimensional system from a two-dimensional view point. In the recent years the surface effects over those films have been studied [5-8], by two different phenomena, the surface disordering and the surface melting, where the difference between them is that melting consists on destruction of the lattice and disordering preserves the lattice and the atoms move around it [6]. In this paper we work with a Cu<sub>3</sub>-Au thin film near the order-disorder transition temperature, and we describe the degree of ordering of the atoms of the lattice by means of the equilibrium order parameter. The order parameter in this work is a quantitative measurement of the crystalline sample, where t=1 means that the sample is completely ordered and t=0 is completely disordered.

## 2. THEORY

Consider a fcc binary alloy A<sub>x</sub>B<sub>1-x</sub> that consists of N atoms in the direction (111) of the crystallographic plane (figure 1), where we suppose that the temperature of it is near to 0 K, in order that all the atoms are fixed in the showed positions. We divide the crystalline structure in two sublattices:  $\alpha$ , the sites of the corners and  $\beta$ , the centers of the faces of the cube. We suppose that our thin film is formed by n planes parallel to the direction (111). Introducing probabilities of sites, such as PA <sub>$\alpha$</sub> , PA <sub>$\beta$</sub> , PB <sub>$\alpha$</sub>  and PB <sub>$\beta$</sub> , that correspond to the probabilities of find atoms A in the sublattice  $\alpha$ , A in the sublattice  $\beta$ , B in the sublattice  $\alpha$  and B in the sublattice  $\beta$ , respectively, we express the order parameter  $t(i) = PA_{\alpha}(i) - PA_{\beta}(i) = PB_{\beta}(i) - PB_{\alpha}(i)$  and the composition  $x(i) = PA_{\alpha}(i)F_{\alpha} + PA_{\beta}(i)F_{\beta}$ , for i=1,..,n.

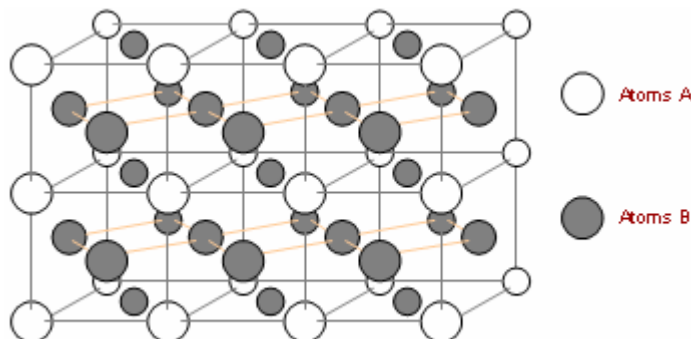


Figure 1. An alloy AB<sub>3</sub> with crystalline structure fcc.

Now we introduce the free energy:

$$F(x(i), t(i), T) = U(x(i), t(i)) - T S(x(i), t(i)) \quad (1)$$

where  $U$  is the internal energy,  $T$  is the temperature and  $S$  is the entropy. In the plane  $i$ , one atom A in the sublattice  $\alpha$  will have atoms B and A as first neighbors in the sublattice  $\alpha$  or  $\beta$  of the planes  $i$ ,  $i+1$  or  $i-1$ . Then, the internal energy is expressed as [5,9]:

$$U(x, t) = -N \sum_{i, C, C'} \left[ \langle \varrho_{CC'} \rangle_{ii} V_{CC'}^{ii} + \langle \varrho_{CC'} \rangle_{ii+1} V_{CC'}^{ii+1} + \langle \varrho_{CC'} \rangle_{ii-1} V_{CC'}^{ii-1} \right] \quad (2)$$

where:  $i=1, \dots, n$ , and  $C, C' = A, B$ . The values  $\langle \varrho_{CC'} \rangle_{ii}$  are all the possibilities of find two atoms on the layer  $i$ , with interaction energies  $V_{CC'}^{ii'}$ .

Here the entropy (Bragg-Williams approximation) is:

$$S(x, t) = k_B N \sum_{i, C, \gamma} F_\gamma P_C^\gamma(i) \ln P_C^\gamma(i) \quad (3)$$

### 3. RESULTS

We minimize the free energy (1):

$$\frac{\partial F}{\partial x(i)} = \lambda \text{ and } \frac{\partial F}{\partial t(i)} = 0 \quad (4)$$

under the condition:

$$\sum_i x(i) = nc \quad (5)$$

where  $c$  is the concentration of A atoms in each layer and  $\lambda$  is a Lagrange multiplier.

Solving (4) and (5), we obtain  $x(i)$  and  $t(i)$ , for temperatures from 0 to 663 K, with  $n=17$  monolayer of Cu<sub>3</sub>Au,  $c=0.25$  [7]; figures 2 and 3 show our results.

We observe from figure 2 that all the atoms A have a value of  $x = 0.25$  at  $T=0$  K and  $T = 663$  K, but at the surface  $x(1)$  and  $x(17)$  decrease when the temperatures is increasing from 0 to 663. For atoms in the bulk  $x(5)-x(13)$ , the composition increase. In figure 3 we observe that the order parameter in each one of the layers goes to zero when the temperature is increasing. The values  $t(1)$  and  $t(17)$  first goes to zero continuously in comparison with the others. However, all take the value of zero at the transition temperature.

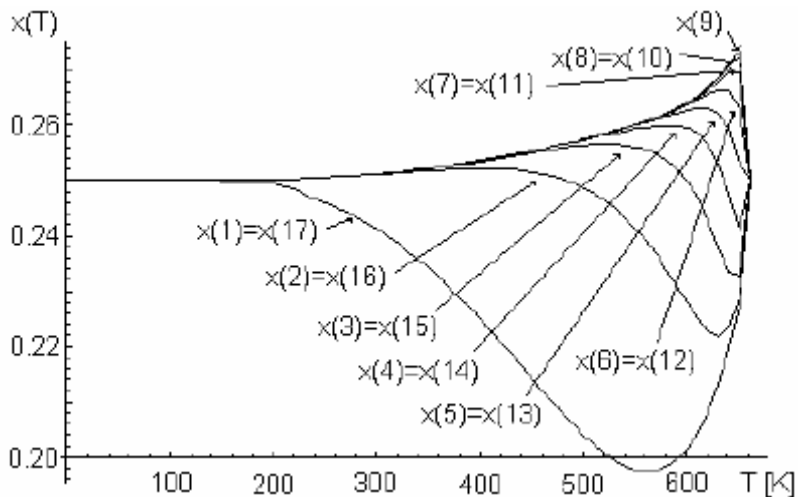


Figure 2. Composition of atoms Au for T from 0 to 663 K and n=17.

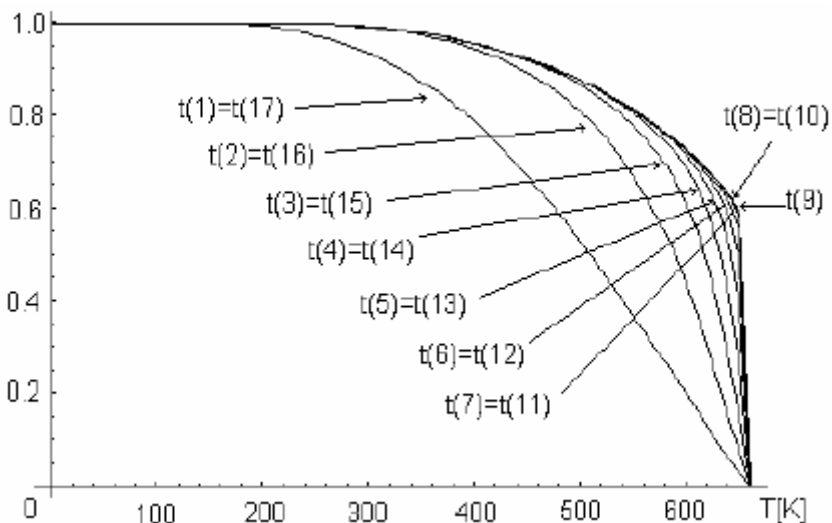


Figure 3. Long range order parameter for T from 0 to 663 K and n = 17.

#### 4. CONCLUSIONS

In the (111) direction of our  $\text{Cu}_3\text{Au}$  thin film,  $x$  has the same value of 0.25 at the beginning as at the end of the process. The disorder begins always at the surface and the order parameter is symmetric around the center of the sample. In the bulk we obtain a first order phase transition and at the surface a second order phase transition, which are in concordance with the experiments.

## ACKNOWLEDGMENT

Work partially supported by CONACyT-MEXICO.

## REFERENCES

- [1] T. L. Hill, *J. Chem. Phys.* 36, 3182 (1962).
- [2] J. L. Morán-López and L. M. Falicov, *Physical Review B*, Volume 18, Number 6 (1978) 2542.
- [3] J. L. Morán-López and L. M. Falicov, *Physical Review B*, Volume 18, Number 6 (1978) 2549.
- [4] J. L. Morán-López, F. Mejía-Lira, K. H. Bennemann, *Phys. Rev.* 54 (1985) 1936.
- [5] F. L. Castillo-Alvarado, A. Sukiennicki, L. Wojtczak, I. Zasada, *Physica B* 344 (2004) 477.
- [6] L. Wojtczak, I. Zasada, A. Sukiennicki, F. L. Castillo Alvarado, *Phys. Rev. B* 70 (2004) 195416.
- [7] L. Wojtczak, I. Sazada, A. Sukiennicki and F. L. Castillo, Order-disorder phenomena at the surfaces of alloy thin films, Bulletin de la Société des Sciences et des Lettres de Lódz, Vol. XXXV, Poland, 2001.
- [8] L. Wojtczak, I. Sazada, T. Rychtelska, *Surface Science*. 600 (2006) 851-860.
- [9] L. Valenta, A Sukiennikcki, *Phys. Stat. Sol.* 17 (1966) 903.



*Chapter 13*

## **GREEN'S FUNCTION TIGHT-BINDING FORMALISM FOR LINE-SHAPE DESCRIPTION OF VIRTUAL ELECTRONIC STATES**

**S. J. Vlaev**

Unidad Académica de Física, Universidad Autónoma de Zacatecas,  
Calzada Solidaridad esq. Paseo La Bufa s/n  
Zacatecas 98068, ZAC., México

### **ABSTRACT**

The possibility of line-shape description for virtual electronic states within the framework of the Green's function formalism is discussed. The consideration is carried out for a semi-empirical tight-binding model. A new scheme based on the Green's function imaginary part is proposed to calculate the full width at half maximum (FWHM) and the mean-life time of virtual electronic states.

### **RESUMEN**

Consideramos la posibilidad de determinar la forma de la línea de estados electrónicos virtuales dentro del formalismo de las funciones de Green en el contexto del modelo de enlace fuerte semi-empírico. Proponemos un nuevo esquema numérico basado en la parte imaginaria de la función de Green para calcular la anchura a media altura (FWHM) y el tiempo de vida media de estados electrónicos virtuales.

### **1. INTRODUCTION**

The study of the electron structure of atoms, molecules, clusters, nanostructures and condensed matter objects of different dimensionality is a main purpose of the modern experimental and theoretical investigations in the atomic, molecular and solid state physics,

materials science and quantum chemistry [1]. All new physical phenomena discovered in the last decades in these fields and their practical applications are strongly related to the basic electronic properties of the matter [2-4]. The rigorous description of the electronic structure can be achieved through quantum mechanical methods and precise measurements based on quantum mechanics [2-4].

The direct observation of the occupied and non-occupied electronic states is possible in the photo-emission, inverse photo-emission and scanning tunneling spectroscopy measurements [5,6]. These experimental techniques permit to obtain detailed total density of states curves and in many cases the band structure and the local density of states in some points of the Brillouin zone for periodic structures [7]. These quantities can be calculated within the framework of different molecular or solid state physics theoretical methods based on the quantum mechanics [8]. The empirical, semi-empirical and first principles methods in discrete and continuous models give the eigenvalues and the eigenvectors of the system related directly to the energy position and the intensity of the maxima in the density of states curves [8].

Each maximum of a given density of states curve obeys two fundamental characteristics: the energy position and the intensity. The energy position determines qualitatively the electronic structure and the chemical composition of the system and the intensity contains also quantitative information. The parameter for each energy maximum in the spectroscopy measurements which describes the line-shape is the full width at half maximum (FWHM) [6].

It is well known that the electronic energy spectrum of each quantum-mechanical system may have discrete and continuum part. The discrete part contains bound states and the states in the continuum are unbound states. Energy bands appear in a bulk crystal and their states propagate through the crystal having the behavior of Bloch extended states. In some cases, for instance crystal with defects, the so called quasi-bound (virtual) states appear in the continuum [9,10]. These quasi-bound states possess normally very strong energy and spatial localizations and obey specific features. These states, occupying the place between the bound and the extended states, have attracted recently the attention of many researchers because of their specific characteristics. The possibility to design the energy position and the FWHM parameter of the quasi-bound states in quantum well structures taking into account the fundamental analogy between photon and electron optics makes the investigations in this direction very interesting and promising from the point of view of technological applications [9].

A bound state is a delta-like state. Measurements and calculations with a given precision "see" this delta-like state as a state with a final energy width. This energy width is an artificial fact and not an intrinsic feature of the physical system. In the measurements this width depends on the experimental technique and in the numerical calculations on the method of calculation. If the precision is sufficient to resolve the maxima, the area of each maximum conserves when the line-shape (FWHM parameter) changes. The only important information is the energy position of the maximum. Theoretically each bound state has a zero width and the corresponding mean-life time is infinity.

An extended state in the quasi-continuum of a crystal band has the same delta-like state behavior. We can measure or calculate a continuous density of states curve with different precisions but each maximum of this curve will be always a delta-like state and, as a result, its mean-life time will be equal to infinity.

The fundamental difference between the bound and extended states from one side and the quasi-bound (virtual) states from other is the fact, that the virtual states have intrinsically finite value of the FWHM parameter and, as a consequence, finite mean-life times. The physical reasons for this intrinsic feature of the virtual states can be different. For instance, the un-restricted Hartree-Fock treatment of the Anderson impurity model [10] derives analytical solutions which reveal the physical mechanism for the creation of virtual states in case of bulk and surface impurities in metals. In many complicated physical systems where analytical solutions are not found, there is not a transparent quantitative explanation for the existence of virtual states.

The virtual states can be observed and studied experimentally using time-resolved spectroscopy measurements [11]. The interpretation of the experimental data and the systematical theoretical study of the quasi-bound states in real systems need the development of stable numerical schemes to calculate the FWHM parameter of the virtual states.

The Green's function formalism has been widely applied in the electronic structure calculations [12,13]. The Green function contains by definition a vanishing imaginary part added to the energy. In the numerical calculations this imaginary part is a small but finite one and it corresponds to the energy resolution of the experimental measurements. To the best of our knowledge there are very few studies within this formalism to calculate the FWHM parameter of quasi-bound states. The aim of the present work is to discuss how the Green's function formalism can be applied to describe the line-shape of the virtual states. We propose a numerical scheme based on the Green's function methodology in the context of the semi-empirical tight-binding model. A brief review of some results for real systems obtained by us previously is presented as an illustration.

## 2. GENERAL DESCRIPTION OF THE NUMERICAL SCHEME

The quantum-mechanical formula to calculate the density of states  $\rho(E)$  in the Green's function formalism is given by:

$$\rho(E) = -1/\pi \lim_{s \rightarrow 0} [\text{Im } G(E + is)] \quad (1)$$

where  $G(E + is)$  is the Green function of the system and  $s$  is the vanishing imaginary part added to the energy. This formula has been widely applied in the literature to obtain the electronic spectrum of different kind of physical systems. The common interpretation of the imaginary part as the precision of the calculation restricts the application of formula (1) and a full description of the line-shape for virtual states can not be done. An intrinsic feature of the virtual states is the finite energy width of their maximum  $\Gamma$ . The full width at half maxima (FWHM) parameter  $\Gamma$  contains additional physical information – the mean-life time  $\tau$  of the virtual state.

$$\tau = \hbar/\Gamma \quad (2)$$

If we want to extract this information from the line-shape of the electronic state we have to calculate this intrinsic FWHM parameter. The problem is to find the procedure which permits the determination of the FWHM.

The idea of the proposed numerical scheme which may determine the FWHM is very simple. We have to calculate the position of the maximum and its energy width for different values of the imaginary part  $s$  decreasing the value of  $s$  in the sequence of calculations. The step energy value in each cycle of the calculation has to be properly chosen providing correct result. Observing what kind of behavior the FWHM values have one can determine the type of the electronic state and in the case of virtual states we are able to find the intrinsic FWHM value thus describing the line-shape and finding the mean-life time of the virtual state.

To clarify better the proposed procedure we consider below typical bound, extended and virtual states.

## 2.1. Bound States

Let's consider the simple example of an isolated bound S state. Its Green function  $G_b(E + is)$  has the form:

$$G_b(E + is) = (E - E_0 + is)^{-1} \quad (3)$$

where  $E_0$  is the energy position of the level,  $s$  the small imaginary part and  $i$  the imaginary unit. The density of states  $\rho_b(E)$  is given by the well known formula:

$$\rho_b(E) = -1/\pi \lim_{s \rightarrow 0} [Im G_b(E + is)] \quad (4)$$

In this trivial case we obtain

$$\rho_b(E) = 1/\pi \lim_{s \rightarrow 0} [s/[(E - E_0)^2 + s^2]] = \delta(E - E_0) \quad (5)$$

The Eq. (5) describes the bound state at energy  $E_0$  with  $FWHM = 0$  and mean life time  $\tau = \hbar/\Gamma = \infty$ . If we perform a numerical calculation where  $s$  has a finite small value, we will observe this discrete level with  $\Gamma = s$ . The situation is analogous to a measurement with energy resolution  $s$ . For smaller  $s$  values we find smaller  $\Gamma$  values, conserving the area of the pick. It is impossible to obtain equal numerical values for  $\Gamma$ , decreasing the small imaginary part  $s$  during the calculations. For complicate real systems where the analytical form of the Green function is not known, numerically the procedure is the same. However, in the case of quasi-bound states the numerical scheme is quite different, as we demonstrate in the subsection 2.3.

Figure 1 illustrates the above considerations for the ground bound state in Al(x)Ga(1-x)As/GaAs quantum well with  $x=0.3$  and well width of 50 monolayers. The energy of this state is 10meV measured from the bottom of the well. A typical delta-like behavior is

observed. The numerical procedure falls down when the imaginary part takes values of the order of the machine zero.

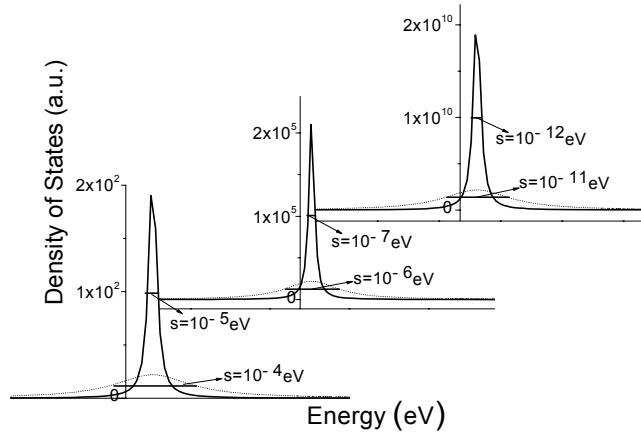


Figure 1. Line-shape of the ground electronic bound state in 50 monolayers rectangular Al(0.3)GaAs(0.7)/GaAs quantum well calculated with different values of the imaginary part  $s$ . A typical delta-like behavior is observed for the energy maxima. The energy of the state measured from the bottom of the well is 10 meV.

## 2.2. Extended States

If we consider now any energy maximum of the density of states curve in a band of a bulk crystal, we obtain the same behavior in the numerical calculation of the FWHM parameter as in the previous subsection. The numerical procedure again falls down when the imaginary part takes values of the order of the machine zero. Figure 2 presents the results for bulk GaAs. The maximum has energy  $E_0=0.48$  eV measured from the bottom of the GaAs conduction band.

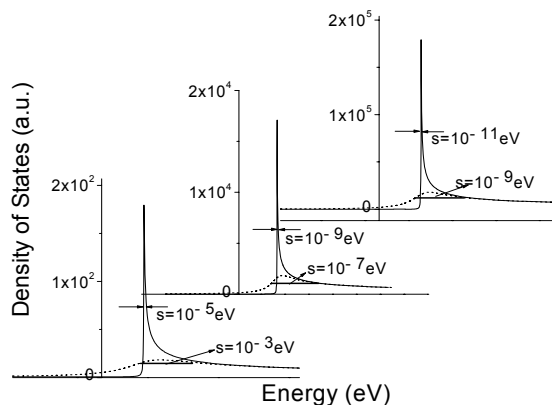


Figure 2. Line-shape of the extended bulk state in the GaAs conduction band with energy 0.48 eV measured from the band edge calculated with different values of the imaginary part  $s$ . A delta-like behavior is observed again for the energy maxima.

## 2.3. VIRTUAL STATES

Let's consider now a single quasi-bound S state. A well known case is, for instance, the virtual impurity level in metals. The un-restricted Hartree-Fock solution of the Anderson impurity model gives analytical solution for the Green function of the impurity  $G_{qb}(E + is)$ :

$$G_{qb}(E + is) = (E - E_0 + is + i\Gamma)^{-1} \quad (6)$$

where  $\Gamma$  is the intrinsic finite *FWHM* parameter. The parameter  $\Gamma$  depends on the metal band structure and the local impurity-host interaction. The Eq. (4) now derives

$$\rho_{qb}(E) = 1/\pi \{ \Gamma / [(E - E_0)^2 + \Gamma^2] \}, \quad (7)$$

a pick of Lorentzian line-shape. What about the numerical procedure in this case? If the small imaginary part  $s \geq \Gamma$ , we observe a Lorentzian pick, but its *FWHM* parameter has a value different from  $\Gamma$ . Only if  $s \ll \Gamma$ , the density of states gives us the right *FWHM* parameter equal to  $\Gamma$ . The mean life time  $\tau = \hbar / \Gamma$  calculated in the case when  $s \ll \Gamma$  has the correct value. Decreasing  $s$  during the calculations, we must find  $s$  value after which the *FWHM* does not change. It is important to mention that the step of the energy has to be properly chosen.

Figure 3 shows the line-shape description of the quasi-bound state in in 500 monolayers rectangular Al(0.3)Ga(0.7)As/GaAs quantum well. There are not changes in the line-shape of the pick for values of the imaginary part less than  $10^{-8}$  eV. The Lorentzian pick has a finite energy width. The calculated value for the FWHM parameter is  $10^{-6}$  eV.

In a general case we don't have analytical solution and the interpretation about the physical reasons which create quasi-bound states is not clear as in the case of the Anderson impurity model cited above.

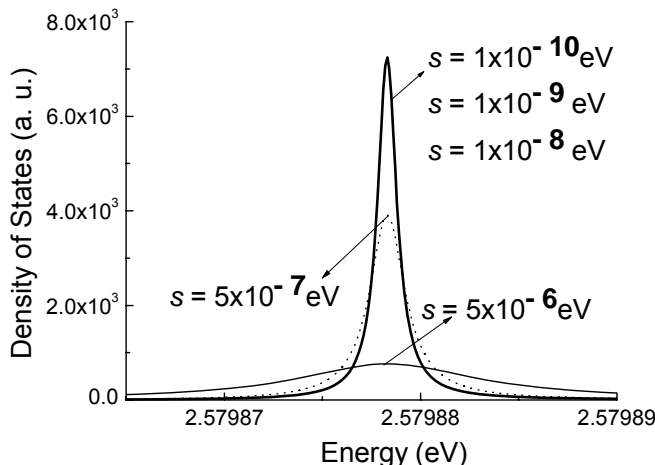


Figure 3. Line-shape of the first virtual electronic state in 500 monolayers rectangular Al(0.3)Ga(0.7)As/GaAs quantum well calculated with different values of the imaginary part  $s$ . A Lorentzian pick is observed at and its FWHM parameter is found when the imaginary part is less than  $10^{-8}$  eV. The energy of this state is 0.479eV measured from the bottom of the well.

### 3. APPLICATION TO VIRTUAL STATES IN SOME QUANTUM WELLS STRUCTURES

We have applied the methodology described in this work to study quasi-bound states in rectangular, parabolic and delta-doped quantum wells structures [14-17]. We have calculated the FWHM parameters and the mean-life times of many virtual states varying the physical conditions. The delta-doped quantum wells create virtual states with stronger energetic and spatial localizations than the rectangular and parabolic quantum wells and barriers. The mean-life times of the quasi-bound states in these wells are sufficiently large to be measured experimentally. It seems that the potential profile of the delta-doped wells creates quasi-bound states which can be converted in Capasso states [9] if a delta-doped well is embedded in a superlattice.

### CONCLUSION

The proposed numerical scheme can be used for a full line-shape description of virtual electronic states created by different physical reasons. A detailed analysis of the virtual states formed in different quantum wells embedded in superlattices is in progress.

### REFERENCES

- [1] Walter A. Harrison, "Elementary Electronic Structure", *World Scientific*, Singapore (1999).
- [2] B. Vinter and C. Weisbuch, "Quantum Semiconductor Structures", Academic Press, San Diego (1991).
- [3] H. T. Grahn, "Semiconductor Superlattices: Growth and Electronic Properties", *World Scientific*, Singapore (1995).
- [4] Paul Harrison, "Quantum Wells, Wires and Dots: Theoretical and Computational Physics", John Wiley, Chichester (2000).
- [5] C. J. Chen, W. F. Smith, "Introduction to Scanning Tunneling Microscopy", *American Journal of Physics*, v. 62, No6, pp.573-574 (1994).
- [6] Stefan Hüfner, "Photoelectron Spectroscopy: Principles and Applications", Springer (2003).
- [7] S. D. Kevan, "Angle-resolved Photoemission", Elsevier (1992).
- [8] MC Desjonquères, D Spanjaard, "Concepts in Surface Physics", Springer (1996).
- [9] F. Capasso, S. Datta, "Quantum electron devices", *Physics Today, Physics Today*, V. 43, No 2, pp.74-82 (1990).
- [10] J. A. White, "Self-consistent Green functions for the Anderson impurity model", *Phys. Rev. B* v. 45, No3, pp.1100 - 1106 (1992)
- [11] Jagdeep Shah, "Ultrafast Spectroscopy of Semiconductors and Semiconductor Nanostructures", Springer (1999).
- [12] A. Gonis, "Green functions for ordered and disordered systems", Elsevier (1992).

- [13] Federico García Moliner, Víctor R. Velasco, “The Method of Surface Green Function Matching: Theory of Single and Multiple Interfaces”, *World Scientific* (1992).
- [14] S. J. Vlaev, I. Rodríguez-Vargas, L. M. Gaggero-Sager, Mean life times of quasi-bound states in delta-doped GaAs quantum wells, *Microelectronics Journal*, v.36, pp.347-349 (2005).
- [15] S. J. Vlaev, I. Rodríguez-Vargas, and L. M. Gaggero Sager, Resonant states in n-type delta-doped GaAs quantum wells, *phys. stat. sol. (c)*, v.2, No10, pp.3649-3652 (2005).
- [16] S. J. Vlaev, I. Rodríguez-Vargas, L. M. Gaggero-Sager, Mean life times of quasi-bound states in delta-doped GaAs quantum wells, *Microelectronics Journal*, v.36, pp.347-349 (2005).
- [17] S. Jelev Vlaev, J. Madrigal Melchor, V. M. González Robles, D. A. Contreras Solorio, “Quasi-bound electronic states in parabolic GaAs/AlGaAs quantum wells and barriers”, *Microelectronics Journal*, accepted (2007).

***Chapter 14***

# **GENDER AND SOCIAL INTERACTION IN MEXICAN NANOTECHNOLOGY AND NANOSCIENCES RESEARCH GROUPS**

***Armando Barrañón***

Dept. of Basic Sciences, UAM-Azcapotzalco, Mexico City.

## **ABSTRACT**

Signatures have been obtained about the need to improve women's participation in the Nanotechnology and Nanosciences research groups. A statistical study performed in this kind of research group suggests that they comply with a power law that can be interpreted in terms of the homeostasis of each research group derived from the optimization of Shannon Information Entropy. These N and N research groups are not large enough to assume an institutionalization process, instead a mean value of 5 was detected which suggests that social interaction is the main factor for the formation of these research clusters

## **INTRODUCTION**

Several countries have dedicated important resources to research and development of nanotechnology with the USA as the leader, followed by the European Union, Japan and Korea. A group of countries also contributes to these efforts, namely China, India and Brazil. The worldwide flow of capital devoted to nanotechnology is in the range of three trillion dollars; meanwhile, the USA spent one trillion dollars for its National Nanotechnology Initiative, India and Brazil have spent several tens of millions of dollars, which might lead to a technological breach derived from these asymmetries. The Mexican Program for Teachers Improvement (PROMEP) published on the Internet in 2007 a list of 45 research groups dedicated to Nanosciences and Nanotechnology, funded by the Secretary of Public Education with a mean size equal to 5, comprising a total of 240 researchers [SEP, 2006]. These results are qualitatively equal to those obtained using a similar list published on the Internet by

PROMEP in 2004. These reduced mean values of the N and N research group size are a signature that N and N research groups in Mexico are still dominated by social interaction and have not yet reached the institutionalization level required for creating national networks of research in Nanosciences and Nanotechnology [A. Barrañón, 2007b]. This indicates the need for establishing a Mexican Nanotechnology Initiative to coordinate this institutionalization process all along these networks of research groups. On the other hand, considering gender, a low level of women's participation is observed which could lead to the establishment of quotas for women's participation in this kind of N and N research group, as a part of this institutionalization process [Barrañón, 2007].

## METHODOLOGY

Following the traditional definition of entropy, internal homeostasis indicates that mean entropy of each subsystem remains constant [ Dover, 2004]:

$$\langle s \rangle = - \sum_{i=1}^N p_i(\Omega(x)) \ln(\Omega(x)) = cte$$

where  $\Omega(x)$  is the number of configuration states of subsystem i with parameter x. Hence a Shannon Lagrangian can be defined:

$$\begin{aligned} L &= - \sum_i p_i(\Omega_i(x)) \ln(\Omega_i(x)) - \lambda \left[ \sum_i p_i(\Omega_i(x)) \ln(\Omega_i(x)) - \langle s \rangle \right] - \lambda_2 \left[ \sum_i p_i(\Omega_i(x)) - 1 \right] \\ L &= - \sum_{i=1}^N p_i(\Omega(x)) \ln(\Omega(x)) - \lambda \left[ \sum_i p_i(\Omega(x)) \ln(\Omega(x)) - \langle s \rangle \right] \\ &\quad - \lambda_2 \left[ \sum_i p_i(\Omega(x)) - 1 \right] \end{aligned}$$

For an optimal entropy, its partial derivatives are equal to zero:

$$\frac{\partial L}{\partial p_i} = 1 - \ln[p_i(\Omega(x))] - \lambda \ln[\Omega_i(x)] - \lambda_2 = 0$$

which provides the following probability distributions:

$$p_i(\Omega_i(x)) = e^{-1-\lambda_2} \Omega_i^{-\lambda}(x)$$

Since:

$$\sum_i p_i(\Omega_i(x)) = 1$$

it follows that:

$$e^{-1-\lambda_2} = \frac{1}{\sum_i \Omega_i^{-\lambda}(x)} = \frac{1}{Z}$$

where:

$$p_i(\Omega_i(x)) = \frac{1}{Z} \Omega_i^{-\lambda}(x)$$

which is a power law for the probabilities as a function of the statistical weight of the subsystems.

As is well known, social networks have a typical size between 8 to 12 members due to the great amount of time and resources required by social interaction [Wilson, 2000].

Considering the high complexity of information transmitted by N and N research networks, this kind of information is conveyed by face-to-face interaction [Allen, 1997] rendering new technologies such as cell phones and email as complementary.

## RESULTS

The universities with the larger number of nano researchers are UAM (#4 for some national rankings and with a budget in the range of 400M US dollars), U. de Guadalajara (#3 for some national rankings and with a budget in the range of 600M US dollars), BUAP, UASLP, UA Sonora, all of them considered among the most important universities. Actually UAM, Ude G and U A Sonora belong to the most developed economic regions and UASLP is based in a major city. BUAP has an important concentration of universities and benefited with a large amount of PROMEP funding to credentialize its teachers.

Table I shows the grand mean for the clusters of researchers in N and N with a mean size equal to 5 with a low percentage of women participation in the range of 20% which is far away from the standard proposed by the Helsinski group of 40% of women participation [Laurila y Young, 2001]. Nevertheless the large value of the standard deviation indicates large fluctuations of this value of women participation in these clusters. Figure 1 shows a power law plot of the number of size A cluster versus the size of the Nanosciences and Nanotechnologies clusters in the PROMEP list. As can be seen the frequencies of clusters of a given size A drop to 1 when the cluster size is larger than 6. This is in agreement with the theory of social interaction that precludes a cluster larger than 12 due to the complexity of social interaction. Therefore, Nanotechnology research clusters in Mexico have not achieved yet the institutional level required for large clusters as the National Initiatives of Nanotechnology or the so-called Megaprojects surveyed by CONACYT in 2006 [CONACYT, 2006]. This institutional level could be attained via the financial support of

networks of clusters with funding in the range of 1M US dollars, as was expected to be done by the end of 2007. This could help for a future Mexican National Nanotechnology Initiative in the future.

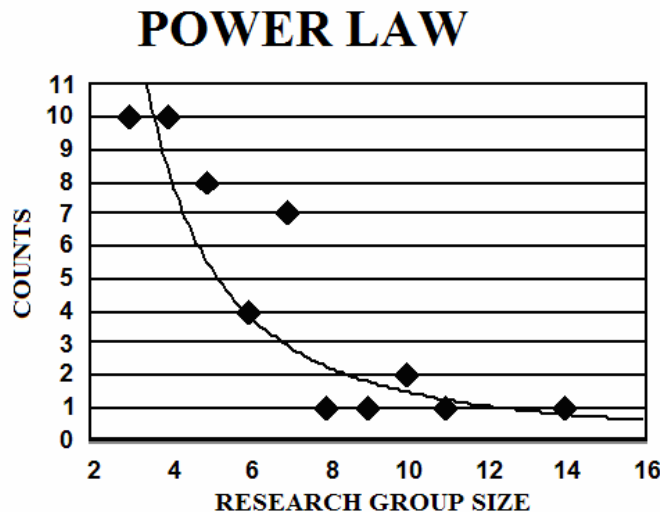


Figure 1. Shows a power law plot of the number of size A cluster versus the size of the Nanosciences and Nanotechnologies clusters in the PROMEP list.

**Table 1.** Shows the grand mean for the clusters of researchers in N and N with a mean size equal to 5 with low percentage of women participation in the range of 20% .

Nevertheless the large value of the standard deviation indicates large fluctuations of this value of women participation in these clusters

PROMEP N%N MEAN SIZE	Hombres	Mujeres	Total	%Actividad Femenina
MEAN SIZE	4	1	5	20
STANDARD DEVIATION	2	2	2	25

## REFERENCES

- T. Allen, 1997. Architecture and Communication Among Product Development Engineers, Sloan School of Management, MIT: Cambridge. pp. 1-35.
- A. Barrañón, 2007. "Perspectivas de la Nanoeducación en México", *Razón y Palabra*, No. 59, Oct.-Nov..
- A. Barrañón, 2007b. La presunción de control en la nanotecnología. *Razón y Palabra*, 58, Agosto-Septiembre.
- CONACYT, 2006. "Resultados de la Convocatoria para Presentación de Ideas para la realización de Megaproyectos de investigación científica o tecnológica 2006", 2006.
- Y. Dover, 2004. *Physica A* vol. 334, No. 3-4, pp. 591-599.
- Pia Laurila P and Kerry Young, 2001 (comps.), *Gender in research*, Bruselas: European Comission.
- Secretaría de Educación Pública, 2006. Programa de Mejoramiento del Profesorado. Un primer análisis de su operación e impactos en el proceso de fortalecimiento académico de las universidades públicas, México, SEP.
- Dr. Ralph F. Wilson, 2000. "The Six Simple Principles of Viral Marketing". *Web Marketing Today*, Issue 70, February 1.

## APPENDIX

Universidad Politécnica de Aguascalientes	8	0	8	0	Automotriz
Universidad Autónoma de Ciudad Juárez	2	1	3	33	Ciencia e Ingeniería de Materiales
Universidad Autónoma de San Luis Potosí	6	1	7	14	INGENIERÍA DE PROCESOS
Universidad Autónoma de San Luis Potosí	4	1	5	20	MATERIALES (FAC. CIENCIAS)
Universidad Autónoma de San Luis Potosí	2	1	3	33	FISICOQUÍMICA DE ALIMENTOS
Universidad Autónoma de San Luis Potosí	3	1	4	25	MATERIALES OPTOELECTRÓNICOS (IICO)
Universidad Autónoma de San Luis Potosí	5	0	5	0	MATERIALES NANOESTRUCTURADOS (INST. FÍSICA)
Universidad Autónoma de San Luis Potosí	3	1	4	25	OPTICA APLICADA (IICO)
Universidad Autónoma de Coahuila	3	0	3	0	FÍSICA
Universidad Autónoma de Nuevo León	9	0	9	0	Síntesis y Caracterización de Materiales
Universidad Autónoma de Nuevo León	6	0	6	0	Fisicoquímica de Materiales
Universidad Autónoma de Nuevo León	4	3	7	43	MATEMÁTICAS APLICADAS
Universidad Autónoma de Nuevo León	0	7	7	100	Nutrición Clínica en la Mujer
Universidad Autónoma de Nuevo León	3	0	3	0	Procesos Termofluidodinámicos y Sistemas Energéticos
Universidad Autónoma del Estado de México	5	1	6	17	INTERACCIÓN DE RADIACIÓN CON MATERIA
Benemérita Universidad Autónoma de Puebla	2	2	4	50	Materiales complejos, inteligentes y nanoestructurados
Benemérita Universidad Autónoma de Puebla	3	1	4	25	Óptica Cuántica
Universidad Juárez Autónoma de	3	1	4	25	Investigación en Nuevos Materiales

Tabasco					
Universidad Veracruzana	6	0	6	0	MICRO Y NANOSISTEMAS
Universidad Autónoma de Baja California	4	0	4	0	FISICA CUANTICA
Universidad Michoacana de S Nicolás de Hidalgo	3	0	3	0	POLÍMEROS, NANOESTRUCTURAS Y ANÁLISIS DE SISTEMAS COMPLEJOS DE REACCIÓN
Universidad Autónoma de Zacatecas	5	0	5	0	Propiedades electrónicas, ópticas y magnéticas de materiales
Universidad de Guanajuato	5	0	5	0	Química teórica y computacional y fisicoquímica de Polímeros
Universidad Politécnica de Pachuca	8	2	10	20	SISTEMAS MECATRÓNICOS
Universidad de Guadalajara	9	1	10	10	SISTEMAS POLIMÉRICOS MULTIFÁSICOS
Universidad de Guadalajara DES:CENTRO UNIVERSITARIO DE LOS LAGOS	3	0	3	0	NANOTECNOLOGÍA DE MATERIALES
Universidad de Guadalajara DES:CENTRO UNIVERSITARIO DE LOS LAGOS	2	2	4	50	BIONANOTECNOLOGÍA
Universidad de Guadalajara DES:CENTRO UNIVERSITARIO DE LOS LAGOS	3	4	7	57	BIOQUÍMICA Y FISIOLOGÍA
Universidad de Guadalajara DES:CENTRO UNIVERSITARIO DE CIENCIAS EXACTAS E INGENIERÍAS	7	0	7	0	CIENCIA Y TECNOLOGÍA DE MATERIALES LIGNOCELULÓSICOS
Universidad de Guadalajara DES:CENTRO UNIVERSITARIO DE CIENCIAS EXACTAS E INGENIERÍAS	4	0	4	0	FISICOQUÍMICA DE MATERIALES ESTRUCTURADOS

## APPENDIX (Continued)

Universidad de Sonora	8	3	11	27	CIENCIA E INGENIERÍA DE PROCESOS
Universidad de Sonora	11	3	14	21	FENÓMENOS ÓPTICOS
Universidad de Sonora	3	0	3	0	FISICA DE MATERIALES AVANZADOS
Universidad de Sonora	4	1	5	20	FISICA DE RADIACIONES
Universidad de Sonora	5	0	5	0	Física Matemática
Universidad de Sonora	6	0	6	0	Propiedades ópticas de materiales
Universidad Autónoma Metropolitana Iztapalapa	3	1	4	25	Desarrollo y aplicaciones de la teoría de funcionales de la densidad
Universidad Autónoma Metropolitana Iztapalapa	3	0	3	0	Diseño de Materiales Catalíticos Avanzados
Universidad Autónoma Metropolitana Iztapalapa	7	0	7	0	Fenómenos Ópticos y de Transporte en la Materia
Universidad Autónoma Metropolitana Iztapalapa DES:CIENCIAS BÁSICAS E INGENIERÍA	3	0	3	0	Fisicoquímica de sistemas nano-estructurados
Universidad Autónoma Metropolitana Iztapalapa	2	1	3	33	Materiales nanoestructurados con porosidad variable y biocompatibilidad para liberación de fármacos
Universidad Autónoma Metropolitana Iztapalapa	4	1	5	20	Materiales Orgánicos e Inorgánicos
Universidad Autónoma Metropolitana Azcapotzalco	2	2	4	50	Universidad Autónoma Metropolitana Azcapotzalco
Universidad Autónoma Metropolitana Azcapotzalco	0	7	7	100	Sociedad y Biotecnología
Universidad Autónoma Metropolitana Azcapotzalco	3	2	5	40	Química de materiales
MEAN	4	1	5	20	
STANDARD DEVIATION	2	2	2	25	

**Chapter 15**

## **ON THE MANIPULATION OF MICROSCOPIC PARTICLES BY OPTICAL TWEEZERS: FLATNESS BASED APPROACH**

***Carlos Aguilar-Ibañez<sup>1\*</sup>, Armando Barrañón Cedillo<sup>2\*</sup>,  
Hebertt Sira-Ramirez<sup>3\*</sup> and Luis Ignacio Rosas Soriano<sup>1\*</sup>***

<sup>1</sup> CIC-IPN; Av. Juan de Dios Bátiz s/n Esq. Manuel Othón de M.  
U.P. Adolfo López Mateos, Col. San Pedro Zacatenco,  
A.P. 75476 México, D.F. 07700.

<sup>2</sup> Depto. de Ciencias Básicas. UAM Azcapozalco; Av. San Pablo No. 180,  
Col. Reynosa Ta. A.P. 02200, México, D.F.

<sup>3</sup> CINVESTAV-IPN, Av. IPN No. 2508, Col. San P. Zacatenco,  
A.P 14740 7300 México, D.F.

### **ABSTRACT**

In this paper we present a control strategy based on a combination of the flatness approach and saturation functions to manipulate the optical tweezers system, which is a flat system, with flat outputs given by the horizontal and vertical positions. The strategy allows the optical tweezers to steer a microscopic particle from an initial position to a final desired position, following a suitable trajectory. The control strategy is proposed under the assumption that the particle is suspended in a frictionless medium. Due to the fact that the particle horizontal and vertical velocities cannot be measurable, a high-gain observer is used. The resulting controller has a relatively simple stability analysis. The control strategy performance is tested by numerical simulations.

**Keywords:** Optical tweezers, flatness based Control, saturation function, high-gain observers.

---

\* caguilar@cic.ipn.mx

\* bca@correo.azc.uam.mx

\* hsira@mail.cinvestav.mx

\* lrosasb08@sagitalario.cic.ipn.mx

## 1. INTRODUCTION

The idea of using light to move objects was introduced by Kepler and has been used to exert forces on objects in the range of piconewtons concentrating laser rays with a high numerical aperture lens. Nowadays this so called optical tweezers can be used to clean microchannels, and will be employed in the future to build up pumps and valves of a micrometric size [15]. Other amazing application of optical tweezers is the use of a rack of optical traps that can be separate distinct phases in a flow attaining the highest particle trapping densities in fluidic microchannels [16]. The last two decades have witnessed an enormous development in the nano technology theory and in the development of nano devices. Optical traps focus a laser beam to trap and manipulate micro particles suspended in a colloid or in a frictionless medium. Optical Tweezers have been widely used by physicians, biologists and chemists in a large range of applications, most of them based in the necessity to hold or move a micro particle. For instance, optical traps have been used to grab a zymmosan particle and put it in contact with a macrophage in order to measure the effect of cytochalasin D on phagocytosis time via cytoskeleton internal motion [10]. In [11] dual beam optical tweezers have been used to measure the distance dependence of colloidal friction coefficients obtaining results in agreement with low-Reynolds number computations. Another useful and common application presented in [1] is to use optical traps to stretch microtubules along an axis by fixing two beds to their ends, which is a standard procedure to measure static forces on extended tubes as well as dynamic effects that happen when these elongations are done at high speeds. Many other examples from medicine, biology or chemistry can be mentioned, however we want to pointing out two issues. The first is that the majority of the applications of optical tweezers have been developed from a very practical point of view and several theoretical aspects remain to be addressed. Secondly, steering microparticles is a rather difficult task in terms of the control and stability problems that arise when we work with dynamical systems. Wallin et. al. have implemented a proportional-gain position-clamping algorithm to control the steering of particles by optical tweezers minimizing the laser power in order to diminish the optical damage [4]. Precise steering of a particle in the specimen plane has been attained using electro-optic deflection obtaining a deflection of the entire beam, attaining a higher trap stiffness and an improved throughput as well as resolving molecular movements of bead bound kinesin motors in the range of 8nm [5]. Optical traps have been used to create 1D channels, which had been already synthesized as long quasicylindrical pores in zeolitic material [6], creating ring-shaped channel structures where colloidal particles are trapped and circulated to model catalytic reactions in zeolitic materials [7]. Also, precise steering of particles in an optical trap has been used to induce cold collisions between cold atoms as well as to deterministically produce light induced collision between atoms confined by a standing wave optical dipole trap into a single potential [8]. In this very work we developed a suitable and useful steering control strategy to accuracy manipulate a micro particle from the perspective of the differential flatness approach, developed in Control Theory and previously introduced in [8]. This approach was applied since an optical traps turns out to be a differentially flat system, with flat outputs defined by the horizontal and vertical position coordinates of the optical trap centroid.

This work is organized as follows. In Section 2 we present the physical model of the optical tweezers and the problem statement. In Section 3, we discuss the flatness property of

the optical tweezers and introduce a flatness based control strategy for solving the trajectory tracking problem. Finally, Section 4 is devoted to conclusions.

## 2. PHYSICAL MODEL OF THE OPTICAL TWEEZERS

Consider a particle of mass  $m$ , which is trapped in a potential field with a Gaussian distribution [9, 13]. Let  $x$  and  $y$  be the horizontal position and vertical position of the particle, with respect to a fixed reference frame. The nonlinear model of this system, which can be obtained from Euler-Lagrange equations is given by

$$\begin{aligned}\ddot{x} &= -\frac{2 \ln(2) p_0 (x-x_0)}{ma^2} \exp \left[ -\ln(2) \left( \frac{(x-x_0)^2}{a^2} + \frac{(y-y_0)^2}{b^2} \right) \right] \\ \ddot{y} &= -\frac{2 \ln(2) p_0 (y-y_0)}{mb^2} \exp \left[ -\ln(2) \left( \frac{(x-x_0)^2}{a^2} + \frac{(y-y_0)^2}{b^2} \right) \right]\end{aligned}\quad (1)$$

where  $p_0$  is the well depth,  $x_0$  and  $y_0$  indicate the center of the trapping potential,  $a$  and  $b$  are related to the beam dimensions (see [9]). Note that  $x_0$  and  $y_0$  are the system control variables. That is, changing adequately the positions of  $x_0$  and  $y_0$  we can force the particle to carry out a specific maneuver task.

It is important to consider that this system is locally controllable if the position of the particle is close enough to the origin, given by  $w_0=(x_0, y_0, 0, 0)$ , which is the geometrical center of the optical tweezers. Conversely, it is not locally controllable if the particle position is far enough to the origin. Indeed, both controllability cases are easy to show by simple linearization of system (1). In the first case the linearization leads to:

$$\delta \dot{x} = \frac{-\ln(2) p_0}{ma^2} \delta x; \quad \delta \dot{y} = \frac{-\ln(2) p_0}{mb^2} \delta y.$$

Where  $\delta x$  and  $\delta y$  can be considered as the horizontal and vertical virtual controllers, respectively. Evidently, the latter linearization system is locally controllable. Hence, the tracking problem can be approximately solved by using the traditionally control theory, with the inconvenient of having a very small domain of attraction. In the second case we only have that  $\delta x=0$  and  $\delta y=0$ , which means that the OT cannot actuate over the particle.

The physically meaning of the first case is that when the particle is located inside of the laser trap, which has an elliptic shape, then the system is locally controllable. On the other hand, when the particle is located outside of the laser beam, that is the second case, the system is not controllable because the real OT attraction force is not enough to move the particle. We can overcome this undesirable case by approaching the OT geometric center towards to the particle to trap it inside of the region of attraction and then be able to manipulate it.

Continuing with our development we introduce the following scaling transformations:

$$\begin{aligned}x_1 &= \frac{x}{a}; & y_1 &= \frac{y}{b}; & x_2 &= \frac{\dot{x}}{ak}; \\y_2 &= \frac{\dot{y}}{bk}; & \lambda &= \frac{b}{a}; & k &= \sqrt{\frac{2 \ln(2)p_0}{a^2 m}} \\ \tau &= kt; & u_x &= \frac{x_0}{a}; & u_y &= \frac{y_0}{b}.\end{aligned}$$

These transformation leads to:

$$\begin{aligned}\dot{x}_1 &= x_2 \\ \dot{x}_2 &= -(x_1 - u_x) \exp \left[ -\ln(2) ((x_1 - u_x)^2 + (y_1 - u_y)^2) \right] \\ \dot{y}_1 &= y_2 \\ \dot{y}_2 &= -\frac{1}{\lambda}(y_1 - u_y) \exp \left[ -\ln(2) ((x_1 - u_x)^2 + (y_1 - u_y)^2) \right]\end{aligned}\quad (2)$$

where, evidently,  $u_x$  and  $u_y$  are the new controllers for the above system.

We end this section with the problem statement formulation:

**Problem statement :** To guarantee that a given particle of mass  $m$ , manipulated by an OT, follows a convenient reference trajectory  $(x_r(t), y_r(t))$ ; with  $t \in [t_0, t_f]$ , where this trajectory must be sufficiently smooth. That is to say, we should move the OT geometrical center, keeping the particle close enough to desired reference.

### 3. A FEEDBACK CONTROL STRATEGY

#### *A Brief on Flatness Approach.*

In general we can say that a nonlinear system is flat if there is a flat output, such that, every system variable can be expressed as a function of this output and its respective time derivatives. Formally speaking this concept is defined as follows.

**Definition 1:** Consider the nonlinear system with the following general form (see [2,3]):

$$\dot{x} = f(x, u); \quad x \in R^n \text{ and } u \in R^k, \quad (3)$$

where  $n > k$ ,  $f = (f_1, \dots, f_n)$  is a smooth function of  $x$  and  $u$ , respectively. System (3) is said to be a flat system if there is a flat output  $y \in R^k$ , such that:

$$x = \phi(y, \dot{y}, \dots, y^{(r)}) \quad u = \eta(y, \dot{y}, \dots, y^{(k)}),$$

where  $r$  and  $k$  are finite integers,  $\phi$  and  $\eta$  are smooth vector functions of the output vector  $y$  and its respective time derivatives.

Now using the previous definition, we show that the OT system is flat.

Define the outputs  $F = x_1$  and  $G = y_1$  we clearly have that the OT system is found to be a flat system, with respect to these outputs, since  $x_2 = F$ ,  $y_2 = G$ , and

$$\begin{aligned}\ddot{F} &= - (F - u_x) \exp \left[ -\ln(2) ((F - u_x)^2 + (G - u_y)^2) \right]; \\ \lambda \ddot{G} &= - (G - u_y) \exp \left[ -\ln(2) ((F - u_x)^2 + (G - u_y)^2) \right].\end{aligned}\quad (4)$$

We most notice that the nonlinear system (4) can only be solved using a numerical method, like the Newton-Rapson method.

The following Lemma gives us the necessary conditions to compute the roots of the last nonlinear system.

**Lemma 1:** Consider the following nonlinear equations:

$$L_i = -v_i \exp \left[ -\ln(2) (v_x^2 + v_y^2) \right]; i = \{x, y\}, \quad (5)$$

where  $|L_i| < L \doteq 2^{-\bar{v}^2} \cong 0.606$ ; with  $\bar{v} = 1/\sqrt{2 \ln(2)} \cong 0.849$ . Then, there is a single  $v_i \in (-\bar{v}, \bar{v})$  satisfying the above equations.<sup>5</sup> ■

Proof: See Appendix.

**Comment:** Lemma 1 gives sufficiently conditions to assure that the algebraic system (5) has an inverse function in some restricted region.

### 3.1. Solving the control of a tracking problem

Since system (1) is a flat system with flat outputs, defined by the two variables  $F$  and  $G$ , we propose the controller  $u_x$  and  $u_y$  that allow us to solve the tracking problem. To this end, we employ a flatness based approach in combination with a saturation function and a high-gain observer.

First of all, we introduce a useful definition:

**Definition 2:** If the function  $\sigma_M(\omega) : R \rightarrow R$  satisfies:

$$\sigma_M(w) = \begin{cases} w & \text{if } |w| \leq M \\ M \text{sign}(w) & \text{if } |w| > M \end{cases}$$

where  $\text{sign}()$  is a sign function and  $M > 0$ , then it is a linear saturation function.

---

<sup>5</sup> Recalling that  $e = 2.71828$ .

Now, we establish the problem of control a tracking, which consists of making the particle to follow a suitable trajectories. The trajectories must satisfy some bound conditions over their first and second time derivatives.

The main goal consist of making that flat outputs  $F$  and  $G$  track the time variant-signals  $F_*(\tau)$  and  $G_*(\tau)$ , respectively; with  $\tau \in [t_0, t_f]$ , where these reference signals must satisfy the inequalities  $|F_*| \leq \bar{k} < L$  and  $|G_*| \leq \bar{k} < L$  to fulfill **Lemma 1**. The latter conditions are necessary in order to compute the inverse function related to the controllers  $u_x$  and  $u_y$ , as we will use them in the sequel.

The tracking errors are defined as:

$$e_x = F - F^*; \quad e_y = G - G^*, \quad (6)$$

and the virtual control variables as

$$v_x = F - u_x; \quad v_y = G - u_y$$

The problem of control a tracking can be reformulated as the problem of finding the virtual controllers  $v_x$  and  $v_y$ , provided that both tracking errors converge to zero. The next proposition help us to find the needful controllers  $v_x$  and  $v_y$  assuring asymptotically exponentially convergence of both tracking errors.

**Proposition 1:** Let  $|F_*| \leq \bar{k}$  and  $|G_*| \leq \bar{k}$  and let  $\{\bar{x}, \bar{y}, k_p, k_d, \bar{k}\}$  be the set of positive constants provided that:

$$\bar{x} + \bar{k} < \bar{L} \quad \text{and} \quad \lambda(\bar{y} + \bar{k}) < \bar{L}. \quad (7)$$

Suppose that  $v_x$  and  $v_y$  satisfy:

$$\begin{aligned} v_x \exp \left[ -\ln(2) (v_x^2 + v_y^2) \right] &= \sigma_x (k_p e_x + k_d \dot{e}_x) - \ddot{F}_*; \\ \lambda v_y \exp \left[ -\ln(2) (v_x^2 + v_y^2) \right] &= \sigma_y (k_p e_y + k_d \dot{e}_y) - \ddot{G}_*, \end{aligned} \quad (8)$$

Then the above controllers globally asymptotically stabilize both tracking errors in (6). ■

**Proof:** According to **Lemma 1**, the implicit control expressions given by (8) are well defined. In other words, there is a single  $v_i \in (-\bar{v}, \bar{v})$ ;  $i=\{x,y\}$  that fulfills the latter equations. Now, computing the second time derivatives of the tracking errors in (6) and after using the expressions given in (4), we have

$$\begin{aligned}\ddot{e}_x - \ddot{F}_* &= v_x e^{-\ln(2)(v_x^2 + v_y^2)}; \\ \ddot{e}_y - \ddot{G}_* &= \lambda v_y e^{-\ln(2)(v_x^2 + v_y^2)}.\end{aligned}\quad (9)$$

Finally, the error dynamic equations are obtained by substituting (8) into (9), as follows:

$$\ddot{e}_x + \sigma_{\bar{x}}(k_p e_x + k_d \dot{e}_x) = 0 \quad ; \quad \ddot{e}_y + \sigma_{\bar{y}}(k_p e_y + k_d \dot{e}_y) = 0. \quad (10)$$

Therefore, both tracking errors locally exponentially converge to zero (see Appendix). ■

We can note that our control strategy is robust with respect to small external perturbations, like the damping force presented in any colloid medium, and it can be probed by a simple linearization of equation (9).

### *A high-gain observer*

The main drawback of the approach described above is that we need accurate estimations of the non-available time derivative outputs, which are directly related to the particle velocity. We overcome this problem by using a high-gain observer to estimate the variables  $x_2$  and  $y_2$ . To this end, we propose the following time derivative estimator based on the previous work of [14]:

$$\frac{d}{dt} \begin{bmatrix} \tilde{y} \\ \dot{\tilde{y}} \end{bmatrix} = \begin{bmatrix} 0 & 1 \\ 0 & 0 \end{bmatrix} \begin{bmatrix} \tilde{y} \\ \dot{\tilde{y}} \end{bmatrix} + (y - \tilde{y}) \begin{bmatrix} \alpha_1/\varepsilon \\ \alpha_2/\varepsilon^2 \end{bmatrix} \quad (11)$$

where  $\alpha_1$  and  $\alpha_2$  are any positive constants, and the parameter  $\varepsilon > 0$  is sufficiently small. The latter estimator allows us to easily obtain the time derivative of state  $y$ . Obviously, to apply the estimator we have to substitute, in system (11), the variables  $e_x$  and  $e_y$  instead of variable  $y$ .

## 4. SIMULATIONS RESULTS

To evaluate the effectiveness and performance of the proposed control strategy we carried out two numerical simulations. In both experiment we make the particle to follows a suitable trajectory. The two experiments used the same physical parameters, taken from a real experiment presented in [12, 9] and defined as:  $a = 1\mu m$ ,  $b = 1\mu m$ ,  $x_0 = 0$ ,  $y_0 = 0$ ,  $p_0 = 1 \times 10^{-5} nJ$  and  $m = 1 \times 10^{-12} Kg$ . For the sake of simplicity, we work in the normalized coordinates.

In the first experiment the particle follows a straight line, with constant velocity and passing through the origin. The straight line trajectory, in the normalized coordinates, was defined as:

$$F_*(t) = mt; \quad G_*(t) = mt,$$

where  $m=1$  and  $t \in [0,10]$ . For this case we have that  $\vec{F}_* = 0$ ,  $\vec{G}_* = 0$ ,  $\lambda=1$ . To ensure condition (7) the normalized controller parameters were set as  $\bar{x} = \bar{y} = 0.5$ . The remaining parameter were chosen as  $k_p=0.81$  and  $k_d=1.27$ . The designed high-gain observer parameters were set as  $\varepsilon=0.1$ ,  $\alpha_1 = 0.81$  and  $\alpha_2 = 1.27$ . Finally, the system initial condition were selected as:

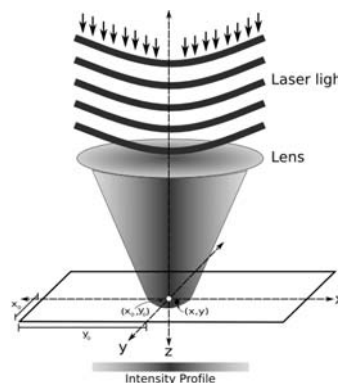
$$x_i(0)=1; \quad y_i(0)=-1.5; \quad \dot{x}(0)=0.1; \quad \dot{y}(0)=0$$

Figure 2 shows the closed-loop trajectories for the state position and the tracking errors in the normalized coordinates of the **OT**. From this figure we can see that even when these conditions are far to the origin of the tracking signal, the system performance stills behaves satisfactory.

In the second experiment the selected trajectory is an ellipse with center at the origin, and axes corresponding to the actual system coordinate axes. The desired flat outputs are nominally specified as,

$$F_*(t) = A \cos \omega t; \quad G_*(t) = B \sin \omega t.$$

where  $A = 3 \times 10^{-5}m$ ,  $B = 2.5 \times 10^{-5}m$ ,  $\omega=0.017 \text{ rad/s}$  and  $t \in [0,\omega/2\pi]$ . To satisfy the condition (7) the normalized controller parameters were set as  $\bar{x} = \bar{y} = 0.35$ , while the all the remainder parameters, including those of the numerical differentiator, were set identically as in the first experiment. The system initial conditions were set as  $x(0) = 2.1 \times 10^{-5}m$ ,  $y(0) = 0.5 \times 10^{-5}m$ ,  $\dot{x}(0) = 0.1m/s$  and  $\dot{y}(0) = 0$ . Figure 3 depicts the position coordinates of the **OT**. From this figure we can see that even though the trap motion starts significantly far away from the desired trajectory, the system performance is quite satisfactory.



**Figure 1.** Optical tweezers.

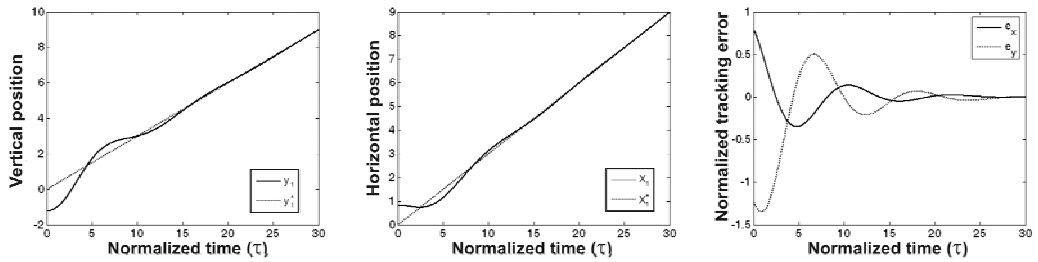


**Figure 2.** Feedback tracking of a straight line.

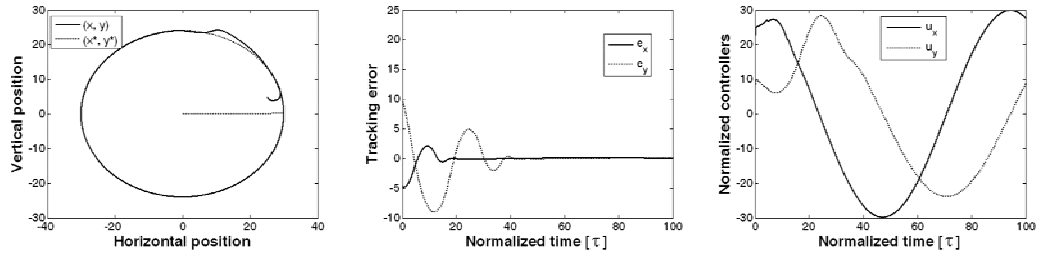


**Figure 3.** Feedback controlled position coordinates for elliptic path tracking.

## 5. CONCLUSIONS

In this work we proposed a control strategy to make a particle to follows a suitable trajectory by manipulating an optical tweezers device. The fact that the optical tweezers system is a flat system, with flat outputs given by their vertical and horizontal positions, allows us to solve the control of a tracking problem. In order to apply the Differential Flatness approach we inverted a two-variables nonlinear function, whose solutions were the needful controllers that solved the tracking problem. The invertibility of this function was assured by using a saturation function. Physically, the strategy places the optical tweezers close enough to the particle. Then, the particle is dragged little by little to the desired tracking trajectory. The controllers needed to accomplish this task were obtained by solving a nonlinear system of algebraic equations, using the well-known Newton-Rapson method. In order to test the effectiveness of the controllers, we used them to successfully make the particle to track a straight line and an elliptic trajectory.

## ACKNOWLEDGMENTS

Luis Ignacio Rosas Soriano is a scholarship holder of the CONACYT.

## 6. APPENDIX

**Proof of Lemma 1:** The idea behind it is to estimate the region where the functions in (5) can be inverted.

For simplicity we fix  $q=(x,y)$ . Now, we define the following surfaces:

$$f(q) = x \exp [-\ln(2)(x^2 + y^2)]; \quad g(q) = y \exp [-\ln(2)(x^2 + y^2)].$$

Using simple Calculus it is easy to show that  $f$  and  $g$  each have a single maximum and a single minimum, given by

$$q_f = \left( \frac{1}{\pm\sqrt{2\log 2}}, 0 \right) \quad q_g = \left( 0, \frac{1}{\pm\sqrt{2\log 2}} \right)$$

where

$$\frac{\partial}{\partial x} f(q) \Big|_{q=q_f} = 0; \quad \frac{\partial}{\partial x} g(q) \Big|_{q=q_g} = 0.$$

On the other hand, as  $f$  and  $g$  are continuous with  $f(0)=0$  and  $g(0)=0$ , then we have

$$\|f(x, y)\| < f(q_f) \hat{=} 2^{-\bar{v}^2} \quad \|g(x, y)\| < g(q_f) \hat{=} 2^{-\bar{v}^2}$$

for all  $x, y \in I_a$ ; with  $I_a = (-\bar{v}, \bar{v})$ . Consequently, if  $|f(q)| < 2^{-\bar{v}^2}$  and  $|g(q)| < 2^{-\bar{v}^2}$ , then, both,  $f$  and  $g$  are unvalued functions. That is,  $f(q)$  and  $g(q)$  have inverse function, for all  $q=(x,y)$ ; such that  $x, y \in I_a$ .

**System stability proof (10).** For simplicity, we only consider the case when  $k_p = k_d = 1$ . Then the stability of (10) can be analyzed by analyzing the stability of:

$$\ddot{x} = -\sigma_T(x + \dot{x}). \tag{12}$$

Now, let us propose the following candidate Lyapunov function

$$V = \frac{1}{2} \dot{x}^2 + \int_0^{x+\dot{x}} \sigma_T(s) ds.$$

Notice that the second term of  $V$  is a strictly positive function. It follows from the definition of saturation function. Then, the time derivative of  $V$  along of the trajectories of (12) is given by

$$\dot{V} = -\dot{x}\sigma_T(k_p x + k_d \dot{x}) + \sigma_T(x + \dot{x})(\dot{x} - \sigma_T(x + \dot{x})) = -\sigma_T(x + \dot{x})^2.$$

As  $V$  is a strictly positive function and is a negative semi-definite, we conclude stability in the Lyapunov sense. However, after using LaSalle's invariance theorem it is easy to see that all the solution of (12) asymptotically converge to the origin  $x=0$  and  $\dot{x}=0$ . On the other hand, the simply linearization of the equation (12), produces

$$\ddot{x} = -x - \dot{x},$$

which is, evidently, exponentially stable around to the origin. Therefore, the closed-loop equations are globally asymptotically stable and locally exponentially stable.

## REFERENCES

- [1] E. Evans and A. Yeung, *Chem. Phys. Lipids.* 73, 39 (1994).
- [2] M. Fliess, J. Levine, P. Martin, P. Rouchon. (1999) A Lie-Backlund approach to equivalence and flatness of nonlinear system, *Automatic Control, IEEE*, Pp. 922-937.
- [3] H. S. Ramirez, S. K. Agrawal, Differential flat system, Marcel Dekker, New York, 2004
- [4] Wallin, A.E., Ojala, H., Haeggstrom, E. and Tuma, R., Stiffer optical tweezers through real-time feedback control. *Applied Physics Letters*, 92 (22), (2008).
- [5] Megan T. Valentine, Nicholas R. Guydosh, Braulio Gutiérrez-Medina, Adrian N. Fehr, Johan O. Andreasson, Steven M. Block. Precision steering of an optical trap by electro-optic deflection. *Optics Letters*, Vol. 33, Issue 6, pp. 599-601 (March 2008).
- [6] J. Weitkamp, H. Kärger, H. Pfeifer, and W. Hölderich, Zeolites and Related Microporous Materials: State of the Art (*Elsevier*, Amsterdam), (1994).
- [7] Q.-H. Wei, C. Bechinger, P. Leiderer. Single-File Diffusion of Colloids in One-Dimensional Channels. *Science*. 287 (5453): 625-627 (2004).
- [8] Y. Miroshnychenko, W. Alt, I. Dotsenko, L. Förster, M. Khudaverdyan, D. Meschede, S. Reick, and A. Rauschenbeutel. Inserting Two Atoms into a Single Optical Micropotential. *Phys. Rev. Lett.* 97, 243003 (2006)
- [9] Y., Lee, K. W., Lyons, T. W., LeBreun, Virtual environment for manipulating microscopic particles with optical tweezers, *Journal of Research of the National Institute of Standards and Technology*, 108(4), 275-287, (2003).
- [10] U. Agero, C. H. Monken, C. Ropert, R. T. Gazzinelli and O. N. Mesquita. Cell surface fluctuations studied with defocusing microscopy. *Phys. Rev. E* 67, 051904 (2003).
- [11] Stuart Henderson, Steven Mitchell, and Paul Bartlett. Direct measurements of colloidal friction coefficients. *Phys. Rev. E* 64, 061403 (2001).
- [12] J. E., Molloy, M. J., Padgett, Lights, action: optical tweezers, *Contemporary Physics*, 43, 241-258, (2002).
- [13] A., Ashkin, Forces of a single-beam gradient laser trap on a dielectric sphere in the ray optics regime, *Biophysical Journal*, 61(2), 569-582, (1992).
- [14] H.K., Khalil, Nonlinear Systems, Prentice Hall, 2002 (third edition).

- [15] Kishan Dholakia, Gabriel Spalding and Michael MacDonald. "Optical tweezers: the next generation". *Physics World*, 31-35, (October 2002).
- [16] F. Merenda, J. Rohner, J. -M. Fournier, and R. -P. Salathé, "Miniaturized high-NA focusing-mirror multiple optical tweezers," *Opt. Express*, 15, 6075-6086 (2007).

**Chapter 16**

## **STRUCTURAL FEATURES AND CATALYTIC ACTIVITY OF $\text{Ce}_{1-x}(\text{La}_x, \text{Ru}_x)\text{O}_2/\text{Bi}_2\text{Mo}_{0.9}\text{W}_{0.1}\text{O}_6$ NANOSTRUCTURED SOLID SOLUTIONS**

***R. Rangel<sup>1</sup>, F. Huerta<sup>1</sup>, P. Bartolo-Pérez<sup>2</sup>,  
F. Morales<sup>3</sup>, D. H. Galván<sup>4</sup> and F. Castillón-Barraza<sup>4</sup>***

<sup>1</sup> Departamento de posgrado, Facultad de Ingeniería Química,  
UMSNH, Edificio K, Ciudad Universitaria, Morelia, Mich., México

<sup>2</sup> CINVESTAV-IPN, Unidad Mérida, Departamento  
de Física Aplicada, Mérida, Yuc., México

<sup>3</sup> Instituto de Investigaciones en Materiales, Universidad Nacional Autónoma de  
México, Apartado Postal 70-360, México Distrito Federal 04510, México.

<sup>4</sup> CNyN-UNAM, Km 107, Carretera Tijuana-Ensenada, B.C.

### **ABSTRACT**

Oxidation features of  $\text{Ce}_{1-x}\text{La}_x\text{O}_2$  and  $\text{Ce}_{1-x}\text{Ru}_x\text{O}_2$  nanostructured solid solutions supported in  $\text{Bi}_2\text{Mo}_{0.9}\text{W}_{0.1}\text{O}_6$  were tested for carbon monoxide. Samples were prepared by citric acid route starting with  $\text{La}(\text{NO}_3)_3$ ,  $\text{Ru}_3\text{C}_{12}\text{O}_{12}$  y  $\text{C}_6\text{H}_9\text{O}_6\text{Ce}$ . The characteristics of structure, morphology, surface composition and surface area were determined by XRD, SEM and the BET method for surface area measurement. Also catalytic activity of samples was studied as a function of composition. High Ce contents ( $>0.9$ ) benefit CO conversion at lower temperatures. Ce-La and Ce-Ru mixed oxides are highly active in the CO oxidation. Regarding Ce-Ru compounds, they become active at lower temperatures than Ce-La compounds.

**Keywords:** solid solutions, carbon monoxide oxidation, catalytic activity, nanostructure, mixed oxides.

---

\* rrangel@umich.mx

## INTRODUCTION

Atmospheric pollution is greatly affecting our planet contributing to Global warming. Last decades, the pollution has been increasing making us to care about the environment, developing efficient catalysts in some reactions to convert contaminants in substances less toxic and lowering their temperature for activation. Catalytic oxidation of CO at low temperature has attracted considerable attention because of its applications in automotive emission control, mainly, and in exhaust abatement for smokestack gases. Commonly, the elements Rh, Pt or Pd were widely used in the automotive industry. The catalysts based on these elements are used to oxidize to the CO and the HC, at the time that reduces the NO<sub>x</sub>. It was the reason because of that their use was extended.. Nevertheless, their shortage and its high cost have caused the necessity to look for a substitute of these elements. At the present time the compounds based on cerium or lanthanum are anticipated that might replace the generally used compounds like Rh, Pt or Pd. The mixed oxides or the solid state combined rare earth solutions with transition metals, have been looked favorable for processes of elimination of polluting agents. Among others cerium oxide has become an important catalyst due to the variety of its applications. It is used as catalytic converter of hydrogenation of unsaturated systems, and has also opened the doors for semiconductors based on metallic oxides; in solar panels for ultra-violet rays absorption, and in luminescent materials for violet blue fluorescence. Also as a part of three way-catalysts it is extensively used for reduction of polluting agents that arisen from the incomplete combustion of hydrocarbons. The importance of oxygen storage capacity of ceria is to be used for making doped catalysts capable to convert CO to CO<sub>2</sub> when Ce is combined with metals as ruthenium, iridium and indium, to form Ce<sub>1-x</sub>M<sub>x</sub>O<sub>2</sub> solid solutions. Having the fluorite structure, ceria promotes the CO oxidation, due to the oxygen vacancies in the ceria lattice, playing an important role in such reaction [1,2]. It is therefore that new possible combinations are tried, wishing to favorably modify the capacity of oxygen storage (OSC). In this sense Deganello and Matorama, [3] reported the capacity of oxygen storage of catalysts based on promoters of lanthanum and cerium oxide, which were synthesized by two different routes; the citrate method and the method of polyethilenglicol, in which the capacity of these compounds to store oxygen was studied by chemiadsorption. They conclude that the increase of the capacity of oxygen storage, based on the increase of the concentration of lanthanum (Ce<sub>1-x</sub>La<sub>x</sub>O<sub>2</sub>), depends on the number of vacancies of oxygen that affect the mobility of oxygen within the cerium oxide network. Recent works have been addressed to study RuO<sub>2</sub> as the oxygen rich phase being catalyst. According the studies CO is adsorbed in Ru sites that are not saturated and it has been suggested that Ru reacts with the closest oxygen lattice to make CO<sub>2</sub> [3]. Also iridium catalysts doped in different metallic oxides have been used to oxidize partially methane, finding good changes in catalytic activity [4]. On the other hand, in previous works, we have demonstrated the efficiency of Bi<sub>2</sub>MoO<sub>6</sub> compounds in the oxidation of carbon monoxide [5, 6]. We assume that one synergistic effect favorable to improve the oxidation reaction of CO to CO<sub>2</sub> could be done by supporting Ce<sub>1-x</sub>M<sub>x</sub>O<sub>2</sub> on Bi-Mo-W compounds.

The present work involves the synthesis of nanostructured catalysts of Ce<sub>1-x</sub>M<sub>x</sub>O<sub>2</sub> nanostructured solid solutions obtained by means of the sol-gel method which were supported on Bi<sub>2</sub>MoWO<sub>6</sub> looking for increasing their efficiency to oxide carbon monoxide to carbon dioxide.

## MATERIALS AND METHODS

The Sol-Gel method was used to synthesize the catalysts by the CIT technique [6]. Stoichiometric amounts of La(NO<sub>3</sub>)<sub>3</sub>.6H<sub>2</sub>O y C<sub>6</sub>H<sub>9</sub>O<sub>6</sub>Ce.H<sub>2</sub>O, Ru<sub>3</sub>C<sub>12</sub>O<sub>12</sub> and citric acid were dissolved in water or isopropilic alcohol and stirred for 4 h at constant temperature (80 °C), to reach the sol and later, the mixture slowly evaporated to gel. The gel received a thermal treatment 110 °C for 12 h and finally we got a fluffy solid that was burned at 600 °C for 4 h with by heating with a ramp 5 °C/min. The support was made by chemical co-precipitation starting from high purity (NH<sub>4</sub>)<sub>6</sub>Mo<sub>7</sub>O<sub>24</sub>·4H<sub>2</sub>O, (NH<sub>4</sub>)<sub>6</sub>W<sub>12</sub>O<sub>6</sub>·H<sub>2</sub>O, Bi(NO<sub>3</sub>)<sub>2</sub> · 5H<sub>2</sub>O compounds and using NH<sub>4</sub>OH 0.1M at pH = 5 and heated in a furnace at 500 °C. Finally, the Ce<sub>1-x</sub>(La<sub>x</sub>, Ru<sub>x</sub>)O<sub>2</sub>/Bi<sub>2</sub>Mo<sub>0.9</sub>W<sub>0.1</sub>O<sub>6</sub> systems were made by impregnation.

## CHARACTERIZATION

The systems under study were characterized by means x-ray diffraction (Siemens, D-5000 model), operating at 30 keV y 20 mA, with a step size 0.02 °/min from 10 to 70°. The images were obtained in a SEM JSM-6400 JEOL Noran Instrument, at 20 keV and 10<sup>-6</sup> Torr. BET surface was measured in Micrometrics Gemini 2060 RIG-100, model with nitrogen adsorption at 77K. The catalytic activity was determined in the interval of 100 to 400 °C. Catalysts were pretreated for one hour by using dried air 30 mL/min at 200 °C and tested for CO oxidation to CO<sub>2</sub>. The initial gasses, CO and O<sub>2</sub>, were diluted in helium at 5% in a ratio of 5/1 (O<sub>2</sub>/CO). The catalyst weight was 200 mg. The products CO<sub>2</sub>, O<sub>2</sub> and CO were analyzed by following their thermal conductivity.

## EXPERIMENTAL RESULTS AND DISCUSSION

### X-ray diffraction analysis

On figures 1 and 2 area we summarize the results concerning the x-ray diffraction analysis. On the top and in the bottom are displayed the La and Ce oxides, respectively, in order to establish comparison when any of them is substituted to form the solid solution. The guidelines were placed to make easier the observation of how the main reflections for La<sub>2</sub>O<sub>3</sub> or CeO<sub>2</sub> are changed while the substitution happens. By example, if observe the La<sub>2</sub>O<sub>3</sub> compound which has its main reflection in 2θ = 29.96°, we see that as the value of the substituent element increases the amount of Ce, the main reflection is run towards the left. For the opposite case in which it is settled CeO<sub>2</sub> as the host compound, we perceived that the main reflection is run towards the right when La is added. There is no doubt about that maximum value exists to carry out the substitution, because will be a limit of solubility for each system. In such case, the appearance of small amounts of initial oxides in balance with the formed solid solution will appear. Observing the compound that initially contains La<sub>2-x</sub>Ce<sub>x</sub>O<sub>3</sub> is probable that in the level of x=0.1, an additional compound to the one of the solid solution has formed, since in that level is observed in addition to the mentioned shifting of some peaks, the appearance of one reflection relative to the La<sub>2</sub>O<sub>3</sub> (2θ = 26 °) compound. It

would be indicative from which we have arrived at the solubility threshold of the Ce in the structure of the  $\text{La}_2\text{O}_3$ . For the case of the  $\text{Ce}_{1-x}\text{La}_x\text{O}_2$  compound substituted with La does not come into view evidence of formation of one secondary phase. Regarding the  $\text{Ce}_{1-x}\text{RuO}_2$  compounds it is observed the corresponding diffractogram in figure 2, at the diverse levels of substitution, that is to say,  $x=0.1, 0.01, 0.05$ , and there is no evidence that has formed any segregation of  $\text{CeO}_2$ ,  $\text{RuO}_2$ ; which in first instance would make suppose that a solid solution in the studied levels has been formed.

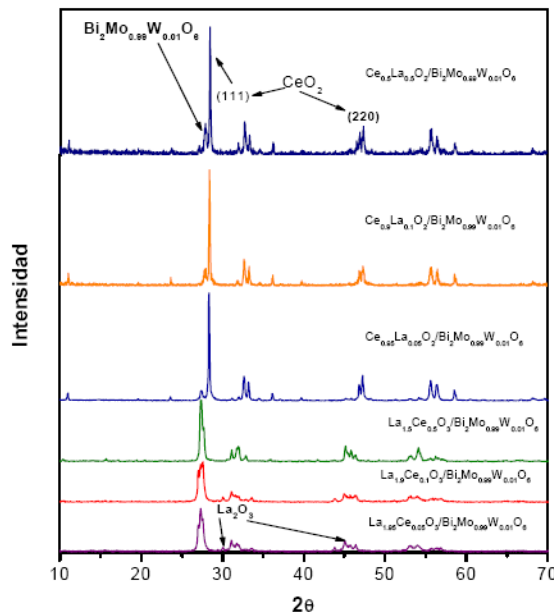


Figure 1. X ray diffraction spectra of  $\text{La}_{2-x}\text{Ce}_x\text{O}_3$  y  $\text{Ce}_x\text{La}_{1-x}\text{O}_2$  compounds. Also the  $\text{La}_2\text{O}_3$  and  $\text{CeO}_2$  are shown.

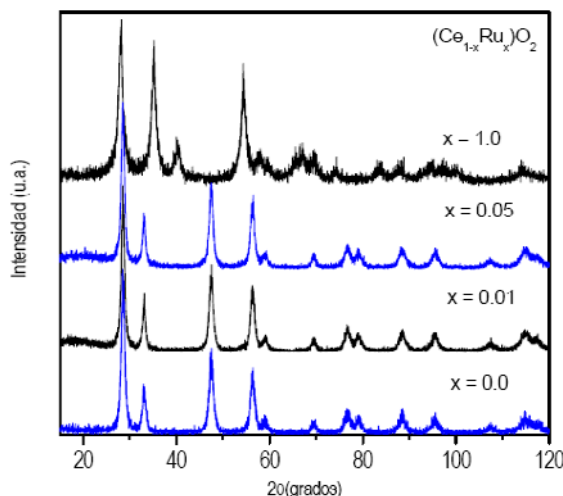


Figura 2. X ray diffraction spectra for the  $\text{Ce}_{1-x}\text{Ru}_x\text{O}_2$  system.

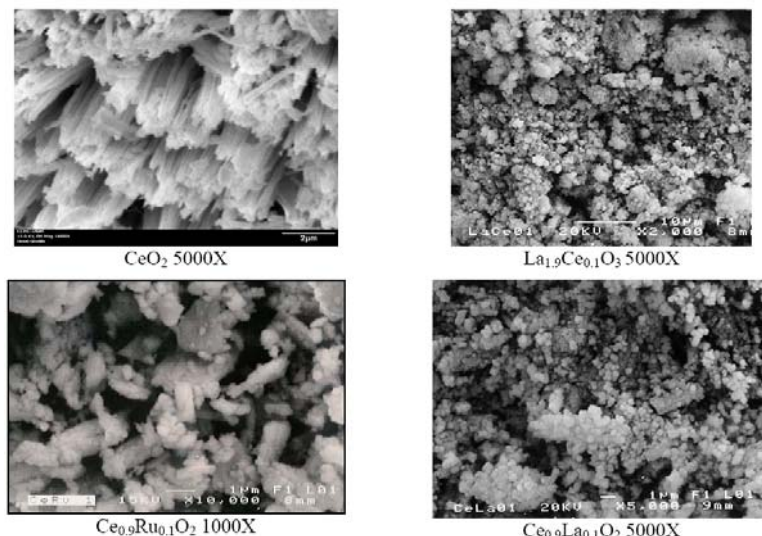


Figure 3. SEM images of  $\text{CeO}_2$ ,  $\text{La}_{1.9}\text{Ce}_{0.1}\text{O}_3$ ,  $\text{Ce}_{0.9}\text{Ru}_{0.1}\text{O}_2$ ,  $\text{Ce}_{0.9}\text{La}_{0.1}\text{O}_2$ , compounds.

## SEM MICROSCOPY

Through this technique the catalysts were analyzed in order to observe their morphology and possible segregation. In principle, it is possible to appreciate that the obtained  $\text{CeO}_2$  has a fiber form elongated with a diameter of  $0.25 \mu\text{m}$ , approximately. The compound is homogenous regarding the shape and size. In the case of Ce-La system for a level of substitution of  $x=0.1$  the formation of one homogeneous phase with crystals around  $0.5\mu\text{m}$  or less it is observed. One similar behavior is appreciated for  $\text{La}_{2-x}\text{Ce}_x\text{O}_3$  compounds. In the case of  $\text{Ce}_{1-x}\text{RuO}_2$  solid solutions, we obtained an agglomerate material consisting of small spheres of  $1 \mu\text{m}$  apparently. In no one of the analyzed cases an important segregation of some oxide was observed, and that confirms that the solid solution structure has been formed.

## SURFACE AREA

The determinations of superficial area, table 1, show compounds with relatively low values in which the cerium oxide has  $9.8 \text{ m}^2/\text{g}$  and the  $\text{Bi}_2\text{Mo}_{0.9}\text{W}_{0.1}\text{O}_6$  system  $6.5 \text{ m}^2/\text{g}$ . It is observed that as increases the La content in the Ce-La system, the surface area is increased; tendency that also is appreciated in the system Ce-Ru, for which, a smaller content of substitution favors an elevated value of area. Some logic may apply here because the La element posses one atomic diameter bigger than the Ru. In the case of La-Ce systems the surface area decreases when Ce is increased. Regarding the differences in surface area among the compounds substituted in 0.5 or 10 % atomic for all the systems are small but significant and proportional to the amount of the substitute material. Because area of the supporting material is initially small and the proportion on Ce-La, Ce-Ru or La-Ce is only 10% (w/w). The resulting materials are also relatively small.

**Table 1. Surface area**

Catalyst	Surface area ( $\text{m}^2/\text{g}$ )
$\text{La}_{1.5}\text{Ce}_{0.5}\text{O}_3/\text{Bi}_2\text{Mo}_{0.90}\text{W}_{0.1}\text{O}_6$	2.2
$\text{La}_{1.9}\text{Ce}_{0.1}\text{O}_3/\text{Bi}_2\text{Mo}_{0.90}\text{W}_{0.1}\text{O}_6$	4.5
$\text{La}_{1.95}\text{Ce}_{0.05}\text{O}_3/\text{Bi}_2\text{Mo}_{0.90}\text{W}_{0.1}\text{O}_6$	4.7
$\text{Ce}_{0.95}\text{La}_{0.05}\text{O}_2/\text{Bi}_2\text{Mo}_{0.90}\text{W}_{0.1}\text{O}_6$	4.7
$\text{Ce}_{0.9}\text{La}_{0.1}\text{O}_2/\text{Bi}_2\text{Mo}_{0.90}\text{W}_{0.1}\text{O}_6$	6.0
$\text{Ce}_{0.9}\text{Ru}_{0.1}\text{O}_2/\text{Bi}_2\text{Mo}_{0.90}\text{W}_{0.1}\text{O}_6$	2.5
$\text{Ce}_{0.95}\text{Ru}_{0.05}\text{O}_2/\text{Bi}_2\text{Mo}_{0.90}\text{W}_{0.1}\text{O}_6$	3.2
$\text{CeO}_2$	9.8
$\text{Bi}_2\text{Mo}_x\text{W}_{(1-x)}\text{O}_6$	6.5

## CATALYTIC ACTIVITY

Regarding the measurements of catalytic activity for the Ce-La or the La-Ce systems, showed us that a small substitution of Ce has the best characteristics of oxidation. If we observe on figure 6 the values concerning the  $\text{CeO}_2$  compound, it is appreciated that this material has an activation temperature around 200 °C reaching 50% conversion at 300 °C. Then, it is interesting to notice that one relatively low temperature of activation of 125°C is obtained, reaching values of 50% conversion at 220 °C for the  $\text{La}_{1.9}\text{Ce}_{0.1}\text{O}_3$ , and  $\text{Ce}_{0.9}\text{La}_{0.1}\text{O}_2$ , compounds. When observing the behavior of solid solutions with greater substitution is appreciated an increase in the temperature of activation. Also one displacement towards greater temperatures to obtain a conversion of 50% of around 325 °C. With respect to compounds of system Ce-Ru a surprising value of activation near the room temperature is observed, with a conversion of the 100% to a temperature below 100°C.

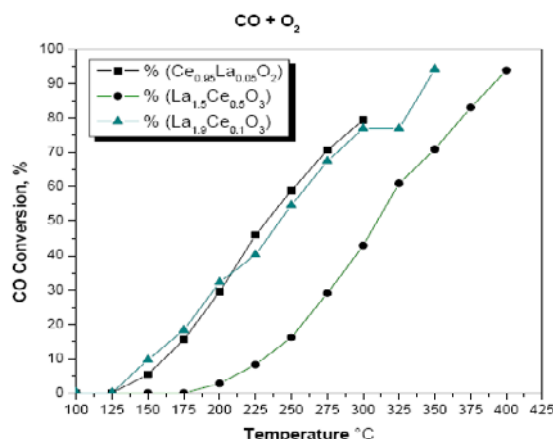


Figure 4. Catalytic activity for carbon monoxide,  $\text{Ce}_{1-x}\text{La}_x\text{O}_2/\text{Bi}_2\text{Mo}_{0.9}\text{W}_{0.1}\text{O}_6$  and  $\text{La}_{2-x}\text{Ce}_x\text{O}_2/\text{Bi}_2\text{Mo}_{0.9}\text{W}_{0.1}\text{O}_6$  systems. Experimental conditions: 1% CO, 0.5% O<sub>2</sub>, 98.5% He; 80 mL/min; 0.1 g.

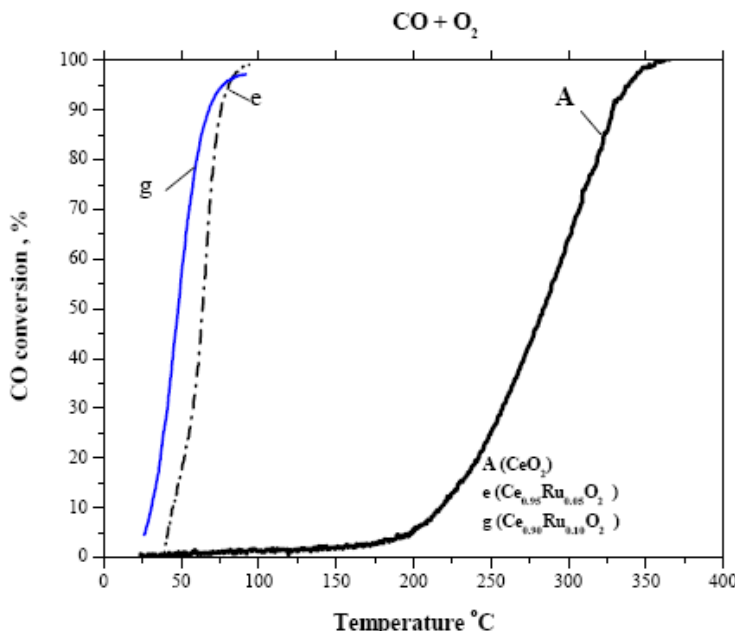


Figure 5. Catalytic activity for carbon monoxide, Ce-Ru system and  $\text{CeO}_2$ . Experimental conditions: 1% CO, 0.5%  $\text{O}_2$ , 98.5% He; 80 mL/min; 0.1 g.

## CONCLUSIONS

The synthesis of  $\text{Ce}_{1-x}(\text{La}_x, \text{Ru}_x)\text{O}_2/\text{Bi}_2\text{Mo}_{0.9}\text{W}_{0.1}\text{O}_6$  compounds was successfully made to compare their structural and reactive characteristics comparing the substituting material and also in comparison to  $\text{CeO}_2$ . On regard of x ray diffraction it is observed one solubility limit higher than  $x=0.05$  and lower than  $x=0.1$ . It is observed one shifting of the principal reflections of  $\text{CeO}_2$  or  $\text{La}_2\text{O}_3$  as indirect indicative of atomic substitution. SEM microscopy revealed homogenous and regular size, of spherical and inferior form to  $1\mu\text{m}$  for La-Ce and Ce-La systems. Both systems are very reactive with conversions of 50% at  $220^\circ\text{C}$ . Surprisingly, the Ce-Ru solid solutions reached 100% conversion under  $100^\circ\text{C}$ . It is concluded that Ce-La, La-Ce and Ce-Ru solid solutions are very reactive and represent an important improvement in comparison to  $\text{CeO}_2$ .

## ACKNOWLEDGMENTS

R. Rangel acknowledges to CIC-UMSNH for financial support under 20.7 project. Also to COECyT-Michoacán grant S08-02/277. P. Bartolo-Pérez acknowledges grant from Conacyt under project 59998. F. Huerta acknowledges the scholarship provided by CONACyT. Authors wish to thank their technical help to V. Luque, F. Solorio from IIM-UMSNH, Wilian Cauich from CINVESTAV-IPN and I. Gradilla from CNyN-UNAM.

## REFERENCES

- [1] T.X.T. Sayle, S.C. Parker, C.R.A. Catlow, "The role of the oxygen vacancies on ceria surfaces in the oxidation of carbon monoxide", *Surface Sci.* 316 (1994) 329-336.
- [2] A. Bueno-López, K. Krishna, M. Makkee, Jacob A. Moulijn, "Active oxygen from CeO<sub>2</sub> and its role in catalyzed soot oxidation", *Cat. Lett. Vol.* 99, (2005), 3-4.
- [3] Francesca Deganello and Antonino Martorana, "Phase Analysis and Oxygen Storage Capacity of Ceria-Lanthana Based TWC Promoters Prepared by Sol-Gel Routes", *J. Sol. State Chem.* 163 (2002), 527-533.
- [4] Y.D. Kim, H.Over, G. Krabbes, G. Ertl, "Identification of RuO<sub>2</sub> as the active phase in CO oxidation on oxygen-rich ruthenium surfaces", *Topics in Cat., Vol.* 14, (2001), 1-4.
- [5] Kiyoharu Nakagawa, Kengo Anzai, Naoko Matsui, Naoki Ikenaga, Toshimitsu Suzuki, Yonghong Teng, Tetsuhiko Kobayashi and Masatake Haruta, "Effect of support on the conversion of methane to synthesis gas over supported iridium catalysts" *Cat. Lett.* 51 (1998) 163-167.
- [6] R. Rangel, P. Bartolo-Pérez, A. Gómez, G. Díaz, D. H. Galván, Comparison between  $\gamma$ -Bi<sub>2</sub>MoO<sub>6</sub> and Bi<sub>2</sub>WO<sub>6</sub> catalysts in the CO oxidation, *Journal of Materials Synthesis and Processing*, vol. 9, No.4 (2001) 207.
- [7] R. Rangel, P. Bartolo-Pérez, A. Gómez, G. Díaz, D. H. Galván, Study of microstructure and catalytic activity of  $\gamma$ -Bi<sub>2</sub>MoO<sub>6</sub> and Bi<sub>2</sub>WO<sub>6</sub> compounds, *Surf. Rev. Lett.*, Vol. 9, No.5 (2002) 1779.
- [8] Mihai Alifanti, Mihaela Florea, Vasile I. Parvulescu, Ceria-based oxides as supports for LaCoO<sub>3</sub> perovskite; catalysts for total oxidation of VOC, *App. Cat. B: Environ.* 70 (2007) 400–405.

***Chapter 17***

## **SILVER NANOPLATES: SYNTHESIS, GROWTH AND FUNCTIONAL PROPERTIES**

***Xuchuan Jiang, Qinghua Zeng, Aibing Yu\****

School of Materials Science and Engineering,  
University of New South Wales, Sydney, NSW 2052, Australia

### **ABSTRACT**

This chapter provides a brief review of the recent research on silver nanoplates, covering the synthesis, growth mechanisms, and functional properties, with a focus on our work in this field. Various methods for the synthesis of silver nanoplates (e.g., triangles, disks, and prisms) are first introduced, including physical technique (e.g., nanosphere lithographic method) and chemical techniques (e.g., photoinduced method, templating method, solvothermal and hydrothermal reduction methods). A synergistic reduction hydrothermal method developed by our lab, namely, the use of three or more reducing agents simultaneously for the synthesis of silver nanoplates at ambient conditions, will be discussed in detail. Then, various experimental and theoretical techniques employed for understanding the principles underlying the growth and shape control of nanoparticles are discussed, including the use of molecular dynamics (MD) and density function theory (DFT) simulations. Finally, the functional properties of silver nanoparticles (e.g., surface enhancement Raman spectrum, and localized surface Plasmon resonances) in chemical and biochemical sensing, as well as the stability and chemical reactivity are summarized based on the recent findings to highlight the potential of silver nanoplates. The need for future research is also briefly discussed.

### **1. INTRODUCTION**

Metal nanoparticles have attracted intensive research interests because of their fascinating physicochemical properties such as optical, electronic, magnetic and chemical properties,

---

\* To whom correspondence should be addressed. Tel: +61-2-93854429, Fax: +61-2-93855956, Email: a.yu@unsw.edu.au.

particularly for low-dimensional gold, silver, and copper nanostructures (e.g., rods, wires, plates, discs).[1-7] This has stimulated not only the development of synthesis, characterization and mechanistic understanding, but also the exploration of functional applications in many areas such as near-field optical probes, surface enhanced Raman spectroscopy (SERS), and biomedical labeling.[8-33] Of the metal nanostructures achieved such far, silver nanoplates (also termed as nanoprisms or nanodisks) become more and more attractive because such morphology possesses an extreme degree of anisotropy together with corners and edges for generating maximum electromagnetic-field enhancement that is useful for optical sensing application.[34-36]

The shape/size-dependent optical properties and applications have propelled the extensive exploitations in synthesis methodology, structural characterization, and mechanistic understanding. Many attempts have been made to control the synthesis/growth of silver nanoparticles with two-dimensional (2D) morphologies, such as plates, prisms, disks, and truncated structures for desirable optical properties. Two main synthetic strategies have been reported, including physical technique (e.g., nanospherical lithography method)[37] and chemical techniques.[38-54] The wet-chemical methods have been proved to be more powerful and versatile in shape control, such as photoinduced method,[38-41] electrochemical method,[42] ultrasonic-assistant method,[43] solvothermal method,[44-48] and templating method (e.g., ‘soft’ reverse micelles and ‘hard’ polystyrene spheres).[49-54] Despite of many successes, some limitations still exist in two major aspects: (i) many of them are empirical in nature and applicable to very specific system(s), and no single approach could be developed as a general synthesis route in view of its potential as an efficient, inexpensive mass production approach for monodispersed silver nanoplates; (ii) some differences still exist about the mechanisms on shape control and growth of silver nanoplates, as highlighted by the fact that various mechanisms have been proposed, such as stacking fault mechanism, twinning-plane mechanism, photoinduced fusion mechanism, and surface selective adsorption mechanism, but none of them is quantitative. The two limitations would impede the progress in exploitation of functional applications of silver nanoplates. How to overcome the limitations has been a major challenge in silver nanoparticle research. In recent years, a lot of efforts have been made in this area. Here we present an attempt to summarize these studies to generate useful information for future development.

In this chapter, we will review the synthesis, growth mechanism and functional properties of silver nanoplates. First, various synthesis methods are briefly introduced, including the synergetic reduction method we recently developed.[55-58] Second, the particle growth and shape control mechanisms are discussed on the basis of both experimental and theoretical methods, where the usefulness of molecular modeling is emphasized. Finally, some functional properties in chemical and biochemical sensing associated with optical properties are presented to demonstrate the potential of silver nanoplates in application.

## 2. SYNTHESIS METHODS

A number of methods have been developed for the synthesis of metal nanoparticles. There have been many reviews on the preparation of metallic nanoparticles.[37, 59-68] Some reviews deal with the synthesis of metallic nanoparticles in general.[62, 67, 68] Some deal

with the synthesis of silver nanoplates,[59] gold nanoparticles,[63, 65] and dendrimer encapsulated metal nanoparticles.[61] In this section, we will briefly introduce the successful approaches developed for shape and size control of silver nanoparticles, including physical and chemical techniques.[37-58] Compared to the physical technique (e.g., nanosphere lithographic approach), chemical technique is much more successful, and shows some advantages such as simple operation condition, diverse choice in solvents, controllable size, and high yield (defined as the percentage of plate-like particles). Here various chemical reduction techniques are mainly discussed, including photoinduced method, templating method, solvothermal reduction method, and hydrothermal reduction method, with a focus on the synergistic hydrothermal reduction method we recently developed.

## 2.1. Nanosphere Lithography Method

Nanosphere lithography (NSL), a physical technique, is an inexpensive, inherently parallel, high throughput, materials general nanofabrication technique capable of producing an unexpectedly large variety of nanoparticle structures and well-ordered 2D nanoparticle arrays. This technique was developed for preparation of silver nanoprisms by Van Duyne and co-workers.[37, 69] It has been demonstrated its usefulness in controlling the size of Ag nanoprisms and the availability of transferring these prisms from substrate (e.g., silicon wafer) to a solvent forming a colloidal dispersion for desirable functional properties.

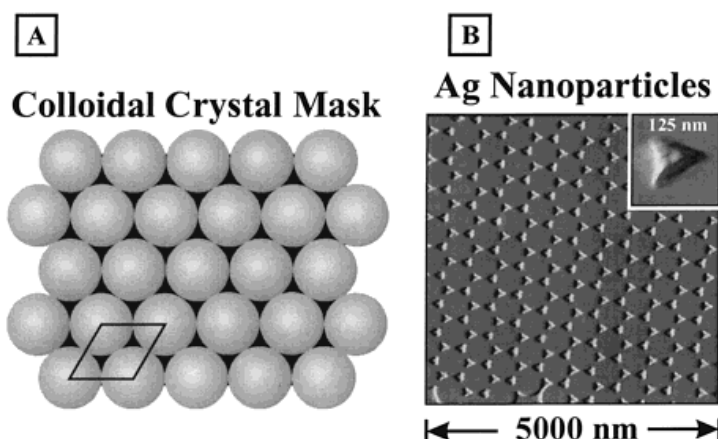


Figure 1. Schematic illustration (A) and representative AFM image (B) of SL PPA. The ambient contact mode AFM image was captured from a SL PPA fabricated with  $D = 542$  nm nanospheres and  $d_m = 48$  nm thermally evaporated Ag metal after 3 min sonication in methylene chloride. (Reprinted with permission from ref. 37. Copyright 2001 The American Chemical Society.)

In the NSL technique, the first step is the self-assembly of hard polystyrene spheres to form a 2D colloidal crystal deposition mask. The deposition requires that the nanospheres are able to freely diffuse across the substrate, seeking their lowest energy configuration. This is often achieved by chemically modifying the nanosphere surface with a negatively charged functional group, such as carboxylate or sulfate that is electrostatically repelled by the negatively charged surface of a substrate (e.g., mica or glass). The solvent (e.g., water)

evaporation of the nanosphere solution could lead to the formation of a monolayer of hexagonally close-packed nanosphere pattern on the substrate due to the capillary forces. As in all naturally occurring crystals, nanosphere masks may include a variety of defects that arise as a result of nanosphere polydispersity, site randomness, point defects (vacancies), line defects (slip dislocations), and polycrystalline domains. A typical defect-free domain could be achieved with ranges from 10 to 100  $\mu\text{m}^2$  (Fig. 1). A monolayer of ordered silver nanoprisms film can be deposited by thermal evaporation, electron beam deposition (EBD), or pulsed laser deposition (PLD) on the substrate through the nanosphere mask to a controllable mass thickness.

Later, Van Duyne et al.[69] reported that such mono-sized silver nanoprisms generated by the NSL technique can be subsequently released into solution because of the weak adhesion of the nanoprisms on the glass substrate. Unfortunately, the use of sonication to release silver nanoplates and the necessary surface coating to protect these nanoprisms from aggregation in solution limit the extensive application of this NSL technique.

To obtain ordered pattern with large areas, Giersig and co-workers[70] reported an alternative strategy in this area. They described the preparation of large-area, two-dimensional metallic structures using shadow nanosphere lithography. By varying the position of the substrate with respect to the evaporation source during the sample preparation, they fabricated morphologies such as cups, rods, and wires, which are not accessible by the standard nanosphere lithography. This technique also allows for an encapsulation of the metallic structures, to prevent them from oxidation.

## 2.2. Photoinduced Method

Photoinduced method means that the synthesis of nanoparticles is performed in solution by illumination of visible light or laser light. A good example in this field was first reported by Mirkin et al.[38, 39] The authors demonstrated an efficient synthesis method for generating nearly monodispersed silver nanoprisms through the illumination of visible light, in which the conversion of citrate-capped Ag colloids into larger particles with triangular morphology and edge length of  $\sim 100$  nm was observed in the presence of stabilizer such as bis(p-sulfonatophenyl) phenylphosphine dehydrate dipotassium salt (BSPP) (Fig. 2). They further proposed that the formation of Ag nanoprisms might be caused by the photoinduced fusion or aggregation of pre-formed nanoparticles which may serve as nuclei in the formation of triangular plates. The BSPP as an adsorbate also played a crucial role in the growth of silver nanoprisms. Later, Junior et al.[71] demonstrated a similar approach in which the replacement of BSPP with poly(vinylpyrrolidone) (PVP), which can also result in the formation of silver nanoprisms. Sun et al.[44] suggested that the role of PVP was used to reduce  $\text{Ag}^+$  ions to generate silver seeds for the growth of Ag nanoplates, and citrate ions played a key role in the transition from spherical to triangular particles due to preferential adsorption on  $\text{Ag}\{111\}$  facets.

Mirkin et al.[39] reported in subsequent work that the excitation wavelengths could be chosen to control the prism size, so that the use of longer excitation wavelength could produce larger particles in the edge length of 30-120 nm. The authors also claimed that a bimodal nanoprism size distribution could be induced by dual-beam illumination, and the so-called secondary beam suppressed the fusion of pre-formed nanoprisms, induced by charge

re-distribution on the particle surface resulting from dipole plasmon excitation. Such a fusion of small prisms would be responsible for the formation of a secondary population of larger ones. The schematic illustration of formation mechanism will be discussed later. Further study was conducted by the same group and they reported an alternative way to regulate the fusion process of nanoprism by adjusting the pH value, which would be suitable for the formation of silver nanoprism on gold seeds, irradiated by a laser beam at 550 nm, so that the gold surface plasmon would be preferentially excited at the start of the aggregation process.[72, 73]

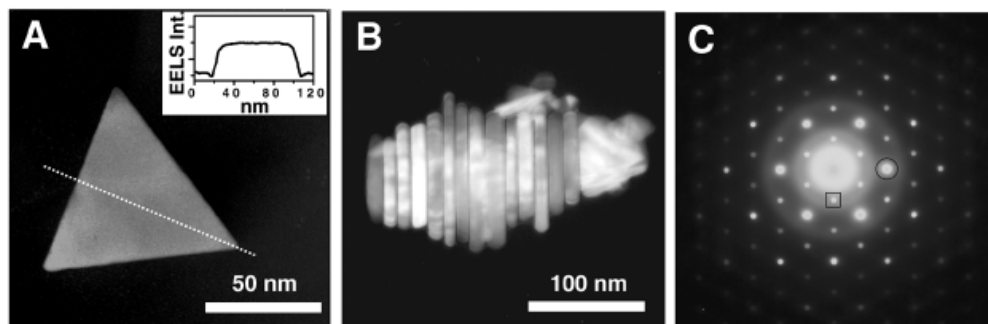


Figure 2. (A) EELS mapping analysis showing the flat-top morphology of the Ag nanoprisms. Inset shows the EELS intensity over the line scan (dotted line through triangle axis). (B) Stacks of Ag nanoprisms assembled in a top-to-base manner on a carbon film coated Cu grid. (C) Electron diffraction analysis of individual Ag nanoprisms. The spot array, diagnostic of a hexagonal structure, is from the [111] orientation of an individual Ag nanoprism lying flat on the substrate with its top perpendicular to the electron beam. On the basis of three-zone axis analysis (not shown), the crystal structure of the Ag nanoprism was determined to be an fcc structure. The intense spots in the [111] zone axis are allowed {220} Bragg reflections (e.g., circled spot, corresponding to the lattice spacing of 1.44 Å), and the sharp weak spot in the center of the triangles formed by the strong spots is indexed as 1/3{422} (e.g., boxed spot, corresponding to the lattice spacing of 2.50 Å). (Reprinted with permission from ref. 38. Copyright 2001 The American Association for the Advancement of Science.)

By extending such a technique, both Maillard[40] and Callegari groups[41] have reported the formation of Ag nanoprisms through photoinduced conversion of silver nanospheres into nanoplates, in which the shape and size can be directly influenced by illumination wavelengths. They reported a two-step growth mechanism for this transfer process, in which the colloids were prepared first in solution by using reducing agents (e.g., NaBH<sub>4</sub>), and then the photo-irradiation technique was used for this conversion. The silver ions could subsequently be photo-reduced and catalyzed on the surface of those initial silver seeds for forming large nanoplates. Again, they found that the photo-reformulation process can be driven by room light, and the shape and size of the silver nanoparticles can be controlled by choosing light wavelengths, but it took a long time (~50 hours).

Liz Marzán and co-workers[74] demonstrated a modified simple method involving illumination of silver seeds with low intensity light emitting diodes (LEDs). The main contribution of this work, compared to previous studies, is the possibility to prepare Ag nanoprisms with dimensions resulting in high absorption coefficients well within the near-infrared region. For example, particles with intense in-plane dipolar bands centred at either 1037 nm or 1491 nm were obtained by using LEDs, and emission bands are centred at 518 nm and 653 nm, respectively. Similarly, the particle size was observed to be dependent upon

illumination wavelength, while the light wavelength produces no significant effect on the shape and thickness of the particles. Their findings indicated consumption of the preformed Ag seeds, but it seemed to rule out Ostwald ripening, as well as fusion of intermediate prisms.[74]

Rocha and co-workers[75-77] described that particle size can be tuned through the choice of the incident wavelength, while the thickness is independent of the illumination conditions, as observed in the photoinduced process.[74] Additionally, these authors[76] confirmed some aspects of the growth mechanism proposed by Maillard et al.[40] and found that the origin of anisotropic growth is not related to local surface plasmon resonance excitation, but related to intrinsic aspects of the seeds, such as structural defects or the capping agent(s) on the seed surface.[77]

### 2.3. Templating Method

An good example in templating method was presented by Pilani and co-workers,[49-52, 78] who used reverse micelles as a ‘soft’ template to control the growth of silver nanodisks, in which the bis(2-ethyl-hexyl)sulfosuccinate (AOT)/isoctane/water reverse micelles played an important role in shape/size control. In this case, they found that the nanodisk size could be tuned between 30 and 100 nm by changing the ratio of reducing agent (hydrazine) to silver ions. The authors also suggested that the stacking faults on Ag{111} facets account for the formation of nanodisks (Fig. 3). Similarly, Carroll and Chen [54] reported a surfactant (e.g., cetyltrimethylammonium bromide, CTAB)-assisted method to generate silver nanodisks in water by ageing at 40 °C for 4 h. The lateral dimensions ranging from 40 to 300 nm were obtained via adjusting the molar ratio of CTAB to silver, however, a mixture of various shapes (e.g., triangle, truncated, and spherical particles) was obtained. The authors described that the adhesion of CTAB on the Ag{111} planes of the silver seeds, along with the formation of silver bromide (AgBr) in contact with these seeds, played a key role in formation of nanodisks. Recently, Zhang et al.[48] used a water/PVP/n-pentanol ternary system, similar as a micellar system, to synthesize silver nanoprisms by heating at 95 °C for 48 h, but a mixture of platelets with various morphologies was generated.

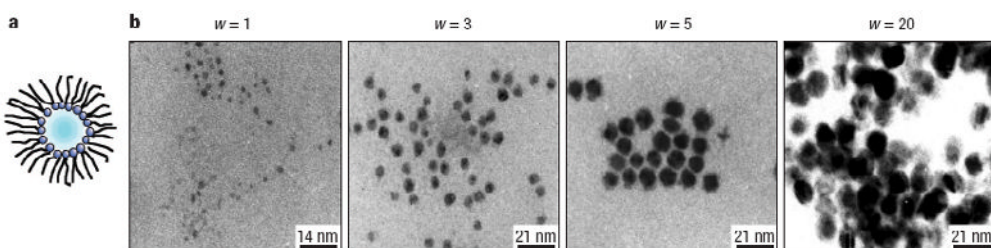


Figure 3. The different shapes of copper nanocrystals produced in colloidal self-assemblies of surfactant-H<sub>2</sub>O-isoctane solution. The surfactant, S, used is either Na(AOT) or Cu(AOT)<sub>2</sub>. The water content  $w = [\text{H}_2\text{O}]/[\text{S}]$  is related to the droplet radius by  $R(\text{nm}) = 0.15 w$ , [AOT] = 0.1 M; [Cu(AOT)<sub>2</sub>] =  $1 \times 10^{-2}$  M; [N<sub>2</sub>H<sub>4</sub>] =  $2 \times 10^{-2}$  M. (a) Reverse micelles; (b) Control of nanocrystal size with  $w$ , that is, control of the size of water-in-oil droplets. (Reprinted with permission from ref. 78. Copyright 2003 Nature Publishing Group.)

Hao and colleagues[54] reported a hard-template (e.g., polystyrene spheres as a template) method to prepare silver nanoplates under the heating of N, N-dimethylformamide (DMF) solution. Here the DMF solution acts as both a solvent and a reducing agent. In this case, an aqueous colloidal suspension of carboxylate-functionalized polystyrene (PS) spheres was mixed with AgNO<sub>3</sub> and ammonium hydroxide solution first. The reducing reaction took only several minutes so that the structure of PS particles was not destroyed, although DMF can slightly decomposes to a more easily oxidized amine upon ageing or upon catalytic decomposition with solid base. The authors demonstrated that the PS particles play an essential templating role through electrostatic binding of Ag ions by surface carboxyl groups of the mesospheres under the surfactant-free conditions. Upon reduction, the adsorbed Ag atoms presumably serve as nucleation centre for particle formation. Once nucleation is initiated, the mesospheres may block growth along certain direction, effectively templating growth in another (lateral) direction, as shown in Fig. 4.

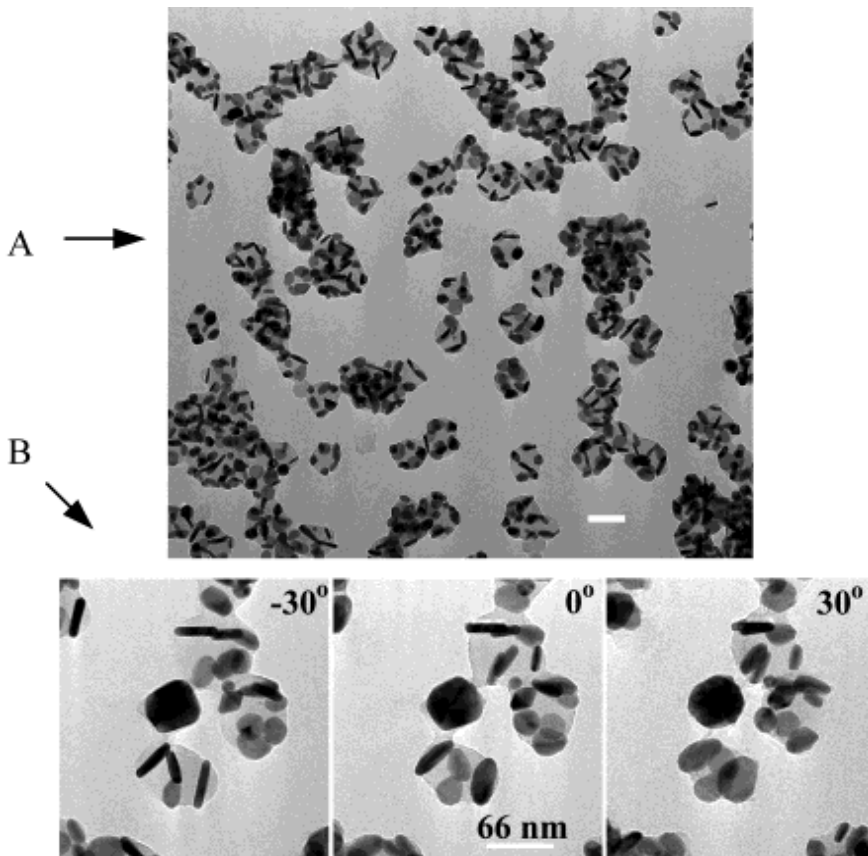


Figure 4. (A) TEM image of a fresh Ag/PS sample with a tool bar 100 nm; (B) TEM images of Ag/PS, tilting the sample plane from  $-30^\circ$  through  $0^\circ$  to  $+30^\circ$ . (Reprinted with permission from ref. 54. Copyright 2002 The American Chemical Society.)

## 2.4. Solvothermal Reduction Method

Solvothermal reduction method has been widely used in preparation of silver nanoplates or nanodisks because of the advantages in bulk volume in product, high yield in the desirable shape, and diverse choices in solvents (e.g., organic solvent, water, or their mixture) and surface capping agents (surfactants, polymers, or both). For example, Carroll et al.[53] presented the CTAB-assisted approach to generate silver nanodisks in water by ageing at 40 °C, and the size ranging from 40 to 300 nm were obtained via adjusting the molar ratio of CTAB to silver, although the reported particles are major in truncated structure. Zhang et al.[48] used PVP as a surfactant to assist the synthesis of silver nanoprisms by heating a water/PVP/n-pentanol ternary system at 95 °C for 48 h. This solvothermal reduction method could generate silver nanoparticles, although various morphologies (triangular, hexagonal, and truncated particles) were obtained in the final product.

Pastoriza-Santos et al.[47] demonstrated a simple procedure leading to truncated silver nanoprisms by simply boiling silver nitrate in DMF in the presence of PVP. The authors also suggested that the DMF can be used as both solvent and reducing agent, and the use of higher concentrations of both AgNO<sub>3</sub> and PVP proved to be a key factor to determine the final morphology in another work of the same group.[79] They proposed the growth mechanism involving the formation of small silver spheres which would then aggregate and subsequently recrystallise into particles with well-defined edges, through a melting-like process. A continuous variation of nanoprism size during the boiling of reaction system was observed. A very similar approach was later used by Jiang et al.[43] who reported the preparation of silver nanoplates in DMF solution and in the presence of PVP molecules, and assisted by an ultrasonic process. They also highlighted the role of PVP as a stabilizer and a shape directing agent to induce triangular shapes through kinetic growth control of various crystal faces (i.e., 111, 110, and 100).

The polyol-mediated synthesis, as another solvothermal reduction method, has been reported by Xia et al.[44-46, 80] who demonstrated the shape control of silver nanoplates through heating ethylene glycol, which could lead to the kinetics or thermodynamics growth depending on experimental parameters. It was demonstrated that the PVP molecules could serve as both a reducing agent and a surfactant for shape control in the synthesis of metal particles. The morphology and dimension of the product were found to strongly depend on reaction conditions such as the molar ratio between the repeating unit of PVP and AgNO<sub>3</sub>. For example, if the molar ratio between the repeating unit of PVP and AgNO<sub>3</sub> was increased from 1.5 to 3, multiply twinned particles became the major product;[45] while the molar ratio of PVP to AgNO<sub>3</sub> was increased or the molecular weight of PVP was decreased, the reduction rate increased, thus nonspherical morphologies (rods, plates, or cubes) were generated. The authors also presented for the first time that the reduction kinetics of AgNO<sub>3</sub> by the hydroxyl end group of PVP can be manoeuvred in at least two different ways to produce Ag triangular nanoplates in high yields. The hydroxyl end groups of PVP reduce silver ions at a sufficiently slow rate so that the growth of Ag nanocrystals became kinetically controlled, leading to the formation of triangular plates, as shown in Fig. 5. This kinetically control could allow one to obtain Ag nanoplates with controllable edge lengths by varying the reaction time.

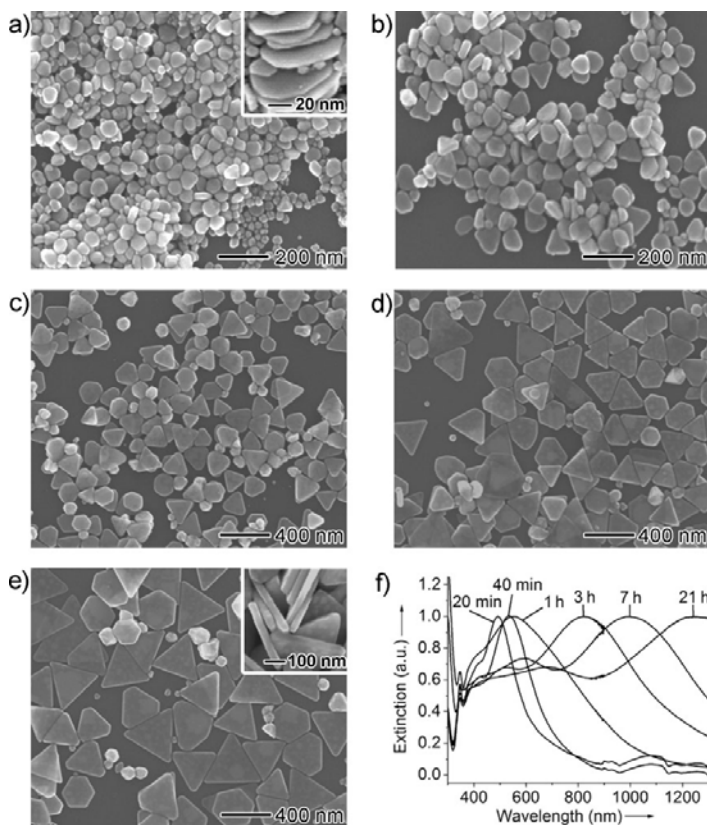


Figure 5. SEM images of products sampled at different stages of a synthesis: (a)  $t = 40$  min; (b)  $t = 1$  h; (c)  $t = 3$  h; (d)  $t = 7$  h; and (e)  $t = 21$  h. (f) UV-vis spectra of these products dispersed in water. The insets of (a) and (e) are SEM images taken from tilted samples. The PVP had an average molecular weight of 29, 000 g mol<sup>-1</sup> and its molar ratio (in terms of the repeating unit) to AgNO<sub>3</sub> was 30. (Reprinted with permission from ref. 46. Copyright 2006 WILEY-VCH Verlag GmbH & Co. KGaA, Weinheim.)

## 2.5. Hydrothermal Reduction Method

As an environmental friendly approach, hydrothermal method becomes more attractive in the synthesis of silver nanoparticles. Carroll et al.[53] presented the CTAB-assisted approach to generate silver nanodisks in water by ageing at 40 °C for 8 h, and the size ranging from 40 to 300 nm were obtained via adjusting the molar ratio of CTAB to silver. They obtained silver nanoparticles with the majority of truncated shape, doped with triangles and disks.

We recently developed a facile synergistic reduction method to synthesize silver triangular nanoplates at ambient conditions (e.g., aqueous solution, room temperature).[55-58] The synergistic reduction approach means that the use of a few reducing agents with different reducing abilities (e.g., citric acid, L-ascorbic acid, and sodium borohydride) toward the reduction of AgNO<sub>3</sub> simultaneously. In our designed approach, the nucleation reaction is initiated by adding trace of NaBH<sub>4</sub> solution, small colloids could be formed at the beginning, and the subsequent growth of silver nanoplates was achieved by the synergistic reduction of both citric acid and L-ascorbic acid in aqueous solution at room temperature. This synthesis

method shows some features such as fast reaction (within 10 minutes), high yield, large quantity, and nearly monodispersed silver nanoparticles. In addition, all operations in this method were performed at room temperature in aqueous solution.

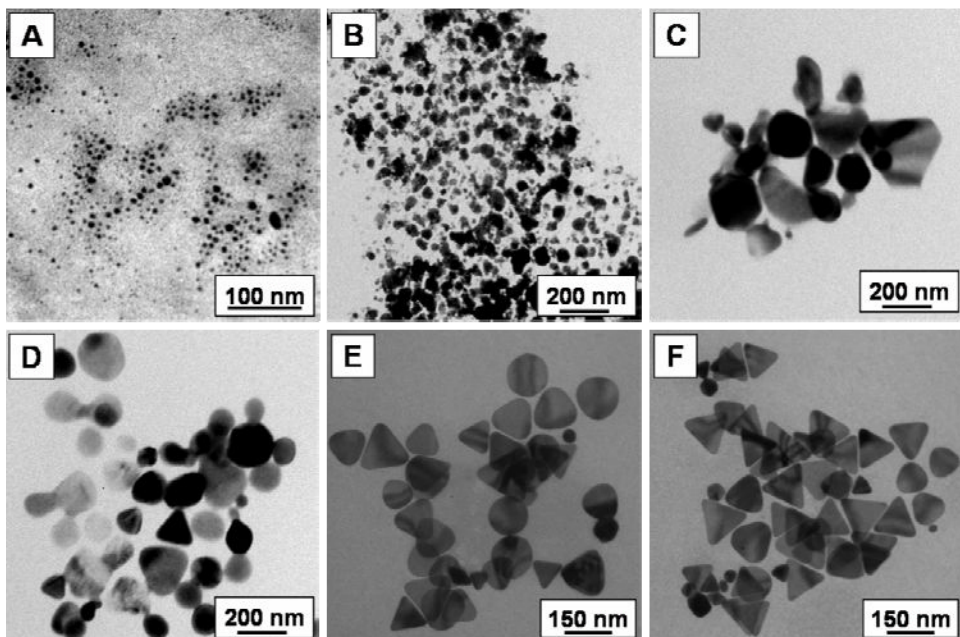


Figure 6. The influence of reducing agents on the morphologies of silver nanoparticles: (A) NaBH4; (B) citric acid + NaBH4; (C) L-ascorbic acid + NaBH4; (D) citric acid + L-ascorbic acid; and (E-F) the synergetic use of citric acid + L-ascorbic acid + NaBH4. Noted that the continuous stirring was employed for those good-quality plates (F).

In this approach, the synergetic effect of three reducing agents of citric acid, L-ascorbic acid, and NaBH4 played a crucial role in determining shape and size of silver nanoparticles.[55-58] As a confirmation, the functioning was examined using any one, any two, or all of the three reducing agents. The corresponding TEM images are shown in Fig. 6. The use of NaBH4 alone could only generate small nanocrystals with diameter of ~5 nm (Fig. 6A), and the sole citric acid could lead to irregular particles over a couple of hours, while the use of sole L-ascorbic acid had no reduction reaction with Ag<sup>+</sup> ions even overnight. The results suggest the combination of any two of these reducing agents could just generate irregular nanoparticles as shown in Figs. 6(B-D). The difference was that the combined use of either NaBH4 and citric acid, or NaBH4 and L-ascorbic acid led to an instant color change of reaction solution, while the combined use of citric acid and L-ascorbic acid took at least 5 min. In the meantime, no triangular silver nanoplates were obtained by the use of any one or two of the three reducing agents. This was because L-ascorbic acid has a weak reducing ability to silver ions at room temperature, and hence leads to extremely slow reaction and generated Ag atoms continuously, as well as different shapes. In contrast, the synergetic reduction by using the three reducing agents could produce high-yield silver nanoplates (Fig. 6E). The stirring of reaction system helped the formation of monodispersed silver nanoplates (Fig. 6F). The exact role of each component played in this reaction system needs further investigations.

### 3. GROWTH MECHANISMS

In the above section, we summarized some of the key advances in the synthesis of silver nanoplates. This section will be focused on the understanding of growth mechanisms of silver nanoplates, based mainly on the experimental measurements and theoretical methods (e.g., density functional theory and molecular dynamics simulation).

#### 3.1. Experimental Observations

Direct measurement of particle shape is critical to exploring the growth mechanisms of nanoparticles. Techniques available for this purpose include scanning tunnelling microscopy (STM), atomic force microscopy (AFM), x-ray diffraction (XRD), transmission electron microscopy (TEM), and high-resolution transmission electron microscopy (HRTEM). Among them, the TEM technique remains the most commonly used technique for characterizing nanoparticle characteristics, in which the particle shape and microstructure could be estimated through the crystallographic analysis of the 2D projection images. The growth mechanisms of silver nanoplates discussed below are derived largely based on the TEM observations.

##### 3.1.1. Stacking Faults Mechanism

Stacking faults occur in a number of crystal structures, in particular the close-packed structures. If the stacking faults occur during crystal growth, it would affect the morphologies of the final crystals. It is known that silver is one of face-centered-cubic (fcc) metals which have two favorable morphologies under thermodynamically controlled growth: truncated nanocubes and multiple twinned particles.[81] Yet, it has been reported that silver may form other kinds of silver morphologies (e.g., plate, disk) under kinetically controlled growth, for instance, at a substantially low silver concentration.[44-52] These silver morphologies are believed to be related to the formation of stacking faults. As an example, Pileni et al.[50] suggested that it is the presence of one or more (111) stacking faults lying parallel to the (111) outer surfaces and extend across an entire silver disk, which are behind the  $1/3\{422\}$  forbidden reflections (Fig. 7). The HRTEM images show a perfect lattice and exhibits 6-fold symmetry. This is well demonstrated by the Fourier transform shown in the insert of Fig. 7A. The lattice spacing is 2.50 Å, corresponding to the  $3\times\{422\}$  lattice spacing of the fcc silver crystal which can be built by 3 sets of  $3\times\{422\}$  spacing. The authors have observed that these  $3\times\{422\}$  fringes have the following features: (a) they build a perfect lattice and extend across the entire disk, include the region with a thickness gradient (for example, at the edge of the disk); and (b) there is not any isolated “island” in the entire image which do not show these  $3\times\{422\}$  fringes. However, it still remains a great challenge to understand the atomic origin of the formation of such stacking faults and to control them during growth process.

Moreover, Pileni et al.<sup>[50]</sup> highlighted that the Ag(111) stacking fault(s) may be the reason for the occurrence of such forbidden reflections and the  $3\times\{-422\}$  superlattice fringes that led to the plate-like shape. It is likely that the growth in parallel to the stacking fault plane is the fastest, favorable for the formation of silver nanodisks. Considering a stacking of hexagonal close-packed (111) layers along the [111] direction with an ABCABCABC... sequence, where A, B and C represent the three stacking positions for the (111) planes, removal or

addition an A layer would cause a distortion in the stacking sequence, the projected potential in A positions will be higher than that in B and C positions by one atom. This is confirmed by their reciprocal spots strongly elongated along the [111] direction in the selected area electron diffraction (SAED) pattern by HRTEM.

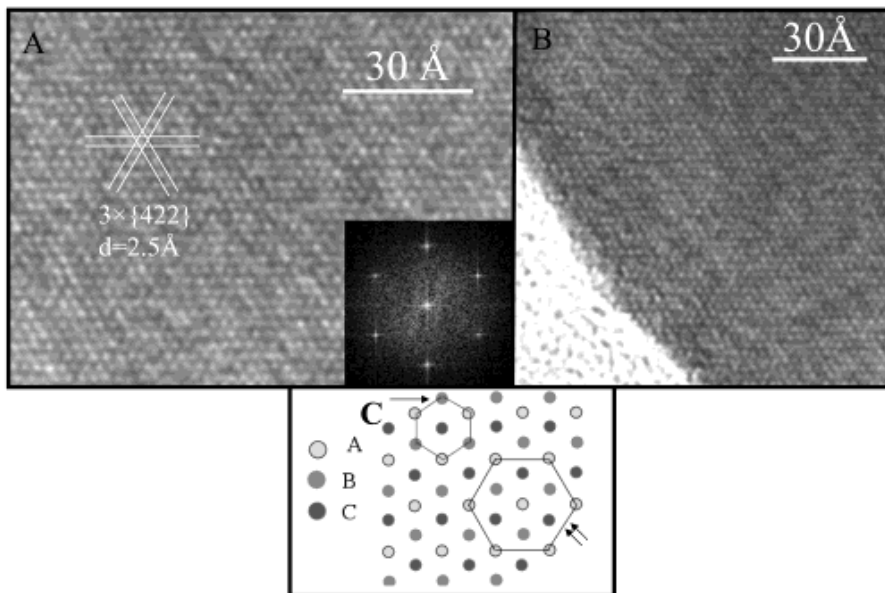


Figure 7. (A) HRTEM image at 400 kV of a silver nanodisk in the [111] orientation. The measured distance is three times the distance of  $\{422\}$ . In the insert, Fourier transform of the same area; (B) [111] HRTEM image of silver nanodisk at the edge region. The  $3 \times \{422\}$  fringes extend over the edge area; (C) Sketch of the fcc stacking of 3 layers of atoms along the [111] direction. The projected positions of the A atoms build a bigger unit cell ( $3 \times \{422\}$  distance). (Reprinted with permission from ref. 50. Copyright 2003 The American Chemical Society.)

Similarly, other researchers suggested that the weak diffraction  $1/3\{422\}$  spots derive from the local hexagonal-like structure observable only for a silver or gold sample with atomically flat, in which the Ag(111) planes of pure fcc structure would slightly distort.[38, 39, 46, 82] These spots to the presence of twin planes parallel to each other would direct the growth of silver nanoplates.[54, 82, 83] In this connection, Lofton et al.[83] suggested that the growth of Ag and Au nanoprisms is similar as silver halide prisms, in which the typical feature is the formation of twinning planes on [111]-type nanoplates. The authors also highlighted that a twinning-plane model can direct the shape of the particles into high aspect-ratio platelets via the formation of re-entrant grooves that are favourable for addition of atoms, which can reduce the nucleation energy to form a new atomic layer in these areas. Whether the forbidden  $1/3\{422\}$  reflections or the [111] twinning planes could be experimentally identified by advanced techniques such as HRTEM.

Takayanagi et al.[84] demonstrated another typical feature of Ag nanoprisms from TEM observations that show the presence of fringes with varying contrast, i.e., dark and bright lines, or bands, or star-like shapes. It was supposed that the origin of these contrast variations was the presence of dislocation networks, which develop on Ag(111) face because the surface layer presents lattice parameters slightly different to those of the bulk material. To

accommodate the lattice difference on the surface layer and inner crystal structure, the reconstruction of the crystalline lattice occurs, which leads to dislocations and to visualization of the stress field in the lattice developing toward the interior. Contrary to the above mechanism, Rodriguez-González et al.[85] suggested that the contrast fringes observed in silver nanoplates by TEM technique are likely originated from the so-called bending contours. These contours, which are well known in TEM characterization of thin films, stem from slight variations in the angle formed between atomic planes of the same plane ( $hkl$ ) at the bent area of a crystal. The origin of the bending is probably due to the stress in the crystalline lattice of nanoprisms, which can be related either to the presence of a hexagonal monolayer on the (111) surfaces or to the presence of stacking faults in the crystal structure.[50]

### 3.1.2. Photoinduced Fusion Mechanism

Mirkin et al.[38, 39] demonstrated a possible photoinduced fusion mechanism in the synthesis of silver nanoplates by using laser or visible light. Although a detailed mechanism for these types of conversions remains to be determined, it is possible that the plasmon excitation does two things: (i) it could redistribute charge on the surfaces of the nanoprisms to either facilitate (in the case of dipole excitation) or inhibit (in the case of quadrupole excitation) particle–particle fusion; and (ii) surface plasmon excitation could facilitate ligand or adsorbate dissociation at the particle edges (as this is where the local fields are the most intensive[38]), allowing the small particles to grow through the Ostwald ripening or surface-plasmon directed fusion process to larger clusters, as shown in Fig. 8. These findings offer a new type understanding of particle size control that is initiated and driven by visible light or laser light.

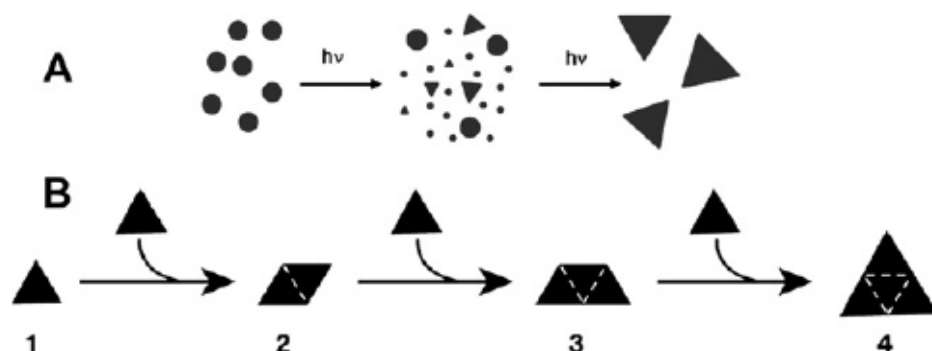


Figure 8. Mechanisms proposed for Ag triangle formation through photoinduced aggregation. (A) Small silver nanoprisms and clusters are formed and subsequently silver nanoprisms act as seeds for growth whereas the small clusters are digested; (B) Light-induced fusion of Ag nanoprisms, where four smaller nanoprisms join together in a stepwise fusion to form one larger nanoprism. (Reprinted with permission from Ref. 38 and 39. Copyright 2001 The American Association for the Advancement of Science and copyright 2003 Macmillan Publishers Ltd., respectively.)

Maillard and colleagues[40] demonstrated another mechanism in the photoinduced growth of silver nanodisks. They supposed that silver particles present a characteristic shape evolution during growth. Starting with a spherical shape, particles grow as spheres and then

evolve into more well-defined, triangular, disklike shapes. The citrate ions play an important role acting as a ligand and a photoreduction agent in the formation of anisotropic silver particles. For spherical shape, the seeds absorb light isotropically (equally for all orientations with respect to the laser polarization). If the inhomogeneity occurs in the deposited silver layer, a particle starts to become ellipsoid-like, and the degenerate plasmon resonance splits into transverse and longitudinal modes. The longitudinal plasmon (along the longer dimension) shifts to longer wavelength, and absorbs this wavelength more strongly, on a rotationally averaged basis in solution, than the transverse mode that shifts to shorter wavelength. If the reduced atoms are deposited in proportion to the near field intensity enhancement at the surface position, then this longer axis grows preferentially. The process accelerates until the longitudinal plasmon wavelength shifts beyond the irradiation wavelength, which will result in the formation of anisotropic geometries. The authors also discussed why the disks formed rather than rods by photoreduction process in the presence of citrate ions.[40]

### **3.1.3. Surface Selective Adsorption Mechanism**

Another experimental explanation on the formation and growth of nanoparticles is generally accepted by most researchers who used polymer(s) or surfactant(s) to control particle shape and size.[38-58] In fact, a great number of polymers or surfactants have been used as surface adsorbates and/or stabilizers for controlling shape/size and protecting from aggregation in the previous studies, such as photoinduced method, templating method, and solvothermal reduction method. The experimental observations revealed that the adsorbates or stabilizers (e.g., polymers or surfactants) could largely affect the morphologies and dimensions of metal nanoparticles by selectively binding or adsorbing on certain crystallographic plane(s), and hence alter the surface energies and lead the preferential growth of nanoparticles to anisotropic structures such as rods, disks, and plates.

The key role of surfactant or polymer molecules played in shape control was also confirmed by our experimental observations. Fig. 9 shows the representative TEM images of silver particles with different morphologies and sizes by using different surfactants, for example, thiols (e.g., 1-dodecanethiol, C12SH) lead to irregular particles with diameter of ~10 nm (Fig. 9A), CTAB results in spherical particles with diameter of ~28 nm (Fig. 9B), and poly(vinyl pyrrolidone) (PVP) leads to truncated nanostructures with edge length of ~32 nm (Fig. 9C). This indicates that different surfactants have different interaction energies with the crystalline planes, and hence leading to different morphologies.

Despite of such efforts, the understanding of the plate growth is far from complete because of the diverse methods used and the complicated growth processes involved. Many possible factors that may affect the final morphologies of silver nanoparticle have been identified. These include the state of initial nuclei or seeds (e.g., amorphous or crystalline), diffusion rate of silver species from solution onto the crystal surface, various crystal defects (e.g., points, lines, or planes), additives (e.g., surfactants, polymers, or reducing agents), as well as synthesis methods and conditions (e.g., template, light illumination, ultrasonic- or microwave-assistance). Moreover, two or more mechanisms may occur concurrently or consecutively during the growth process.

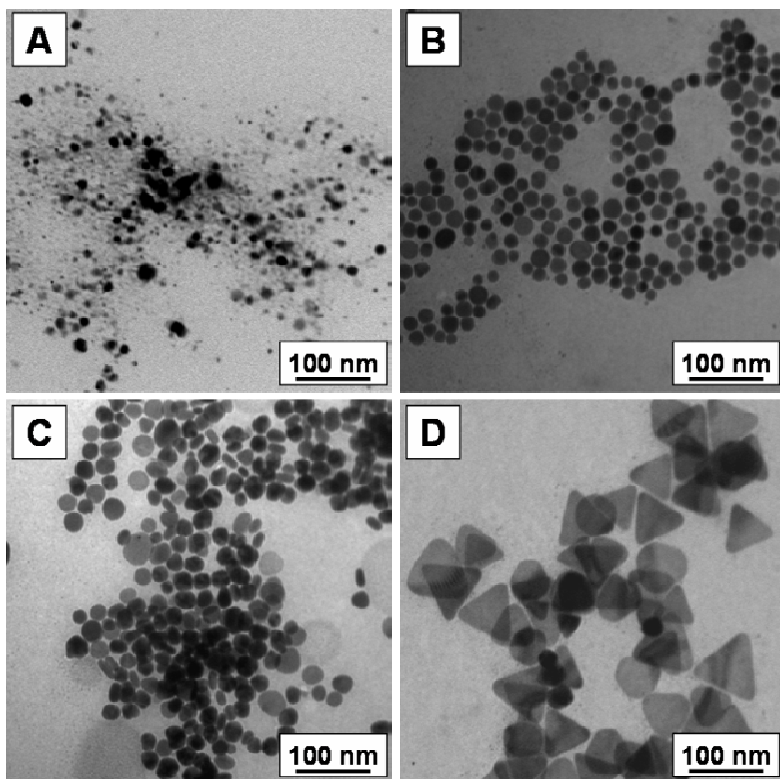


Figure 9. TEM images showing the influence of different capping agents on the morphologies of silver nanoparticles: (A) C12SH; (B) CTAB; (C) PVP; and (D) AOT.

### 3.2. Molecular Modeling

The aforementioned mechanistic understandings are mainly based on experimental analysis. They are very much macroscopic and to some degree phenomenological. The theoretical calculations or computational modelings are required to better understand the principles underlying particle growth and shape control at different scales. Recently, some theoretical efforts have been made to investigate the molecular origins of the growth mechanisms of nanoparticles. The work is largely performed by using density functional theory (DFT) and molecular dynamics (MD) simulation which provide estimates of molecule-crystal interaction, molecular dissociation, surface atom rearrangements and crystal growth.[24–28] Here we will discuss two theoretical studies (DFT and MD) commonly used toward the growth of metal nanoparticles.

#### **DFT Simulation.**

Chemical reduction and directed blocking of different crystal surface can be used to prevent the chemical activity at some specific surfaces while allowing other surface to dissolve or grow.[7] For example, citric acid is an effective capping agent which demonstrated to block the Ag(111) surface while allowing the Ag(100) surface to grow.[45] Recently, Kilin et al.[86] used DFT calculation to study the binding affinity between citric

acid and silver crystal planes. They found that citric acid preferentially binds to Ag(111) plane, promoting crystal growth along the Ag(100) plane and the formation of silver nanoplates as observed in the experiment.

Recently, we have used DFT to calculate the binding energy between gold surfaces and adsorbed atoms or molecules of PVP for understanding the growth mechanism of gold nanorods.[87] The binding energy between gold atoms and carbon atoms of PVP represents the attractive or repulsive force of the adsorbed atoms on certain metal plane, and subsequently affects the growth orientation of gold nanostructures, although there is still limitation in explaining the gold wormlike or complicated structures.

### **MD Simulation.**

MD simulation is another theoretical technique capable of understanding the growth mechanisms of crystal nanoparticles. It can be used to calculate the interaction energy of individual crystal surface and surrounding molecules, and then the selective molecular adsorption. Such information is useful for understanding particle growth at a molecular scale.

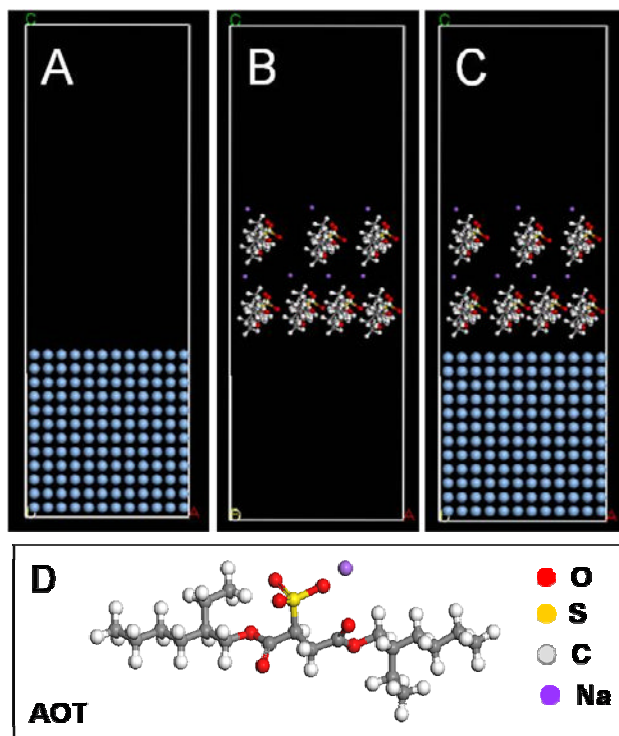


Figure 10. Model system for MD simulation: (A) the initial model for silver {111} plane; (B) the initial model for AOT molecules; (C) the adsorbed AOT molecules on silver {111} plane with an initial model; and (D) the spatial structure of AOT molecule containing O, S, C, and Na atoms with different colors. (Reprinted with permission from ref. 57. Copyright 2007 IOP Publishing Ltd Printed in the UK.)

We have recently applied MD simulation to explain the shape control of silver nanoplates in the presence of surfactants (e.g., AOT molecules).[55-57] To perform such simulation, for each crystalline plane we created a representative molecular model, consisting of the silver

plane and a number of surfactant molecules as shown in Fig. 10. Such a model was subject to energy minimization for the structural optimization before MD simulation. Our MD simulation lasted for 50 ps with the time-step of 1 fs and the data were collected in the last 20 ps. The results showed that the total energies of the bare silver are  $-29978.4$ ,  $-28648.8$ , and  $-28045.8$  kcal·mol $^{-1}$  for (100), (110), and (111) planes, respectively. Their equivalent energies indicate the formation of thermodynamically favored truncated or spherical particles.[81] However, with the addition of surfactants, particle shape is closely related to the difference in interaction energies between each surface and surfactants.

The interaction energies were calculated based the potential energies of the equilibrated MD models of silver plane with surfactant (e.g., AOT) molecules, isolated silver plane, and isolated surfactant molecules. They are  $-249.9$ ,  $-323.4$ , and  $-460.1$  kcal·mol $^{-1}$  corresponding to the three silver planes of (100), (110), and (111), respectively.[55-57] The negative energies indicate that AOT molecules are likely to be adsorbed on the silver crystal planes, and the large negative interaction energy of Ag(111)-AOT indicates that the AOT molecules have a stronger interaction with the (111) plane than with the (110) and (100) planes. Subsequently, the selective adsorption would reduce the sites available for adsorbing silver atoms on the (111) plane. In this AOT-Ag system, the stronger interaction of AOT-Ag{111} planes restrict the growth on this plane, and hence the other two planes {110} and {100} grow faster, which benefits to the formation of silver nanoplates. These molecular methods are anticipated to provide useful information in generating large quantity of nanoparticles with shape control.

In addition, the crystal shape is theoretically determined by the relative diffusion rate and binding strength of particles (e.g., ions, atoms, molecules, or clusters) on crystal surfaces. Thus, the surfaces that grow slowest appear as largely developed surfaces. The growth rates are determined primarily by the binding strength between particles and crystal surface. However, any factors that may change the diffusion rate on a surface will influence on the crystallization habit, including temperature, supersaturation, solvent, additive, and impurity. Due to such complexity, it still remains very challenging to control experimentally the final morphology and to explore theoretically the growth mechanisms of nanoparticles in future.

#### 4. FUNCTIONAL PROPERTIES AND APPLICATIONS

The development of various synthetic methods and better understanding of the growth mechanisms would facilitate the advances toward the functional properties and potential applications of silver nanoplates in different areas. In this section, we aim to describe the optical properties of silver nanoparticles, starting from the origin of the intrinsic optical properties for noble metals (Au, Ag, and Cu). Then, we provide a brief introduction to the numerical methods that have been used for theoretical modelings, such as discrete dipole approximation (DDA) and boundary element method (BEM). Finally, the potential applications of silver nanoparticles associated with optical properties (e.g., SERS and LSPRs) in chemical and biochemical sensing are also presented.

## 4.1. Optical Property

### 4.1.1. Surface Plasmon Resonance

The optical properties of noble metal nanoparticles have been of great interests because of applications in linear and nonlinear optical devices.[21-25] The intense color of metal colloids is originated from their surface plasmon resonance (SPR), which are oscillation modes arising when an electromagnetic field (in the visible range for Au, Ag and Cu) is coupled to the collective oscillations of conduction electrons.[88] The plasmon resonances can be found in different status of metals such as bulk plasmons for bulk metals or surface plasmons for metal films. When the particle size decreases smaller than the incident wavelength, the resonance condition is only fulfilled within a narrow spectral range, which is reflected in the absorption bands in UV-vis spectrum.

The SPR leads to large local electric fields, which results in the enhancement of absorption coefficients and third-order nonlinear susceptibilities at the resonance frequency. The concept of LSPRs was introduced to describe the signature optical property of a metallic nanoparticle.[18] This resonance occurs when the correct wavelength of light strikes a metallic nanoparticle, causing the plasma of conduction electrons to oscillate collectively. The term of LSPRs is used because this collective oscillation is localized within the near surface region of the nanoparticle. The exciting LSPRs are originated from selective photon absorption and generation of locally enhanced or amplified electromagnetic fields at the nanoparticle surface. The LSPRs for noble metal nanoparticles in the size range from 20 to hundreds of nanometers usually appear in the visible and IR regions, identified by UV-vis-IR absorption spectrum.

In addition, LSPRs are commonly characterized by the strong field enhancement at the particle interface, while the electric field vector decays exponentially away from the surface (in the nm range). For small spherical particles only dipolar modes can exist, while bigger particles, particularly those anisotropic ones, can accommodate higher order plasmon modes (e.g., quadrupolar modes). That is, the LSPR frequency is quite sensitive to the particle characteristics (e.g., shape, size, composition, and inter-particle spacing) and the dielectric properties of the surrounding media.[88] For anisotropic particles, their unique LSPR modes arise from different orientations of the particle with respect to the electric field of the incident electromagnetic radiation,[89] as discussed by Schatz's group.[18]

### 4.1.2 Numerical Simulations

Various theories and analytical methods to study the optical properties of noble metallic particles have been reported in the past. The Maxwell-Garnett theory has been successfully applied in the calculation of linear and nonlinear optical properties of metals.[21, 23, 27, 28] In the case of spherical nanoparticles embedded in dielectric materials, the Mie scattering theory[26] has succeeded in describing the extinction spectra in the visible region, including the surface plasmon resonance of dipolar modes, which results in strong attenuation of incident light. The linear optical properties of nanospheres in a nonabsorbing medium can be quantitatively predicted by effective medium theories. Subsequently, various analytical methods including DDA, T-matrix, finite differences in the time domain (FDTD), and boundary element method (BEM), have been used to model the optical properties of particles with virtually arbitrary geometries. Among them, the DDA and BEM methods were more common in previous studies.[19, 30-32, 38, 52, 59, 91-96]

### Discrete Dipole Approximation (DDA)

Extinction spectra of the perfect or truncated triangular Ag nanoprisms were numerically calculated using a DDA method.[19, 38, 52, 59] The DDA simulation, a finite element-based method, was first introduced by Purcell and Pennypacker[30] and later improved by Draine and Flatau.[31, 32] Using DDA, Maxwell's equations can be solved numerically, so that one can study scattering and absorption of electromagnetic radiation by particles with size of the order of the wavelength of the incident light or smaller. The flexibility of this method resides in imposing no restriction on the localization of occupied cubic lattice sites, so that the DDA method can analyse a particle of arbitrary shape and composition by this simulation. The detailed DDA simulation equations has been reviewed by Liz-Marzán and co-workers.[59]

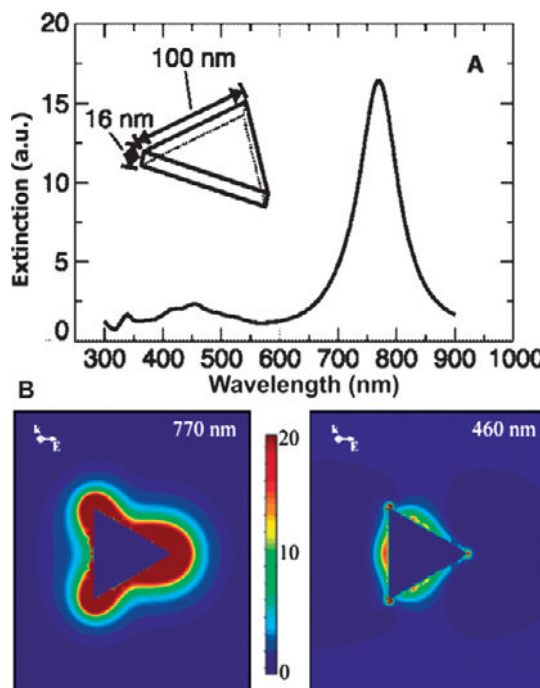


Figure 11. (A) DDA simulations of the orientation averaged extinction efficiency spectra of a perfectly triangular nanoprism; (B) Electron-Field enhancement contours external to the prism, for a plane that is perpendicular to the trigonal axis and that passes midway through the prism. The light is chosen to have  $K$  along the trigonal axis and  $E$  along the abscissa. Left:  $\lambda = 770$  nm. Right:  $\lambda = 460$  nm. Side length of 100 nm; thickness of 16 nm for a silver plate. (Reprinted with permission from refs. 18 and 38, respectively. Copyright 2001 The American Association for the Advancement of Science and copyright 2003 The American Chemical Society, respectively.)

Schatz group[38] reported for the first time the theoretical calculations for Ag nanoprisms using DDA method to interpret experimental observations of the plasmon resonances recorded from nanoprism dispersion in the UV-vis spectrum. In particular, the authors distinguished two quadrupolar LSPR modes for a single metal particle. In the calculations, a model was built taking into account the shape and dimensions of the real particles. For a triangular platelet with edge length of 100 nm and thickness of 16 nm, a spectrum containing four plasmon resonances were present in Fig. 11A, and they qualitatively matched the spectrum measured in similar average dimensions.[38] In this case, four peaks centred at 770,

470, 410, and 340 nm in UV-vis spectrum could be accordingly assigned to in-plane dipole, in-plane quadrupolar, out-of-plane dipolar and out-of-plane quadrupolar resonances, respectively. This assignment was further confirmed by the same group after calculating the extinction efficiency for light polarized along the three primary symmetry axes.[18] This is also supported by the 2D plots of electron-field enhancement around a single particle, which reveals that maximum enhancement occurs at the tips for dipolar resonances, while it peaks at the sides for the quadrupolar modes (Fig. 11B).

Additionally, Schatz and co-workers[38] observed that the field decays away from the surface faster for the quadrupole than for the dipole, especially at the tips. In another paper,[90] the same authors investigated the plasmon properties of a single triangle using dark-field optical microscopy for single-particle spectroscopy, again finding a good agreement between the two LSPRs observed in the measured scattering spectra with the theoretical model. The influence of other parameters on the plasmon resonances has been reported by several groups, including particle size and aspect ratio between lateral dimension and thickness.[39-41, 72, 74, 80] Furthermore, triangular nanoplates are often found to be truncated, the effect of snipping was further studied. The results show that the bands are red-shifted when the snip is decreased. Brioude and Pileni[52] studied theoretically the silver nanodisks by using DDA method, in which the relative contributions of absorption and scattering to the extinction spectra were reported for nanoparticles with different edge lengths but same aspect ratio (e.g., AR= 4). The authors demonstrated that the light-scattering contribution starts to dominate for particle size of ~50 nm, becoming dominant for size above 100 nm; while for small nanoparticles (< 20 nm), the absorption contribution dominates the extinction spectrum, consistent with the study carried out for other geometries.[91]

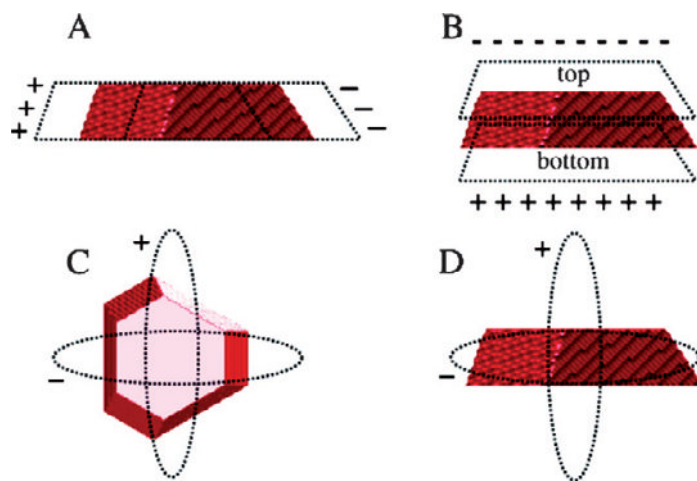


Figure 12. Schematic representation of the resonance plasmon modes involved in metal nanoplates. The dipolar in-plane and out-of-plane modes are represented in (A) and (B), respectively. The corresponding in-plane and out-of-plane quadrupolar modes are represented in (C) and (D), respectively. (Reprinted with permission from ref. 52. Copyright 2005 The American Chemical Society.)

The DDA simulation allows us not only to assign the surface plasmon resonance but also to correlate optical properties to the particle geometry, especially for non-spherical ones,[19,

30-33, 38, 52] based on Mie's scattering theory.[26] The extinction spectra show dipole and quadrupole plasmon resonances for both in-plane and out-of-plane polarizations. Brioude and Pileni[52] have demonstrated theoretically that both the in-plane and the out-of plane excitations can lead to dipolar and quadrupolar resonances for silver triangular nanoplates (Fig. 12). Similarly, the SPR of Ag nanowires with a non-regular cross section have also been calculated by Kottmann et al.[33] These local fields play a key role in nonlinear optical response and in the SERS spectrum. The third-order nonlinear susceptibilities related to both the dipole and quadrupole plasmon resonances of Ag nanoprisms were measured using femtosecond pump-probe spectroscopy.

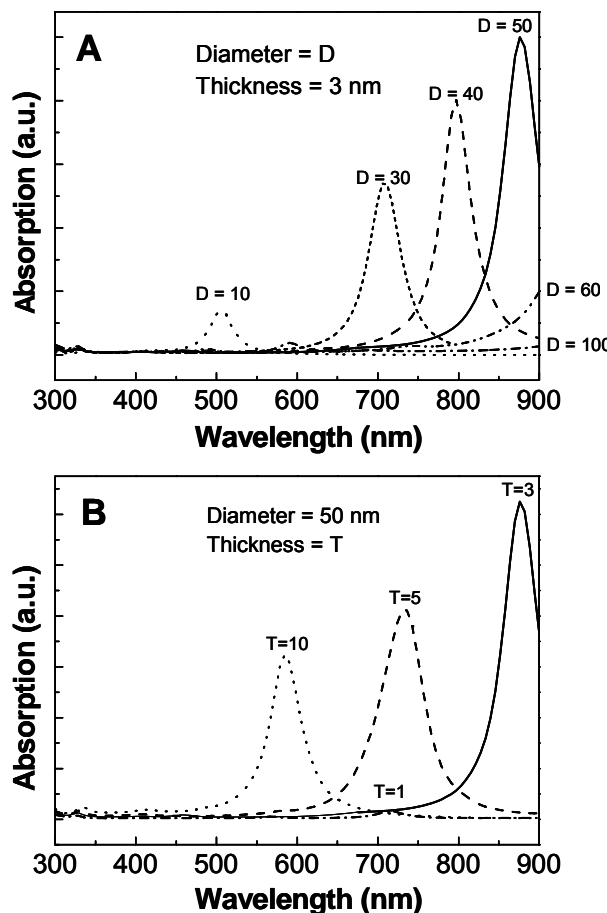


Figure 13. DDA simulations of the orientation averaged extinction efficiency spectra of silver nanodisks in water: (A) nanodisks of thickness ( $T=3$  nm) and different diameters:  $D=10, 30, 40, 50, 60$ , and  $100$  nm; and (B) nanodisks of diameter ( $D=50$  nm) and different thickness:  $T=1, 3, 5$ , and  $10$  nm.

As a further confirmation, our recent work on the study of gold nanorods and silver nanodisks showed that such DDA simulations can be used for quantifying optical properties.[5, 6] The size-dependent optical properties could be clearly identified from the shift of SPR, as shown in Fig. 13. Examination of the induced polarizations associated with

these peaks indicated that the maximum SPRs could be assigned to the in-plane dipolar mode corresponding to different diameters of a disk (i.e., 10, 30, 40, 50, 60, and 100 nm with thickness of 3 nm, Fig. 13A). The maximum SPR shifts toward shorter wavelengths and the absorption intensity decreases obviously for a disk (diameter of 50 nm) with thickness increasing from 1 to 3, 5, and 10 nm, as shown in Fig. 13B). That is, the absorption intensity and position of the SPR are heavily dependent upon the shape and size of nanoparticles.

### **Boundary Element Method.**

Another theoretical method for understanding optical property of metal particles is BEM.[92, 93] This method has proven useful for the calculation of spatially-resolved electron energy loss spectra (EELS) and amplitude maps. This approach allows for the description of metal nanoparticles embedded in a surrounding medium. The BEM is proven to be suitable for the simulation of EELS when the materials under consideration are described by local frequency-dependent response functions. This simulation can be used to derive analytical expressions for the energy loss probability in a simple geometry such as a sphere, a cylinder, or a plate. However, for more complex interfaces, as in the case of a triangle, this theoretical method cannot be worked out analytically.

An important step in this field achieved by Nelayah et al.[94] toward the direct correlation between optical spectra and LSPR modes has been reported. The authors demonstrated that high resolution electron energy-loss spectroscopy allows a direct mapping of plasmon modes in silver nanoprisms. This method relies on the well-known relationship between the energy loss encountered by a fast electron travelling along a linear path at a constant speed through or close to an object, and the object's optical properties.[95, 96] Based on experimental observations, the relative intensity of the modes strongly varied at different positions within a single nanoprism, the distribution and amplitude of the different modes in the triangular plate could be mapped. Compared the measured EEL spectra to the EELS amplitude maps by calculations, the simulated energies of the three main peaks are in good agreement with the experiments, while a qualitative agreement is observed between the measured and the simulated amplitude maps.[92, 93]

## **4.2 Potential Applications**

Potential applications of metal nanoparticles related to chemical and biological sensing are the ones currently receiving much more attention. The functional applications of metal nanoparticles (e.g., Au and Ag) are significantly associated with their SERS and LSPRs, as discussed in the followings.

### **4.2.1 Surface Enhanced Raman Spectroscopy**

Surface enhanced Raman spectroscopy operates by measuring the effective Raman cross-section of the target molecules, which is largely enhanced when the molecule is in contact with a metallic surface. The details related to SERS have been reviewed by several groups in the past.[97-99] Generally, SERS is a spectroscopic technique which combines modern laser spectroscopy with the exciting optical properties of metallic nanostructures, resulting in strongly increased Raman signals when molecules are attached to nanometre-sized gold and silver nanostructures. Although the exact enhancement mechanism has remained

controversial, it is commonly agreed that two processes contribute to the overall enhancement: a chemical effect and an electromagnetic enhancement. This is because of the confinement of the target molecules within the zone of large local electromagnetic fields that generate excitation of the LSPR of the metal nanoparticles.[100-102]

Silver nanoparticles normally exhibit intensive SPR in the wavelength range of 300-900 nm dependent on their dimensions. To date, many studies concentrate on the optical applications (e.g., chemical and biochemical sensors) of silver nanoparticles with various morphologies (e.g., rods, wires, and spheres) or their arrays served as substrates.[8-14, 29] For example, rod-type silver nanoparticles exhibit two characteristic SPR bands, including the transverse SPR ( $\perp$ ) and the longitudinal SPR ( $\parallel$ ), depending on the light polarization direction to the principal axis.[8] The peak position of the transverse SPR is similar to that of spherical particles. However, the peak position of the longitudinal SPR depends dramatically on the axial ratio (b/a).[9]

Later, Yang, et al.[10] reported that Langmuir-Blodgett silver nanowire monolayer served as a substrate for SERS enhancement of thiols, 2,4-dinitrotoluene, and Rhodamine 6G molecules. Shanmukh et al.[11] described the sensitive detection of respiratory virus molecular signatures using the array of silver nanorods as a SERS substrate. Van Duyne et al.[110] reported a SERS study of trans-1,2-bis(4-pyridyl)ethylene that adsorbed onto silver film over nanosphere electrodes. The SERS enhancement can be attributed to the increased local optical fields near the silver surface as a result of the excitation of surface plasmon resonances. In the above studies on SPR, the electromagnetic-field enhanced SERS spectrum requires coupling of the incident radiation to the metal surface, particularly on roughened or defected metallic substrates. Different from anisotropic structures, Henglein and Mulvaney[103-109] demonstrated the effect of the chemisorbed ions or surface modification on the SPR band both in intensity and in spectrum shape of spherical silver nanoparticles and/or gold nanorods in aqueous system, in which the changes could be attributed to the changes of electronic properties, or the refractive index of the medium surrounding particles.

Despite demonstrating silver nanoparticles to be efficient SERS substrates,[111] their SERS properties are less understood. The dispute on the SERS enhancement effect of silver nanoplates with respect to their geometries can be found in different work. Zhang et al.[112] observed that Ag nanoplates are less efficient than wires or spheres (on the basis of more favourable interactions of active crystal faces with organic molecules), while Yang et al.[110] reported a higher activity of triangular plates for SERS detection, due to sharper corners and edges. Thus, it is hard to drive a general conclusion, since the existing reports have not taken into account all factors that potentially influence SERS enhancement. Moreover, the recent findings showed that the aggregated silver nanoplates[113] or sandwich structures made of silver nanoplates–probing molecule–gold(silver)[114] present stronger Raman enhancement than a single Ag nanoplate, due to strong electromagnetic coupling between neighbouring nanoplates. Apparently, there is plenty of room for development of efficient metal nanostructures where the SERS enhancement can be optimised.

#### **4.2.2 Localized Surface Plasmon Resonance**

The giant enhancement of electric fields around metal nanoparticles driven by LSPRs makes them extremely sensitive toward changes in the local dielectric environment. While LSPR sensors are operated by transducing changes in local refractive index (produced by the chemisorption or biomolecular adsorption) to wavelength shifts of the LSPR extinction band

maximum.[115] For the case of LSPR, light is required to interact with particles much smaller than the incident wavelength, which leads to a plasmon that oscillates locally around the nanoparticle with a frequency known as the LSPR. Van Duyne group[12, 17, 116-119] explored the optical properties of Ag nanoparticles (in-plane width of 100 nm and out-of-plane height of 50 nm) chemically modified with alkanethiol self-assembled monolayers by measuring the LSPRs using UV-vis spectroscopy. The authors suggested that silver nanoparticles of different shapes show different refractive-index sensitivities, for instance, rods show the highest sensitivity followed by triangles, and then spheres. Individual silver nanoparticles or their arrays were applied for real-time optical sensors based on localized surface plasma resonance.[17-20] Additionally, silver nanoparticles were also used to evoke intensive chemiluminescence with tris(2,2'-bipyridyl) ruthenium(II) and cerium(IV).[103] Coupled planar silver nanoparticle arrays were used for refractive index sensors.[120]

The LSPRs are generally affected by particle morphology, size, distribution, and aspect ratio (the ratio of lateral dimension and thickness for nanoplates). Theoretically, it was also observed that both the in-plane dipolar and quadrupolar modes shifted toward longer wavelength when the edge length of triangular plates increased, while the quadrupolar mode is less sensitive to particle size because the induced polarization of the mode is localized at the central portion of the triangle.[18, 52, 121]

Moreover, the LSPR frequency is also affected by the refractive index of the medium surrounding the particles, which is the basis for LSPR-based biosensors. Pastoriza-Santos et al.[47] described that upon solvent exchange from DMF to water (refractive indices of 1.426 and 1.333, respectively), the in-plane dipolar resonance of Ag nanoprisms dispersion shifted toward shorter wavelengths by nearly 40 nm, while only 5 nm shift was observed for spherical silver nanoparticles.[122] Mirkin group[72] observed the color changes in thin films fabricated by deposition of silver nanoprisms from a colloidal solution onto a glass surface, when the films were immersed in water, as compared to air (refractive indices of 1.333 and 1.0, respectively). Measurements show that the dipolar plasmon wavelength of Ag nanoprisms depends linearly on the refractive index of surrounding medium, though the agreement was not found with the corresponding slopes.[18] Recently, Van Duyne et al.[90] reported the environmental sensitivity of silver nanoprisms by measuring dark-field scattering spectra of individual single nanoprisms in different dielectric environments.

#### **4.2.3 Sensing Detection of Inorganic Ions**

The SPR spectrum can provide thermodynamic and real-time kinetic data for chemical adsorption/desorption processes. The following discussion is focused on our recent work on the sensitivity and selectivity of silver nanoplates toward inorganic anions (e.g., halides, phosphate, and thiocyanate ions) in aqueous system.[58] The experimental results for the first time showed that the sensitivity of silver nanoplates toward halides (e.g., Cl<sup>-</sup>, Br<sup>-</sup>, and I<sup>-</sup>), phosphate and thiocyanate ions can be down to the order of 1×10<sup>-6</sup> M based on the shift in the intensive SPR band. A typical example was addressed here to show that the SPR shifts remarkably during the sensing detection of some inorganic ions such as halides (Fig. 14).

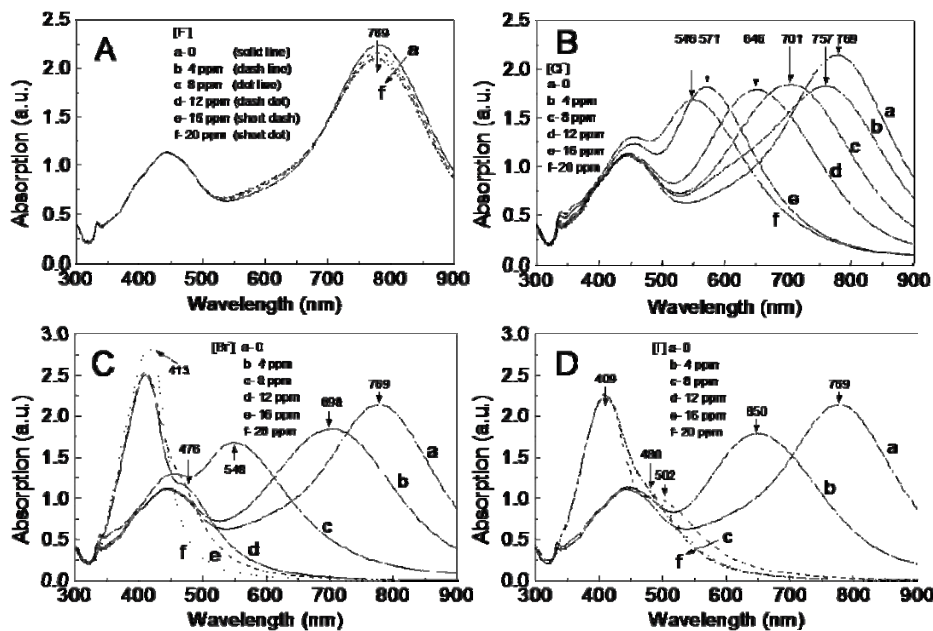


Figure 14. UV-vis spectra showing that silver nanoplates can be used for sensing detection of halides in aqueous solution: (A)  $\text{F}^-$ ; (B)  $\text{Cl}^-$ ; (C)  $\text{Br}^-$ ; and (D)  $\text{I}^-$ . Note that the unit of ppm stands for  $1 \times 10^{-6}$  M in all the Figures. (Reprinted with permission from ref. 58. Copyright 2008 The American Chemical Society.)

These silver nanoplates also show a high selectivity in detection of inorganic ions, including  $\text{NO}_3^-$ ,  $\text{ClO}_4^-$ ,  $\text{CH}_3\text{COO}^-$ ,  $\text{SO}_4^{2-}$  anions and  $\text{Zn}^{2+}$ ,  $\text{Cu}^{2+}$ ,  $\text{Cd}^{2+}$  cations. No significant shifts were observed in all the three SPR bands of silver nanoplates even if the concentration of these ions was increased to  $20 \times 10^{-6}$  M, indicating that these anions could not significantly alter the surface dielectric properties of silver nanoplates and the SPR bands (Fig. 15A). In contrast, a remarkable SPR shift (i.e.,  $\Delta\lambda_{\max} = 233$  nm) for  $\text{Cl}^-$  ions with the concentration of  $16 \times 10^{-6}$  M was observed under the similar conditions. No significant shift for the intensive SPR was observed when inorganic cations were added into the dispersion of silver nanoplates (Fig. 15B).[58]

Several perturbations might affect the SPR wavelength shifting, such as refractive index changes to the surrounding media, particle geometry (shape, size), and/or particle surface electron charging.[104-109, 123] It is expected according to the Mie theory[26] that a change in refractive index would lead solely to a shift in the SPR band and would not significantly influence the width of the band. However, the experimental observations in the UV-vis spectra suggested that the effect of the refractive index to the surroundings is not significant. In the meantime, the changes in the particle shape/size distributions could be hardly observed according to the TEM and AFM analysis, indicating that the particle geometry played a slight effect on the SPR shift in the silver nanoplate system.[55-58] A possible sensing mechanism was postulated that the surface electron charging of silver nanoplates may be responsible for the shift in the SPR band, which could be caused by the electron injection via different means like adding reducing agents or negatively charged ions. In doing this, an interesting

phenomenon was found for the case of silver nanoplates that are highly sensitive to halides, phosphates and thiocyanate anions but not to  $\text{F}^-$ ,  $\text{NO}_3^-$ ,  $\text{ClO}_4^-$ ,  $\text{CH}_3\text{COO}^-$  and  $\text{SO}_4^{2-}$  ones, albeit they all are negatively charged.

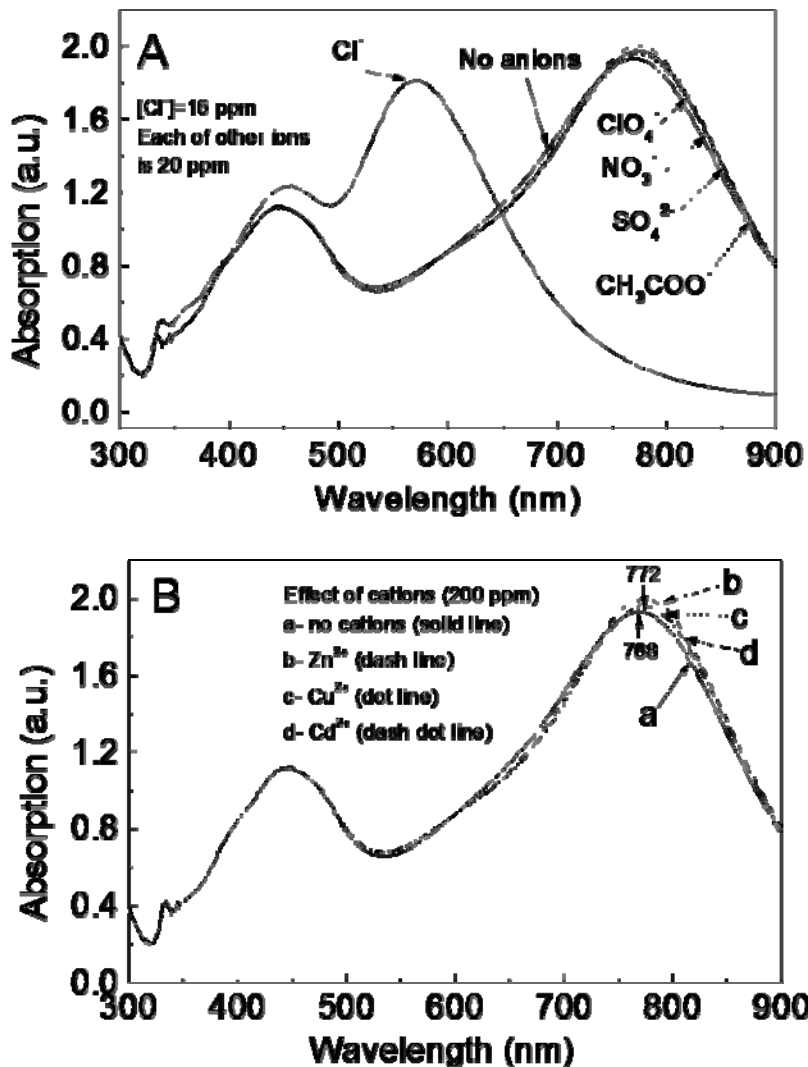


Figure 15. UV-vis spectra showing that the silver nanoplates are sensitive to  $\text{Cl}^-$  ions ( $16 \times 10^{-6} \text{ M}$ ) but not  $\text{NO}_3^-$ ,  $\text{ClO}_4^-$ ,  $\text{CH}_3\text{COO}^-$ , or  $\text{SO}_4^{2-}$  ions with individual concentration of  $20 \times 10^{-6} \text{ M}$  (A) and inorganic cations such as  $\text{Zn}^{2+}$ ,  $\text{Cu}^{2+}$ , and  $\text{Cd}^{2+}$  (B). (Reprinted with permission from ref. 58. Copyright 2008 The American Chemical Society.)

The concept of solubility of silver compounds was used to interpret the SPR shift mechanism in our study.[58] The solubility constant ( $K_{\text{sp}}$ )[124] (see Table 1) of silver compounds determines thermodynamically the interaction tendency between the surface silver atoms and the injected anions. The difference in the interaction tendency to form silver compounds (e.g.,  $\text{AgCl}$ ,  $\text{AgBr}$ , and  $\text{AgI}$ ) within an Ag-anion bond would result in different surface electron charging or affect the electron mean free path, and hence the shift in the

plasma frequencies. For example, the  $K_{sp}$  order of silver compounds in water is  $\text{F}^- > \text{Cl}^- > \text{Br}^- > \text{I}^-$ , and the  $K_{sp}$ ,  $\text{AgF}$  is at least 12 order magnitudes (182 g/100 ml water at 15 °C) larger than those of other three halides (see Table 1). This means that the surface electron charging is readily achieved for  $\text{Cl}^-$ ,  $\text{Br}^-$ , and  $\text{I}^-$  ions but not for  $\text{F}^-$  ions under the similar conditions. Similar results have been observed in sensing detection of phosphate ( $\text{PO}_4^{3-}$ ) and thiocyanate ( $\text{SCN}^-$ ) ions that have strong interaction tendency with silver surface atoms.[66] Such a mechanism could be further supported by the addition of anions such as  $\text{NO}_3^-$ ,  $\text{ClO}_4^-$ ,  $\text{CH}_3\text{COO}^-$ , and  $\text{SO}_4^{2-}$ , which have large solubility in water[81] and hence weak interaction with silver atoms leading to insignificant shifts in the SPR. That is, the interaction tendency between silver atoms and anions plays a dominant role in the surface electron charging, and subsequently affect the shifts in the intensive surface plasma resonance.

**Table 1. The solubility of silver compounds in water[81]**

Silver compounds	$K_{sp}$ (conditions)
$\text{AgF}$	182g/100 ml water (15.5 °C)
$\text{AgCl}$	$1.76 \times 10^{-10}$
$\text{AgBr}$	$5.32 \times 10^{-13}$
$\text{AgI}$	$8.49 \times 10^{-17}$
$\text{AgSCN}$	$1.03 \times 10^{-12}$
$\text{Ag}_3\text{PO}_4$	$1.05 \times 10^{-16}$
$\text{AgNO}_3$	122g /100 ml water
$\text{AgClO}_4$	5.57g/100 ml water
$\text{Ag}(\text{CH}_3\text{COO})$	1.02g/100 ml water
$\text{Ag}_2\text{SO}_4$	$1.19 \times 10^{-5}$

Additional evidence to the proposed explanation on the surface electron charging is that using sulphur-containing molecules to modify silver surfaces. It was found the addition of anions (e.g.,  $\text{Cl}^-$ ) could hardly cause any shifts in the SPR once again when C12SH (Fig. 16A) or cysteine (Fig. 16B) was added into the sensing system containing silver nanoplates. This means that the surface modification by sulphur-containing molecules could hinder the anions (e.g.,  $\text{Cl}^-$  ions) to reach the silver surface, and hence maintain the surface electron density and the subsequent SPR shifts. This is also consistent with our observations that the thiols could be used to freeze and stabilize the shape evolution of silver nanoplates in aqueous solution.[56]

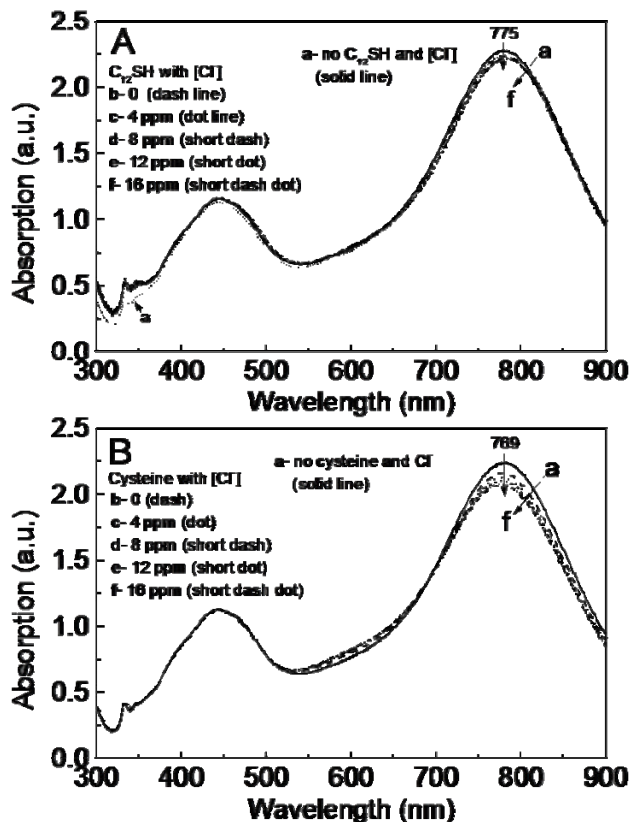


Figure 16. UV-vis spectra showing that the sensitivity of silver nanoplates towards halide anions (e.g., Cl<sup>-</sup> ions) is largely reduced when the silver atomic surfaces were modified by molecules: (A) C12SH; and (B) cysteine. (Reprinted with permission from ref. 58. Copyright 2008 The American Chemical Society.)

On the contrary, spherical silver colloids exhibit only one single SPR band centered at ~422 nm for particle size of ~5 nm under our reported conditions. No any shifts in the SPR were observed during sensing detection toward F<sup>-</sup>, Cl<sup>-</sup>, Br<sup>-</sup> and I<sup>-</sup> ions, even if their individual concentration was increased to 120×10<sup>-6</sup> M.[58] The absorption intensity was kept the same except for a slight damping in I<sup>-</sup> ionic system, consistent with the study on the surface plasmon damping of silver colloids (6-nm mean diameter) by chemisorbed I<sup>-</sup> ions. Henglein and Mulvaney[103-109] demonstrated that the I<sup>-</sup> ions could lead to a distinctive damping in the plasma band of silver colloids due to possible redox reduction. There is no simple way to account for the intensity of this damping at present, but the damping strength is correlated with the strength of the Ag-anion bond. The effect is not simply due to the reduction in the electron mean free path and the channeling of the surface plasmon energy into excitation modes of the surface metal-adsorbate complex.[80]

### 4.3. Stability and Chemical Reactivity

#### 4.3.1 Stability

Many studies focused on the shape control of particles in their formation and growth stage. However, little attention has been paid to the stability of nanostructures during their storage. The structural and optical stability of nanoparticles directly influences on their application involving plasmon-enhanced spectrometers. For example, the plasmon-enhanced spectroscopy requires stable and well-defined resonances. A shift of plasmon resonance, even if only a few nanometers, can reduce signal intensities by orders of magnitude, particularly if nonlinear optical enhancements are involved.[124-127] This is an important problem that should be properly addressed.

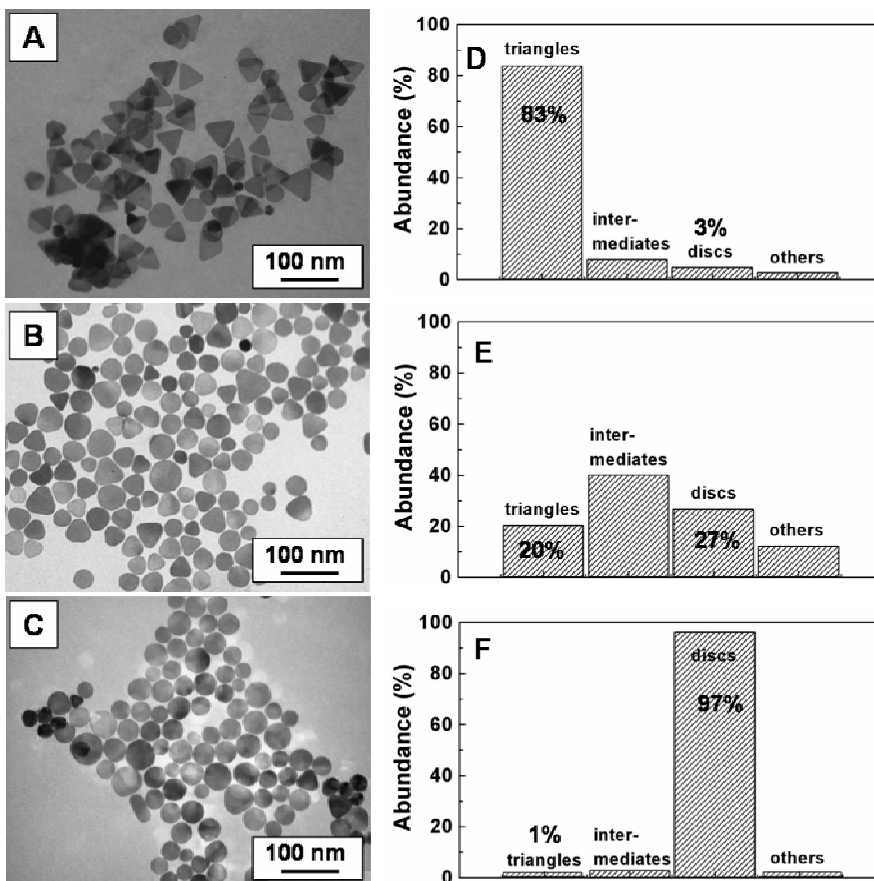


Figure 17. TEM images showing the influence of ageing time on the morphology of silver nanoplates: (A) triangles; (B) intermediates ageing for 24 h; and (C) disks ageing for 100 h; and (D-F) the shape distributions of silver nanoplates corresponding to the TEM images (A-C), respectively.

Our experimental observations showed that the silver nanoplates stabilized by AOT molecules in aqueous solution could evolve in shape and transform into other morphologies such as intermediate of triangle and disks, and disks (Fig. 17). The MD simulation can also be used to explain the shape transformation of silver nanoplates to disks, as discussed in our work. [56] The aforementioned MD calculation shows that there is a small difference ( $\Delta E_{int} =$

73 kcal·mol<sup>-1</sup>) in the interaction energies between (110) and (100) silver planes but a relatively large difference ( $\Delta E_{\text{int}} \geq 136$  kcal·mol<sup>-1</sup>) from (111) plane, which would generate a driving force for atom migration between these two planes. That is, the quantitative calculation can be used to explain not only the growth of silver nanoplates but also the shape transformation from triangular to circular ones as depicted in the scheme (Fig. 18).

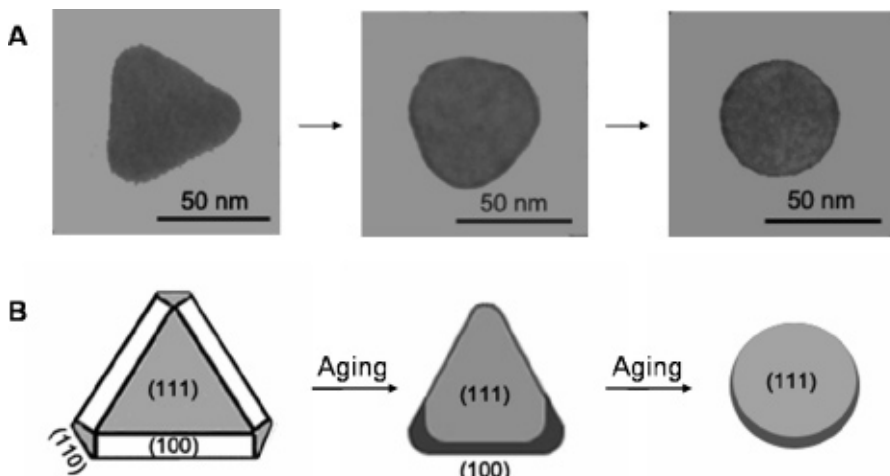


Figure 18. Schematically illustrating the shape evolution of silver nanoplates from triangles to circular disks. (Reprinted with permission from ref. 56. Copyright 2007 The American Chemical Society.)

A facile and effective method, namely the thiol-frozen approach, was developed by our laboratory to stabilize triangular silver nanoplates. Thiols ( $\text{CnH}_{2n+1}\text{SH}$ ) with different carbon chain lengths of C6, C8, C12, and C16 were chosen to modify the surface of silver nanoplates. Similarly, the addition of thiol(s) or cysteine could prevent silver nanoplate surface sensitivity toward inorganic ions, also indicating the surface functionality of thiols on metallic nanoparticles. The MD simulation was again performed to understand the thiol-frozen mechanism of triangular silver nanoplates. It is believed that the strong affinity of -SH head groups on metals (e.g., Au, Ag, Cd and Zn) could lead to intensive surface adsorption of thiol molecules on silver surfaces in this system.[36, 116, 117, 129-135] The calculated results,  $\text{C12H25SH-Ag}\{100\}$ -308.6,  $\text{Ag}\{110\}$ -361.1, and  $\text{Ag}\{111\}$ -959.0 kcal/mol, indicate that the thiol has much stronger interaction strength with  $\text{Ag}\{111\}$  plane than that with other planes (e.g., 110, and 100). Comparing with AOT molecules, the binding ability of C12H25SH to the silver surfaces is much stronger.[55-57] Such simulation will undergo a large shift in particle growth and shape-controlled synthesis from experimental or empirical choices to quantified determination.

#### 4.3.2 Chemical Reactivity

Silver nanoplates and nanodisks have higher surface-to-volume ratios and higher surface areas than spherical particles, such that they exhibit high chemical activity and can be applied in many areas of physics, chemistry and material science. For example, the nanodisks can be used as a scaffold template to fabricate gold rings through a galvanic replacement reaction in aqueous  $\text{AuCl}_4^-$  solution. This process is based on the higher standard reduction potential of

the AuCl<sub>4</sub>–Au<sub>0</sub> pair (0.99V vs. SHE), as compared to that of the Ag<sup>+</sup>/Ag<sub>0</sub> pair (0.80V vs. SHE), which leads to spontaneous oxidation of silver nanoparticles in the presence of HAuCl<sub>4</sub>.[136]

Silver nanoprisms used as a template for the synthesis of gold nanoframes have been previously reported by Xia group[136, 137] via the galvanic displacement. In our approach, Au nanorings other than the closed sealed shells formed (Fig. 19A). This is also supported by XRD pattern (Fig. 19B) and the corresponding UV-vis spectra (Fig. 19C). The diffraction intensity ratios between the different planes indicate no preferential orientation in the gold nanorings. This can also be evidenced from the SAED pattern (inset of Fig. 19A) of the Au nanorings. The plasmon bands of silver nanodisks disappeared (solid line) and a new band emerged around 520 nm (dotted line) that could be attributed to gold nanocrystals.

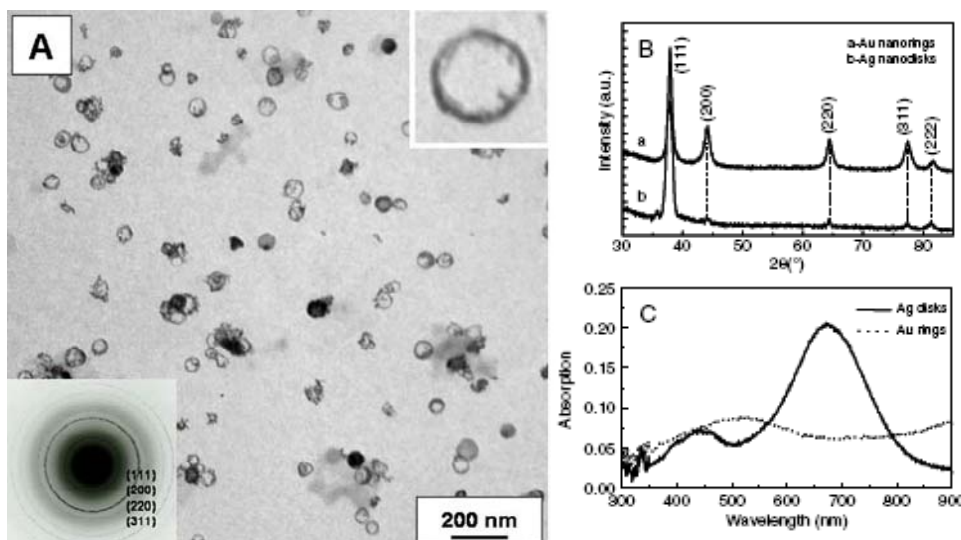


Figure 19. (A) TEM image and the inset SAED pattern of gold nanorings; (B) the XRD patterns of gold nanorings (a) and silver nanodiscs (b); and (C) the corresponding UV–vis spectra of gold nanorings (dotted line) and Ag nanodisks (solid line). (Reprinted with permission from ref. 55. Copyright 2006 IOP Publishing Ltd Printed in the UK.)

Considering the formation mechanism of gold rings, the replacement reaction was expected to occur first on the Ag{110} and Ag{100} facets, and then Ag{111} facets, based on the results generated by the aforementioned MD simulation. So a gold ring formed first around the edge bounded by {110} and {100} facets of a disk, and then the ring could serve as nuclei for further growth of gold layer into a complete shell. The crystallographic reconstruction would be favourable for the formation of gold nanorings via the Ostwald ripening process. A similar etching mechanism has been described in making hollow forms of rods, cubes and triangular frames.[136, 137] These results show that the silver template used for generating gold nanorings are disks but not spheres.[136] It is believed that this template approach based on silver nanodisks could be extended to produce other metallic ring-like structures as long as their oxidation potentials are higher than the redox pair of Ag<sup>+</sup>/Ag<sub>0</sub>.[138]

Another example to show the chemical reactivity of silver nanoparticles is to use them as an inducer in the formation of selenium (Se) nanorods and nanowires, as demonstrated in Our

recent work.[139, 140] This method exhibits some advantages in fabricating single-crystalline t-Se nanowires (diameter of ~23 nm and lengths over hundreds of nanometers), including no need to use stabilizers and sonichemical process, avoidance of toxic reducing agents (e.g. NaBH<sub>4</sub>, N<sub>2</sub>H<sub>4</sub>), and all operations being proceeded in aqueous media and at room temperature. In this approach, the silver particles show a high chemical reactivity as an inducer, even they have different shapes and sizes, such as colloids (5-15 nm in diameter), spheres (~45 nm in diameter), and nanoplates (~60 nm in edge length and thickness of ~2 nm). The as-prepared selenium nanowires or nanobelts induced by such silver nanoparticles are shown in Fig. 20.

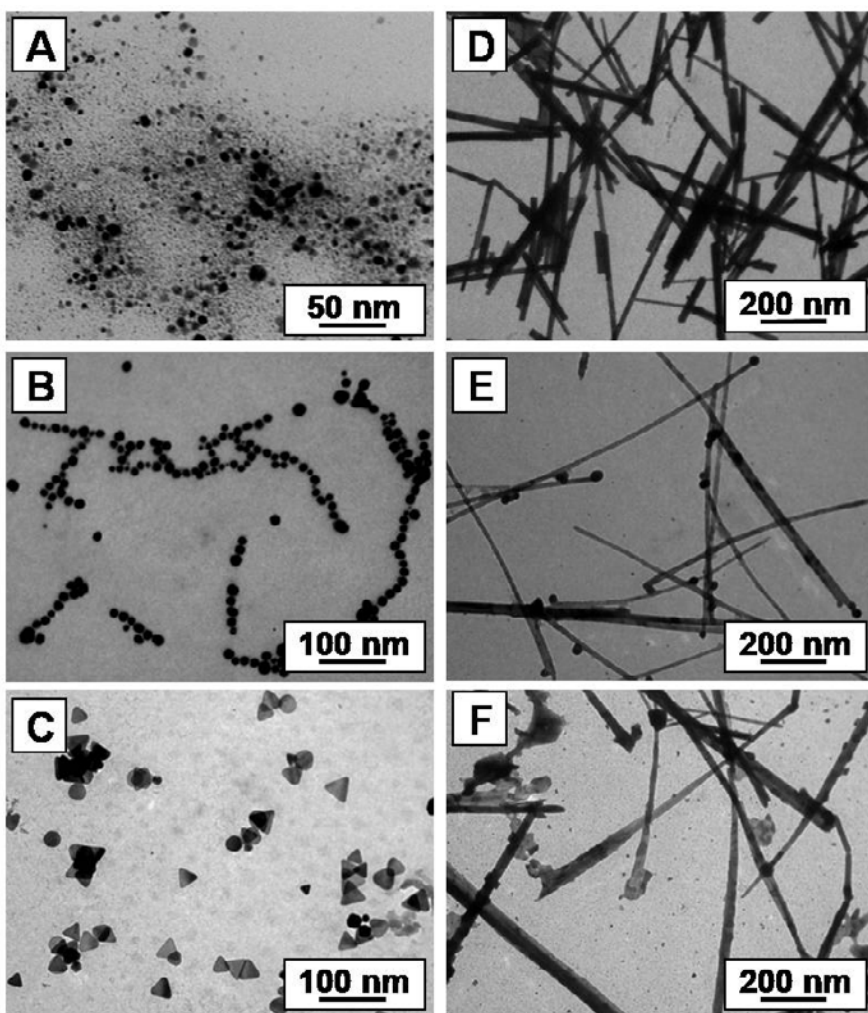


Figure 20. (A, D), TEM images of silver colloids (5-15 nm in diameter) and the corresponding selenium nanowires; (B, E) TEM images of silver particels (~45 nm in diameter) and the corresponding selenium nanowires; and (C, F) TEM images of silver nanoplates (~60 nm in edge length and ~2 nm in thickness) and the corresponding flat selenium nanowires.

A possible growth mechanism for selenium nanowires, namely the “bonding-epitaxy” growth, was proposed on the basis of experimental observations.[139, 140] The so-called

'bonding' means that the surface silver atoms are so chemically active that they can bond with Se atoms to form silver selenide ( $\text{Ag}_2\text{Se}$ ). These particles can further serve as nuclei for 'epitaxy' of selenium atoms on their surface to form nanowires. This is because the lattice match in the crystallographic structures between hexagonal-Se ( $a = 0.437 \text{ nm}$ ) and orthorhombic- $\text{Ag}_2\text{Se}$  ( $a = 0.434 \text{ nm}$ ) or between hexagonal-Se ( $c = 0.495 \text{ nm}$ ) and tetragonal- $\text{Ag}_2\text{Se}$  ( $c = 0.498 \text{ nm}$ ) plays a vital role, consistent with the literature.[141-145] The perfect lattice match would lead to the further nucleation and growth of selenium atoms on the surface of  $\text{Ag}_2\text{Se}$  particles to form Se nanowires. This approach for generating selenium nanowires could be extended to other semiconductor systems with similar lattice parameters (e.g.,  $\text{Ag}_2\text{Se}$  and  $\text{CdSe}$ ).

## 5. SUMMARY

The unique optical properties and promising applications in biological and chemical sensing of silver nanoplates have stimulated considerable research toward their synthesis, growth mechanisms and functional properties. Many approaches have been proposed and investigated in recent years. Two main synthetic strategies have been studied, including physical technique and chemical techniques. Compared to the physical technique, chemical technique is much more successful, and shows some advantages such as simple operation condition, diverse choice in solvents, controllable size from a few to hundreds of nanometers, and high yield in desired morphology. Therefore, many efforts have been made to the development of chemical methods in this area. Some methods have been demonstrated to be effective in the synthesis of silver nanoplates with shape and size control, including the photoinduced method, templating method, solvothermal and hydrothermal reduction method. Despite of many successes, the limitations still exist in the synthesis strategy. In fact, many of the methods developed thus far are empirical in nature and their application is very specific. Therefore, much more work is needed to develop an efficient and inexpensive mass production route for the synthesis of silver nanoplates with controllable shape and size, and such development should be coupled with better fundamental understandings.

Many efforts have been made in exploring the underlying mechanisms through the experimental observations and molecular modelings. Due to the versatility and complexity of the demonstrated synthetic approaches, there are different mechanisms proposed on shape control and growth of silver nanoplates, as highlighted by the stacking faults mechanism, twinning-plane mechanism, photoinduced fusion mechanism, and surface selective adsorption mechanism. Most of them are proposed on the basis of experimental observations, where the information generated is rarely quantitative. This would impede the progress in development of a general synthesis method for shape control. To better understand the formation mechanisms of silver nanoplates, theoretical efforts must be there. Molecular modeling has demonstrated some success in understanding the principles governing particle growth and shape control at a molecular scale. Such theoretical work will facilitate the development of reliable and versatile synthesis methods. However, constrained by the current computer capacity, the DFT and MD simulations thus far are largely limited to the study of the thermodynamics, with little effort made on the kinetics. Future work is therefore needed to overcome this limitation while investigating more complicated systems.

Silver nanoplates have exhibited specific optical properties in the wavelength range of 300-900 nm because of the anisotropic nanostructure with corners, edges, and large aspect ratios that can generate maximum electromagnetic-field enhancement. The strong SERS and LSPRs spectra have been exploited for functional applications in the area of chemical and biochemical sensing. Silver nanoplates have been used in sensing detection of inorganic ions in aqueous solution based on the SPR shift in the wavelength. In addition, the relationship between surface plasmon resonances and particle geometry can be correlated by DDA and BEM methods. However, generally speaking, such studies are limited to the laboratory tests to demonstrate the potentials. In the future, more efforts are needed to exploit the practical application while exploring and understanding their functional properties of silver nanoplates.

## ACKNOWLEDGMENTS

We gratefully acknowledge the financial support of the Australia Research Council (ARC) and Natural Science Foundation of China in the past years.

## REFERENCES

- [1] El-Sayed M A. *Acc Chem Res*, 2001, 34: 257-264
- [2] Kamat P V. *J Phys Chem B*, 2002, 106: 7729-44
- [3] Pérez-Juste J, Pastoriza-Santos I, Liz-Marzán L M, Mulvaney P. *Coord Chem Rev*, 2005, 249: 1870-1901
- [4] Shankar S S, Rai A, Ankamwar B, Singh A, Ahmad A, Sastry M. *Nat Mater*, 2004, 3: 482-488
- [5] Jiang X C, Brioude A, Pileni M P. *Colloids and Surf A*, 2006, 227: 201-206
- [6] Brioude A, Jiang X C, Pileni M P. *J Phys Chem B*, 2005, 109: 13138-42
- [7] Yin Y, Alivisatos P. *Nature*, 2005, 437: 664-70
- [8] Bohren C F, Huffman D R. *Absorption and scattering of light by small particles*, Wiley, New York, 1983.
- [9] Bloember M J, Buncick M C, Warmack R J, Ferrell T L. *J Opt Soc Am B*, 1988, 5: 2552-59
- [10] Tao A, Kim F, Hess C, Goldberger J, He R, Sun Y, Xia Y, Yang P D. *Nano Lett*, 2003, 3: 1229-33
- [11] Shanmukh S, Jones L, Driskell J, Zhao Y-P, Dluhy R, Tripp R A. *Nano Lett*, 2006, 6: 2630-36
- [12] McFarland A D, Young M A, Dieringer J A, Van Duyne R P. *J Phys Chem B*, 2005, 109: 11279-85
- [13] Hulteen J C, Treichel D A, Smith M T, Duval M L, Jensen T R, Van Duyne R P. *J Phys Chem B*, 1999, 103: 3854-63
- [14] Muniz-Miranda M. *Chem Phys Lett*, 2001, 340: 437-443
- [15] Hashimoto N, Hashimoto T, Teranishi T, Nasu H, Kamiya K. *Sensors and Actuators B: Chemical*, 2006, 113: 382-388

- [16] Nicewarner-Peña S R, Freeman R G, Reiss B D, He L, Peña D J, Walton Ian D, Cromer R, Keating C D, Natan M J. *Science*, 2001, 294: 137-141
- [17] Katherine A, Willets K A, Van Duyne R P. *Annual Rev Phys Chem*, 2007, 58: 267-97
- [18] Kelly K L, Coronado E, Zhao L, Schatz G C. *J Phys Chem B*, 2003, 107: 668-77
- [19] Miller M M, Lazarides A A. *J Phys Chem B*, 2005, 109: 21556-65
- [20] Nie S, Emory S R. *Science*, 1997, 275: 1102-06
- [21] Hache F, Ricard D, Flytzanis C. *J Opt Soc Am B*, 1986, 3: 1647-55
- [22] Haglund R F Jr, Yang L, Magruder R H III; Wittig J E, Becker K, Zuhir R A. *Opt Lett*, 1993, 18: 373-375
- [23] Uchida K, Kaneko S, Omi S, Hata C, Tanji H, Asahara Y, Ikushima A J, Tokizaki T, Nakamura A. *J Opt Soc Am B*, 1994, 11: 1236-43
- [24] Tokizaki T, Nakamura A, Kaneko S, Uchida K, Omi S, Tanji H, Asahara Y. *Appl Phys Lett*, 1994, 64: 941-943
- [25] West R, Wang Y, Goodson III T. *J Phys Chem B*, 2003, 107: 3419-26
- [26] Mie G. *Ann Phys*, 1908, 25: 377-445
- [27] Maxwell-Garnett J C. *Philos Trans R Soc London Ser A*, 1904, 203: 385-420
- [28] Hamanaka Y, Nakamura A, Omi S, Del Fatti N, Vallee F, Flytzanis C. *Appl Phys Lett*, 1999, 75: 1712-14
- [29] Kneipp K, Kneipp H, Itzkan I, Dasari R R, Feld M S. *J Phys: Condens Matter*, 2002, 14: R597
- [30] Purcell E M, Pennypacker C R. *Astrophys J*, 1973, 186: 705-714
- [31] Draine B T, Goodman J J. *Astrophys J*, 1993, 405: 685-697
- [32] Draine B T, Flatau P J. *J Opt Soc Am A*, 1994, 11: 1491-99
- [33] Okada N, Hamanaka Y, Nakamura A, Pastoriza-Santos I and Liz-Marzán L M. *J Phys Chem B*, 2004, 108: 8751-55
- [34] Kowshik M, Ashtaputre S, Kharrazi S, Vogel W, Urban J, Kulkarni S K, Paknikar K M. *Nanotechnology*, 2003, 14: 95-100
- [35] Mukherjee P, Ahmad A, Mandal D, Senapati S, Sainkar S R, Khan M I, Ramani R, Parischa R, Ajayakumar P V, Alam M, Sastry M, Kumar R. *Angew Chem Int Ed*, 2001, 40: 3585-88
- [36] Prasad B L V, Stoeva S I, Sorensen C M, Klabunde K J. *Langmuir*, 2002, 18: 7515-20
- [37] Haynes C L and Van Duyne R P. *J Phys Chem B*, 2001, 105: 5599-5611
- [38] Jin R, Cao Y, Mirkin C A, Kelly K L, Schatz G C, Zheng J G. *Science*, 2001, 294: 1901-1903
- [39] Jin R, Cao Y, Metraux G S, Schatz G C, Mirkin C A. *Nature*, 2003, 425: 487-490
- [40] Maillard M, Huang P, Brus L. *Nano Lett*, 2003, 3: 1611-1615
- [41] Callegari A, Tonti D, Chergui M. *Nano Lett*, 2003, 3: 1565-68
- [42] Sun Y. *Chem Mater*, 2007, 19: 5845-5847
- [43] Jiang L P, Xu S, Zhu J M, Zhang J R, Zhu J J, Chen H Y. *Inorg Chem*, 2004, 43: 5877-83
- [44] Sun Y, Mayers B, Xia Y. *Nano Lett*, 2003, 3: 675-679
- [45] Sun Y, Xia Y. *Science*, 2002, 298: 2176-79
- [46] Washio I, Xiong Y, Yin Y, Xia Y. *Adv Mater*, 2006, 18: 1745-49
- [47] Pastoriza-Santos I, Liz-Marzán L M. *Nano Lett*, 2002, 2: 903-905
- [48] Zhang J, Liu H, Zhan P, Wang Z, Ming N. *Adv Funct Mater*, 2007, 17: 1558-66

- [49] Maillard M, Giorgio S, Pileni M P. *J Phys Chem B*, 2003, 107: 2466-70
- [50] Germain V, Li J, Ingert D, Wang Z L. *J Phys Chem B*, 2003, 107: 8717-8720
- [51] Germain V, Brioude A, Ingert D, Pileni M P. *J Chem Phys B*, 2005, 122: 124707
- [52] Brioude A, Pileni M P. *J Phys Chem B*, 2005, 109: 23371-77
- [53] Chen S, Carroll D L. *Nano Lett*, 2002, 2: 1003-7
- [54] Hao E, Kelly K L, Hupp J T, Schatz G C. *J Am Chem Soc*, 2002, 124: 15182-83
- [55] Jiang X C, Zeng Q H, Yu A B. *Nanotechnology*, 2006, 17: 4929-35
- [56] Jiang X C, Zeng Q H, Yu A B. *Langmuir*, 2007, 23: 2218-23
- [57] Zeng Q H, Jiang X C, Yu A B, Lu G. *Nanotechnology*, 2007, 18: 035708
- [58] Jiang X C, Yu A B. *Langmuir*, 2008, 24: 4300-09
- [59] Pastoriza-Santos I, Liz-Marzán L M. *J Mater Chem*, 2008, 18: 1724-37
- [60] Jiang Y. Forced Hydrolysis and Chemical Co-Precipitation. In *Handbook of Nanophase and Nanostructured Materials*; Wang Z L, Liu Y, Zhang Z. Eds.; Kluwer Academic: New York, 2003, p 59.
- [61] Crooks R M, Zhao M, Sun L, Chechik V, Yeung L K. *Acc Chem Res*, 2001, 34: 181
- [62] Shenhar R, Rotello V M. *Acc Chem Res*, 2003, 36: 549
- [63] Thomas K G, Kamat P V. *Acc Chem Res*, 2003, 36: 888
- [64] Xia Y, Rogers J A, Paul K E, Whitesides G M. *Chem Rev*, 1999, 99: 1823
- [65] Shipway A N, Lahav M, Willner I. *Adv Mater*, 2000, 12: 993
- [66] Schrtl W. *Adv Mater*, 2000, 12: 1899
- [67] Khabashesku V N, Billups W E, Margrave J L. *Acc Chem Res*, 2002, 35: 1087
- [68] Burda C, Chen X, Narayanan R and El-Sayed M A. *Chem Rev*, 2005, 105: 1025-1102
- [69] Haes A J, Zhao J, Zou S, Own C S, Marks L D, Schatz G C and Van Duyne R P. *J Phys Chem B*, 2005, 109: 11158-62
- [70] Kosiorek A, Kandulski W, Chudzinski P, Kempa K and Giersig M. *Nano Lett*, 2004, 4: 1359-63
- [71] Junior A M, de Oliveira H P M, Gehlen M H. *Photochem Photobiol Sci*, 2003, 2: 921-925
- [72] Xue C, Mirkin C A. *Angew Chem Int Ed*, 2007, 46: 2036-38
- [73] Xue C, Millstone J E, Li S and Mirkin C A. *Angew Chem Int Ed*, 2007, 46: 8436-8439
- [74] Bastys V, Pastoriza-Santos I, Rodriguez-González B, Vaisnoras R and Liz-Marzán L M. *Adv Funct Mater*, 2006, 16: 766-773
- [75] Rocha T C R and Zanchet D. *J Nanosci Nanotechnol*, 2007, 7: 618
- [76] Rocha T C R and Zanchet D. *J Phys Chem C*, 2007, 111: 2885-91
- [77] Rocha T C R and Zanchet D. *J Phys Chem C*, 2007, 111: 6989- 93
- [78] Pileni M P. *Nat Mater*, 2003, 2: 145-150
- [79] Pastoriza-Santos I, Liz-Marzán L M. *Langmuir*, 2002, 18: 2888-94
- [80] Xiong Y, Siekkinen A R, Wang J, Yin Y, Kim M J, Xia Y. *J Mater Chem*, 2007, 17: 2600-2602
- [81] Balleto F, Ferrando R. *Rev Mod Phys*, 2005, 77: 371-423
- [82] Kirkland I, Jefferson D A, Duff D G, Edwards P P, Gameson I, Johnson B F G, Smith D J. *Proc: Math Phys & Sci*, 1993, 440: 589-609
- [83] Lofton C, Sigmund W. *Adv Funct Mater*, 2005, 15: 1197-08
- [84] Takayanagi K, Tanishiro Y, Yagi K, Kobayashi K and Honjo G. *Surf Sci*, 1988, 205: 637-651

- [85] Rodriguez-González B, Pastoriza-Santos I and Liz-Marzán L M. *J Phys Chem B*, 2006, 110: 11796-799
- [86] Kilin D S, Xia Y and Prezhdo O V. *Chem. Phys Lett*, 2008, 458: 113-116
- [87] Kemal L, Jiang X C, Wong K and Yu A B. *J Phys Chem C*, 2008, 112: 15656-64
- [88] Kreibig U and Vollmer M. *Optical Properties of Metal Clusters*, Springer-Verlag, Berlin, 1996.
- [89] Liz-Marzán L M. *Langmuir*, 2006, 22: 32-41
- [90] Sherry L J, Jin R, Mirkin C A, Schatz G C and Van Duyne R P. *Nano Lett*, 2006, 6: 2060-2065
- [91] Rodriguez-Fernández J, Pérez-Juste, J, García de Abajo F J and Liz-Marzán L M. *Langmuir*, 2006, 22: 7007-7010
- [92] García de Abajo F J and Howie A. *Phys Rev Lett*, 1998, 80: 5180-5183
- [93] García de Abajo F J and Howie A. *Phys Rev B*, 2002, 65: 115418-1-17
- [94] Nelayah J, Kociak M, Stéphan O, García de Abajo F J, Tencé M, Henrard L, Taverna D, Pastoriza-Santos I, Liz-Marzán L M and Colliex C. *Nat Phys*, 2007, 3: 348-353
- [95] Ritchie R H. *Phys Rev*, 1957, 106: 874-881
- [96] Chen C H, Silcox J. and Vincent R. *Phys Rev B*, 1973, 12: 64-71
- [97] Kneipp K, Kneipp H, Itzkan I, Dasari R R and Feld M S. *Chem Rev*, 1999, 99: 2957-75
- [98] Otto A. In *Light scattering in solids IV. Electronic scattering, spin effects, SERS and morphic effects*; Cardona M, Güntherodt G, Eds.; Springer-Verlag: Berlin, Germany, 1984.
- [99] Moskovits M. *Rev Mod Phys*, 1985, 57: 783-826
- [100] Jeanmaire D L and Van Duyne R P. *J Electroanal Chem Interfacial Electrochem*, 1977, 84: 1-20
- [101] Albrecht M G and Creighton J A. *J Am Chem Soc*, 1977, 99: 5215-5217
- [102] Haynes A J and Van Duyne R P. *J Am Chem Soc*, 2002, 124: 10596-7
- [103] Gorman B A, Francis P S, Dunstan D E, Barnett N W. *Chem Commun*, 2007, 395-397
- [104] Henglein A, Mulvaney P, Linnert T. *Faraday Discuss*, 1991, 92: 31-44
- [105] Henglein A, Meisel D. *Langmuir*, 1998, 14: 7392-96
- [106] Henglein A. *Chem Mater*, 1998, 10: 444-450
- [107] Linnert T, Mulvaney P, Henglein A. *J Phys Chem*, 1993, 97: 679-682
- [108] Mulvaney P. *Langmuir*, 1996, 12: 788-800
- [109] Mulvaney P, Pérez-Juste J, Giersig, M, Liz-Marzán L M, Pecharromán C. *Plasmonics* 2006, 1: 61-66
- [110] Yang W H, Hulteen J, Schatz G C and Van Duyne R P. *J Chem Phys*, 1996, 104: 4313-23
- [111] Haynes C L and Van Duyne R P. *J Phys Chem B*, 2003, 107: 7426-7433
- [112] Zhang J, Li X, Sun X and Li Y. *J Phys Chem B*, 2005, 109: 12544
- [113] Zou X and Dong S. *J Phys Chem B*, 2006, 110: 21545-21550
- [114] Wang Y, Zou X, Ren W, Wang W and Wang E. *J Phys Chem C*, 2007, 111: 3259-3265
- [115] Brockman J M, Nelson B P and Corn R M. *Annu Rev Phys Chem*, 2000, 51: 41-63
- [116] Malinsky M D, Kelly K L, Schatz G C and Van Duyne R P. *J Am Chem Soc*, 2001, 123: 1471-82
- [117] Mcfarland A D and Van Duyne R P. *Nano Lett*, 2003, 3: 1057-62

- [118] Haes A J, Chang L, Klein W L and Van Duyne R P. *J Am Chem Soc*, 2005, 127: 2264-71
- [119] Haes A J, Hall W P, Chang L, Klein W L and Van Duyne R P. *Nano Lett*, 2004, 4: 1029-34
- [120] Malynych S, Chumanov G. *J Opt A: Pure Appl Opt*, 2006, 8: S144-S147
- [121] Hao E, Schatz G C and Hupp J T. *J Fluoresc*, 2004, 14: 331-341
- [122] Pastoriza-Santos I, Hamanaka I, Fukuta K, Nakamura A, Liz-Marzán L M. In Low-Dimensional Systems. Theory, Preparation and Some Applications. Eds. Liz-Marzán L M and Giersig M. *NATO Science Series II, vol. 91*, Kluwer, Dordrecht, 2003, pp 65-75.
- [123] Person B N. *J Surf Sci*, 1993, 281:153-162
- [124] *Handbook of Chemistry & Physics*, Weast 64th Edition, CRC Press, 1983-84.
- [125] Wei A. In *Nanoparticles: Scaffolds and Building Blocks*; Rotello, V. M., Ed.; Kluwer Academic: New York, 2004, pp173-200.
- [126] Genov D A, Sarychev A K, Shalaev V M, Wei A. *Nano Lett*, 2004, 4: 153-8
- [127] Imura K, Nagahara T, Okamoto H. *J Am Chem Soc*, 2004, 126: 12730-31
- [128] Zweifel D A, Wei A. *Chem Mater*, 2005, 17: 4256-61
- [129] Martin J E, Wilcoxon J P, Odinek J, Provencio P. *J Phys Chem B*, 2000, 104: 9475-86
- [130] Sastry M, Lala N, Patil V, Chavan S P, Chittiboyina A G. *Langmuir*, 1998, 14: 4138-42
- [131] Sastry M, Mayya K S, Patil V, Paranjape D V, Hegde S G. *J Phys Chem B*, 1997, 101: 4954-58
- [132] Weisbecker C S, Merritt M V, Whitesides G M. *Langmuir*, 1996, 12: 3763-72
- [133] Song Y, Huang T, Murray R W. *J Am Chem Soc*, 2003, 125, 11694-701
- [134] Ingram R S, Hostetler M J, Murray R W. *J Am Chem Soc*, 1997, 119: 9175-78
- [135] Ulman A. *Chem Rev*, 1996, 96: 1533-54
- [136] Sun Y and Xia Y. *Adv Mater*, 2003, 15: 695
- [137] Sun Y and Xia Y. *Adv Mater*, 2002, 14: 833
- [138] Kotz J C and Purcell K F. *Chemistry and Chemical Reactivity* 2nd edn, Philadelphia, PA: Saunders College Publishing, 1991.
- [139] Jiang X C, Kemal L, Yu A B. *Mater Lett*, 2007, 61: 2584-88
- [140] Jiang X C and Yu A B. *J Nanoparticle Res*, 2008, 10: 477-489
- [141] Gates B, Mayers B, Cattle B, Xia Y. *Adv Funct Mater*, 2002, 12: 219-227
- [142] Mayers B T, Liu K, Sunderland D, Xia Y. *Chem Mater*, 2003, 15: 3852-58
- [143] Zhang B, Dai W, Ye X, Hou W, Xie Y. (2005) *J Phys Chem B*, 2005, 109: 22830-35
- [144] Zhang B, Dai W, Ye X, Zuo F, Xie Y. *Angew Chem Int Ed*, 2006, 45: 2571-74
- [145] Chizhikov D M and Shchastlivyi V P. *Selenium and selenides* (Translated from the Russian by Elkin EM). Collet's Ltd, London and Wellingborough, 1968.

***Chapter 18***

## **STUDY OF THE PROPERTIES OF IRON OXIDE NANOSTRUCTURES**

***Arturo I. Martinez<sup>1</sup>, M.A. Garcia-Lobato<sup>1</sup> and Dale L. Perry<sup>\*2</sup>***

<sup>1</sup>Center for Research and Advanced Studies of the National Polytechnic Institute,  
Cinvestav-Saltillo, Carr. Saltillo-Mty. Km 13, 25900 Ramos Arizpe, Coahuila, Mexico.

<sup>2</sup>Lawrence Berkeley National Laboratory, Berkeley, California 94720

### **1. INTRODUCTION**

Iron oxides exist in a rich variety of structures and occur in a great variety of settings, from geological to nanoscale technological applications. Ferrous and ferric iron oxides present seven crystalline phases, the more common are  $\alpha\text{-Fe}_2\text{O}_3$  (hematite),  $\gamma\text{-Fe}_2\text{O}_3$  (maghemite),  $\text{Fe}_3\text{O}_4$  (magnetite) and  $\text{Fe}_{1-x}\text{O}$  (wustite); the less commonly found are the  $\beta$ - and  $\varepsilon\text{-Fe}_2\text{O}_3$  phases and the low-temperature rhombohedral structure of magnetite. Thanks to their fascinating properties, all of these oxides have been widely investigated by chemists, engineers, and physicists. These phases have been used successfully in many applications; e.g., magnetite nanoparticles have been used in cancer diagnosis and therapy [1], drug delivery vehicles [2], and in water remediation [3]. Magnetite thin films lend themselves to room temperature applications in the construction of different devices such as tunneling magnetoresistance, giant magnetoresistance and magnetic random-access memory devices [4]. Maghemite is used in magnetic resonance imaging [5], magnetic recording media [6], fabrication of biocompatible magnetic fluids [7], and electrochromic devices [8]. Hematite nanostructures have been explored in the development of electrochromic devices [8], as cathodes in lithium batteries [9], and in the construction of photoelectrochemical systems to produce hydrogen from water using solar radiation [10]. Thin films of wustite/maghemite have been used in solar radiation filters [11].

---

\* [mtz.art@gmail.com](mailto:mtz.art@gmail.com)

## 1.1. Nanostructures of Iron Oxides

Hematite exhibits a rhombohedral structure which is antiferromagnetic below its Morin transition ( $T_M$ ) of about 260 K. Between this temperature and the Néel temperature ( $T_N$ ) of about 948 K, it exhibits a weak ferromagnetic behavior. The weak ferromagnetic behavior is due to a slight disorder of the spin axis from exact antiparallelism. The dependence of the particle size on  $T_M$  has been studied, and it was found that the  $T_M$  is lower for smaller particles; however,  $T_M$  is strongly dependent on the sample preparation method, lattice defects, and the incorporation of water and OH groups into the hematite structure [12]. The magnetic properties of this phase are strongly related to the morphology and size of the nanoparticles. The coercivity ( $H_c$ ) ranges from 31 to 530 Oe [13-16], and remanent magnetizations ( $M_r$ ) are from 0.6 to 16 memu/g [13-16]. The higher  $H_c$  and  $M_r$  are associated with greater sizes; otherwise, small particles of hematite with different morphologies above the blocking temperature ( $T_b$ ) acquire a single magnetic domain behavior showing superparamagnetic properties [13, 17].

Magnetite and maghemite are ferrimagnetic, and both crystallize in the inverse spinel cubic structure. At ambient conditions, these phases are thermodynamically less stable than hematite [18]; despite this, it has been found that for smaller nanocrystals of maghemite, the stability increases. This can be inferred because its surface energy is lower than that of hematite [19]. Maghemite is an insulator with an energy gap of 2 eV, while magnetite is a  $\text{Fe}^{2+}$ - $\text{Fe}^{3+}$  mixed valence metal. Magnetite has a Curie temperature ( $T_C$ ) of 860 K, while the  $T_C$  is 900 K for maghemite. Furthermore, magnetite shows an order-disorder transition at the Verwey transition  $T_V$ , at about 120 K, in which the electrical conductivity decreases by almost two orders of magnitude [20]. According to Verwey, below  $T_V$  magnetite exhibits an orthorhombic structure, although other researchers argue for a monoclinic structure [20]. The absence of the structural transition for magnetite nanoparticles smaller than 10 nm and the observation of the nonexistence of  $T_V$  have been reported [21].

Wustite is an antiferromagnet; with a  $T_N$  of about 200 K, it crystallizes in the rock salt structure. The iron deficiency in wustite leads to the formation of vacancies located on interstitial, tetrahedral sites clustered around  $\text{Fe}^{3+}$  ions [22]. Wustite exhibits semiconductor properties. Thermoelectric measurements record a drop in the thermoelectric power taking place below 120 K, and a change in the sign from positive to negative is observed [23]. Wustite is metastable, yielding metallic iron and magnetite; this metastability has been used to prepare mixed-phase nanoparticles with both composition and magnetic properties controlled by the fabrication technique [24, 25]. In order to stabilize the wustite phase with controlled stoichiometry, the nanoparticles have been capped with organic ligands [24-26].

## 1.2. Other Ferrites

Ferrites have the general formula of  $\text{MFe}_2\text{O}_4$ , where M can be one or more metal atoms with different ratios between them; they crystallize in the inverse spinel structure. A great variety of metal ferrite nanoparticles has been reported in the literature. Very important properties can be found, such as in  $\text{CoFe}_2\text{O}_4$ , which exhibits light-induced changes in the coercive field; this property, called photomagnetism, may be used in the fabrication of hybrid data storage [27]. The superparamagnetic properties of nanoparticles cover a broad range of

particle sizes of ferrites such as  $\text{MgFe}_2\text{O}_4$  [28],  $\text{Ni}_{0.20}\text{Zn}_{0.44}\text{Fe}_{2.36}\text{O}_4$  [29],  $\text{NiFe}_2\text{O}_4$  [30], and  $\text{MnFe}_2\text{O}_4$  [31]. In order to satisfy the current technological demands, other ferrites such as  $\text{BiFeO}_3$  [32] and ferrites with more complex compositions, such as the  $\text{Mg}_{0.55-x}\text{Cu}_x\text{Zn}_{0.45}\text{O}(\text{Fe}_2\text{O}_3)_{0.97}$  [33] and  $\text{Ba}_{(1-x)}\text{Sr}_x\text{Fe}_{12}\text{O}_{19}$  compounds [34] are extensively studied because of their ferroelectric, ferroelastic, and ferromagnetic properties.

## 2. PREPARATION OF IRON OXIDES NANOSTRUCTURES

### 2.1. Synthesis of Nanoparticles

Iron oxide nanoparticles have been synthesized by a variety of techniques. The most commonly used methods for the preparation of hematite, maghemite, magnetite, wustite, and other ferrite nanoparticles are: co-precipitation [27, 28, 35], the polyol process [36, 37], thermal decomposition of metal-organic compounds [3, 24, 26], microemulsion [29, 32, 38], hydrothermal synthesis [13-17], aerosol pyrolysis [39], high energy ball milling [25, 31], sol-gel [6, 40], and some vacuum methods such as sputtering have also been used for the preparation of core-shell nanoparticles [41]. Obtaining nanoparticles with a controlled size, morphology, and composition is the main challenge for all the techniques mentioned above; also, a simple, reliable, and cheap process is needed for large-scale syntheses. Figure 1 shows a comparison of the size distribution of iron oxide nanoparticles prepared by different techniques.

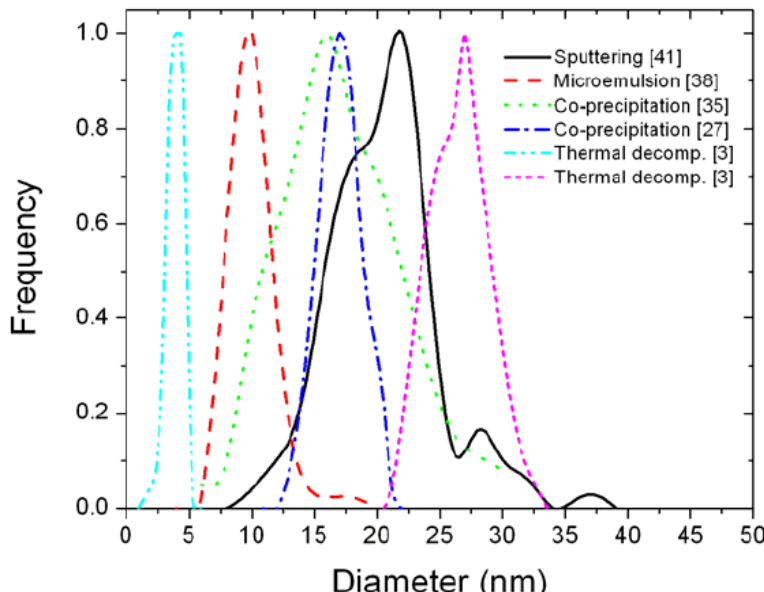


Figure 1. Size distribution of iron oxides nanoparticles obtained by different preparation methods. Very narrow distributions are seen in smaller particles prepared by thermal decomposition and microemulsion. Nanoparticles prepared by co-precipitation and sputtering shows spread size distributions.

Co-precipitation methods are simple methods of synthesizing magnetite and other ferrite nanoparticles from ferric and ferrous salts such as nitrates, chlorides, sulfates, perchlorates, etc. With the appropriate ratios of the precursor salts, it is possible to obtain narrow size distribution of spherical nanoparticles [27, 28, 35]. As an alternative method, the polyol process uses polyols such as ethylene glycol; polyols are high-boiling solvents, reducing agents, and stabilizers that control the growth and prevent the aggregation of nanoparticles. This method is useful for the preparation of dispersed magnetite nanoparticles with tailor-made size and tuneable magnetic properties [36, 37]. The thermal decomposition at appropriate conditions yields monodispersed nanocrystals in one reaction without a further size-selection process; large scale amounts of material are available because inexpensive reagents can be used [26]. With this method, wustite, magnetite and maghemite nanoparticles have been prepared [24, 26]. In the microemulsion method, co-precipitation occurs in the aqueous phase of water-in-oil emulsions controlling the particle size and size distribution in the desired proportions. Particles of a great variety of ferrites including magnetite, nickel zinc and bismuth ferrite have been successfully prepared by this method [29, 32, 38]. The hydrothermal method involves high-temperature aqueous solutions at high vapor pressures; this technique is very effective to control the size and shape of nanocrystals. The hydrothermal syntheses of nanorods, nanotubes, nanocubes, and rhombohedral crystals of maghemite and hematite have been reported [13-17]. Aerosol pyrolysis is a technique that involves a series of reactors with a temperature gradient. In these reactors the aerosol droplets travel following the next step in the processes: evaporation of the solvent, solute condensation within the droplet, drying, and the thermolysis of the precipitated particle. This method is useful for obtaining particles of predictable shape, size and composition; maghemite hollow spheres have been prepared by this method [39]. By ball milling, the mechanosynthesis of nanostructures is promoted by the mechanical activation of the chemical reactions involved in the formation of the oxides. Wustite nanoparticles from metallic iron and hematite have been prepared by this method [25]. The sol-gel process uses metallic alkoxides as precursors; it allows the preparation of ceramic nanoparticles of a great variety of compounds, including ellipsoidal single-crystalline nanoparticles of hematite and polycrystalline spherical nanoparticles of hematite. With a proper reduction-reoxidation process, magnetite and maghemite nanoparticles that retain their shape can be obtained [6].

## 2.2. Thin Film Growth

Iron oxide thin films of hematite, maghemite, magnetite and wustite have been prepared by a variety of techniques including chemical vapor deposition (CVD) [42, 43], sputtering [4, 10, 11, 44], sol-gel [8, 45], pulsed laser deposition (PLD) [46, 47, 48, 49], molecular beam epitaxy (MBE) [50, 51], and spray pyrolysis [52, 53]. The quality of the film depends on the technique of growth and diverse operating parameters. For physical techniques such as PLD and sputtering, the most important parameters are target-substrate distance, chamber pressure, substrate temperature, deposition time, oxygen partial pressure, laser energy density, laser frequency, and the power of the RF or DC source [37]. For the chemical techniques, the most important parameters that affect the quality and properties of iron oxide films are the type of chemical precursors, deposition rate, carrier gas pressure, substrate temperature, precursor temperature, and annealing temperature. MBE is a technique that grows films with excellent

crystal quality at low deposition rates and low substrate temperatures, but it is an expensive technique.

Thin films of magnetite, maghemite and hematite have been successfully prepared by PLD [46, 47, 48]. Using different substrates, hematite targets, vacuum pressure, and substrate temperatures from 623 to 773 K, the formation of thin films exhibiting the maghemite or magnetite phases has been observed [46, 47, 48]. Hematite films have been prepared by using oxygen at working pressures ranging from 2 to 7 Pa [46]. PLD allows the preparation of smooth films at reasonable deposition rates with a controlled phase; the only drawback of this technique is that only small areas can be coated. As an alternate method, sputtering is a technique that allows depositing iron oxide films on large areas; films of iron oxides have been prepared on soda-lime glass of  $60 \times 30 \times 3$  mm<sup>3</sup> at residual pressures of 700 Pa. In order to change the reflectance properties, these films were heated in a reducing atmosphere of H<sub>2</sub> and N<sub>2</sub>, yielding mixed phase films of maghemite and wustite. These films have been successfully used as solar radiation filters for saving energy in warm weather [11]. Sputtered magnetite films have been prepared at room temperature by introducing an external RF power; without this, mixed phase films of Fe<sub>2</sub>O<sub>3</sub> and Fe<sub>3</sub>O<sub>4</sub> are obtained [44]. Saturation magnetizations ranging from ~70 to ~440 emu/cm<sup>3</sup> were reported for magnetite films prepared at different substrate temperatures with different thicknesses; higher magnetizations are obtained for films prepared at substrate temperatures higher than 523 K and thicker than 10 nm [4, 44]. Additionally, wustite films have been prepared by DC magnetron sputtering; these films exhibit large  $M_s$  and low temperature  $H_c$  [54]. This unusual behavior is attributed to the existence of 16:5 spinel type defect clusters coherently embedded in the FeO matrix [54].

Hematite thin films have been obtained by CVD using iron (III) tert-butoxide at substrate temperatures ranging from 623 to 673 K, while magnetite films can be prepared at 773 K. Intermediate temperatures yield films crystallized with both phases [43]. In addition, films crystallized in the cubic  $\beta$ -Fe<sub>2</sub>O<sub>3</sub> phase have been obtained by CVD using iron (III) acetylacetone as a precursor at temperatures ranging from 623 to 673 K; these films were studied for electrochromic applications [42]. Using spray pyrolysis techniques, hematite films were prepared by spraying aqueous solutions of iron (III) chloride at 773 K [52]. While iron (III) chloride dissolved in methanol sprayed at 633 K yields maghemite/hematite films, the formation of maghemite is promoted under a reducing atmosphere promoted by the organic solvent [53]. The spray deposition of iron (II) sulfate onto glass substrates has not yielded films of iron oxides [52]. Using the sol-gel method, hematite films have been formed at annealing temperatures of 623 to 873 K in air [8, 45]; annealing at 873 K in nitrogen/hydrogen atmosphere yields metallic iron films, and with a subsequent heat treatment at the same temperature in nitrogen, the generation of maghemite is observed [45].

### **3. CHARACTERIZATION TECHNIQUES FOR IRON OXIDES NANOSTRUCTURES**

#### **3.1. Magnetic and Electrical Properties**

The vibrating sample magnetometer (VSM) and the superconducting quantum interference device (SQUID) magnetometer are used to measure the magnetic properties of

materials. SQUID magnetometers are very sensitive; they are used to measure extremely small magnetic fields, based on the properties of electron-pair wave coherence and Josephson junctions. In a VSM, a sample is placed in a uniform magnetic field, and the sample is vibrated sinusoidally. The magnetic flux generated by the vibrating sample induces a current, which is proportional to the magnetization of the sample. The electrical properties of films are usually measured by the Van der Pauw method; this is useful for the determination of resistivity and the Hall parameters of films of arbitrary shape.

Experimentally and theoretically, the relationship between the size and the magnetic properties of nanoparticles has attracted much attention [3, 5-6, 13, 15, 21, 27-28, 37-39]. It has been found that nanoparticles smaller than a critical size ( $\sim 40$  nm) present a variety of size-dependent behaviors [3]; e.g., the cooperative phenomenon in ferromagnetism is no longer observed, and the particles behave like single domains, showing magnetic susceptibilities higher than the bulk, and the superparamagnetic behavior appears. The size of superparamagnetic nanoparticles can be obtained from the slope of their magnetization loop near zero magnetic field; for samples with a wide size distribution, the major contribution comes from the largest particles. Therefore, the upper limit of the magnetic size ( $D_m$ ) is given by [17]:  $D_m = [(18 k_B T / \pi)(\chi_i / \rho M_s^2)]^{1/3}$ , where  $k_B$  is the Boltzmann constant,  $T$  the temperature,  $\chi_i$  the initial magnetic susceptibility ( $\chi_i = (dM/dH)_{H \rightarrow 0}$ ),  $\rho$  the density of the nanoparticle and  $M_s$  the saturation magnetization. Additionally, it is frequently observed that the saturation magnetization decreases for smaller particles; this is due to the increase of spin order effects at the particle surface, which yields smaller net magnetic moments.

The correlation between the superparamagnetic properties of ferrite nanoparticles and size is related to the size dependence of the magnetocrystalline anisotropy energy ( $E_A$ ) in the nanoparticles. According to the Stoner-Wohlfarth theory,  $E_A$  of a single domain particle is approximated by [28]:  $E_A = KV \sin^2 \theta$ , where  $K$  is the magnetocrystalline anisotropy constant,  $V$  is the volume of the nanoparticles, and  $\theta$  is the angle between the direction of field-induced magnetization and the easy axis of the nanoparticles. This anisotropy is the energy barrier that prevents the change of magnetization direction [28]. When  $E_A$  is comparable with thermal activation energy ( $k_B T$ ), the magnetization direction is moved away from the easy axis by thermal activation or an external magnetic field. The coercivity of nanoparticles is closely related to  $E_A$ . At a constant temperature below  $T_B$ ,  $H_c$  corresponds to the magnetic field strength at which the magnetic field provides the required energy in addition to  $k_B T$  to overcome the magnetic anisotropy. Hence,  $H_c$  of nanoparticles increases with nanoparticle size; in addition, the  $H_c$  is affected by the shape anisotropy contribution, since high changes in  $H_c$  have been reported for iron oxide nanoparticles with different aspect ratios, such as nanorods, nanocubes, ellipsoidal, spherical and polyhedral shaped nanoparticles [6, 13]. Table 1 shows some characteristics of iron oxide nanoparticles with a variety of shapes and sizes, the effects of the size on the coercive field, saturation magnetization, and remanent magnetization as explained above is seen in these data which were extracted from the literature.

Typically, the magnetization of magnetite films is not easily saturated because of the localized antiphase boundaries (APB) present in the films [51]; however, some films reach their saturation magnetization easily, see figure 2. Sputtered magnetite films prepared at optimal conditions on Si (100) and MgO (100) substrates showed saturated magnetization loops, while those prepared at coarse conditions are not easily saturated [4, 44]. The

observation of  $M_s$  lower than the bulk value ( $\sim 477$  emu/cm $^3$ ) can be due to the presence of other phases at the interfaces between the substrate and to the presence of voids between the grains and *APB*.

**Table 1. Particle size, shape and magnetic parameters determined at room temperature of different iron oxide nanoparticles reported in the literature**

Iron oxide	Particle size (nm)	Shape	$M_s$ (emu/g)	$H_C$ (Oe)	$M_r$ (emu/g)	Ref.
Magnetite $Fe_3O_4$	4	spherical	31.8	12	0	[21]
	11.5	spherical	60.1	34	3.9	
	47.7	spherical	65.4	156	16.4	
	$\sim 150$	spherical	75.6	323	18.9	
	$\sim 200$	tubes	60.9	340.2	18.6	[14]
Hematite $\alpha\text{-}Fe_2O_3$	9-12	rodlike	-	250	0.02	[16]
	215×28	rodlike	-	46.94	$2.754\times 10^{-3}$	
	$\sim 400$	rhombohedral	-	99.21	$1.657\times 10^{-3}$	[15]
	$\sim 230$	rhombohedral	-	77.75	$1.043\times 10^{-3}$	
	19	rodlike	-	31	$1.6\times 10^{-3}$	[13]
Maghemite $\gamma\text{-}Fe_2O_3$	46	cubes	-	10	$6.1\times 10^{-4}$	
	36	cubes	8.6	106	1.9	[13]
	8.7	roughly spherical	72**	200**	-	
	4.6	roughly spherical	55* <sup>**</sup>	510**	-	[5]
	2.7	roughly spherical	48* <sup>**</sup>	680**	-	
	$\sim 200$	tubes	42.7	342.2	13.56	[14]

\*The measurement was made under non-saturated magnetic hysteresis loops.

\*\*Determination at a temperature of 5 K.

Electrical resistivity measurements in magnetite films prepared by different techniques reveal that the metal-insulator transition in the films is dependent on the deposition conditions and the film thickness;  $T_v$  estimations lie between 75 and 165 K for magnetite films prepared by different methods [4, 44, 47, 48, 49]. Figure 3 shows the temperature dependence of the electrical resistivity ( $\rho$ ) for magnetite films prepared by different authors using PLD. For all samples, the semiconductor like behavior can be observed at lower temperatures; however, at higher temperatures of around 100 K, abrupt decreases of  $\rho$  are observed. From this abrupt change of  $\rho$ , the  $T_v$  values are measured. The difference of  $T_v$  for films with respect to the bulk value ( $\sim 120$  K) has been associated with the residual strain of lattice mismatch between the substrate and the film. However, the lowest value ( $\sim 75$  K), which differs substantially from the bulk, is due to the presence of  $Fe_2O_3$  [44]. Pure magnetite exhibits magnetoresistance ( $MR$ ); this is defined as  $MR = [R_{(H)} - R_{(0)}] / R_{(0)}$ , where  $R_{(0)}$  is the resistance at zero magnetic field ( $H$ ) and  $R_{(H)}$  is the measurement at the applied field. Typical  $MR$  measurements with respect to temperature show a peak close to  $T_v$  [48]. For sputtered films

with magnetic fields in the range of 1-5 T [44], the  $MR$  remained around 8% to 10% at diverse temperatures; for comparison,  $MR$  up to 16% in a magnetic field of 7.7 T was observed for a magnetite single crystal near  $T_v$  [49]. The small  $MR$  values exhibited in sputtered magnetite films have been attributed to the intergranular transport of spin polarized electrons.

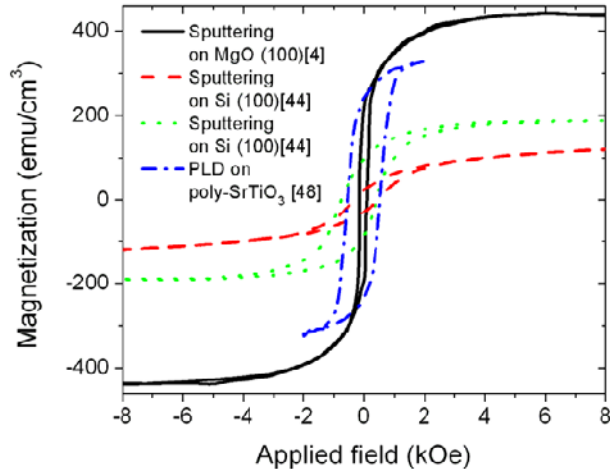


Figure 2. Magnetization hysteresis curves measured at 300 K for magnetite films prepared by sputtering and PLD on different substrates at various deposition conditions. Films deposited at optimal conditions with appropriate thicknesses display clear saturation magnetizations such as the sputtered films prepared by Soeya et al. and Hong et al. [4, 44]. The difference in the magnetization saturation values is due to the difference in the deposition temperature. Films deposited at room temperature show a  $M_s = 190.6$  emu/cm<sup>3</sup> [44], while the films deposited at 573 K show a  $M_s$  of 430 emu/cm<sup>3</sup> [4].

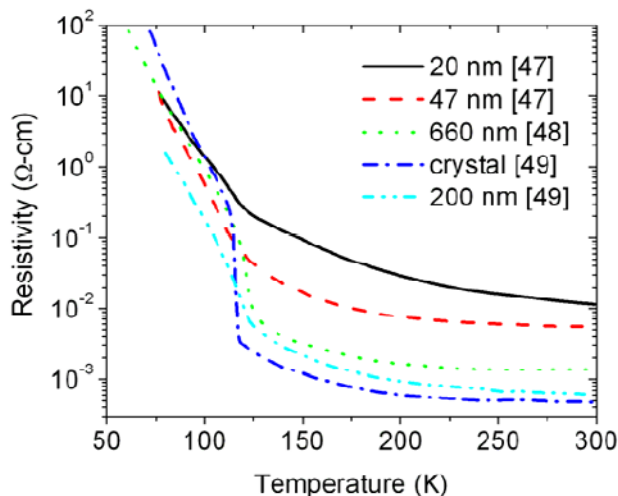


Figure 3. Electrical resistivity as a function of temperature for magnetite films with different thicknesses prepared by PLD for different authors. For comparison, the resistivity of single crystal magnetite is included.

### 3.2. Optical Properties

The optical properties of iron oxides are very important for designing electrochromic devices, photoelectrochemical generation of hydrogen, solar radiation filters, etc. [8, 9, 10, 11]. Magnetite and wustite show thermally induced electronic transitions assigned to intervalence charge transference; for this reason they exhibit absorption in the visible and near-IR region [55]. Maghemite and hematite are insulators and do not present any absorption in the near-IR region. The oxidation process of magnetite nanoparticles to maghemite has been monitored by the loss of optical absorption in the near-IR region [55]. For hematite films, the direct optical band gap determined through Tauc plots ranges from 2.0 to 2.7 eV [43, 52, 53], while the indirect transition energy is around 1.9 eV [52]. Direct band gaps of 1.73 and 1.97 eV are reported for amorphous and  $\beta$ -Fe<sub>2</sub>O<sub>3</sub> films, respectively [42]. The band gap of bulk maghemite is 2.0 eV [54], while maghemite nanoparticles exhibit an energy gap of 2.47 eV due to the quantum confinement effects [56].

### 3.3. Mossbauer Spectroscopy and X-Ray Photoelectron Spectroscopy (XPS)

Mossbauer spectroscopic studies of iron oxide nanostructures have been extensively reported. One group reported a study on the iron oxides, noting that there was difficulty in guaranteeing complete stoichiometry [57]. Similar studies have been conducted on nanoparticle iron oxides as part of a composite system with polymers [58], while yet another study was directed at the iron oxides and their stability against further oxidation [41]. Mossbauer studies have been reported for nanoparticles and thin films of several of the polymorphic phases such as hematite [9, 17, 40], maghemite [5, 39], magnetite [21, 24, 50] and wustite [24, 54], and other ferrites, as well as nanoparticles of iron oxides that have been coated with other oxides [35, 38]. Additionally, Mossbauer studies have shown the evidence of the presence of an amorphous, spin-glass like phase due to spin frustration at the Fe<sub>x</sub>O/Fe<sub>3</sub>O<sub>4</sub> interface [24].

X-ray photoelectron spectroscopy (XPS) has been widely used for determination of the composition and chemical states of many systems, including magnetite films [44], hematite films [8, 52], iron oxide nanotubes [14], crystals synthesized using copolymer micelles [59], and the production of iron oxide nanoparticles by laser precursors [60]. Nanoparticles of maghemite made by electrodeposition also have been studied by X-ray photoelectron spectroscopy [61]. The Fe 2p<sub>1/2</sub> and Fe 2p<sub>3/2</sub> orbitals can be used for the study of the iron oxide phases such as magnetite, hematite, and wustite. However, there is a wide deviation in the published values at the NIST XPS-Database [62]; e.g., wustite presents a variation of 1.1 eV in the Fe 2p<sub>1/2</sub> peak, while magnetite exhibits a difference of 1.5 eV in the same orbital, which lies at around 710.4 eV [62]. Despite this, XPS is a powerful characterization technique used to determine the purity of magnetite films; e.g., the features that distinguish magnetite from maghemite are the broadening of the Fe 2p<sub>1/2</sub> and Fe 2p<sub>3/2</sub> peaks and the absence of a satellite line located at ~718 eV [44].

## REFERENCES

- [1] L.D. Marks. *Rep. Prog. Phys.* 57 (1994) 603-649.
- [2] B. Chertok, B.A. Moffat, A.E. David, F. Yu, C. Bergemann, B.D. Ross, V.C. Yang. *Biomaterials.* 29 (2008) 487-496.
- [3] C.T. Yavuz, et al. *Science.* 314 (2006) 964-967.
- [4] S. Soeya, J. Hayakawa, H. Takahashi, K. Ito, C. Yamamoto, A. Kida, H. Asano, M. Matsui. *Appl. Phys. Lett.* 80 (2002) 823-825.
- [5] D. Fiorani, A. M. Testa, F. Lucari, F. D'Orazio, H. Romero. *Physica B* 320 (2002) 122-126.
- [6] H. Itoh, T. Sugimoto. *J. Colloid Interface Sci.* 265 (2003) 283–295.
- [7] M. H. Sousa, J. C. Rubim, P. G. Sobrinho and F. A. Tourinho. *J. Magn. Magn. Mater.* 225 (2001) 67-72.
- [8] Z. Wang, X. Hu, P. Kall, U. Helmersson. *Chem. Mater.* 13 (2001) 1976-1983.
- [9] D. Larcher, C. Masquelier, D. Bonnin, Y. Chabre, V. Masson, J.-B. Leriche, J.-M. Tarascona. *J. Electrochem. Soc.* 150 (2003) A133-A139.
- [10] E.L. Miller, D. Paluselli, B. Marsen, R.E. Rocheleau. *Solar Energy Mater. Solar Cells.* 88 (2005) 131–144
- [11] J. Chavez-Galan, R. Almanza. *Solar Energy.* 81 (2007) 13-19.
- [12] R.F. Vandenberghe, C.A. Barreto, GM. da Costa, E. Van San, E. De Grave. *Hyp. Interact.* 126 (2000) 247-259.
- [13] Y.C. Zhang, J.Y. Tang, X.Y. Hu. *J. Alloys Compounds.* 462 (2008) 24–28.
- [14] B. Lv, Y. Xu, D. Wu, Y. Sun. *Particuology.* (2008), doi:10.1016/j.partic.2008.04.006.
- [15] Z. Jing, S. Wu. *Mater. Lett.* 58 (2004) 3637 – 3640.
- [16] S. Mandal, A.H.E. Muller. *Mater. Chem. Phys.* 111 (2008) 438–443.
- [17] S. Giri, S. Samanta, S. Maji, S. Ganguli, A. Bhaumik. *J. Magn. Magn. Mater.* 285 (2005) 296–302.
- [18] A. Navrotsky, L. Mazeina, J. Majzlan. *Science.* 319 (2008) 1635-1638.
- [19] T. Chen, H. Xu, Q. Xie, J. Chen, J. Ji, H. Lu. *Earth Planetary Sci. Lett.* 240 (2005) 790-802.
- [20] F. Walz. *J. Phys.: Condens. Matter.* 14 (2002) R285-R340.
- [21] G.F. Goya, T.S. Berquo, F.C. Fonseca, M.P. Morales. *J. Appl. Phys.* 94 (2003) 3520-3528.
- [22] F.Koch J. B.Cohen. *Acta Crystallogr. B* 25 (1969) 275-287.
- [23] J.D. Hodge, H.K. Bowen. *J. Am. Ceram. Soc.* 64 (1981) 220 – 223.
- [24] G.C. Papaefthymiou, F.X. Redl, C.T. Black, R.L. Sandstrom, M. Yin, C.B. Murray, S.P. O'Brien. *Hyperfine Interact.* 165 (2005) 239–245.
- [25] M. Gheisari, M. Mozaffari, M. Acet, J. Amighian. *J. Magn. Magn. Mater.* 320 (2008) 2618– 2621.
- [26] M. Yin, Z. Chen, B. Deegan, S. O'Brien. *J. Mater. Res.* 22 (2007) 1987-1995.
- [27] A.K. Giri, E.M. Kirkpatrick, P. Moongkhamklang, S. A. Majetich, V.G. Harris. *Appl. Phys. Lett.* 80 (2002) 2341-2443.
- [28] Q. Chen, Z.J. Zhang. *Appl. Phys. Lett.* 73 (1998) 3156-3158.
- [29] S.A. Morrison, C.L. Cahill, E.E. Carpenter. *J. Appl. Phys.* 95 (2004) 6392-6395.

- [30] S. Son, M. Taheri, E. Carpenter, V. G. Harris, M. E. McHenry. *J. Appl. Phys.* 91 (2002) 7589-7591.
- [31] F. Padella, C. Alvani, A. La Barbera, G. Ennas, R. Liberatore, F. Varsano. *Mater. Chem. Phys.* 90 (2005) 172–177.
- [32] N. Das, R. Majumdar, A. Sen, H.S. Maiti. *Materials Letters.* 61 (2007) 2100-2104.
- [33] M.M. Haque, M. Huq, M.A. Hakim. *J. Magn. Magn. Mater.* 320 (2008) 2792– 2799.
- [34] S.B. Narang, C. Singh, Y. Bai, I.S. Hudiara. *Mater. Chem. Phys.* 111 (2008) 225–231.
- [35] P. C. Morais. *Hyperfine Interact.* (2008), doi 10.1007/s10751-008-9609-9.
- [36] H.L. Liu, S.P. Ko, J.H. Wu, M.H. Jung, J.H. Min, J.H. Lee, B.H. An, Y.K. Kim. *J. Magn. Magn. Mater.* 310 (2007) e815–e817.
- [37] W. Cai, J. Wan. *J. Colloid Interface Sci.* 305 (2007) 366-370.
- [38] T. Tago, T. Hatsuta, K. Miyajima, M. Kishida, S. Tashiro, K. Wakabayashi. *J. Am. Ceram. Soc.* 85 (2002) 2188–2194.
- [39] B. Martinez, A. Roig, E-Molins, T. Gonzalez-Carreno, C. J. Serna. *J. Appl. Phys.* 83 (1998) 3256-3262.
- [40] S. Figueroa, J. Desimoni, P.C. Rivas, M.M. Cervera, M.C. Caracoche. *Chem. Mater.* 17 (2005) 3486-3491.
- [41] L.T. Kuhn, A. Bojesen, L. Timmermann, M. M. Nielsen, S Morup. *J. Phys.: Condens. Matter.* 14 (2002) 13551–13567
- [42] T. Maruyama, T. Kanagawa. *J. Electrochem. Soc.* 143 (1996) 1675-1677.
- [43] S. Mathur, V. Sivakov, H. Shen, S. Barth, C. Cavelius, A. Nilsson, P. Kuhn. *Thin Solid Films.* 502 (2006) 88-93.
- [44] J.P. Hong, S.B. Lee, Y.W. Jung, J.H. Lee, K.S. Yoon, K.W. Kim, C.H. Lee, M.H. Jung. *Appl. Phys. Lett.* 83 (2003) 1590-1592.
- [45] C.D. Park, D. Magana, A. E. Stiegman. *Chem. Mater.* 19 (2007) 677-683
- [46] T. Tepper, C.A. Ross. *J. Appl. Phys.* 91 (2002) 4453-4456.
- [47] M.G. Chapline, S.X. Wang. *J. Appl. Phys.* 97 (2005) 123901.
- [48] X.W. Li, A. Gupta, G. Xiao, G.Q. Gong. *J. Appl. Phys.* 83 (1998) 7049-7051.
- [49] M. Ziese, H.J. Blythe. *J. Phys.: Condens. Matter.* 12 (2000) 13-28.
- [50] T. Hibma, F.C. Voogt, L. Niesen, P.A.A. van der Heijden, W.J.M. de Jonge, J.J.T.M. Donkers, P.J. van der Zaag. *J. Appl. Phys.* 85 (1999) 5291-5293.
- [51] S. K. Arora, R.G.S. Sofin, I.V. Shvets, M. Luysberg. *J. Appl. Phys.* 100 (2006) 073908.
- [52] L. Dghoughi, B. Elidrissi, C. Bernede, M. Addou, M.A. Lamrani, M. Regragui, H. Erguig. *Applied Surface Science.* 253 (2006) 1823–1829
- [53] J.D. Desai, H.M. Pathan, S.K. Min, K.D. Jung, O.S. Joo. *Appl. Surf. Sci.* 252 (2006) 2251-2258.
- [54] D.V. Dimitrov, K. Unruh, G.C. Hadjipanayis, V. Papaefthymiou, A. Simopoulos. *Phys. Rev. B* 59 (1999) 14 499- 504.
- [55] J. Tang, M. Myers, K.A. Bosnick, L.E. Brus. *J. Phys. Chem. B* 107 (2003) 7501-7506.
- [56] C.T. Wang. *J. Non-Cryst. Solids* 353 (2007) 1126-1133.
- [57] S. Kamali-M., T. Ericsson, R. Wappling. *Thin Solid Films.* 215, (2006) 721-723.
- [58] A. A. Novakova, V. Y. Lanchinskaya, A. V. Volkov, T. S. Gendler, T. Y. Kiseleva, M. A. Moskvina, S. B. Zezin. *J. Magn. Magn. Mater.* 258-259, (2003) 354-357.
- [59] S.H. Yun, B.H. Sohn, J.C. Jung, W.C. Zin, J.K. Lee, O. Song. *Langmuir.* 21 (2005) 6548-6552.

- [60] S. Martell, A. Mancini, R. Giorgi, R. Alexandrescu, S. Cojocaru, A. Crunteanu, I. Voicu, M. Balu, I. Morjan. *Appl. Surf. Sci.* 154-155 (2000) 353- 359.
- [61] H. Park, P. Ayala, M. A. Deshusses, A. Mulchandani, H. Choi, N. V. Myung. *Chem. Engineer. J.* 139 (2008) 208-212.
- [62] NIST X-ray Photoelectron Spectroscopy Database. NIST Standard Reference Database 20, Version 3.5. <http://srdata.nist.gov/xps>.

# INDEX

## A

- A $\beta$ , 90  
abatement, 138  
absorption, 22, 23, 46, 58, 59, 70, 71, 138, 149, 162, 163, 164, 166, 172, 191  
absorption coefficient, 149, 162  
academic, 9  
accidental, 43  
accuracy, 126  
acetylene, 18, 28  
acid, 21, 94, 95, 96, 101, 102, 137, 139, 153, 154, 159  
acidic, 70  
activation, 138, 142, 186, 188  
activation energy, 188  
active site, 15  
additives, 158  
adhesion, 148, 150  
adjustment, 64  
administration, 94, 97, 100  
adsorption, 15, 69, 70, 71, 72, 73, 76, 77, 139, 146, 148, 160, 161, 167, 168, 174, 177  
adults, 80  
aerosol, 185, 186  
aerospace, 33  
AFM, 15, 18, 19, 27, 147, 155, 169  
Africa, 32, 38  
Ag, 147, 148, 149, 150, 151, 152, 154, 155, 156, 157, 159, 161, 162, 163, 165, 166, 167, 168, 170, 171, 172, 174, 175  
age, 10, 17, 37, 80  
ageing, 150, 151, 152, 153, 173  
agent, 61, 63, 96, 150, 151, 152, 158, 159  
agents, 70, 138, 145, 149, 152, 153, 154, 158, 159, 169, 176, 186  
aggregates, 22  
aggregation, 63, 148, 149, 157, 158, 186  
aggregation process, 149  
aid, 10, 65  
air, 19, 30, 46, 62, 64, 139, 168, 187  
alcohol, 139  
alcohols, 63  
algorithm, 4, 126  
alkaline, 21, 64  
alkaline media, 64  
alloys, 46  
alternative, 42, 148, 149, 186  
aluminum, 42, 43, 44, 48  
American Association for the Advancement of Science, 149, 157, 163  
amine, 151  
amino, 26, 69, 70, 71, 75, 77  
amino acids, 26  
amino groups, 69, 70, 71, 75, 77  
ammonium, 151  
ammonium hydroxide, 151  
amorphous, 158, 191  
amplitude, 166  
Amsterdam, 8, 135  
analgesic, 100  
analytical techniques, 77  
anisotropy, 146, 188  
annealing, 19, 186, 187  
anodes, 18, 27  
antiferromagnet, 184  
antiferromagnetic, 184  
antigen, 96  
application, vii, 21, 58, 61, 62, 80, 111, 126, 146, 148, 173, 177, 178  
aqueous solution, 22, 26, 153, 169, 171, 173, 178, 186, 187  
aqueous solutions, 26, 186, 187  
ARC, 178  
Argentina, 37

arsenic, 69, 70, 71, 76, 77  
 ascorbic, 153, 154  
 ascorbic acid, 153, 154  
 aspect ratio, 164, 168, 178, 188  
 assignment, 164  
 assimilation, 11  
 asymptotically, 130, 135  
 atmosphere, 187  
 atomic force microscopy, 10, 155  
 atomic force microscopy (AFM), 155  
 atomic theory, 41, 47  
 atoms, 18, 62, 63, 104, 105, 106, 109, 126, 151, 154, 156, 158, 160, 161, 170, 177, 184  
 attachment, 77  
 Au nanoparticles, 62, 63, 64, 65, 67  
 Australia, 145, 178  
 autonomy, 11  
 availability, 62, 147  
 avoidance, 176  
 awareness, 10

**B**

backscattered, 19  
 band gap, 191  
 bandgap, 21  
 barrier, 58, 100, 188  
 barriers, 115, 116  
 batteries, 183  
 beams, 55  
 behavior, 18, 28, 53, 55, 110, 112, 113, 141, 142, 184, 187, 188, 189  
 benchmarks, 80  
 bending, 157  
 benefits, 10, 32, 37, 161  
 benzene, 18, 27  
 bias, 21  
 binding, 22, 109, 111, 151, 158, 159, 160, 161, 174  
 binding energies, 22  
 binding energy, 160  
 biocompatible, 183  
 biodegradable, 93, 94, 95  
 biodegradables, 93  
 biomolecular, 167  
 biomolecules, 96, 102  
 biosensors, 168  
 biotechnology, 14, 34  
 bipolar, 53  
 bismuth, 186  
 blocks, 73  
 blood, 96, 101  
 blood stream, 101

blood vessels, 101  
 Bohr, 47, 57  
 boiling, 152, 186  
 Bolivarian Republic of Venezuela, 39  
 Boltzman constant, 58  
 Boltzmann constant, 188  
 bonding, 176  
 bottom-up, vii  
 boundary conditions, 4, 50  
 brain, 33  
 brain drain, 33  
 branched polymers, 70  
 Brazil, 33, 36, 37, 117  
 Brazilian, 36  
 bremsstrahlung, 42, 43, 44  
 bulk crystal, 110, 113

**C**

cadmium, 21, 41  
 calibration, 44  
 Canada, 32, 71  
 cancer, 183  
 candidates, 63  
 capillary, 148  
 caprolactone, 96, 102  
 capsule, 100  
 carbon, 18, 19, 27, 28, 61, 64, 65, 101, 137, 138, 142, 143, 144, 149, 160, 174  
 carbon atoms, 160  
 carbon dioxide, 101, 138  
 carbon film, 149  
 carbon monoxide, 137, 138, 142, 143, 144  
 carbon nanotubes, 18  
 carboxyl, 70, 75, 151  
 carboxyl groups, 75, 151  
 Caribbean, 32  
 carrier, 186  
 catalysis, 15, 61, 62, 67, 70  
 catalyst, 64, 65, 66, 67, 138, 139  
 catalytic activity, 63, 64, 137, 138, 139, 142, 144  
 catalytic effect, 64  
 cathode, 63  
 cell, 5, 15, 21, 119, 156  
 cell lines, 15  
 cell phones, 119  
 ceramic, 186  
 cerium, 138, 141, 168  
 cesium, 43  
 chalcogenides, 22  
 channels, 70, 126  
 charge density, 50  
 charged particle, 3

- chemical deposition, 22, 27  
chemical energy, 62  
chemical interaction, 77  
chemical properties, 70, 145  
chemical reactions, 186  
chemical reactivity, 145, 175  
chemical sensing, 177  
chemical vapor deposition, 186  
chemiluminescence, 168  
chemisorption, 167  
children, 10, 11, 12, 13, 80  
Chile, 33, 34, 35, 36  
China, 117, 178  
chitosan, 96, 102  
chloride, 147, 187  
chromium, 69, 70, 71, 76, 77  
classical, 3  
clean energy, 62  
clinical trial, 97, 98  
clinical trials, 98  
closed-loop, 132, 135  
clusters, 63, 72, 109, 117, 119, 120, 157, 161, 187  
Co, 45, 47, 153, 168, 180, 186  
CO<sub>2</sub>, 138, 139  
coal, 18  
coatings, 21, 27  
cognitive development, 80, 89, 91  
cognitive level, 86, 89  
cognitive science, vii  
coherence, 188  
collaboration, 12, 13  
colleges, 90  
collisions, 126  
colloidal particles, 2, 126  
colloids, 62, 148, 149, 153, 162, 172, 176  
colors, 160  
community, 9, 12, 13, 26  
compensation, 49  
competitiveness, 33, 36, 37  
complex systems, 2  
complexity, 119, 161, 177  
compliance, 98  
components, 11, 46, 67, 97, 103  
composites, 26, 69, 70, 74, 76  
composition, 47, 62, 70, 104, 105, 110, 137, 162, 163, 184, 185, 186, 191  
compounds, 68, 70, 94, 137, 138, 139, 140, 141, 142, 143, 144, 170, 171, 185, 186  
computational modeling, 159  
computer science, 12  
computer simulation, 8  
computer simulations, 2  
computing, 130  
concentration, 71, 105, 119, 138, 155, 169, 170, 172  
conceptualization, 86  
concordance, 106  
concrete, 80, 86, 87  
condensation, 186  
condensed matter, 109  
conduction, 113, 162  
conductivity, 139, 184  
conductor, 49  
configuration, 2, 4, 51, 55, 118, 147  
confinement, 58, 59, 167, 191  
confrontation, 89  
conservation, 6, 79, 83, 86, 87, 89  
construction, 18, 28, 183  
consumption, 62, 150  
contaminants, 138  
control, 26, 62, 63, 64, 70, 74, 83, 86, 87, 97, 98, 100, 121, 125, 126, 127, 129, 130, 131, 133, 135, 138, 145, 146, 147, 148, 150, 152, 155, 157, 158, 159, 160, 161, 173, 177, 186  
convergence, 4, 130  
conversion, 21, 62, 137, 142, 143, 144, 148, 149  
cooling, 99  
copolymer, 191  
copolymer micelles, 191  
copper, 42, 65, 146, 150  
core-shell, 185  
correlation, 79, 87, 166, 188  
Costa Rica, 37  
cost-effective, 62  
costs, 62  
coupling, 70, 167  
covering, 145  
CRC, 182  
Croatia, 15  
cross-sectional, 22  
crystal growth, 59, 155, 159, 160  
crystal structure, 74, 75, 149, 155, 157  
crystal structures, 155  
crystalline, 22, 74, 104, 157, 158, 160, 176, 183, 186  
crystallization, 161  
crystals, 20, 26, 43, 59, 60, 141, 148, 155, 186, 191  
CSVT, 22  
CTAB, 150, 152, 153, 158, 159  
cultural factors, 13  
culture, 15  
curiosity, 9, 10  
curriculum, 28, 93  
CVD, 186, 187

cycles, 43  
cysteine, 171, 172, 174  
cytoskeleton, 126

**D**

damping, 131, 172  
danger, 11  
data collection, 42  
database, 46  
decay, 21, 42, 49, 55  
decisions, 27  
decomposition, 18, 27, 151, 185, 186  
defects, 110, 148, 158, 184  
deficiency, 17, 184  
definition, vii, 111, 118, 129, 134  
degenerate, 158  
dehydrate, 148  
delivery, 96, 102  
dendrimers, 69, 70, 71, 73, 74, 75, 76, 77, 78  
density, 2, 6, 50, 82, 110, 111, 112, 113, 114, 145, 155, 159, 171, 188  
density functional theory, 155, 159  
Department of Education, viii  
depolarization, 43  
deposition, 15, 19, 22, 27, 147, 168, 186, 187, 189, 190  
deposition rate, 186, 187  
derivatives, 118, 128, 129, 130  
desorption, 168  
destruction, 104  
detection, 167, 168, 169, 171, 172, 178  
developed countries, 33, 35, 36  
developing countries, 32, 33  
developing world, 37  
deviation, 191  
DFT, 145, 159, 160, 177  
didactic teaching, 80  
dielectric constant, 3  
dielectric materials, 162  
dielectric permittivity, 3  
diffraction, 49, 55, 60, 69, 72, 74, 139, 140, 143, 149, 155, 156, 175  
diffuse reflectance, 72  
diffusion, 26, 158, 161  
dimensionality, 109  
dimethylformamide, 151  
diodes, 149  
diphtheria, 96  
dipole, 126, 149, 157, 161, 164, 165  
direct observation, 110  
disappointment, 12  
discipline, vii

discourse, 37  
discs, 1, 2, 3, 146  
dislocation, 156  
dislocations, 148, 157  
disorder, 104, 106, 107, 184  
disordered systems, 115  
dispersion, 62, 64, 100, 147, 163, 168, 169  
displacement, 142, 175  
dissatisfaction, 11  
dissociation, 157, 159  
distilled water, 71  
distribution, 1, 2, 6, 7, 19, 20, 27, 61, 65, 80, 127, 148, 166, 168, 185, 186, 188  
distribution function, 6, 7  
diversity, 78  
DMF, 151, 152, 168  
DNA, 94, 96  
doors, 138  
doped, 59, 115, 116, 138, 153  
DRIFT, 69, 75  
drug delivery, 183  
drugs, 13, 94, 100, 101  
drying, 186  
duration, 43  
dyes, 26, 78  
dynamical systems, 126

**E**

ears, 34, 58  
earth, 138  
economic development, 33  
economic resources, 11  
education, viii, 11, 14, 117  
educational research, 80  
educators, 10, 12, 13, 14  
Einstein, Albert, 18, 28  
electric arc, 18  
electric energy, 62  
electric field, 49, 52, 53, 54, 55, 162, 167  
electrical characterization, 27  
electrical conductivity, 184  
electrical properties, 188  
electricity, 43  
electrodeposition, 22, 191  
electrodes, 18, 21, 28, 167  
electromagnetic, 26, 49, 50, 146, 162, 163, 167, 178  
electromagnetic fields, 162, 167  
electromagnetic wave, 49  
electron, 5, 10, 18, 19, 20, 26, 42, 58, 59, 66, 72, 109, 110, 115, 148, 149, 155, 164, 166, 169, 170, 171, 172, 188

electron beam, 19, 66, 148, 149  
electron charge, 5  
electron density, 171  
electron diffraction, 66  
electron microscopy, 10, 18, 65, 155  
electronic structure, 110, 111  
electrons, 42, 43, 59, 162, 190  
electrostatic interactions, 1, 2, 76  
elementary particle, 27  
elementary school, 9  
email, 119  
emancipation, 27  
emerging economies, vii  
emission, 47, 58, 110, 138, 149  
employers, 29  
emulsions, 96, 186  
encapsulated, 42, 78, 94, 99, 147  
encapsulation, 96, 99, 148  
energy, 1, 2, 3, 4, 5, 6, 7, 15, 17, 21, 23, 26, 32, 41, 42, 44, 46, 47, 57, 58, 59, 62, 66, 70, 72, 83, 103, 105, 110, 111, 112, 113, 114, 147, 156, 160, 161, 166, 172, 184, 185, 186, 187, 188, 191  
energy consumption, 62  
energy density, 186  
England, 80  
enthusiasm, 10  
entrainment, 53, 55  
entropy, 103, 105, 118  
environment, 135, 138, 167  
environmental protection, 13  
epistemology, 79  
epitaxy, 177, 186  
epoxy, 19  
equilibrium, 103, 104  
erosion, 18, 27  
estimator, 131  
estrangement, 11  
etching, 175  
ethanol, 65  
ethylene, 68, 152, 167, 186  
ethylene glycol, 68, 152, 186  
Euler-Lagrange equations, 127  
European Union, 117  
evaporation, 26, 96, 148, 186  
evolution, 157, 171, 174  
EXAFS, 29  
excitation, 19, 44, 47, 148, 150, 157, 167, 172  
experimental design, 99  
exploitation, 36, 146  
exports, 32, 33  
exposure, 43  
extinction, 162, 163, 164, 165, 167

extraction, 98

## F

fabricate, 174  
fabrication, 59, 183, 184  
face-to-face interaction, 119  
family, 11, 78  
faults, 150, 155, 157, 177  
feedback, 135  
ferrite, 184, 185, 186, 188  
ferrocenyl, 70  
ferromagnetic, 184, 185  
ferromagnetism, 188  
Feynman, 18, 19, 26  
fiber, 18, 28, 141  
fibers, 18, 27  
film, 19, 20, 21, 22, 24, 25, 103, 148, 149, 167, 186, 189  
film thickness, 103, 189  
films, 21, 104, 162, 168, 183, 186, 187, 188, 189, 190, 191  
filters, 47, 183, 187, 191  
financial support, 14, 27, 119, 178  
financing, 34, 36, 37  
finite differences, 162  
first principles, 110  
flatness, 125, 126, 129, 135  
flexibility, 163  
flow, 64, 82, 83, 87, 99, 117, 126  
flow of capital, 117  
flow rate, 99  
fluctuations, 82, 119, 120, 135  
fluid, 82, 83  
fluorescence, 41, 42, 47, 138  
focusing, 136  
Fourier, 66, 69, 155, 156  
free energy, 103, 105  
friction, 83, 126, 135  
frustration, 11, 191  
fuel, 61, 62  
fuel cell, 61, 62  
funding, 10, 119, 120  
funds, vii, 34, 35, 36  
fusion, 146, 148, 150, 157, 177  
FWHM, 45, 109, 110, 111, 112, 113, 114, 115

## G

G8, 38  
GaAs, 59, 112, 113, 114, 116  
games, 13

- gamma-ray, 42  
 gas, 97, 144, 186  
 gases, 138, 139  
 Gaussian, 127  
 GDP, 36  
 gel, 139  
 gels, 70  
 gender, 118  
 generation, 19, 26, 32, 42, 47, 49, 62, 69, 70, 71, 77, 162, 187, 191  
 Germany, 181  
 glass, 19, 21, 24, 27, 59, 147, 148, 168, 187  
 glasses, 59  
 gold, 61, 67, 72, 146, 147, 149, 156, 160, 165, 166, 167, 174, 175  
 gold nanoparticles, 147  
 government, iv, 37  
 grades, 87  
 grafting, 70  
 grains, 19, 189  
 graph, 19  
 graphite, 18, 27  
 Gross Domestic Product (GDP), 36  
 ground state energy, 57, 58  
 group size, 118  
 groups, vii, viii, 12, 69, 70, 71, 72, 73, 74, 75, 77, 85, 117, 149, 151, 152, 164, 166, 174, 184  
 growth, 18, 27, 32, 33, 59, 62, 63, 145, 146, 148, 149, 150, 151, 152, 153, 155, 156, 157, 158, 159, 160, 161, 173, 174, 175, 176, 177, 186  
 growth mechanism, 145, 146, 149, 150, 152, 155, 159, 160, 161, 176, 177  
 growth rate, 161  
 guidelines, 139

**H**

- $H_2$ , 62, 63, 64, 187  
 handling, 26, 27  
 health, 70  
 heat, 43, 64, 187  
 heating, 62, 139, 150, 151, 152  
 heavy metal, 70, 71  
 heavy metals, 70, 71  
 height, 66, 82, 168  
 helium, 71, 139  
 hematite, 183, 184, 185, 186, 187, 191  
 hepatitis B, 96, 102  
 heterojunctions, 21  
 heuristic, vii  
 hexagonal lattice, 69  
 high resolution, 18, 66, 166  
 high tech, 33

- high temperature, 47  
 higher education, 36  
 homeostasis, 117, 118  
 homogeneity, 19  
 homogenisation, 96, 97, 98, 102  
 homogenous, 48, 141, 143  
 host, 114, 139  
 HRTEM, 155, 156  
 human, 12, 18, 27, 29, 70, 93  
 human resources, 12, 29  
 hybrid, 70, 184  
 hydrazine, 150  
 hydro, 70, 78, 138  
 hydrocarbon, 62  
 hydrocarbons, 138  
 hydrogen, 18, 183, 187, 191  
 hydrogenation, 62, 63, 138  
 hydrophilic, 70, 78  
 hydrophobic, 70, 78  
 hydrothermal, 70, 145, 147, 153, 177, 185, 186  
 hydrothermal synthesis, 185  
 hydroxide, 21, 64, 65, 66, 151  
 hydroxides, 64  
 hydroxyl, 71, 73, 74, 77, 152  
 hydroxyl groups, 71, 73, 74, 77  
 hypothesis, 49, 86  
 hysteresis, 189, 190  
 hysteresis loop, 189

**I**

- IBM, 18  
 ICM, 33, 34, 35, 38  
 id, 38, 85  
 identification, 15, 42, 61, 83, 86  
 illumination, 21, 55, 148, 149, 150, 158  
 images, 18, 19, 139, 141, 151, 153, 154, 155, 158, 159, 173, 176  
 imaging, 72, 183  
 immune response, 102  
 impregnation, 61, 62, 64, 66, 139  
 impurities, 47, 111  
 in situ, 61  
 in vivo, 97  
 incomplete combustion, 138  
 incompressible, 81, 82, 83  
 India, 117  
 indication, 21  
 indices, 168  
 indium, 138  
 inducer, 175  
 industrial, 15, 32, 33  
 industrial application, 15

industrial revolution, 32  
industry, vii, 12, 32, 33, 37, 138  
inequity, 37  
inertia, 58  
infants, 11, 13  
infinite, 57, 58, 59  
infrared, 72, 75, 76, 149  
infrared spectroscopy, 75  
infrastructure, 10, 33  
inhomogeneity, 158  
initiation, 79  
injection, 169  
innovation, 32, 33, 36, 38  
inorganic, 26, 70, 168, 169, 170, 174, 178  
inspection, 47  
inspiration, 80  
institutionalization, 117, 118  
institutions, 33, 36, 37  
instruction, 10, 12, 42, 91  
instructors, viii, 13  
instruments, vii, 47  
insulators, 191  
integration, 4, 50  
intellect, 10  
intellectual development, 80, 90, 91  
intelligence, 26  
interaction, 3, 4, 5, 19, 61, 62, 64, 65, 66, 93,  
105, 114, 117, 118, 119, 158, 159, 160, 161,  
170, 174  
interactions, 1, 2, 4, 76, 77, 167  
interface, 162, 191  
interference, 187  
internet, 117  
interstitial, 184  
interstitials, 18, 27  
interval, 44, 82, 139  
intrinsic, 110, 111, 112, 114, 150, 161  
investigations, 47  
investment, 33  
ionic, 1, 2, 3, 6, 7, 8, 63, 70, 172  
ionic liquids, 1, 8  
ionic solutions, 2  
ionization, 43  
ions, 15, 21, 62, 76, 77, 148, 149, 150, 151, 152,  
154, 158, 161, 167, 168, 169, 170, 171, 172,  
174, 178, 184  
IOP, 160, 175  
Ireland, 33  
iridium, 138, 144  
iron, 48, 183, 184, 185, 186, 187, 188, 189, 191  
iron deficiency, 184  
irradiation, 45, 149, 158  
island, 155

isotherms, 71  
Israel, 14

## J

Japan, 117  
Jefferson, 180  
job satisfaction, 11  
Josephson junction, 188  
Jung, 193

## K

kinetic energy, 83  
kinetics, 152, 177  
Kirchhoff, 49  
knowledge economy, 31, 36  
Korea, 117

## L

labeling, 146  
labor, vii, 11  
lactic acid, 96, 101, 102  
Lagrangian, 118  
Langmuir, 78, 167, 179, 180, 181, 182, 193  
Langmuir-Blodgett, 167  
language, 11, 37, 38  
lanthanum, 138  
large-scale, 185  
laser, 18, 30, 126, 127, 135, 148, 149, 157, 158,  
166, 186, 191  
lasers, 26  
Latin America, 31, 32, 33, 34, 35, 37, 38  
Latin American countries, 34  
lattice, 18, 26, 103, 104, 138, 149, 155, 156, 163,  
177, 184, 189  
lattice parameters, 26, 156, 177  
law, 35, 36, 47, 117, 119, 120  
laws, 83  
learning, 10, 11, 79, 80  
lens, 126  
lidocaine, 100  
ligand, 157, 158  
ligands, 63, 184  
light emitting diode, 149  
light-induced, 157  
limitation, 160, 177  
limitations, 146, 177  
linear, 20, 26, 29, 44, 129, 162, 166  
linear regression, 44  
links, 13, 33, 35

liquid crystals, 2  
 liquid nitrogen, 72  
 liquid phase, 63  
 liquids, 1, 8  
 lithium, 43, 183  
 lithography, vii, 146, 147, 148  
 living conditions, 11  
 localization, 89, 163  
 London, 38, 48, 67, 101, 102, 179, 182  
 losses, 83  
 low-temperature, 183  
 Lyapunov, 134, 135  
 Lyapunov function, 134  
 lying, 149, 155

## M

M1, 64, 65  
 macrophage, 126  
 maghemite, 183, 184, 185, 186, 187, 191  
 magnetic, 49, 50, 145, 183, 184, 186, 187, 188, 189  
 magnetic field, 50, 188, 189  
 magnetic fluids, 183  
 magnetic moment, 188  
 magnetic properties, 184, 186, 187, 188  
 magnetic resonance imaging, 183  
 magnetite, 183, 184, 185, 186, 187, 188, 189, 190, 191  
 magnetization, 188, 190  
 magnetizations, 184, 187, 190  
 magnetoresistance, 183, 189  
 magnetron sputtering, 187  
 management, 12  
 manipulation, 2, 18  
 manufacturing, 96, 97, 98, 99  
 mapping, 149, 166  
 market, viii, 32, 47  
 Marx, 18  
 Marxism, 28  
 mask, 147  
 mass transfer, 15  
 materials science, 1, 110  
 mathematics, vii, 9  
 matrix, 162, 187  
 MBE, 22, 186  
 MCA, 42, 43  
 measurement, 19, 104, 112, 137, 155, 189  
 measures, 33  
 media, 26, 64, 109, 162, 169, 176, 183  
 medicine, 9, 12, 13, 39, 126  
 melt, 59  
 melting, 104, 152  
 memory, 183  
 men, 13  
 Mesoporus, 78  
 metal ions, 22  
 metal nanoparticles, 63, 146, 158, 159, 162, 166, 167  
 metal-organic compounds, 185  
 metals, 61, 62, 66, 70, 111, 114, 138, 155, 161, 162, 174  
 meteorites, 48  
 methane, 138, 144  
 methanol, 187  
 methyl group, 75  
 methyl groups, 75  
 methylene, 147  
 methylene chloride, 147  
 Mexican, vi, viii, 28, 37, 117, 120  
 Mexico, viii, 1, 10, 11, 14, 15, 28, 29, 33, 36, 37, 57, 60, 71, 93, 101, 117, 118, 119, 183  
 Mexico City, 15, 117  
 mica, 147  
 micelles, 2, 146, 150  
 microemulsion, 185, 186  
 micrometer, 59  
 microorganisms, 93, 94  
 microparticles, 96, 126  
 microscope, 72  
 microscopy, 10, 18, 135, 143, 155, 164  
 microspheres, 102  
 microstructure, 144, 155  
 microtubules, 126  
 microwave, 158  
 migration, 174  
 millennium, 31, 33, 34, 35, 36, 38, 39  
 Millennium Project, 33, 38  
 mining, 35  
 MIT, 121  
 mixing, 99  
 mobility, 138  
 modeling, 146, 177  
 models, 110, 161  
 modern society, 70  
 modules, 80  
 molar ratio, 61, 63, 64, 150, 152, 153  
 molecular beam, 186  
 molecular beam epitaxy, 186  
 molecular biology, vii  
 molecular dynamics, 1, 2, 3, 6, 7, 145, 155, 159  
 molecular weight, 152, 153  
 molecules, 2, 15, 18, 30, 62, 93, 94, 95, 109, 152, 158, 160, 161, 166, 167, 171, 172, 173, 174  
 monochromator, 47  
 monolayer, 19, 105, 148, 157, 167

monolayers, 112, 113, 114, 168  
 monomers, 70  
 Monte Carlo method, 7  
 morphology, 15, 19, 77, 137, 141, 146, 148, 149, 152, 161, 168, 173, 177, 184, 185  
 motion, 3, 4, 6, 81, 82, 83, 126, 132  
 motivation, viii  
 motors, 126  
 movement, 58  
 MSI, 33, 34, 35, 38  
 mucosa, 100  
 mucosal barrier, 94, 101  
 multidisciplinary, 13  
 multiplication, 22  
 multiplier, 105

## N

NaCl, 64, 65  
 nanobelts, 176  
 nanobiotechnology, 34  
 nanocapsules, 35, 93, 94, 95, 96, 97, 99  
 nanocrystal, 150  
 nanocrystals, 59, 150, 152, 154, 175, 184, 186  
 nanocubes, 155, 186, 188  
 nanodevices, 29  
 nanofabrication, 147  
 nanometer, 18  
 nanometers, vii, 17, 58, 162, 173, 176, 177  
 nanoparticles, 61, 62, 63, 64, 65, 66, 67, 68, 96, 97, 102, 145, 146, 148, 149, 152, 153, 154, 155, 158, 159, 160, 161, 162, 164, 166, 167, 168, 173, 174, 175, 183, 184, 185, 186, 188, 189, 191  
 nanorods, 160, 165, 167, 175, 186, 188  
 nanoscience, 9, 10, 11, 12, 13, 26, 34, 35  
 nanostructures, vi, 57, 58, 59, 60, 70, 109, 115, 146, 158, 160, 166, 167, 173, 183, 184, 185, 186, 187, 191  
 nanotechnology, vii, viii, 9, 10, 11, 12, 13, 15, 17, 18, 26, 29, 31, 32, 34, 35, 36, 117  
 nanotubes, 18, 26, 186, 191  
 nanowires, 19, 165, 175, 176  
 nation, 11  
 National Academy of Sciences, 18  
 National Institute of Standards and Technology, 135  
 NATO, 182  
 natural, vii, 36, 70, 79, 80  
 natural resources, 36, 70  
 natural sciences, vii  
 neoliberal, 38  
 network, 33, 36, 37, 78, 138

networking, 36  
 New South Wales, 145  
 New York, 27, 38, 47, 90, 135, 178, 180, 182  
 Newton, 3, 83, 129, 133  
 next generation, 93, 136  
 Ni, 44, 45, 47  
 nickel, 42, 186  
 Nielsen, 193  
 NIST, 191, 194  
 nitrate, 43, 152  
 nitrates, 186  
 nitrogen, 71, 72, 73, 139, 187  
 noble metals, 161  
 noise, 46  
 non-destructive, 41, 42  
 nonlinear optical response, 165  
 normal, 54, 62  
 novel materials, 67, 68  
 n-type, 116  
 nucleation, 15, 151, 153, 156, 177  
 nuclei, 35, 36, 37, 148, 158, 175, 177  
 nucleus, 86  
 Nuevo León, 122  
 numerical aperture, 126

## O

observations, 18, 155, 156, 158, 163, 166, 169, 171, 173, 176, 177  
 OCs, 62  
 OECD, 36, 38  
 oil, 96, 150, 186  
 opposition, 80  
 optical, 19, 20, 21, 23, 26, 27, 29, 49, 53, 55, 58, 59, 125, 126, 127, 133, 135, 136, 145, 146, 161, 162, 164, 165, 166, 167, 168, 173, 177, 178, 191  
 optical absorption coefficient, 21  
 optical density, 22, 23, 59  
 optical microscopy, 164  
 optical properties, 26, 58, 146, 161, 162, 164, 165, 166, 168, 177, 191  
 optical tweezers, 125, 126, 127, 133, 135, 136  
 optics, 19, 29, 56, 110, 135  
 optimization, 117, 161  
 optoelectronic, 21, 62  
 optoelectronic devices, 21, 62  
 organic, 26, 62, 70, 94, 96, 152, 167, 184, 185, 187  
 organic compounds, 62  
 organic solvent, 96, 152, 187  
 Organisation for Economic Co-operation and Development, 38

organometallic, 27  
 orientation, 19, 149, 156, 160, 163, 165, 175  
 orthorhombic, 177, 184  
 oscillation, 162  
 oscillations, 162  
 oscillator, 58  
 Ostwald ripening, 150, 157, 175  
 oxidation, 62, 67, 137, 138, 139, 142, 144, 148, 175, 191  
 oxide, 138, 141, 185, 186, 187, 188, 189, 191  
 oxide nanoparticles, 185, 188, 189, 191  
 oxides, 137, 138, 139, 144, 183, 185, 186, 187, 191  
 oxygen, 138, 144, 186, 187

## P

pain, 98  
 parabolic, 115, 116  
 parameter, 3, 4, 103, 104, 105, 106, 110, 111, 112, 113, 114, 118, 131, 132  
 parents, 11, 13  
 particle morphology, 168  
 particle shape, 155, 158, 161, 169  
 particles, 2, 3, 4, 6, 18, 27, 28, 53, 55, 62, 63, 66, 72, 73, 74, 102, 103, 126, 135, 147, 148, 149, 150, 151, 152, 154, 155, 156, 157, 158, 161, 162, 163, 166, 167, 168, 173, 174, 176, 177, 178, 184, 185, 186, 188  
 partnerships, 37  
 patents, vii  
 path tracking, 133  
 Pb, 44, 45  
 PbS, 22  
 pedagogical, 80  
 pedagogy, 79  
 PEMFC, 62  
 perception, 10, 11, 12, 86  
 periodic, 4, 5, 58, 78, 110  
 permit, 46, 47, 58, 110  
 perovskite, 144  
 perturbations, 99, 131, 169  
 petrochemical, 62  
 pH, 64, 66, 71, 76, 77, 99, 139, 149  
 phagocytosis, 126  
 pharmaceutical, 96, 102  
 pharmaceuticals, 33  
 pharmacological, 94  
 Philadelphia, 182  
 philosophical, viii  
 philosophy, vii, 17  
 phosphate, 168, 171  
 phosphates, 170  
 photoelectron spectroscopy, 191  
 photon, 43, 110, 162  
 photonic, 18  
 photonics, 17  
 photons, 42  
 photosensitivity, 20  
 photovoltaic, 21  
 photovoltaic devices, 21  
 physical properties, 10, 46, 70  
 physicians, 126  
 physicists, 183  
 physicochemical, 67, 145  
 physicochemical properties, 145  
 physics, vii, 8, 9, 12, 28, 29, 41, 57, 59, 60, 91, 109, 110, 174  
 placebo, 99  
 planar, 168  
 planning, 80  
 plasma, 162, 168, 171, 172  
 plasmons, 162  
 platelet, 163  
 platelets, 150, 156  
 platinum, 61, 67  
 play, 13, 18, 37, 151, 158, 165  
 PLD, 148, 186, 187, 189, 190  
 PLGA, 96  
 point defects, 148  
 poisoning, 62  
 Poland, 103, 107  
 polarization, 42, 43, 53, 158, 167, 168  
 politicians, 27  
 politics, 17  
 pollutants, 30, 62  
 pollution, 70, 138  
 poly(vinylpyrrolidone), 148  
 polycrystalline, 148, 186  
 polydispersity, 148  
 polymer, 62, 63, 64, 67, 69, 96, 100, 158  
 polymer molecule, 158  
 polymeric materials, 60  
 polymerization, 70, 94  
 polymers, 70, 94, 95, 152, 158, 191  
 polystyrene, 146, 147, 151  
 polyvinyl alcohol, 62, 96  
 polyvinylpyrrolidone, 63  
 poor, 10, 37  
 population, 11, 37, 85, 86, 149  
 pore, 70, 72, 73, 74, 77  
 pores, 69, 70, 73, 74, 75, 126  
 porous, 69, 71  
 powder, 22, 25, 61, 69, 72  
 powders, 64, 75  
 power, 43, 117, 119, 120, 126, 184, 186, 187

PPA, 147  
 practical activity, 87  
 precipitation, 139, 185, 186  
 president, 32  
 pressure, 37, 82, 83, 96, 99, 102, 186, 187  
 private, 33, 37  
 probabilistic reasoning, 86  
 probability, 118, 166  
 probability distribution, 118  
 probe, 165  
 problem solving, 79, 80  
 production, 6, 18, 28, 33, 96, 97, 102, 146, 177, 191  
 program, 1, 2, 3, 7, 30, 98  
 propagation, 50  
 property, 126, 162, 166, 184  
 proportionality, 79  
 proposition, 130  
 protection, 13, 97  
 prototype, 33  
 psychology, 80  
 public, 10, 13, 36, 37  
 public resources, 36  
 public-private partnerships, 37  
 pulsed laser, 148, 186  
 pulsed laser deposition, 148, 186  
 pumps, 126  
 pupils, 11  
 purification, 32, 101  
 PVA, 96  
 PVP, 63, 148, 150, 152, 153, 158, 159, 160  
 pyrolysis, 185, 186, 187

**Q**

quadrupole, 157, 164, 165  
 quality of life, 11  
 quantum, 57, 58, 59, 110, 111, 112, 113, 114, 115, 116, 187, 191  
 quantum chemistry, 110  
 quantum confinement, 58, 59, 191  
 quantum devices, 57  
 quantum mechanics, 57, 59, 110  
 quantum structure, 57  
 quantum well, 58, 59, 110, 112, 113, 114, 115, 116  
 questionnaire, 89  
 questionnaires, 83, 87  
 quizzes, 86  
 quotas, 118

**R**

R and D, 33  
 radar, 30  
 radial distribution, 1, 2, 6, 7  
 radiation, 26, 42, 43, 44, 49, 54, 162, 163, 167, 183, 187, 191  
 radio, 55  
 radius, 50, 53, 150  
 Raman, 145, 146, 166, 167  
 Raman spectroscopy, 146, 166  
 random, 183  
 randomness, 148  
 range, 1, 2, 5, 21, 26, 49, 70, 71, 72, 87, 99, 106, 117, 119, 120, 126, 162, 167, 178, 184, 190  
 rare earth, 138  
 raw material, 70  
 raw materials, 70  
 REA, 123  
 reaction time, 152  
 reactivity, 145, 176  
 reagents, 26, 71, 73, 186  
 reality, 86  
 reasoning, 79, 80, 81, 83, 86, 87, 89  
 recall, 18  
 recognition, 10, 11, 12  
 reconstruction, 157, 175  
 recrystallization, 26  
 redox, 70, 78, 172, 175  
 reductionism, vii  
 reference frame, 127  
 refining, 62  
 reflection, 139  
 refractive index, 167, 168, 169  
 refractive indices, 168  
 regular, 70, 143, 165  
 regulation, 97  
 relationship, 166, 178, 188  
 relativity, 28  
 relaxation, 26  
 relaxation time, 26  
 relevance, 9, 62  
 remediation, 183  
 research and development, 33, 70, 117  
 research funding, 37  
 resin, 19  
 resistance, 189  
 resistivity, 21, 188, 189, 190  
 resolution, 10, 18, 43, 66, 111, 112, 155, 166  
 resources, 10, 11, 12, 29, 33, 35, 36, 70, 117, 119  
 respiratory, 167  
 Reynolds number, 126  
 RFT, 66

rhombohedral, 184, 186, 189  
 rings, 174, 175  
 rods, 146, 148, 152, 158, 167, 168, 175  
 room temperature, 26, 58, 59, 142, 153, 154, 176,  
   183, 187, 189, 190  
 royalty, 34, 35, 36  
 Russian, 182  
 ruthenium, 138, 144, 168

## S

salt, 62, 63, 64, 148, 184  
 salts, 61, 186  
 sample, 19, 43, 44, 65, 66, 74, 76, 80, 86, 89,  
   103, 104, 106, 148, 151, 156, 184, 187  
 satellite, 191  
 satisfaction, 10, 11  
 saturation, 125, 129, 133, 134, 188, 190  
 SBA, 78  
 scaffold, 174  
 scaling, 127  
 scanning electron microscopy, 15, 72  
 scanning tunnelling microscopy, 155  
 scarcity, 34  
 scattering, 162, 163, 164, 165, 168, 178, 181  
 scholarship, 133, 143  
 school, 9, 10, 13, 79, 80, 85, 86  
 scientific community, 9, 26  
 scientific knowledge, vii, 9, 80  
 SCN, 171  
 search, 10, 22, 35  
 secondary education, 37  
 seed, 150  
 seeds, 148, 149, 150, 157, 158  
 segregation, 140, 141  
 selected area electron diffraction, 156  
 selectivity, 62, 168, 169  
 selenium, 175, 176  
 self, 19, 115  
 self-asassembly, 147  
 SEM, 15, 19, 20, 22, 24, 26, 72, 137, 139, 141,  
   143, 153  
 SEM micrographs, 72  
 semantic, vii  
 semiconductor, 21, 57, 58, 59, 177, 184, 189  
 semiconductors, 17, 26, 28, 57, 59, 138  
 sensing, 145, 146, 161, 166, 168, 169, 171, 172,  
   177, 178  
 sensitivity, 168, 172, 174  
 sensors, 20, 62, 167  
 sensory experience, 80  
 separation, 70, 71  
 series, 33, 59, 60, 186

shape, 19, 62, 65, 109, 110, 111, 112, 113, 114,  
   115, 127, 141, 145, 146, 147, 149, 150, 152,  
   153, 154, 155, 156, 157, 158, 159, 160, 161,  
   162, 163, 166, 167, 169, 171, 173, 174, 177,  
   186, 188, 189  
 shares, 12  
 sharing, vii, 13, 33  
 shortage, 138  
 Siemens, 72, 139  
 sign, 3, 129, 184  
 signals, 66, 69, 74, 75, 130, 166  
 silane, 70  
 silica, 69, 70, 71, 72, 73, 74, 75, 78  
 silicon, 147  
 silver, 145, 146, 147, 148, 149, 150, 151, 152,  
   153, 154, 155, 156, 157, 158, 159, 160, 161,  
   163, 164, 165, 166, 167, 168, 169, 170, 171,  
   172, 173, 174, 175, 176, 177, 178  
 simple linear regression, 44  
 simulation, 3, 5, 6, 7, 8, 155, 159, 160, 163, 164,  
   166, 173, 174, 175  
 simulations, 1, 2, 4, 6, 7, 8, 125, 131, 145, 163,  
   165, 177  
 Singapore, 115  
 single-crystalline, 176, 186  
 SiO<sub>2</sub>, 67  
 sites, 15, 104, 138, 161, 163, 184  
 skills, 12, 87  
 smart materials, 10, 13  
 social network, 119  
 social perception, 10, 12  
 socialization, 10  
 sodium, 153  
 software, 66  
 solar, 20, 21, 138, 183, 187, 191  
 solar cell, 20, 21  
 solar cells, 20  
 solar panels, 138  
 sol-gel, 138, 185, 186, 187  
 solid solutions, 137, 138, 141, 142, 143  
 solid state, 42, 43, 57, 58, 59, 60, 73, 109, 110,  
   138  
 solubility, 78, 139, 143, 170, 171  
 solvent, 1, 2, 3, 96, 98, 147, 151, 152, 161, 168,  
   186  
 solvent molecules, 2  
 solvents, 147, 152, 177, 186  
 soot, 144  
 South Korea, 33, 36  
 spatial, 26, 110, 115, 160  
 species, 2, 158  
 specific surface, 159

- spectroscopy, 47, 59, 72, 75, 110, 111, 164, 165, 166, 168, 173  
spectrum, 22, 23, 24, 41, 43, 44, 45, 46, 47, 75, 110, 111, 145, 162, 163, 164, 165, 167, 168  
speed, 82, 83, 87, 89, 90, 166  
spheres, 141, 146, 147, 151, 152, 157, 167, 168, 175, 176, 186  
spin, 181, 184, 188, 190, 191  
spin polarized electrons, 190  
SPR, 162, 165, 167, 168, 169, 170, 171, 172, 178  
sputtering, 22, 185, 186, 187, 190  
SQUID, 187  
stability, 26, 42, 99, 100, 125, 126, 134, 135, 145, 173, 184, 191  
stabilization, 63  
stabilize, 44, 62, 130, 171, 174, 184  
stabilizers, 158, 176, 186  
stages, 86, 98, 153  
stainless steel, 97  
standard deviation, 119, 120  
standardization, 89  
standards, 37  
State Department, 60  
steel, 97  
stiffness, 126  
stimulus, 100  
STM, 15, 18, 19, 155  
stoichiometry, 191  
storage, 138, 173, 184  
strain, 189  
strategies, 10, 12, 13, 146, 177  
strength, 46, 47, 48, 161, 172, 174, 188  
stress, 12, 13, 157  
stretching, 75  
strikes, 162  
strong interaction, 171  
structural defect, 150  
structural defects, 150  
students, viii, 9, 10, 11, 12, 13, 29, 41, 42, 47, 58, 59, 79, 80, 81, 83, 85, 86, 87, 89  
substances, 17, 26, 70, 94, 96, 138  
substitutes, 96  
substitution, 139, 141, 142, 143  
substrates, 167, 187, 188, 190  
sulfate, 147, 187  
sulphur, 171  
summaries, 34  
superconducting, 187  
superlattice, 115, 155  
superlattices, 115  
superposition, 45  
supply, 43  
surface area, 69, 70, 72, 73, 74, 76, 77, 137, 141, 174  
surface chemistry, 76  
surface energy, 184  
surface layer, 156  
surface modification, 70, 167, 171  
surface region, 162  
surface tension, 8  
surfactant, 75, 150, 151, 152, 158, 161  
surfactants, 63, 70, 152, 158, 160  
susceptibility, 188  
suspensions, 2  
sustainability, 31, 36, 37  
symbolic, 86  
symmetry, 155, 164  
synergistic, 138  
synergistic effect, 138  
synthesis, 2, 28, 29, 61, 62, 63, 64, 65, 66, 70, 138, 143, 144, 145, 146, 148, 152, 153, 155, 157, 158, 174, 175, 177, 185  
systems, 2, 4, 5, 26, 59, 86, 98, 102, 111, 112, 138, 139, 141, 142, 143, 177, 183, 191
- T**
- talent, 33  
tantalum, 42  
targets, 11, 187  
taxonomy, 79  
teachers, 10, 11, 12, 13, 119  
teaching, 9, 10, 12, 13, 41, 57, 58, 80, 90  
teaching strategies, 13  
technological developments, 13  
technology, vii, 8, 11, 12, 26, 30, 32, 33, 36, 62, 70, 97, 126  
tellurium, 21  
TEM, 29, 61, 65, 67, 151, 154, 155, 156, 158, 159, 169, 173, 175, 176  
temperature, 1, 2, 4, 5, 6, 7, 19, 43, 47, 48, 58, 61, 63, 65, 71, 72, 76, 99, 104, 105, 138, 139, 142, 153, 161, 183, 184, 186, 187, 188, 189, 190  
temperature dependence, 189  
temperature gradient, 186  
Texas, viii, 28, 41  
textbooks, 57, 58  
therapy, 183  
thermal activation, 188  
thermal activation energy, 188  
thermal analysis, 26  
thermal decomposition, 185, 186  
thermal evaporation, 22, 148  
thermal treatment, 139

thermodynamic, 7, 103, 168  
 thermodynamics, 152, 177  
 thermolysis, 186  
 thin film, 19, 21, 22, 103, 104, 106, 107, 157,  
   168, 183, 186, 187, 191  
 thin films, 21, 22, 107, 157, 168, 183, 186, 187,  
   191  
 thinking, 86, 87, 90  
 Third World, 32, 38  
 three-dimensional, 104  
 threshold, 140  
 time consuming, 98  
 tissue, 100  
 title, 34, 35  
 top-down, 33  
 toxic, 138, 176  
 toys, 13  
 trace elements, 42  
 tracking, 127, 129, 130, 131, 132, 133  
 trade, 33  
 training, 33, 35, 37  
 trajectory, 4, 82, 125, 127, 128, 131, 132, 133  
 trans, 167  
 transfer, 33, 149  
 transference, 30, 191  
 transformation, vii, 36, 70, 128, 173  
 transformations, 127  
 transition, 43, 80, 104, 105, 106, 138, 148, 184,  
   189, 191  
 transition metal, 138  
 transition temperature, 104, 105  
 transitions, 191  
 transmission, 65, 155  
 transmission electron microscopy, 15, 65, 155  
 transparent, 26, 33, 34, 49, 111  
 transport, 1, 62, 190  
 traps, 126  
 travel, 186  
 trial, 97, 98  
 Trojan horse, 93, 94  
 tunneling, 110, 183  
 twinning, 146, 156, 177  
 two-dimensional (2D), 8, 103, 104, 146, 148

**U**

UK, 160, 175  
 undergraduate, 57, 59  
 underlying mechanisms, 177  
 UNICEF, 10  
 uniform, 22, 63, 74, 80, 188  
 United Nations, 32

United Nations Industrial Development Organization, 32  
 United States, 33, 36, 80  
 universe, 26  
 universities, viii, 37, 96, 119  
 university students, 80  
 updating, 11  
 urban areas, 62

**V**

vacancies, 138, 144, 148, 184  
 vaccine, 96, 97, 102  
 vacuum, 3, 43, 71, 185, 187  
 valence, 184  
 values, 4, 5, 7, 47, 53, 58, 59, 65, 105, 112, 113,  
   114, 118, 141, 142, 189, 190, 191  
 vapor, 186  
 variables, 83, 86, 87, 89, 127, 129, 130, 131, 133  
 variation, 152, 191  
 vector, 4, 50, 129, 162  
 vehicles, 183  
 velocity, 4, 131  
 Venezuela, 35, 39  
 versatility, 177  
 vessels, 97, 101  
 video games, 13  
 virus, 93, 96, 167  
 viruses, 94  
 viscosity, 99  
 visible, 148, 157, 162, 191  
 visualization, 10, 15, 157  
 vitreous, 26  
 voids, 189

**W**

wages, 10  
 Wales, 145  
 water, 32, 71, 83, 84, 85, 87, 89, 90, 96, 99, 101,  
   139, 147, 150, 152, 153, 165, 168, 171, 183,  
   184, 186  
 wavelengths, 71, 148, 149, 166, 168  
 weak interaction, 171  
 wealth, 11  
 web, 14, 18  
 weight ratio, 99  
 wells, 59, 115  
 wires, 18, 146, 148, 167  
 women, 85, 117, 118, 119, 120  
 workability, 46  
 workers, vii, 33, 147, 148, 149, 150, 163, 164

World Bank, 31, 33, 34, 35, 38, 39  
writing, 89

**X**

XPS, 22, 25, 29, 191  
x-ray diffraction, 72, 74, 77, 139, 155  
X-ray photoelectron spectroscopy (XPS), 191  
X-rays, 19, 41, 42, 44, 48  
XRD, 22, 24, 26, 61, 65, 67, 69, 137, 155, 175

**Y**

yield, 41, 42, 43, 99, 147, 152, 154, 177, 187

**Z**

zinc, 186  
Zn, 19, 45, 46, 174  
ZnO, 18, 19, 20, 21, 27